

June 1988

**HYDROGEOLOGY OF FORMATIONS USED
FOR DEEP-WELL INJECTION,
TEXAS GULF COAST**

by

Charles W. Kreitler
M. Saleem Akhter
Andrew C. A. Donnelly
Warren T. Wood

Prepared for the
U.S. Environmental Protection Agency under
Cooperative Agreement ID No. CR812786-01-0

Bureau of Economic Geology
W. L. Fisher, Director
The University of Texas at Austin
Austin, Texas 78713

CONTENTS

| | |
|--|----|
| 1. ABSTRACT..... | xi |
| 2. INTRODUCTION..... | 1 |
| 2.1 Scope of Work..... | 1 |
| 2.2 Previous Work on Geohydrologic Description of the Gulf Coast..... | 3 |
| 3. THE TEXAS GULF COAST HYDROGEOLOGIC ENVIRONMENT..... | 3 |
| 3.1 SHALLOW FRESH TO MODERATELY SALINE SECTION..... | 4 |
| 3.2 BRINE HYDROSTATIC SECTION..... | 6 |
| 3.3 GEOPRESSURED SECTION..... | 6 |
| 3.4 THE INJECTION ZONES..... | 8 |
| 3.4.1 Structure..... | 8 |
| 3.4.2 Geologic and Hydrologic Description..... | 10 |
| 3.4.3 Geochemistry..... | 10 |
| 4. PHYSICAL HYDROLOGY..... | 16 |
| 4.1 Data Acquisition and Sources..... | 16 |
| 4.2 Logistics of Data Processing..... | 16 |
| 4.2.1 Data Description..... | 16 |
| 4.2.2 Methodology..... | 18 |
| 4.2.3 Quality Control..... | 20 |
| 4.3 Pressure-Depth Plots..... | 26 |
| 4.4 Regional Potentiometric Surfaces, Frio Formation..... | 27 |
| 5. CASE ANALYSIS, VICTORIA COUNTY, TEXAS..... | 49 |
| 5.1 Pressure-Depth Plot..... | 49 |
| 5.2 Potentiometric Surfaces..... | 49 |
| 5.3 Residual Surface..... | 55 |
| 6. DISCUSSION--PHYSICAL HYDROLOGY..... | 63 |
| 6.1 Regional Trends..... | 63 |
| 6.2 Victoria County Hydrologic Trends..... | 63 |
| 6.3 Reservoir Parameters and Fluid Velocities..... | 66 |
| 6.4 Sensitivity of Potentiometric Surfaces to Data Selection and Fluid Density..... | 69 |
| 6.5 Implications of Depressurization..... | 70 |
| 6.6 Implications of Overpressurization..... | 74 |

| | |
|---|-----|
| 7. WATER CHEMISTRY - INTRODUCTION..... | 87 |
| 7.1 Hydrochemical Environment..... | 87 |
| 7.2 Construction of Potentiometric Surfaces..... | 87 |
| 7.3 Hydrochemical Interpretation of the Hydrogeology of Saline Formations..... | 88 |
| 8. WATER CHEMISTRY - METHODOLOGY..... | 90 |
| 8.1 Sample Selection..... | 118 |
| 8.2 Sample Collection..... | 118 |
| 8.3 Sample Analysis..... | 129 |
| 8.4 Quality Assurance..... | 132 |
| 9. WATER CHEMISTRY - RESULTS..... | 132 |
| 9.1 Trilinear Diagrams..... | 135 |
| 9.2 Major Anion (Cl, SO ₄) Distributions..... | 135 |
| 9.3 Major Cation (Na, Ca) Distributions..... | 141 |
| 9.4 Minor Elements (Br), and Cl/Br and Na/Cl Ratios..... | 141 |
| 9.5 Alkalinity..... | 160 |
| 9.6 Gas Chromatographic Analysis of Oil..... | 165 |
| 9.7 Estimated In-Situ pH..... | 172 |
| 9.8 Oxygen and Hydrogen Isotopes..... | 173 |
| 9.9 Age Determination..... | 178 |
| 10. WATER CHEMISTRY - DISCUSSION..... | 181 |
| 10.1 Hydrochemical Environment..... | 181 |
| 10.2 Hydrochemical Interpretation of Hydrogeologic Environment..... | 182 |
| 11. SUMMARY AND CONCLUSIONS..... | 184 |
| 12. FUTURE RESEARCH DIRECTIONS..... | 188 |
| 12.1 Better Understanding of Depressurization..... | 188 |
| 12.2 Research in Overpressure Formation Mechanisms..... | 188 |
| 12.3 Potential for Biodegradation..... | 189 |
| 12.4 Thermal Regimes..... | 191 |
| 12.5 Hydrogeologic Computer Modeling..... | 191 |
| 12.6 Other Gulf Coast Formations Used for Injection..... | 191 |
| 13. ACKNOWLEDGMENTS..... | 193 |
| 14. REFERENCES..... | 194 |
| 15. APPENDIX..... | 201 |

ILLUSTRATIONS

Figures

| | |
|---|----|
| 1. Ground-water regimes and circulation pathways within the Tertiary basin fill of the northwestern Gulf Coast Basin..... | 5 |
| 2. Base of fresh to moderately saline water along the Texas Gulf Coast..... | 7 |
| 3. County map with deep-well injection locations, Texas Gulf Coast..... | 9 |
| 4. Computer-generated structure map of the top of Frio Formation, with major fault features..... | 11 |
| 5. Structure map of the top of Miocene Formation..... | 12 |
| 6. Computer-generated structural configuration on top of middle Wilcox Formation..... | 13 |
| 7. Generalized stratigraphic cross section, Gulf of Mexico..... | 14 |
| 8. Stratigraphic and hydrogeologic dip section FF' through Victoria County, Texas Gulf Coast..... | 15 |
| 9. Schematic flow diagram for data processing..... | 17 |
| 10. Salinity (total dissolved solids)-depth plot, Texas Gulf Coast Tertiary formations..... | 19 |
| 11. Pressure-depth diagram, Frio regions A, B, and C data..... | 21 |
| 12. Geographical distribution of Frio data, from 0 to 14,000 ft subsea depth..... | 22 |
| 13. Histogram for FSIP/ISIP ratio, Frio regions A, B, and C data..... | 24 |
| 14. Pressure gradient (psi/ft) versus convergence ratio (FSIP/ISIP) for DST data, Frio regions A, B, and C..... | 25 |
| 15. Pressure-depth diagram, Frio region C data..... | 28 |
| 16. Histogram of formation fluid pressure gradients (psi/ft), region C data..... | 29 |
| 17. Pressure-depth diagram, Frio region C, wildcat wells..... | 30 |
| 18. Pressure-depth diagram, Frio region C, oil wells..... | 31 |
| 19. Pressure-depth diagram, Frio region C, gas wells..... | 32 |
| 20. Pressure gradient versus time plot, Frio region C..... | 33 |
| 21. Regional potentiometric surface for Frio regions A-B-C, all class data, 1975-84, 0-2,000 ft horizontal slice..... | 35 |

| | |
|---|----|
| 22. Regional potentiometric surface, Frio regions A-B-C, all class data, 1975-84, 2,000-4,000 ft horizontal slice..... | 36 |
| 23. Regional potentiometric surface, Frio regions A-B-C, all class data, 1975-84, 4,000-6,000 ft horizontal slice..... | 37 |
| 24. Regional potentiometric surface, Frio regions A-B-C, all class data, 1975-84, 6,000-8,000 ft horizontal slice..... | 38 |
| 25. Regional potentiometric surface, Frio regions A-B-C, all class data, 1975-84, 8,000-10,000 ft horizontal slice..... | 40 |
| 26. Regional potentiometric surface, Frio regions A-B-C, all class data, 1975-84, 10,000-12,000 ft horizontal slice..... | 41 |
| 27. Frio residual potential surface, 2,000-4,000 ft minus 0-2,000 ft slice (4K-2K), all classes, 1975-84 data..... | 42 |
| 28. Frio residual potential surface, 4,000-6,000 ft minus 2,000-4,000 ft slice (6K-4K), all classes, 1975-84 data..... | 43 |
| 29. Frio residual potential surface, 4,000-6,000 ft minus 0-2,000 ft slice (6K-2K), all classes, 1975-84 data..... | 45 |
| 30. Frio residual potential surface, 6,000-8,000 ft minus 0-2,000 ft slice (8K-2K), all classes, 1975-84 data..... | 46 |
| 31. Frio residual potential surface, 6,000-8,000 ft minus 2,000-4,000 ft slice (8K-4K), all classes, 1975-84 data..... | 47 |
| 32. Frio residual potential surface, 6,000-8,000 ft minus 4,000-6,000 ft slice (8K-6K), all classes, 1975-84 data..... | 48 |
| 33. Pressure-depth diagram, Victoria County data..... | 50 |
| 34. Salinity (total dissolved solids)-depth plot for Tertiary formations, Victoria County..... | 51 |
| 35. Isometric view of structure tops, Tertiary system, Victoria County..... | 52 |
| 36. Hydraulic head values, 0-2,000 ft horizontal slice, Victoria County, all formations, all classes, 1965-84 data..... | 53 |
| 37. Potentiometric surface, 0-2,000 ft slice, Victoria County, all formations, all classes, 1965-84 data..... | 54 |
| 38. Hydraulic head values, 2,000-4,000 ft horizontal slice, Victoria County, Frio and Catahoula, all classes, 1965-84 data..... | 56 |
| 39. Potentiometric surface, 2,000-4,000 ft horizontal slice, Victoria County, Frio and Catahoula, all classes, 1965-84 data..... | 57 |
| 40. Hydraulic head values, 4,000-6,000 ft horizontal slice, Victoria County, Frio Formation, all classes, 1965-84 data..... | 58 |

| | |
|--|----|
| 41. Potentiometric surface, 4,000-6,000 ft slice, Victoria County, Frio Formation, all classes, 1965-84 data..... | 59 |
| 42. Hydraulic head values, 4,000-4,900 ft slice, Victoria County, Frio and Catahoula, all classes, 1945-84 data..... | 60 |
| 43. Potentiometric surface, 4,000-4,900 ft slice, Victoria County, Frio and Catahoula, all classes, 1945-84 data..... | 61 |
| 44. Isometric view of potentiometric surface, 4,000-4,900 ft slice, Victoria County, Frio and Catahoula, all classes, 1945-84 data..... | 62 |
| 45. Residual potential surface, 4,000-6,000 ft (Frio) minus 0-2,000 ft (Miocene) slice, Victoria County, all classes, 1965-84 data..... | 64 |
| 46. Isometric view of residual potential surface, 4,000-6,000 ft minus 0-2,000 ft slice, Victoria County, all formations, all classes, 1965-84 data..... | 65 |
| 47. Permeability distribution in Texas Gulf Coast Tertiary formations, 4,000-6,000 ft interval..... | 67 |
| 48. Location of average flow gradients in the 4,000-6,000 ft interval, Frio Formation, Texas Gulf Coast..... | 68 |
| 49. Hydraulic head values, 4,000-4,900 ft slice, Victoria County, with 0.465 gradient, include extreme head values, all classes, Frio and Catahoula, 1945-84 data..... | 71 |
| 50. Potentiometric surface, 4,000-4,900 ft slice, Victoria County, with 0.465 gradient, includes extreme heads, all classes, all formations, 1945-84 data..... | 72 |
| 51. Potentiometric surface, 4,000-4,900 ft slice, Victoria County, with 0.433 gradient, Frio and Catahoula, all classes, 1945-84 data..... | 73 |
| 52. Base of saline hydrostatic section along the Texas Gulf Coast..... | 75 |
| 53. Top of geopressed section along the Texas Gulf Coast..... | 77 |
| 54. Overlap between base of hydrostatic and top of geopressed sections..... | 78 |
| 55. Pressure-depth diagram, Kenedy County data..... | 79 |
| 56. Pressure-depth diagram, Brazoria County data..... | 80 |
| 57. Pressure-depth diagram, Brooks County data..... | 81 |
| 58. Pressure-depth diagram, Refugio County data..... | 82 |
| 59. Top of geopressed section along the Texas Gulf Coast..... | 83 |
| 60. Difference between structure top of geopressure based on > 0.465 gradient and top of geopressure based on > 0.7 gradient..... | 84 |

| | |
|---|-----|
| 61. Pressure-depth diagram, middle Wilcox Formation, regions A-B-C data..... | 85 |
| 62. Pressure-depth diagram, undifferentiated Miocene Formation, regions A-B-C data..... | 86 |
| 63. Location of wells sampled for this study..... | 128 |
| 64. Titration of organic alkalinity versus sum of acetate, propionate, and butyrate..... | 131 |
| 65. Comparison of gas chromatograph traces for samples ARCO-1989 (BEG-1) to ARCO-2000 and ARCO-1997 (BEG-29) to ARCO-2001..... | 133 |
| 66. Trilinear diagrams for Northgulf, Northcentral, Southcentral, and Southgulf regions of the Frio Formation..... | 136 |
| 67. Chloride distribution for the Frio Formation for various depths from Northgulf, Northcentral, Southcentral and Southgulf regions..... | 140 |
| 68. Cl versus depth, Nueces and San Patricio Counties..... | 142 |
| 69. Sulfate concentrations versus chloride in the Frio Formation collected for this study..... | 143 |
| 70. Sodium concentration in the Frio Formation from data collected for this study..... | 145 |
| 71. Calcium concentrations versus chloride in the Frio Formation from data collected for this study..... | 147 |
| 72. Plot of bromide versus chloride from data collected for this study..... | 149 |
| 73. Br versus Cl for high Br trend and low Br trend based on EPA data and Southgulf region data..... | 151 |
| 74. Plot of Cl/Br versus chloride, Frio Formation, from data collected for this study..... | 152 |
| 75. Na/Cl versus chloride, Frio Formation, from data collected for this study..... | 153 |
| 76. Geographic distribution of the two different populations of data..... | 154 |
| 77. Plot of Br versus Ca, Frio Formation. Data from this study..... | 156 |
| 78. Plot of Br versus Sr..... | 157 |
| 79. Plot of Br versus depth..... | 158 |
| 80. Plot of Na/Cl versus Cl/Br, Frio Formation..... | 159 |
| 81. Plot of total field alkalinity versus sum of organic acids..... | 161 |
| 82. Plot of total field alkalinity versus sum of organic alkalinity from Lundegard (1985)..... | 162 |

| | |
|--|-----|
| 83. Plot of total alkalinity versus the individual organic acids, acetate, propionate, and butyrate..... | 163 |
| 84. Total organic acids versus depth..... | 164 |
| 85. Gas chromatograph trace of whole oil sample BEG-15..... | 166 |
| 86. Gas chromatograph trace of whole oil sample BEG-16..... | 166 |
| 87. Gas chromatograph trace of whole oil sample BEG-17..... | 167 |
| 88. Gas chromatograph trace of whole oil sample BEG-26..... | 167 |
| 89. Gas chromatograph trace of whole oil sample BEG-29..... | 168 |
| 90. Gas chromatograph trace of whole oil sample BEG-31..... | 168 |
| 91. Gas chromatograph trace of whole oil sample BEG-3..... | 169 |
| 92. Gas chromatograph trace of whole oil sample BEG-11..... | 169 |
| 93. Gas chromatograph trace of whole oil sample BEG-12..... | 170 |
| 94. Gas chromatograph trace of whole oil sample BEG-1..... | 170 |
| 95. Gas chromatograph trace of whole oil sample BEG-34..... | 171 |
| 96. Inorganic alkalinity (total field alkalinity minus total titrated organic acids) versus pH..... | 174 |
| 97. Hydrogen versus oxygen isotopic composition of waters from the Frio Formation..... | 175 |
| 98. $\delta^{18}\text{O}$ versus depth..... | 176 |
| 99. $\delta^2\text{H}$ versus depth for waters in the Frio Formation..... | 177 |
| 100. Comparison of $\delta^{18}\text{O}$ composition of Wilcox waters with that of Frio waters..... | 180 |
| 101. Pressure-depth diagram, Frio regions A-B-C data..... | 190 |
| 102. Temperature-depth profile, Frio Formation, region C..... | 192 |

Tables

| | |
|---|----|
| 1. Hydrologic properties of Tertiary formations in injection zones..... | 66 |
| 2. Average horizontal linear velocities in 4,000-6,000-ft depth interval..... | 69 |
| 3a. Major ion chemistry, Frio Formation, Northgulf region..... | 91 |

| | |
|---|-----|
| 3b. Major ion chemistry, Frio Formation, Northcentral region..... | 96 |
| 3c. Major ion chemistry, Frio Formation, Southcentral region..... | 98 |
| 3d. Major ion chemistry, Frio Formation, Southgulf region..... | 105 |
| 4. Major and minor ion chemistry, Frio Formation..... | 113 |
| 5. All chemical analyses of Frio waters collected for this study..... | 119 |
| 6. Samples (with location and operator information) of Frio waters collected for this study..... | 121 |
| 7. Oxygen and hydrogen isotopic data, Frio and Wilcox Formations..... | 127 |
| Appendix | |
| Chloride versus depth for Gulf Coast counties..... | 201 |

1. ABSTRACT

This research program was conducted to investigate fluid migration potential and fluid direction and velocities in the regional hydrologic environment of the Texas Gulf Coast Tertiary formations in the context of deep-well injection of hazardous chemical wastes. The study has focused on the Frio Formation because it is the target of massive waste injection and because a large data base exists on formation pressures and water chemistry in the Frio.

Pressure data gathered from drill-stem tests and bottomhole pressure measurements in onshore oil and gas wells were used in evaluating pressure regimes. Pressure-depth profiles and potentiometric surfaces constructed from the pressure data reflect existence of three hydrologic regimes: a shallow fresh to moderately saline water section in the upper 3,000-4,000 ft, an underlying 4,000- to 5,000-ft-thick, essentially saline hydrostatic section, and a deeper overpressured section with moderate to high salinities. The complexity of the hydrologic environment is enhanced by extensive depressurization in the 4,000- to 8,000-ft depth interval. This presumably results from the estimated production of more than 10 billion barrels of oil equivalent and associated brines from this interval alone in the past 50 years. A composite potentiometric surface of the entire Frio to determine "natural" flow gradients or "natural" points of discharge cannot be constructed.

Potentiometric surfaces representing discrete depth intervals were mapped. These values and the flow gradients determined from potentiometric surfaces and published permeability and porosity data were used to compute linear fluid flow velocities ranging from 0.01 ft/year to 105 ft/year in the lateral direction.

Potential for vertical fluid migration was investigated with equivalent environmental hydraulic head maps. The presence of widespread pockets of depressured formations significantly affects the direction and value of fluid gradients, inasmuch as these depressured oil and gas fields may become potential sinks for the injected chemical wastes.

Published water chemistry data were supplemented by field sampling of waters from 32 oil fields. Active recharge of Frio by continental waters does not appear to be occurring. All waters sampled appear to be in isotopic equilibrium with the rock

matrix. In the northern section salt dome dissolution is the primary reaction controlling water chemistry in this region. Brines from the deeper geopressed section may be leaking into the hydrostatic section of the central and southern Gulf Coast Frio.

The lack of organic acids and the alteration of Frio oils from samples shallower than approximately 7,000 ft suggest biodegradation. This has a useful implication for degradation of injected chemical wastes.

A detailed analysis of the localized hydrodynamics in Victoria County, Texas, as a case study shows the applicability of the developed techniques to injection facility siting and monitoring process, where depressurization was observed on a local, county-size scale.

2. INTRODUCTION

Within the past 30 years, subsurface disposal of liquid industrial wastes generated by chemical and manufacturing industries into deep formations has become an acceptable and increasingly conventional technology. More than twenty states in the continental United States now allow this form of industrial waste disposal. In Texas, deep-well injection is the major method of chemical waste disposal, with projected volumes of 2.2 billion gallons (9.1 billion kilograms) in 1988 (Carpenter, 1987). Since this is a geological method of disposal, it is regulated by federal and state agencies and laws similar to the ones governing the oil and gas and other extractive industries. These laws have evolved in response to environmental concerns, to prevent contamination of ground-water resources from unsafe underground injection practices. The U.S. Congress passed the Safe Drinking Water Act, Public Law 93-523, in 1974, to ensure protection of underground sources of drinking water by subsurface injection of industrial wastes. The Environmental Protection Agency (EPA) has been mandated through this law to develop regulations for underground injection control.

The proposed rule-changes for the U.S. Environmental Protection Agency's Underground Injection Control Program (Federal Register, August 27, 1987) require a Class I injection well operator to show through a permit application that either the injected hazardous wastes will degrade to nontoxic materials or these wastes will not migrate to a point of discharge in 10,000 years. This report provides an approach in which Class I injection well operators can characterize the original injection zone hydrology that surrounds an injection well being considered for a permit. Using this methodology and with greater integration of regional geologic information such as depositional facies and fault distributions, it is possible to build a hydrodynamic model to describe the injection fluid pathways and velocities and its hydrologic interaction with formation fluids.

2.1 Scope of Work

The objective of the overall study is to evaluate regional trends in pressure regimes and the potential, direction, and velocity of fluid migration in the Texas Gulf Coast Tertiary formations. To complement this hydrologic investigation, we also studied the chemical composition of the brines. The preliminary activity plan for this study outlined the following topics for investigation:

A. Basin Hydrology: Map potentiometric surfaces of major injection zones in Texas Gulf Coast to assess horizontal directions and velocities of saline ground-water flow.

1. Injection zones to be studied with data availability- Frio/Catahoula, Wilcox, Undifferentiated Miocene, Oakville, Yegua.
2. Data sources- Petroleum Information Corp. (PI Corp.) data files, Railroad Commission of Texas files, available oil company files.
3. Evaluate data quality prior to mapping.
4. Mapping methods to be considered => fresh-water head equivalent, salt-water heads, pressure surfaces, bond surfaces, kriging.
5. Map cross sections of hydraulic potential to assess vertical flow potential.
6. Assess available permeability and porosity data from injection zones for integration into velocity calculations.

B. Basin Geology: Evaluate available geologic information.

1. Collect relevant geologic maps of Texas Gulf Coast onshore Tertiary formations.
2. Develop base maps for fresh-water, saline hydrostatic, and geopressured sections.

C. Integrate Geologic and Hydrologic Data: Synthesis of geologic and hydrologic information for regional characterization.

1. Investigate influence of facies change, existence of faults and salt domes.
2. Regional generic and site-specific modeling of ground-water flow.

D. Basin Geochemistry: Enhance our understanding of the hydrochemical environment of Gulf Coast brine aquifers used for deep-well injection.

1. Review available water-chemistry data to describe regional trends.
2. Obtain and analyze water samples from selected oil fields.
3. Integrate hydrochemical and hydrologic interpretation of regional and local features.

This report focuses on the Frio Formation, which has a large data base and which is the target of most of the hazardous chemical waste disposed of by deep-well injection. It summarizes the methodology and results and includes a discussion of a hydrologic study based on the analysis of formation-pressure data. As a sample case, an in-depth evaluation of hydrologic investigations in Victoria County, Texas, is presented here. Victoria County was chosen because of its large pressure data base and because of the presence of a large injection facility for which pressure data were available in the literature.

Results of the hydrologic investigation are presented in the form of pressure-depth profiles reflecting the pressure regimes in the Frio Formation and as potentiometric and residual surfaces defining regional trends and migration potential for formation fluids. Potentiometric surfaces were based on either fresh-water or salt-water head equivalent corresponding to the prevalent brine densities in the formation. These potentiometric surfaces were further utilized to evaluate flow patterns, to estimate flow velocities, and to compile a generic hydrodynamic model of the Gulf Coast aquifer system. Integration of faults and salt domes in the model and analysis of transient pressure data for delineation of oil field depressurization has been deferred pending additional data acquisition. Detailed discussion of the chemical composition of formation brines is contained in Sections 1 through 10 of this report.

2.2 Previous Work on Geohydrologic Description of the Gulf Coast

The regional hydrologic and geochemical environment of the saline sections of the Gulf Coast sedimentary basin controls the transport and ultimate fate of the injected liquid wastes. In Texas, the Gulf of Mexico basin is a relatively young (Tertiary-age) compacting basin. In the deeper brine sections, fluid movement is driven by shale compaction and is up the stratigraphic dip or up fault zones. The basin is still being filled with fine-grained clastic sediments (mud) and has undergone extensive growth faulting that may have restricted lateral fluid movement but could provide likely pathways for upward migration of waters (Kreitler, 1986). An earlier report by Kreitler and Richter (1986) reviewed previously published data on the hydrochemistry of Gulf Coast formation brines.

3. THE TEXAS GULF COAST HYDROGEOLOGIC ENVIRONMENT

The unconsolidated Tertiary sandstones designated for chemical waste disposal are part of a larger Gulf of Mexico sedimentary basin, deposited continuously for nearly 70 million years. The Frio Formation of Oligocene-Miocene age is one of the major progradational wedges of the Texas Gulf Coastal Plain and contains prolific hydrocarbon-producing plays. This wedge, which consists of interfingering marine and nonmarine sands and shales, extends in a band that is as much as 50 mi wide and in places more than 12,000 ft thick along the Texas Gulf Coast (Galloway and others, 1982).

Ground waters in the Coastal Plain aquifers are considered to have two origins: meteoric waters, introduced into shallow aquifers by precipitation, and formation

waters, from original depositional environments (Kreitler, 1979). These two types of waters coexist in the basin in the following three hydrologic regimes:

- (1) The uppermost permeable strata are continuously recharged by meteoric waters, forming a fresh to moderately saline water regime, where flow is directed toward the Gulf of Mexico. This regime may extend to a depth of 3,000 to 4,000 ft below land surface.
- (2) A brine hydrostatic section lies beneath the fresh to moderately saline section. Waters within this essentially saline section are assumed to be original formation waters or at least several million years old, or they may be meteoric in origin (Kreitler and Richter, 1986). Hydraulic connection between the hydrostatic and the overlying meteoric sections prevents excessive pressure buildup within the hydrostatic zone.
- (3) Deeper, the underlying strata represent the overpressured or geopressed zone where abnormally high fluid pressures exist due to restricted drainage conditions. Figure 1 schematically delineates these three hydrologic regimes and identifies the possible migratory pathways for deep waters.

Various researchers have found evidence of deep penetration of fresh meteoric waters into the saline sections of the Gulf Coast Basin (Bachman, 1979; Carothers and Kharaka, 1978; Lundegard, 1985). Deep basinal ground water from the geopressed zone is presumed to be leaking upward into shallower aquifer systems (Jones, 1968; Fisher, 1982). Downward flow of fresh meteoric water, upward movement of deep basinal brines, and the possible presence of original depositional waters suggest existence of a hydrologically dynamic system. However, flow rates within this environment need to be considered in the context of geologic time--that is, millions of years. The existence of complex fault systems and literally hundreds of thousands of oil- and gas-related holes adds a new dimension to the consideration of potential pathways for the movement of the various types of waters. Within this context, the injection and long-time confinement of toxic chemical wastes present an interesting topic of study.

The Texas Gulf Coast sedimentary basin can be classified into three hydrologic units: a shallow fresh to moderately saline hydro pressured section, a brine hydrostatic section, and a deep overpressured section. The following paragraphs briefly describe the hydrology of each of these units.

3.1 Shallow Fresh to Moderately Saline Section

This near-surface to 4,000-ft-deep section is characterized by water of less than 10,000 parts per million total dissolved solids, with fluid pressure gradient of

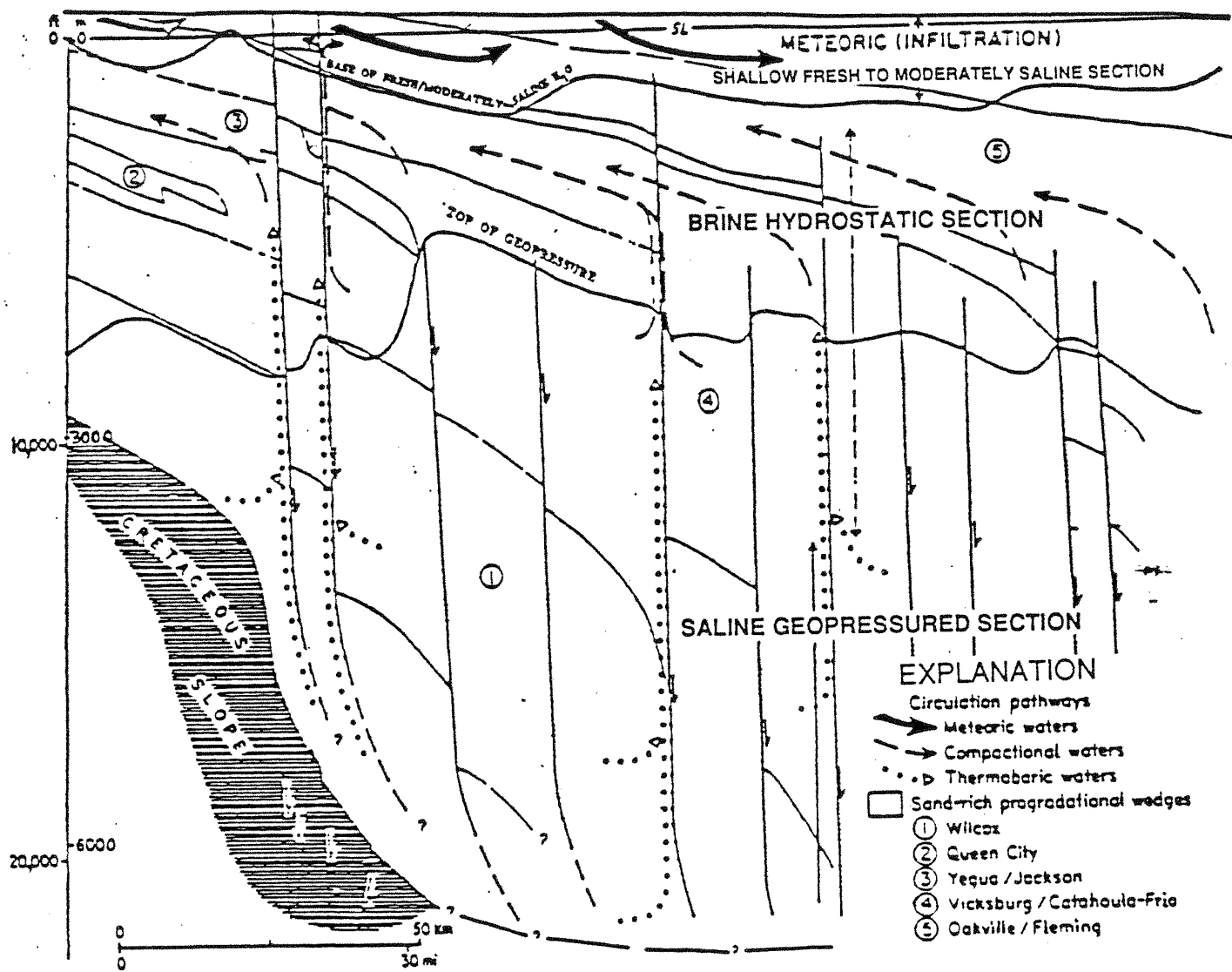


Figure 1. Ground-water regimes and circulation pathways within the Tertiary basin fill of the northwestern Gulf Coast Basin (modified from Galloway, 1982).

0.433 psi/ft. Within this regime, surface waters penetrate permeable strata and ground-water flow is directed toward the Gulf of Mexico (Kreitler and Richter, 1986). Figure 2 (Kreitler and Richter, 1986) outlines the base of the fresh to moderately saline section in the Texas Gulf Coast. The hydraulic heads in this section rise to near land surface and vertical hydraulic gradients are +0.01 or less.

3.2 Brine Hydrostatic Section

From about 4,000 to 10,000 ft deep, this essentially brine hydrostatic section underlies the fresh to moderately saline section. Hydraulic communication between the two sections prevents buildup of excessive pressures within the brine hydrostatic section. The upper part of this section is a transition zone characterized by mixing of meteoric water with in situ formation water. Salinities vary laterally and vertically, ranging from 10,000 ppm to 50,000 ppm TDS. In the lower parts of the brine hydrostatic section, waters are assumed to be original formation waters and several million years old, and salinity values range from 80,000 to 150,000 ppm TDS. The hydrology of this section is very complex due to the presence of divergent pressure regimes. Numerous hydrocarbon plays found in this section have been extensively developed and exhibit a large degree of depressurization. At the same time, a transition zone of weakly overpressured sediments is interspersed within and underlies this section.

3.3 Geopressured Section

At 7,000 to 10,000-14,000 ft in depth, the overpressured zone extends from on-shore beyond the coast into the continental shelf. Previous researchers (such as Galloway and Hobday, 1983) reported top of the overpressured sediments between 9,500 and 11,000 ft, whereas the current research encounters a transition to overpressured gradients as shallow as 6,000 ft. The overpressured regime is not confined to any single hydrostratigraphic unit, but cuts across most of them. Fisher (1982) described a relationship between formation lithology and the top to this zone. Numerous investigators have also suggested release of ground water from overpressured zone into shallower regional aquifer systems. These hypotheses were based on the study of thermal maturity of hydrocarbons, studies of organic acids in deep-basin brines, and the tracking of isotherms in the deep formations. Traditionally, top of geopressured zone has been delineated using either drilling engineering criteria, that is, from a need to increase mud weight to control oil/gas kicks, or from shale resistivity measurements with electrical logs, or by using an arbitrary 0.7 psi/ft

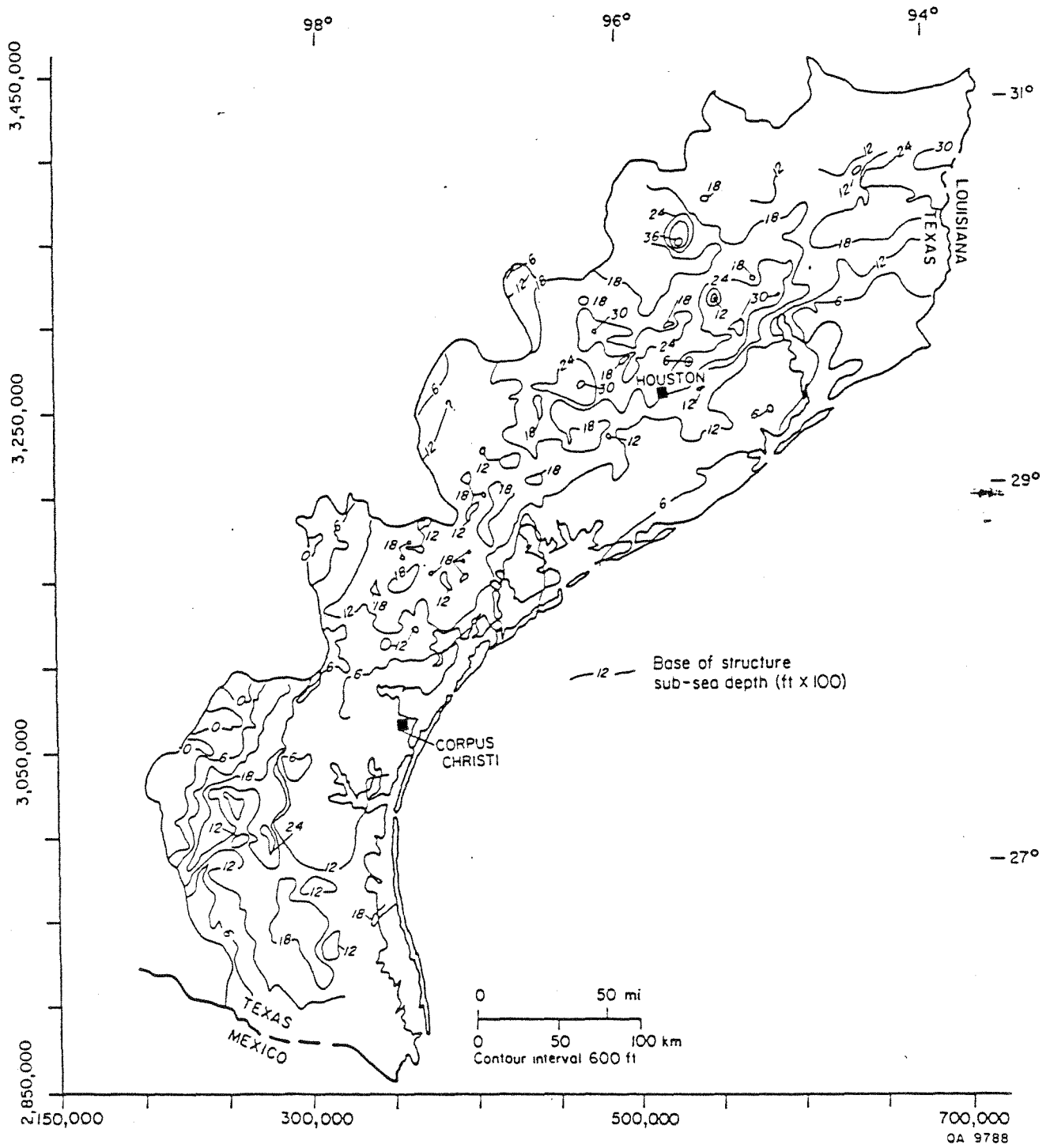


Figure 2. Base of fresh to moderately saline water along the Texas Gulf Coast (after Wood and others, 1963)

pressure gradient. These definitions did not necessarily correlate to the in situ fluid pressures. This report departs from the often used "soft" and "hard" geopressure concept and proposes that very similar processes control the formation of overpressures in both previously defined regions. Thus, for the purpose of differentiating the brine hydrostatic regime from the overpressured regime, a hydrologic criteria of fluid pressures is applied, whereby fluid pressure gradients in excess of 0.465 psi/ft are considered overpressured.

3.4 The Injection Zones

Tertiary saline formations of the Texas Gulf Coast have been used for more than 20 years for deep-well disposal of chemical wastes. The depths of waste disposal range from 2,000 to 8,250 ft below land surface in the Oakville, Catahoula, Yegua, and Frio Formations, the undifferentiated Miocene formations, and the Wilcox Group. Most injection operations are concentrated in the Miocene, Frio, Yegua, and Catahoula aquifers. To date, more than 80 billion gallons (10.7 billion ft³) of industrial waste have been injected in these zones (Kreitler and Richter, 1986). In Victoria County, large volumes of chemical waste (nearly 16 billion gallons) have been injected since 1953 at the E. I. Du Pont de Nemours facility in selected intervals between 3,800 and 4,900 ft below land surface (Texas Water Commission, 1987). Figure 3 reflects the overall area of investigation covered by this regional study, identifies the location of major concentrations of deep-well injection facilities, and delineates the regions A, B, and C into which the data were separated for convenience in handling the large computer data base.

3.4.1 Structure

The Frio and its updip equivalent, the Catahoula Formation, consist of deposits of two large fluvial and associated deltaic systems, centered in the Houston and Rio Grande Embayments (Galloway and others, 1982). Structural history in the Houston Embayment is dominated by syndepositional deformation of underlying Jurassic salt. Mobilization of thick, undercompacted prodelta and slope muds characterized the tectonic evolution of the deltaic sequence in the Rio Grande Embayment. These two major deltaic depocenters are separated by a vertically stacked, strike-parallel coastal barrier and strandplain system, called the San Marcos Arch. The Houston Embayment of East Texas is characterized by salt diapirism and associated faulting and large salt withdrawal subbasins (Bebout and others, 1978). Across the San Marcos Arch and southward toward the Rio Grande Embayment, underlying salt is thin or absent, and long linear belts of growth faults and deep-seated shale ridges and

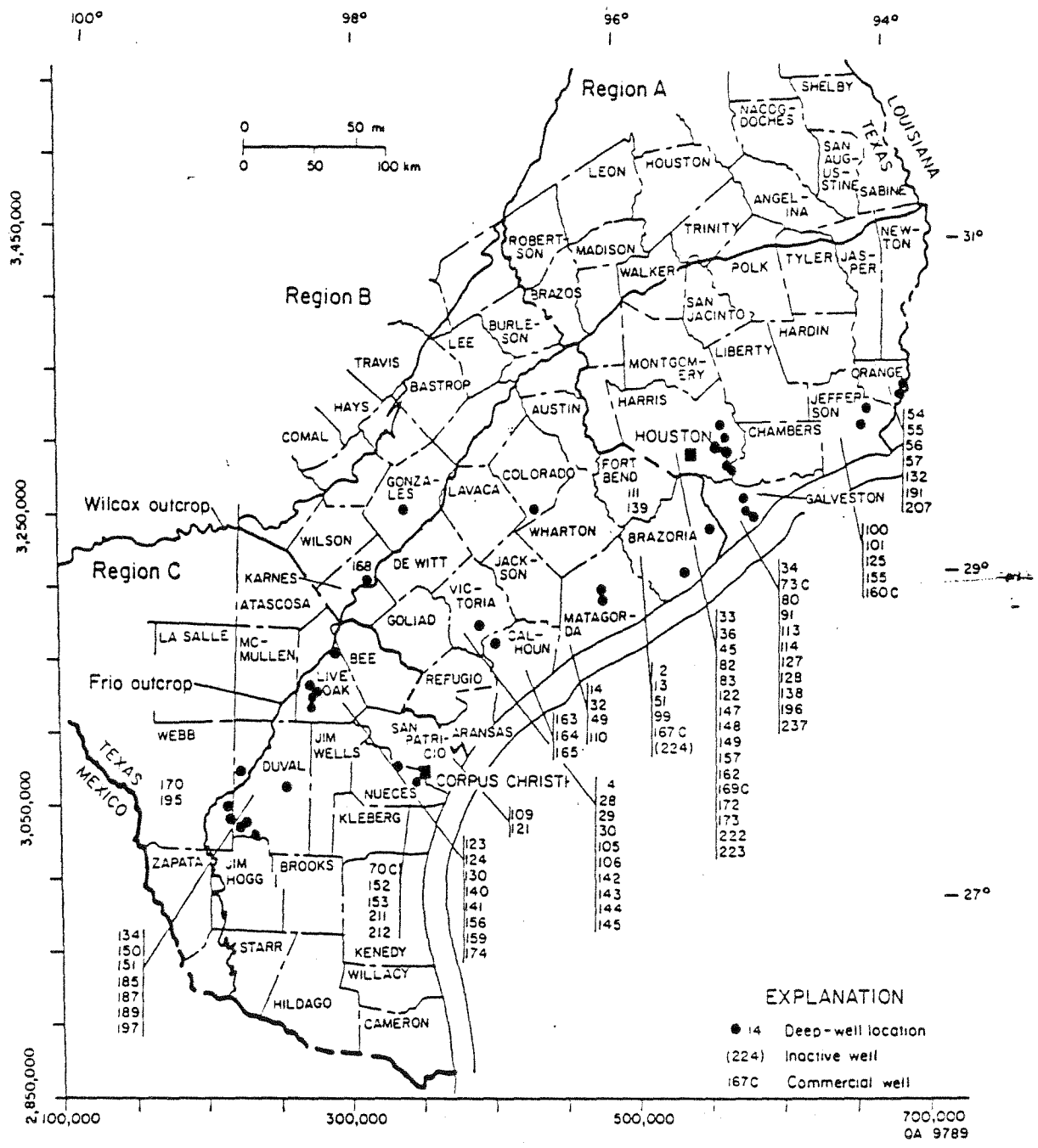


Figure 3. County map with deep-well injection locations, Texas Gulf Coast.

massifs occur. The frequency of faulting gradually decreases in updip portions of the Frio. But in the thick gulfward sections, major faulting and increasingly complex and segmented structure are encountered. The Vicksburg flexure forms the updip limit of significant structural deformation of the Frio. It is a continuous, narrow band of faults characterized by extreme vertical displacement of the underlying section. Figure 4 outlines the major structural elements on a structural map of the Frio. Structure contours for the Miocene and Wilcox are presented in figures 5 and 6.

All Frio depositional systems contain major, geologically defined, hydrocarbon-producing plays (Galloway and others, 1982). Extensive development and production over the past 55 years has yielded nearly 20 billion barrels of oil equivalent and has presumably caused widespread disequilibrium in the hydrodynamic system through depressurization. These depressured zones are encompassed by negative hydraulic contours on the potentiometric surfaces.

3.4.2 Geologic and Hydrologic Description

As a means of consolidating the available geologic information on the Gulf Coast saline formations, earlier published and unpublished maps, including structure, isopach, and net-sand-thickness maps done by various investigators, were acquired. The structure maps were digitized and reproduced using a computerized contouring program. These computer-generated structure maps were used for verifying the formation codes of test wells in the PI data base, as well as for assigning formation codes to test intervals where such information was missing in the data base. Figure 7 is a generalized cross section representing the various stratigraphic units of the Gulf Coast saline formations. A steep thickening of the Frio below the 2,000-ft subsea depth is evident (fig. 7). Stratigraphic and hydrogeologic dip section FF', through the middle section of the Texas Gulf Coast including Victoria County, is represented in figure 8. Major hydrologic units including the Frio and its updip equivalent, the Catahoula Formation, are delineated in figure 8. Exclusion of faulting from the dip section in figure 8 presents a simplistic picture of hydraulic continuity. In reality, the faults may either act as barriers to fluid flow or provide pathways for vertical communication.

3.4.3 Geochemistry

Kreitler and Richter (1986) have provided a detailed description of the chemical composition of Gulf Coast formation fluids. Most of the brines are NaCl type, with salinities varying vertically and laterally, ranging from less than 10,000 mg/L to greater than 250,000 mg/L; most values lie between 30,000 and 80,000 mg/L. Salt

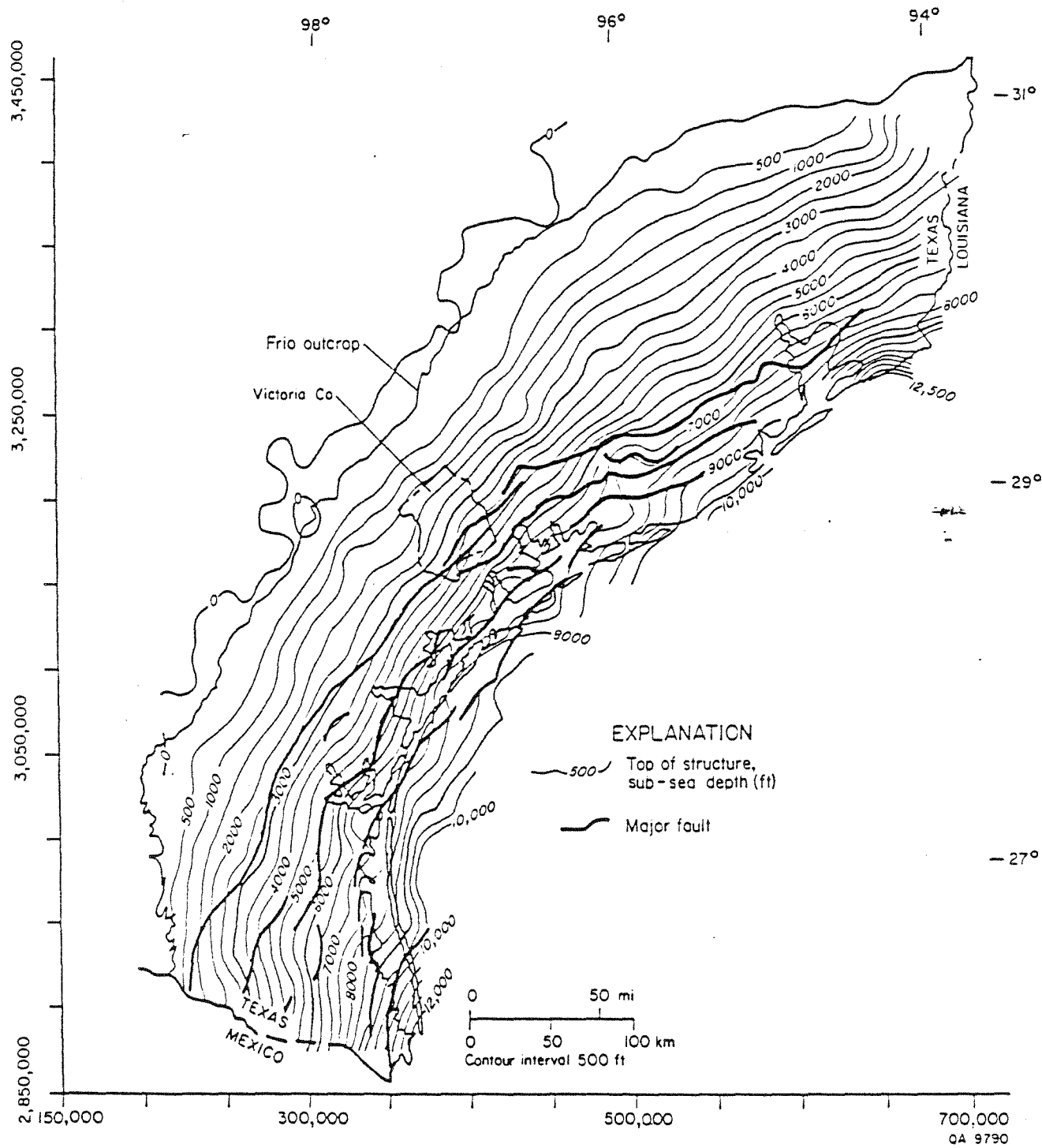


Figure 4. Computer generated structure map of the top of Frio Formation, with major fault features (after Dodge and Posey, 1981; Galloway and others, 1982).

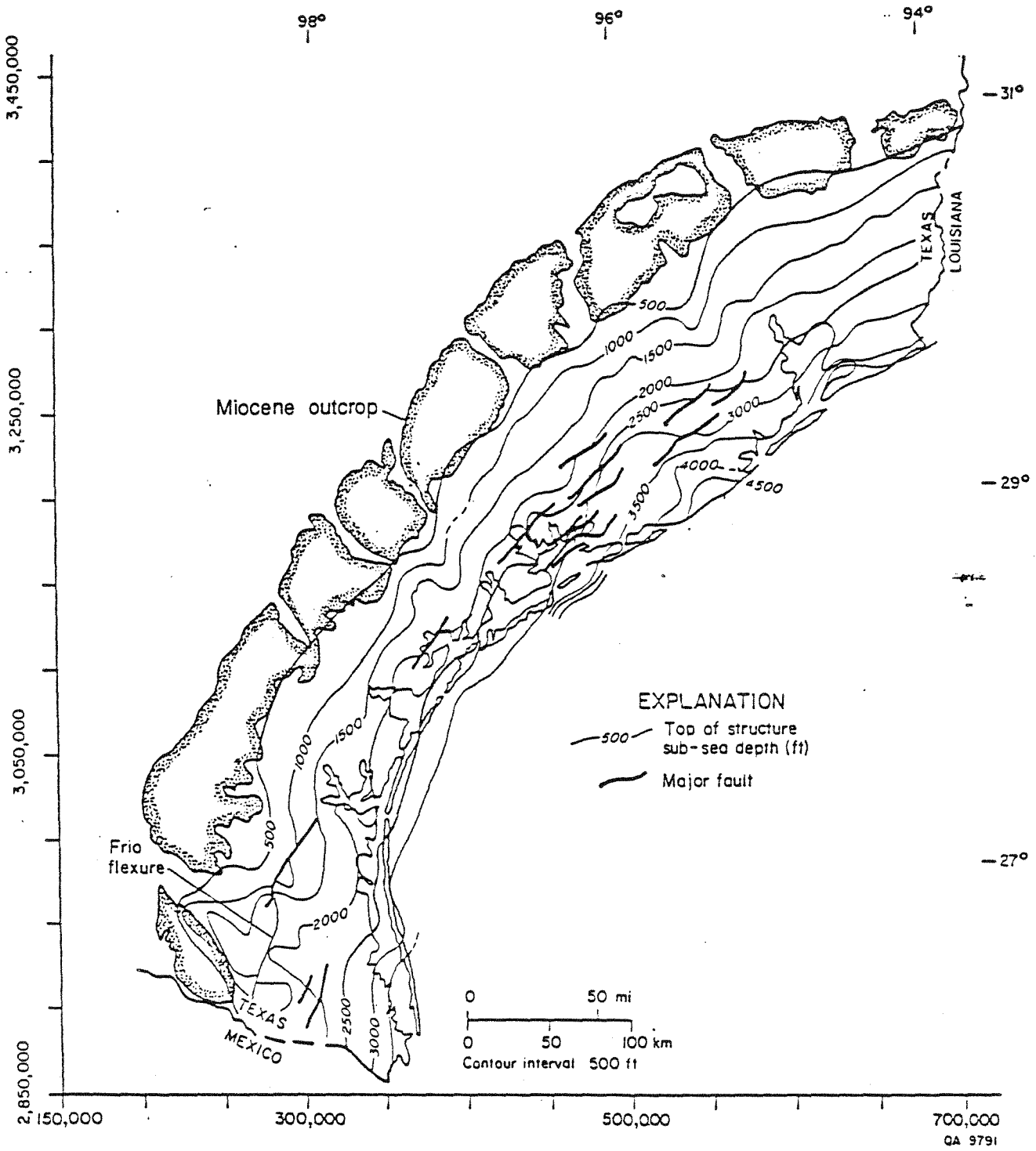


Figure 5. Structure map of the top of Miocene Formation (from DuBar, 1982).

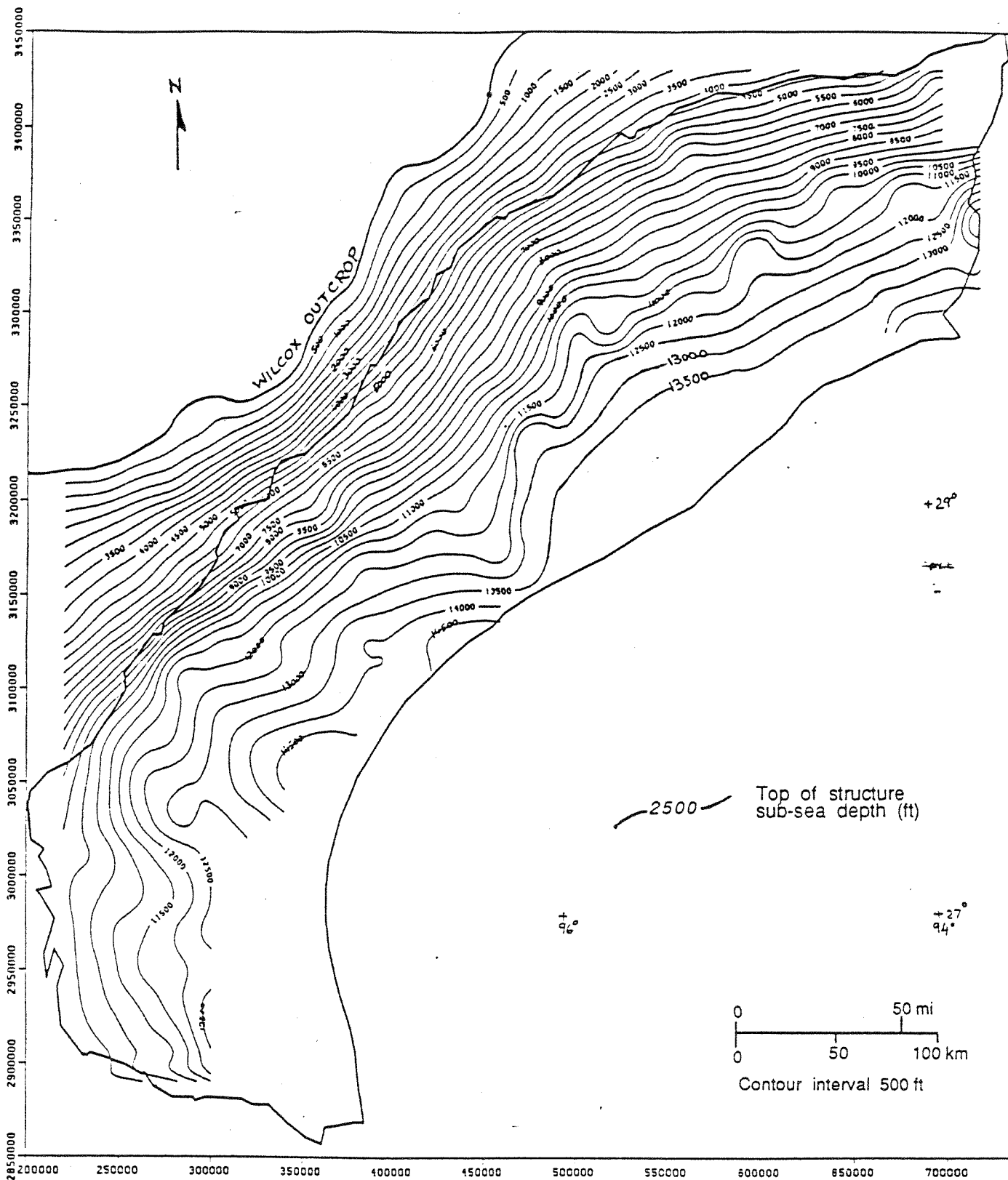


Figure 6. Computer generated structural configuration on top of middle Wilcox Formation (after Dodge and Posey, 1981).

dissolution in northern Gulf Coast causes higher salinities in that region. However, mixing of fresh water and brines may cause some of the low salinities at depths ranging from 4,000 ft to 9,000 ft along the southern Gulf Coast. High alkalinity values are contributed from organic acids as well as by bicarbonates. Estimates of pH range between 4 and 6. Deep-basin brines reflect a preponderance of reducing conditions. Detailed geochemistry of the formation waters is discussed in the second section of this report.

4. PHYSICAL HYDROLOGY

4.1 Data Acquisition and Sources

Pressure data used for the investigation of the pressure regimes and the hydrology in this project were acquired from the Petroleum Information Corporation (PI Corp.), Denver, Colorado, under a cooperative agreement with the U.S. Geological Survey and the Environmental Protection Agency. The data base, obtained on magnetic tapes, consists of drilling, completion, and testing information on nearly 147,000 new and worked-over wells. Originally compiled by PI Corp. from well-data records of the Railroad Commission of Texas and private oil companies, the data base includes bottomhole-pressure information gathered during drill-stem tests, and initial flow-potential tests, and by other bottomhole-pressure-measuring techniques. Hydrologic parameters (porosity and permeability values) were gathered from reports submitted by the injection facility operators to the regulating authorities (the Texas Water Commission and the Railroad Commission of Texas).

4.2 Logistics of Data Processing

Due to the size and complexity of the acquired pressure data, significant time and computing resources were expended in sorting, screening and processing. The following sections describe the data manipulation.

4.2.1 Data Description

The large data base acquired from the Petroleum Information Corporation (PI Corp.), Denver, Colorado, was contained on three magnetic tapes. In-house computer programs developed at the Bureau of Economic Geology (BEG) were utilized for reading the magnetic tapes and for retrieving the relevant information from them. Figure 9 is a flow chart that was used for processing the data base. A major part of the data manipulation was executed on the Dual-Cyber system at The University of Texas, and the subsequent graphics plotting was done on the BEG's VAX 11/780

FLOWCHART FOR PROCESSING OF P.I. DATA TAPES

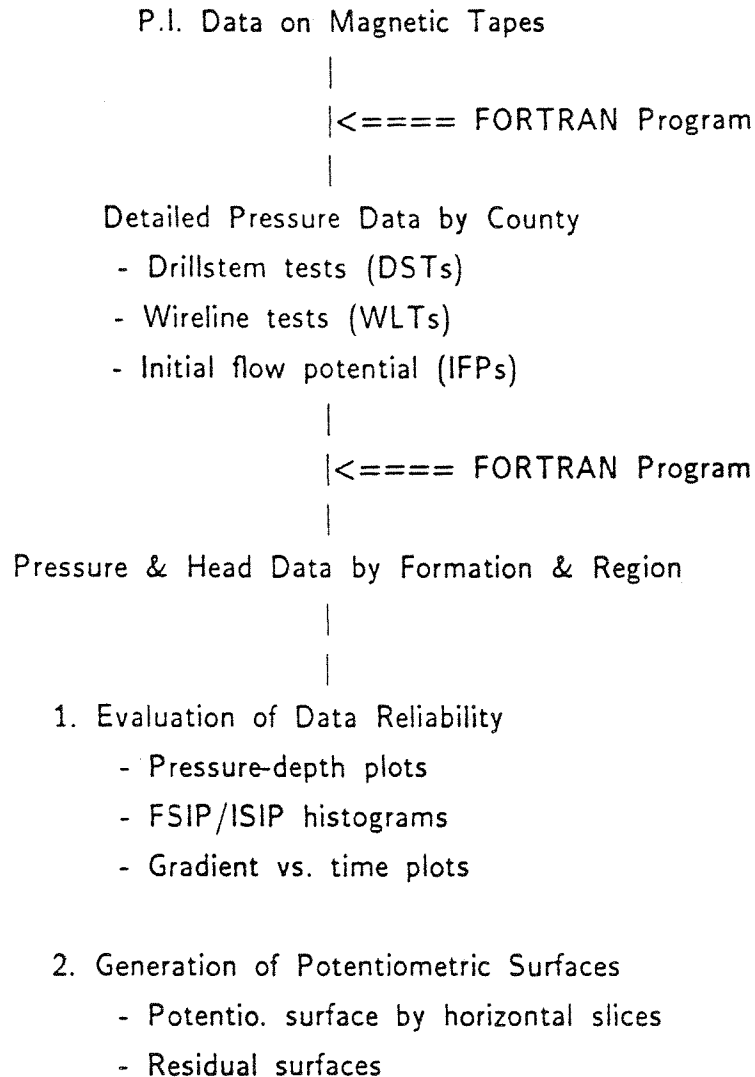


Figure 9. Schematic flow diagram for data processing.

computer. A commercially available contouring package, CPS-1 by Radian Corporation, Austin, was used for plotting the potentiometric surfaces. Although the data base spanned the years 1940 through 1985, scant pressure information was available for the years 1940-44, and wells included after 1984 lacked geographical location coordinates; hence, data from 1945 through 1984 were used for this research. A total of 64,400 pressure values pertaining to some 25,500 wells were retrieved from the PI files. Many wells had multiple pressure values for different test intervals. Thus, a data base of nearly 38,700 pressure values for the Tertiary formations spanning 81 counties along the Texas Gulf Coast was compiled for use in this research. Out of these, about 17,400 pressure values were assigned to the Frio Formation.

4.2.2 Methodology

The formation pressures used to construct the pressure-depth profiles and the potentiometric surfaces are predominantly final shut-in pressures (FSIPs) from DST records and static bottomhole pressures taken with wireline testers during the initial completion or initial production-potential testing of oil and gas wells. A small percentage (<10%) of data are from wells recompleted during a workover. In the case of DSTs where two pressures, the initial and final shut-in pressures (ISIP and FSIP), were available, the higher of the two values was used. The pressures were converted to equivalent fresh-water heads; thus, the potentiometric surface represents the elevation from a datum (sea-level), to which an equivalent fresh-water head would rise in a well completed to the midpoint depth of the DST interval.

Thus,

$$\text{hydraulic head (ft)} = \text{subsea depth (ft)} + \frac{\text{measured fluid pressure (psi)}}{\text{fresh-water pressure gradient (psi/ft)}}$$

The subsea depth is calculated as the difference of the well elevation and the midpoint of the measured test-depth. Initially, a fresh-water pressure gradient of 0.433 psi/ft was used for computing the equivalent hydraulic heads. The use of fresh-water heads is commonly accepted for determining heads in aquifers with variable fluid density. On a regional scale, such application provides good results for evaluation of flow directions and flow gradients in a lateral direction. Brine chemistry data gathered by Kreitler and Richter (1986) exhibit higher salinity values in the deeper sections of the brine hydrostatic zone (fig. 10). Hence, potentiometric maps with equivalent salt-water heads (gradient of 0.465 psi/ft) were also compiled for the Frio.

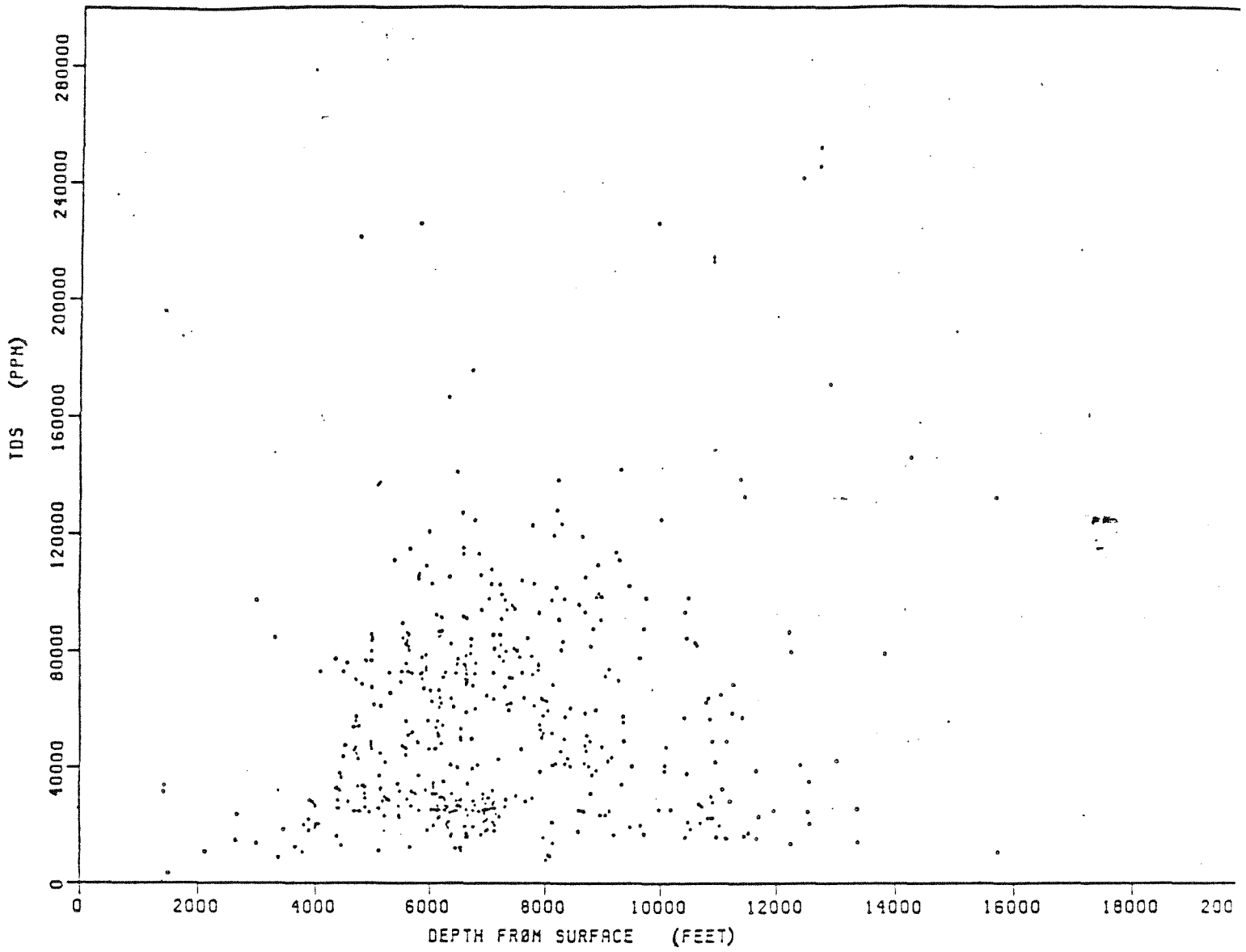


Figure 10. Salinity (total dissolved solids)-depth plot for Texas Gulf Coast Tertiary formations (from Kreitler and Richter, 1986).

These brine head potentiometric surfaces were utilized for mapping residual flow potential in the vertical direction.

Choice of fresh-water or salt-water heads is based on hydrochemistry and applicability. Strictly speaking, in fluids of variable density it is very difficult to construct potentiometric surfaces (Hubbert, 1957; Bond, 1972), due to existence of vertical flow gradient. Vertical components of potential gradients cannot be identified from the potentiometric contours. Moreover, the fresh-water head is a function of pressure, which itself depends on the local density of the formation fluid (Toth, 1978). By differentiating the Frio Formation in separate hydrologic sections (fresh to moderately saline hydro pressured, brine hydrostatic), on the basis of brine chemistry, and through the use of horizontal slices, a generic model was created. Thus, the potentiometric surface of a thick slice within a relatively homogeneous hydrologic section is a valid representation of the average energy distribution. Also, the use of fresh-water or brine heads within each corresponding hydrologic environment provides reasonably accurate lateral potential gradients. This technique is also valid for estimation of vertical flow potential by mapping residual potential surfaces.

Figure 11 is a pressure-depth plot of the Frio data from regions A, B, and C. A careful look identifies two distinct trends on figure 11 that seem to match the gradient trends for 0.433 and 0.465 psi/ft, corresponding to fresh-water and brine densities. Figure 12 reflects the geographical distribution of Frio data from surface down to a depth of about 14,000 ft (datum: sea level). This is a representative sample of the overall dataset and indicates the high data density in regions B and C. Data density in region A is relatively lower.

4.2.3 Quality Control

An important initial step was to evaluate the reliability of pressure measurements contained in the PI data base. Pressure-depth plots were used as a diagnostic tool to assess the range and variability of pressure data, as well as an interpretive technique to delineate major trends for hydrologic regimes in the Frio.

DST pressures comprised nearly 6,000 data points and were culled to obtain about 1,000 data values, each having a minimum of two pressures: an initial shut-in pressure (ISIP) and a final shut-in pressure (FSIP). An assessment of reliability of the drillstem test pressures was performed at this stage. Histograms for the ratio FSIP/ISIP exhibited a very high degree of convergence between the two pressures. The mean value was 0.975. Nearly 82% of the ratio values ranged between 0.9 and 1.1, and an additional 10% of the values ranged within 30 percent of a

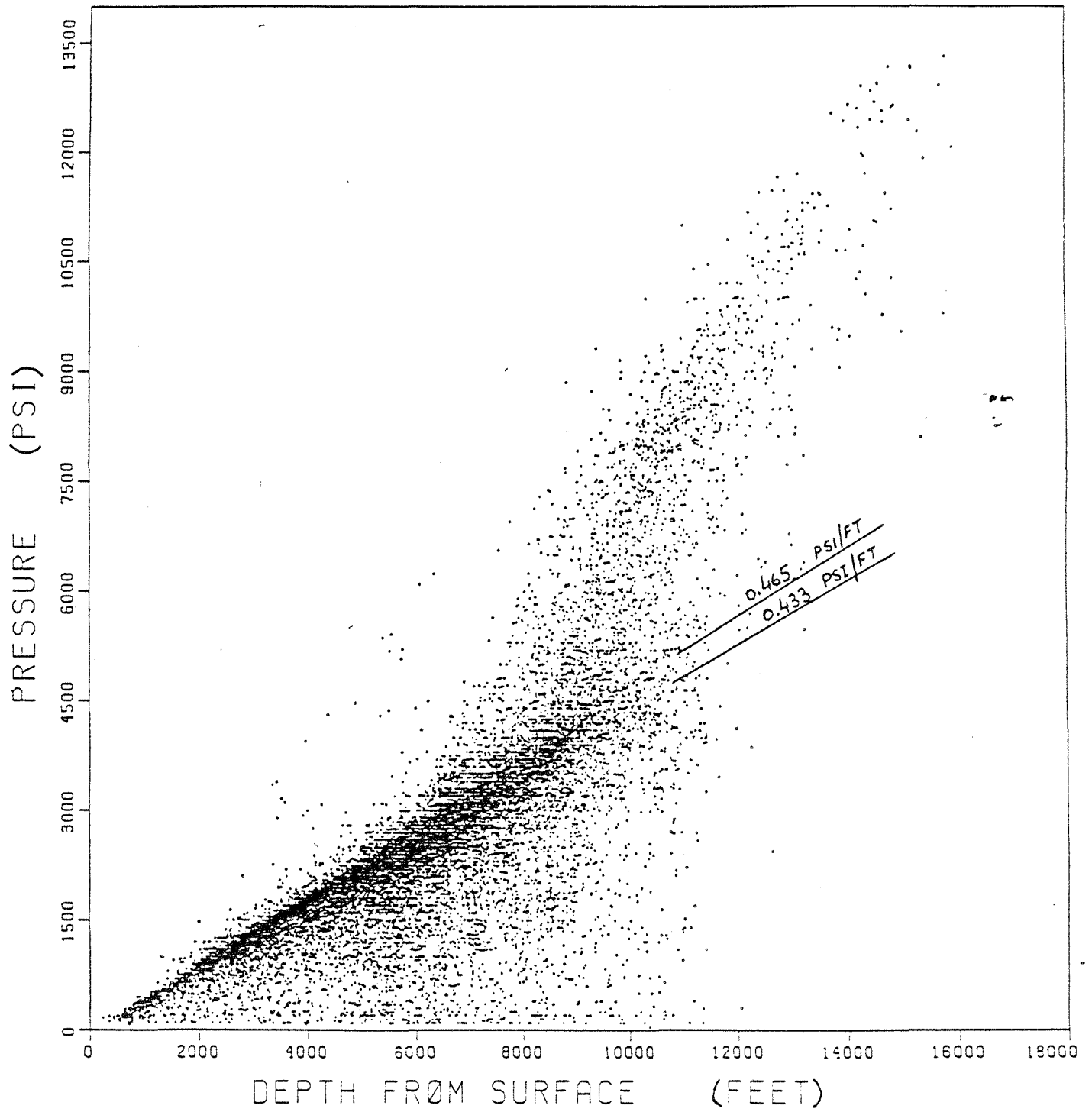


Figure 11. Pressure-depth diagram for Frio regions A, B, and C data.

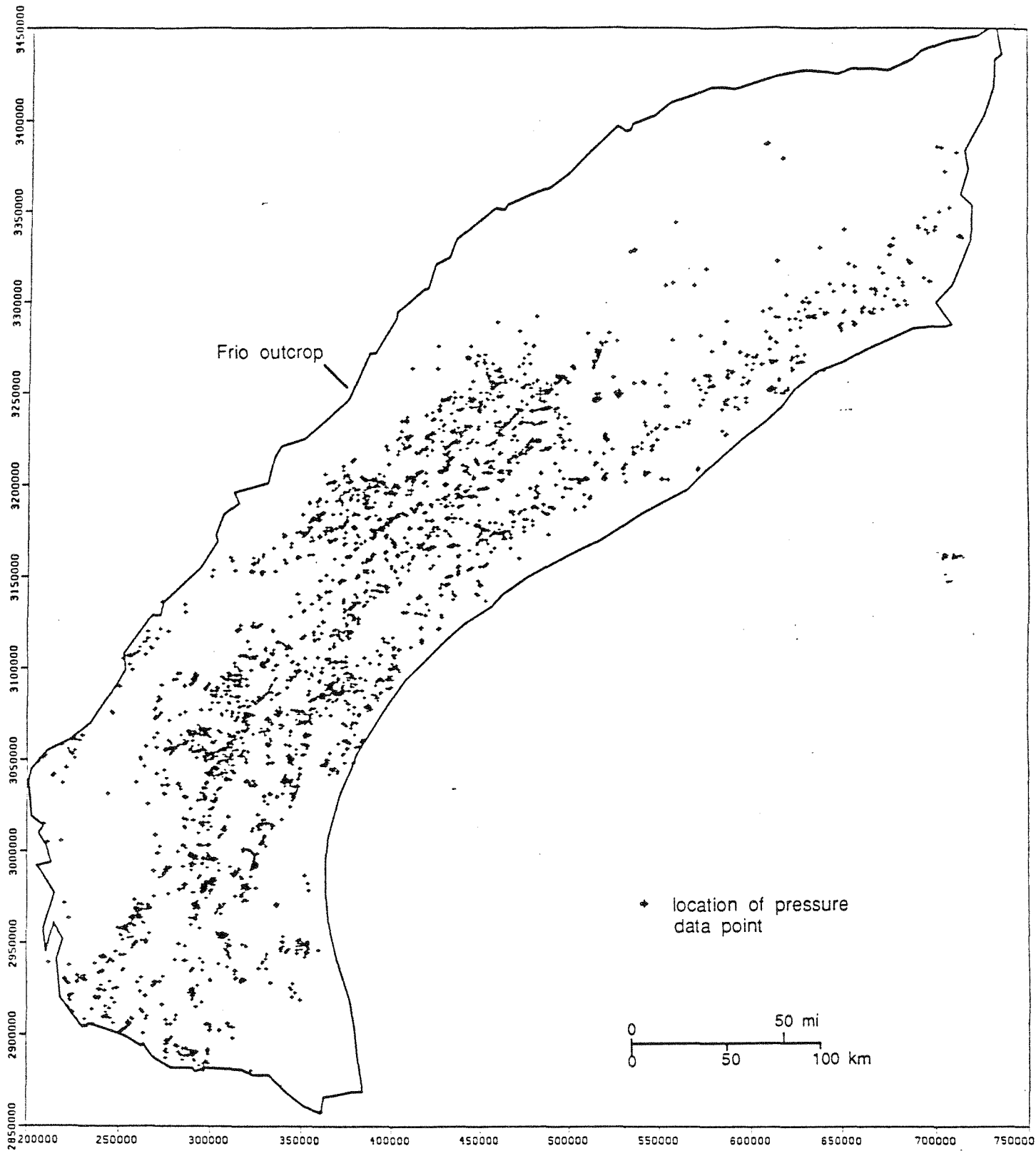


Figure 12. Geographical distribution of Frio data, from 0 to 14000 ft subsea depth.

1.0 ratio. Figure 13 is a histogram showing the convergence of the two shut-in pressures for DSTs. The formation pressure gradient (psi/ft) was plotted versus the FSIP/ISIP ratio, in order to identify any possible correlation between different pressure levels and their frequency of convergence. Figure 14 confirms that a close convergence (ratio = ~1.0) of pressures is prevalent in all pressure levels, moreso in the 0.3-0.5 psi/ft range, where most of the data lie. This enhances the level of confidence in the DST pressures and in the entire pressure data base from which the DST pressures are drawn. To promote further quality assurance, a classification and screening scheme for the entire data base was applied:

Data Classification

Class A data: Tests in which ISIP and FSIP agree within 10%

Class B data: Tests in which ISIP and FSIP diverge by more than 10%

Class C data: Tests where only one pressure (ISIP or FSIP) is available

Class D data: Pressures that convert to equivalent fresh-water heads
higher than ground elevation (flowing wells)

Class Z data: Class A data within class D

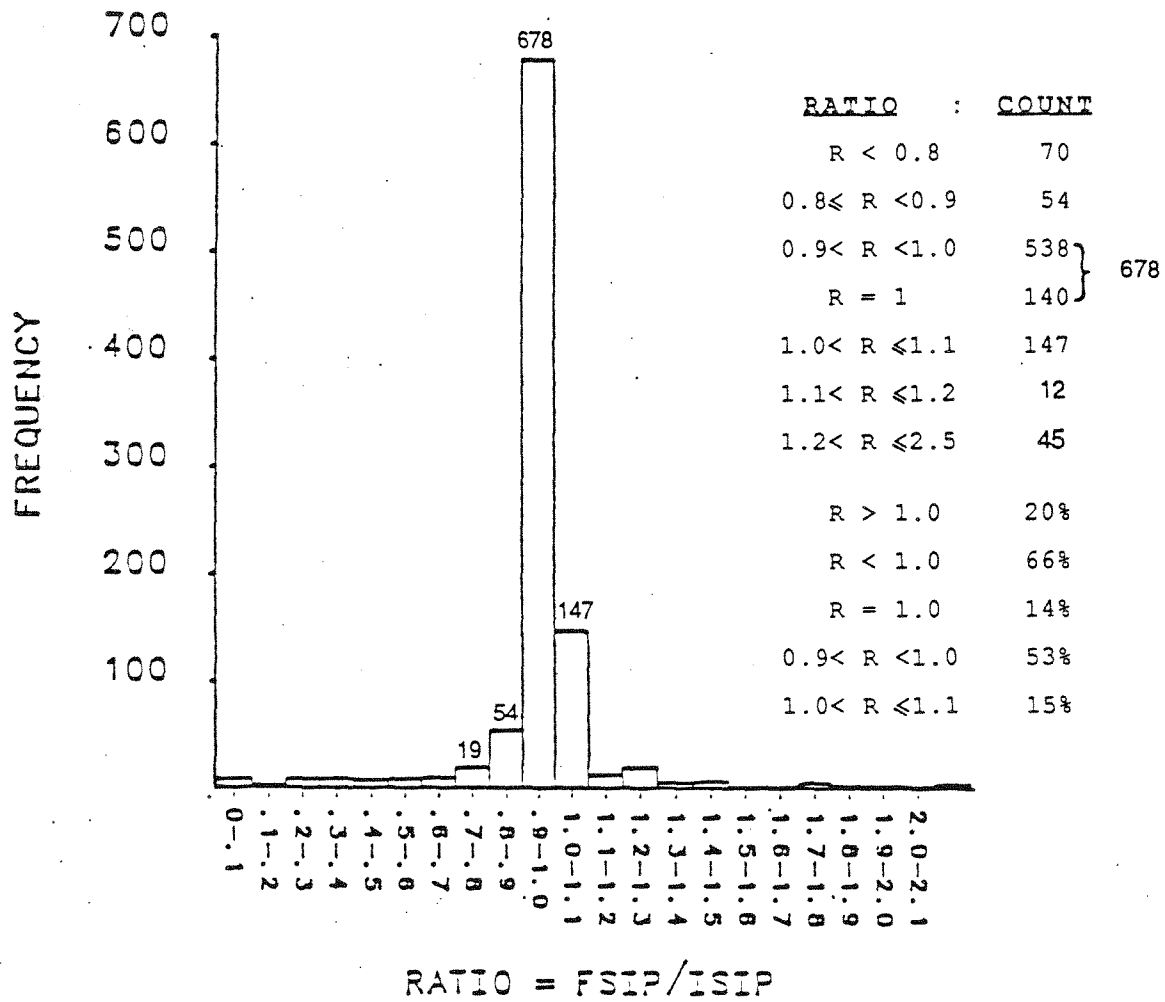
The data were sorted according to aquifer (undifferentiated Miocene, Catahoula, Vicksburg, Jackson, Frio, and Wilcox).

Data Screening

1. Nonrepresentative pressures: data with pressure gradients greater than 2.0 or less than 0.05 were deleted
2. Multiple pressure points: in case of multiple pressure data for a single well in one formation-depth interval, only the highest class and the highest pressure from the same class were retained.

Additionally, at various stages, data were also sorted by well types (wildcat, oil, and gas) and by timespan intervals for definition of trends. Identified as wildcat were wells drilled for exploration purposes in new productive zones. Development wells drilled for production were classified as oil and gas wells. During the posting of head values for contouring, anomalous data that drastically differed from local surrounding values were culled. The data classification scheme served a useful purpose in this culling process, since during comparison, the higher class (class A) was preferentially retained against the lower class (class B or C).

One of the limitations of the PI Corp. data base was a large number of missing formation codes for the pressure-test intervals. This problem was partly resolved by



N= 1006 MEAN= 0.975 STD DEV= 0.204

Figure 13. Histogram for FSIP/ISIP ratio, Frio regions A, B, & C data. A, B, and Z class data included.

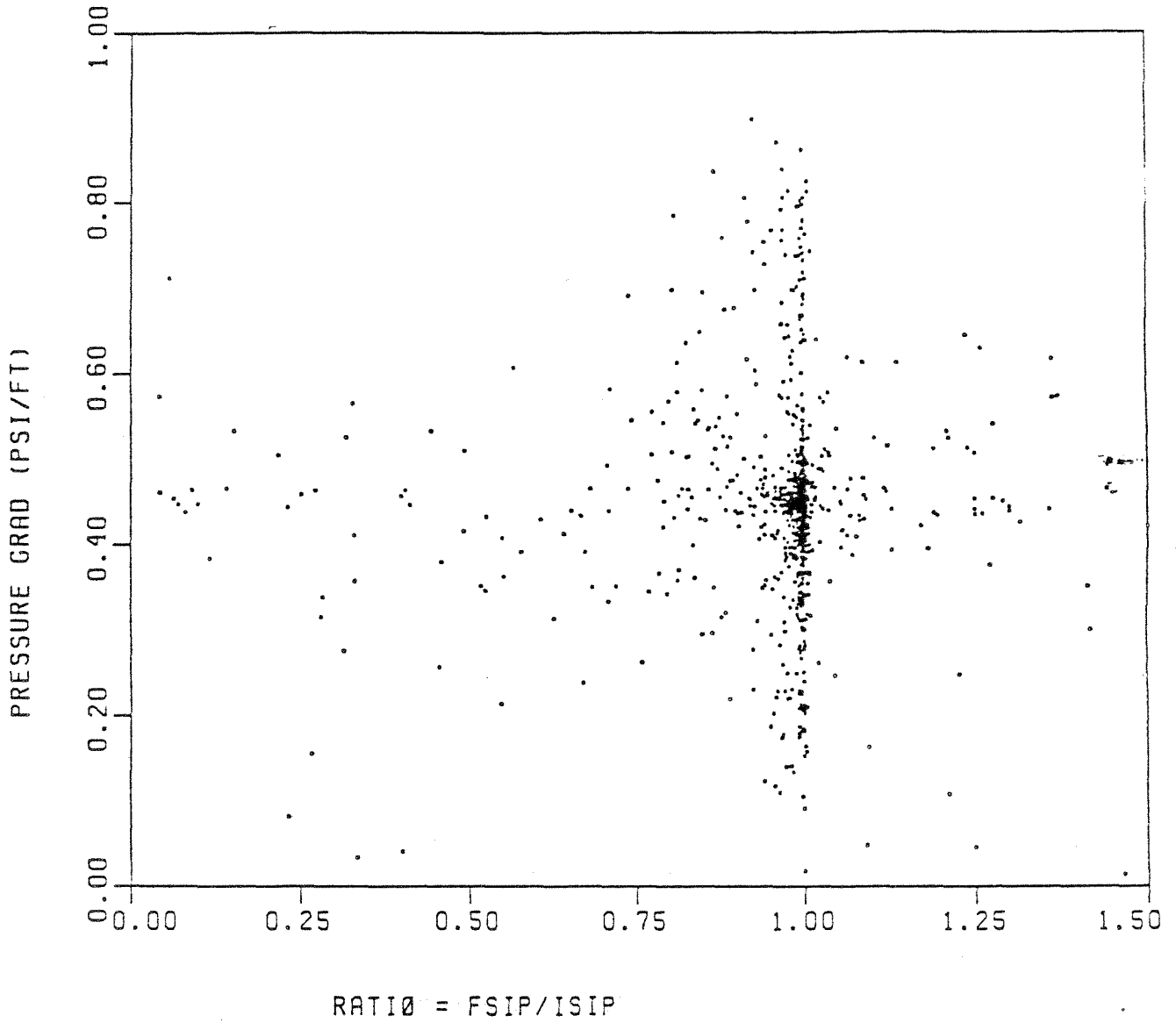


Figure 14. Pressure gradient (psi/ft) versus convergence ratio (FSIP/ISIP) for DST data, Frio regions A, B, C.

assigning interpolated formation codes in such missing cases, with the help of the contouring program CPS-1. The structure tops for the Tertiary formations were digitized and transformed into a grid network. Then the tested depths were correlated to these interpolated stratigraphic picks and their values assigned reasonable formation codes. Where no reliable match was obtained between the tested intervals and the computerized structure contour surfaces, the data were culled from the data base.

The contouring program CPS-1 used for mapping the potentiometric surfaces requires careful handling. The continuous contour lines are defined by the irregularly spaced head data, which are transformed to a regular X-Y grid mesh. The density of data in each grid cell is different, and the program averages all the data from each cell to determine the values at the nodes (corners) of the grid cells. Thus, the data density and grid-cell size influence the value of the averaged contour line passing through that cell. The size of the grid cells and the averaging algorithm were carefully selected in this study to produce representative surfaces. This data averaging approach is necessary because of the high density of data. Contouring of individual data points is impossible. This technique does, however, provide an averaged surface. Moreover, mapping of potentiometric surfaces on a county-size scale facilitated a closer scrutiny of the data.

4.3 Pressure-Depth Plots

The fluid pressures retrieved from the PI data were plotted versus the corresponding depths to obtain a pressure-depth profile for the entire Frio Formation. This P-D profile (fig. 11) was used as a diagnostic tool to scan the complete range of fluid pressures existing in the Frio, as well as an interpretive technique for evaluating the presence of different hydrologic regimes. Two trend lines are drawn on the P-D plot: one with a 0.433 psi/ft slope, and the other with a 0.465 psi/ft slope. These slopes were not computed from any regression analysis, but merely represent the dominant trends visible on the P-D plot. These slopes also delineate the fresh-water and brine hydrostatic gradients in the Gulf Coast. Additionally, the following observations are relevant to the P-D profile:

1. a significant volume of data lie along the fresh-water gradient line
2. the overpressured regime is represented by data above the brine hydrostatic line
3. a large body of data lies in the underpressured zone below the 0.433 psi/ft gradient line.

The pressure data were then plotted separately for the three regions (A, B, and C), and similar trends were observed. Figure 15 is the pressure-depth profile for region C. A histogram of the pressure gradients in region C (fig. 16) reveals the larger groupings into which the pressure measurements are differentiated, and once again it reinforces the significance of the 0.433 and 0.465 gradient trends.

For investigating the variability in the pressure-depth profiles as a function of well type and time, several P-D plots were compiled for region C for various well categories; wildcat, oil, and gas (figs. 17, 18, and 19, respectively). There are basic similarities between these plots and the integrated plot shown in figure 11. Figure 20 is the gradient versus time plot for region C. No distinguishing trends can be observed from this plot. Thus, the influence of time on the nature of hydrologic regimes can be isolated only indirectly, and it has been addressed in the context of potentiometric surfaces compiled for different time segments.

4.4 Regional Potentiometric Surfaces, Frio Formation

Regional potentiometric surfaces of the Frio were constructed using equivalent fresh-water and salt-water heads calculated from the highest available shut-in pressures. The initial surface was generated from the screened class A, B, and Z data. This surface contained several localized highs and lows (bulls-eyes) and represented complex variations in flow trends. The enormous thickness of the Frio and the variability in hydraulic gradients as reflected on the stratigraphic cross section (fig. 7) and the pressure-depth plot (fig. 11) made it difficult to discern any specific flow trends in this regional surface. Consequently, potentiometric surfaces were generated for separate slices through the Frio. This allowed a rough delineation between the top fresh to moderately saline hydro pressured zone, the next lower brine hydrostatic zone, and the deep overpressured formations. As part of the preliminary investigations, potentiometric surfaces were generated for 2,000-ft-thick horizontal slices of the Frio, from land surface down to a 14,000-ft depth. These surfaces are presented in figures 21 through 26. Outlined on these maps are the boundaries of reliable data regions, beyond which sparseness and boundary effects make any viable interpretation difficult. Most of these surfaces cover regions B and C, and only partially extend into region A, due to scarcity of data in region A. Data from years 1975-84, within classes A, B, C, and D were selected for constructing these potentiometric surfaces.

The large pressure dataset provides good areal coverage on a regional scale, and reliable regional potentiometric surfaces can be generated. Kriging, a geostatistical analysis method used for minimizing variance in a regionalized variable such as

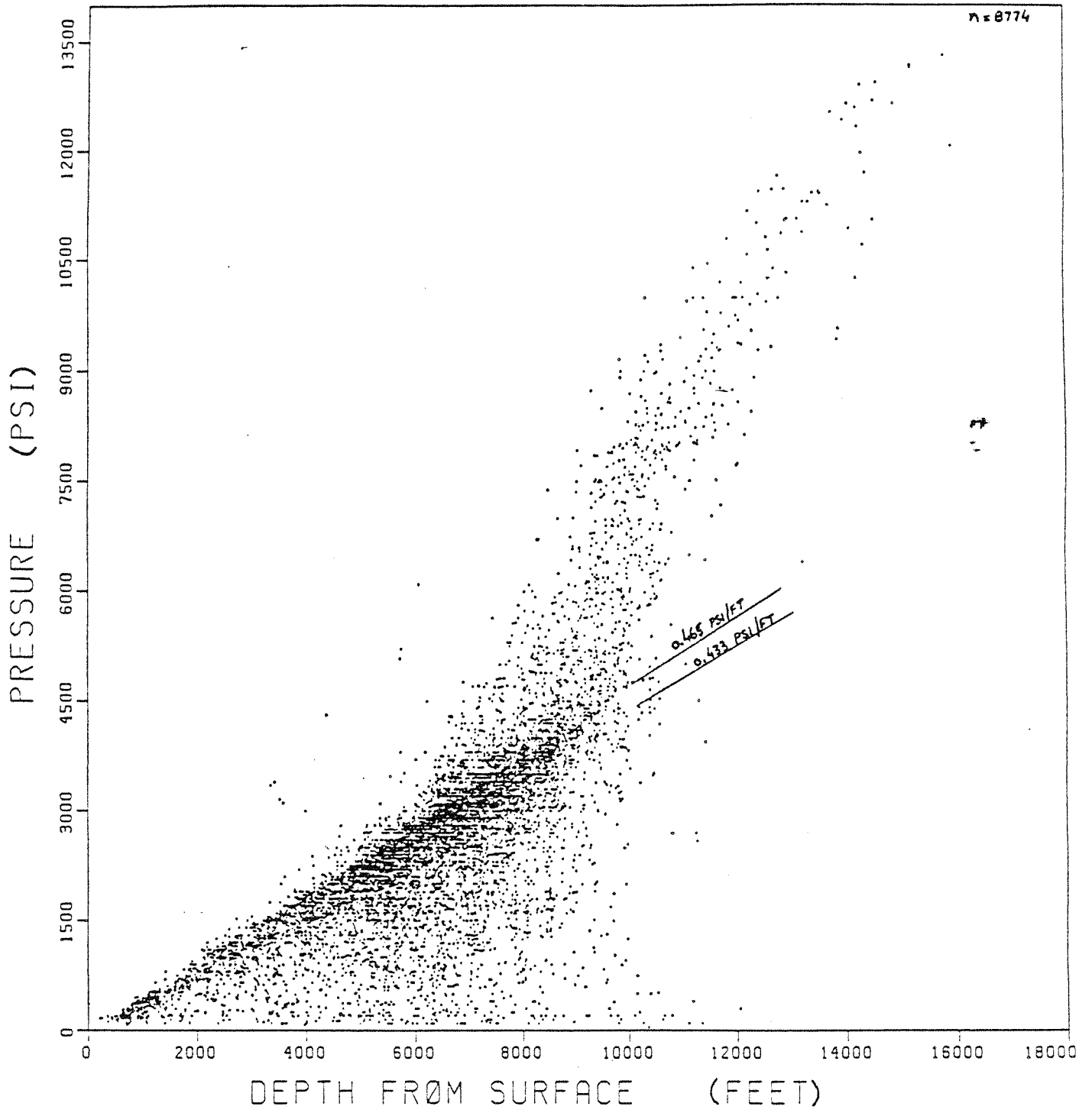
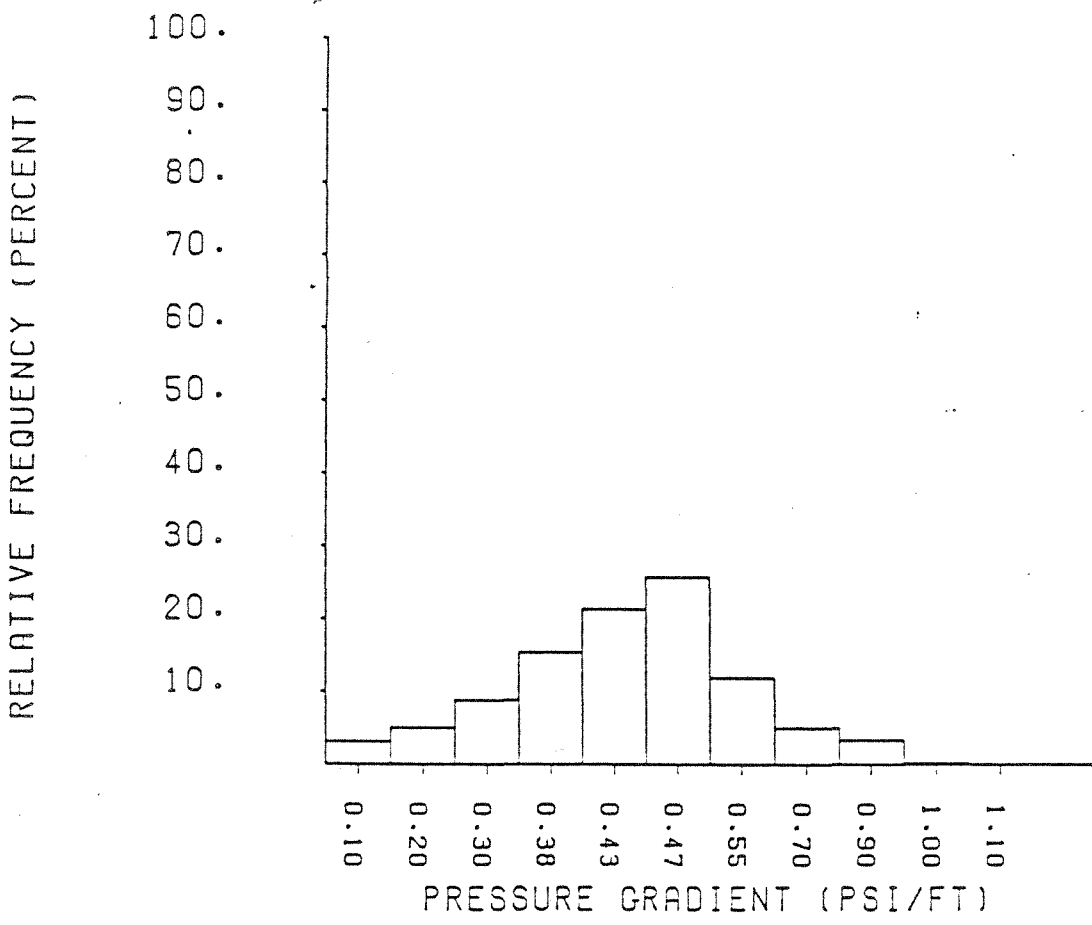


Figure 15. Pressure-depth diagram for Frio region C data.



N= 8773 MEAN= 0.406 STD DEV= 0.139

Figure 16. Histogram of formation fluid pressure gradients (psi/ft), region C data.

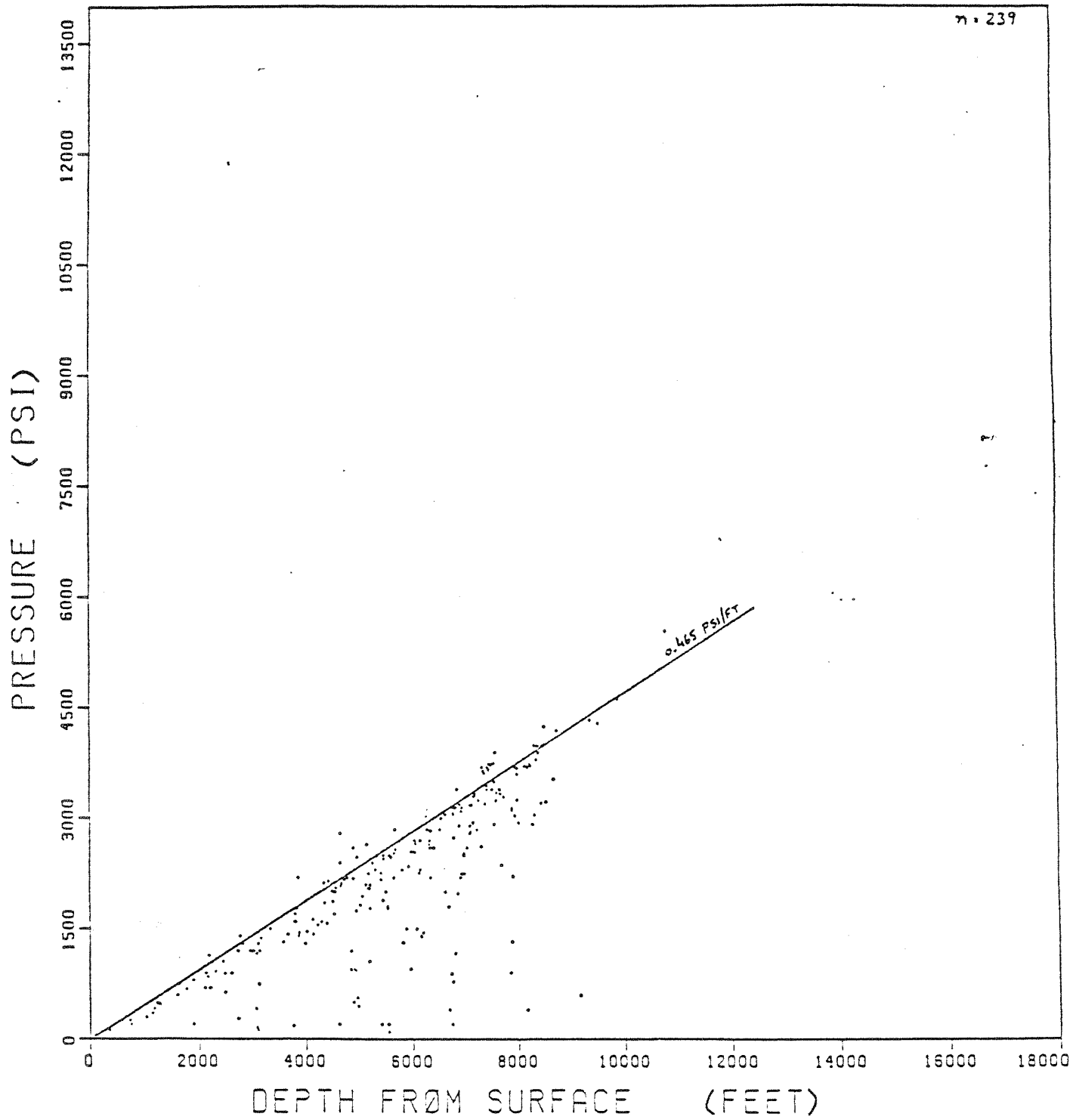


Figure 17. Pressure-depth diagram for Frio region C, wildcat wells.

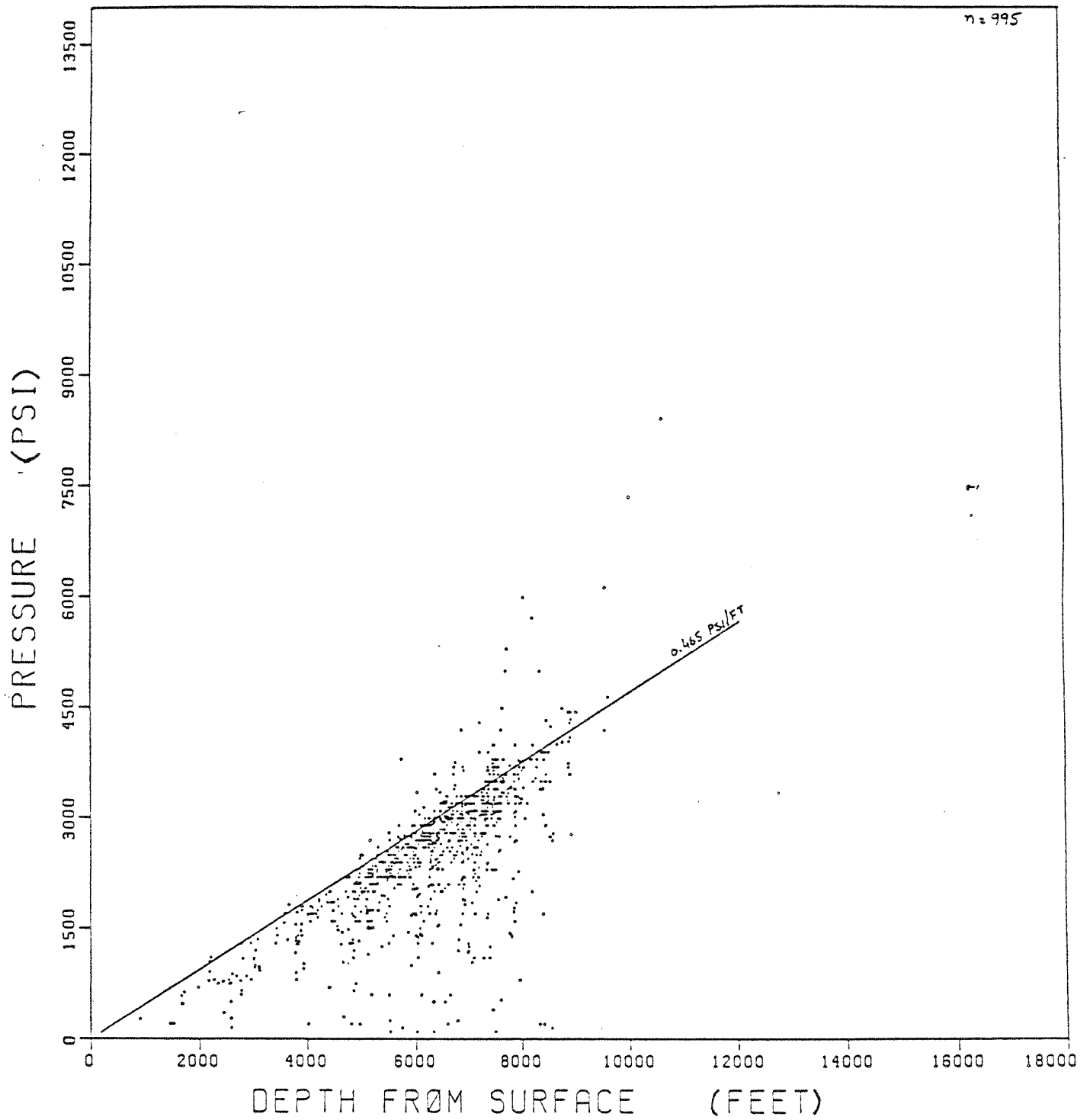


Figure 18. Pressure-depth diagram for Frio region C, oil wells.

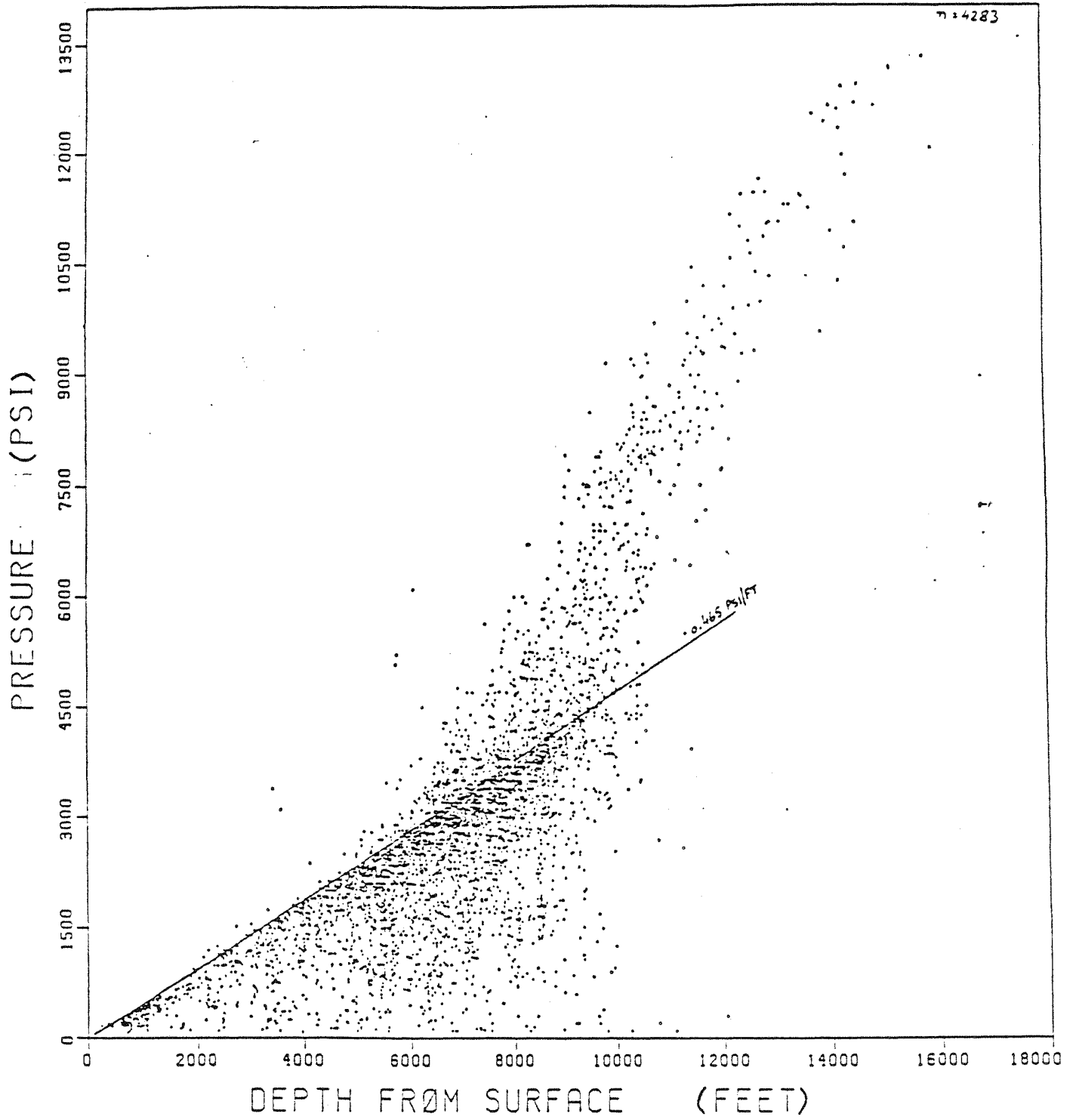


Figure 19. Pressure-depth diagram for Frio region C, gas wells.

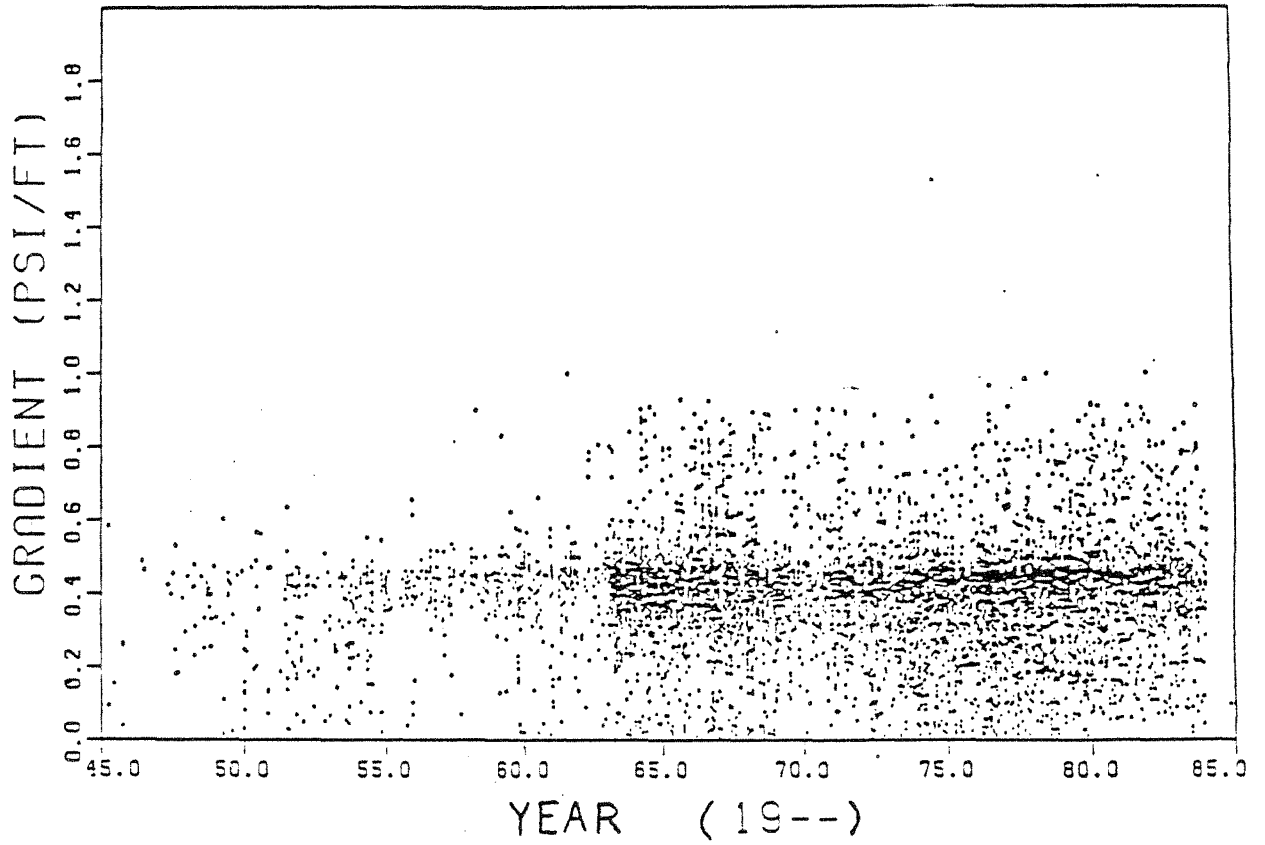


Figure 20. Pressure gradient versus time plot for Frio region C.

potentiometric level, may be needed when data are sparse. High data density, separation of data by horizontal slices, and the capability of analyzing county-size maps combined to make kriging unnecessary. As discussed earlier, equivalent fresh-water and salt-water heads proved adequate for characterizing the lateral flow potentials. Lack of continuous data along the vertical prevents determination of environmental heads. But, within the bounds of the horizontal slices, variations of formation water salinities are small enough so that fresh-water and salt-water heads result in representative surfaces for the corresponding hydrologic regimes. Therefore, at less than a 4,000-ft depth, a fresh-water gradient (0.433 psi/ft) was used to compute hydraulic heads, and in the deeper intervals, a salt-water gradient (0.465 psi/ft) was used.

Following is a brief discussion of the salient features of each of these surfaces.

(a). 0-2,000 ft interval (fig. 21): Most of the surface is flat with hydraulic heads near land elevation (-250- to +250-ft contours). There is a cone of depression in the middle of the map (in north region C) that corresponds to extreme negative contours in Jim Wells County. Individual pressure values for wells in this area reveal a cluster of producing gas wells that presumably have caused the depletion.

(b). 2,000-4,000 ft interval (fig. 22): A majority of hydraulic heads are near land elevation; however, the area covered by depressured contours has expanded. But there are no extreme contrasts in flow gradient. The depressured areas are confined by negative contours, in the central and southern parts of the study area. Normally pressured areas are represented by mildly positive and zero-contour lines and are located on the western flank. Due to coexistence of normally pressured and underpressured areas side-by-side, localized reversals of flow direction are observed.

(c). 4,000-6,000 ft interval (fig. 23): This represents the average potentiometric surface for pressures in the 4,000-6,000-ft slice. Negative depressured contours envelope almost the entire surface. The lower bound of the negative contours (-2000 ft) corresponds to depressurization to the extent of 930 psi below hydrostatic pressure. The large volume of pressure data also reflects extensive hydrocarbon development in this horizon.

(d). 6,000-8,000 ft interval (fig. 24): This surface has a character similar to that of the overlying interval. Underpressured regime occupies a significant part of the surface. The surface becomes positive near the shoreline in the north-central part, which reflects a gradual transition to overpressures. Reversal of flow direction is also observed. Adequate hydraulic communication over a large overlapping segment of the two slices probably exists there.

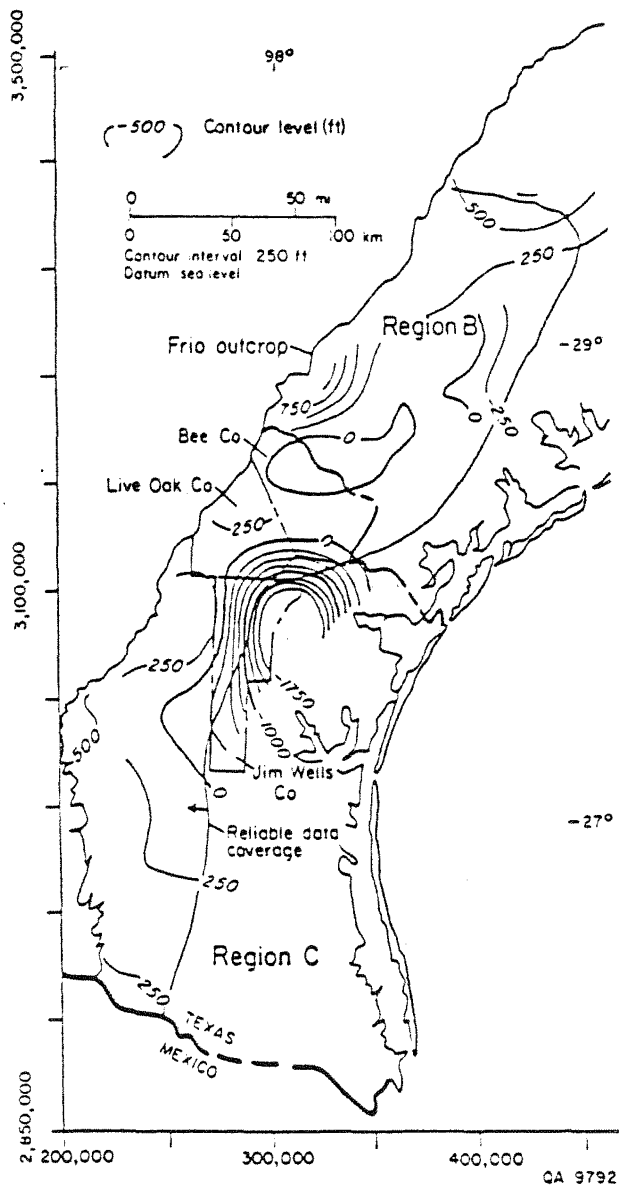


Figure 21. Regional potentiometric surface, Frio regions A-B-C, all class data, years 1975-84, 0-2,000 ft horizontal slice. Equivalent fresh-water heads.

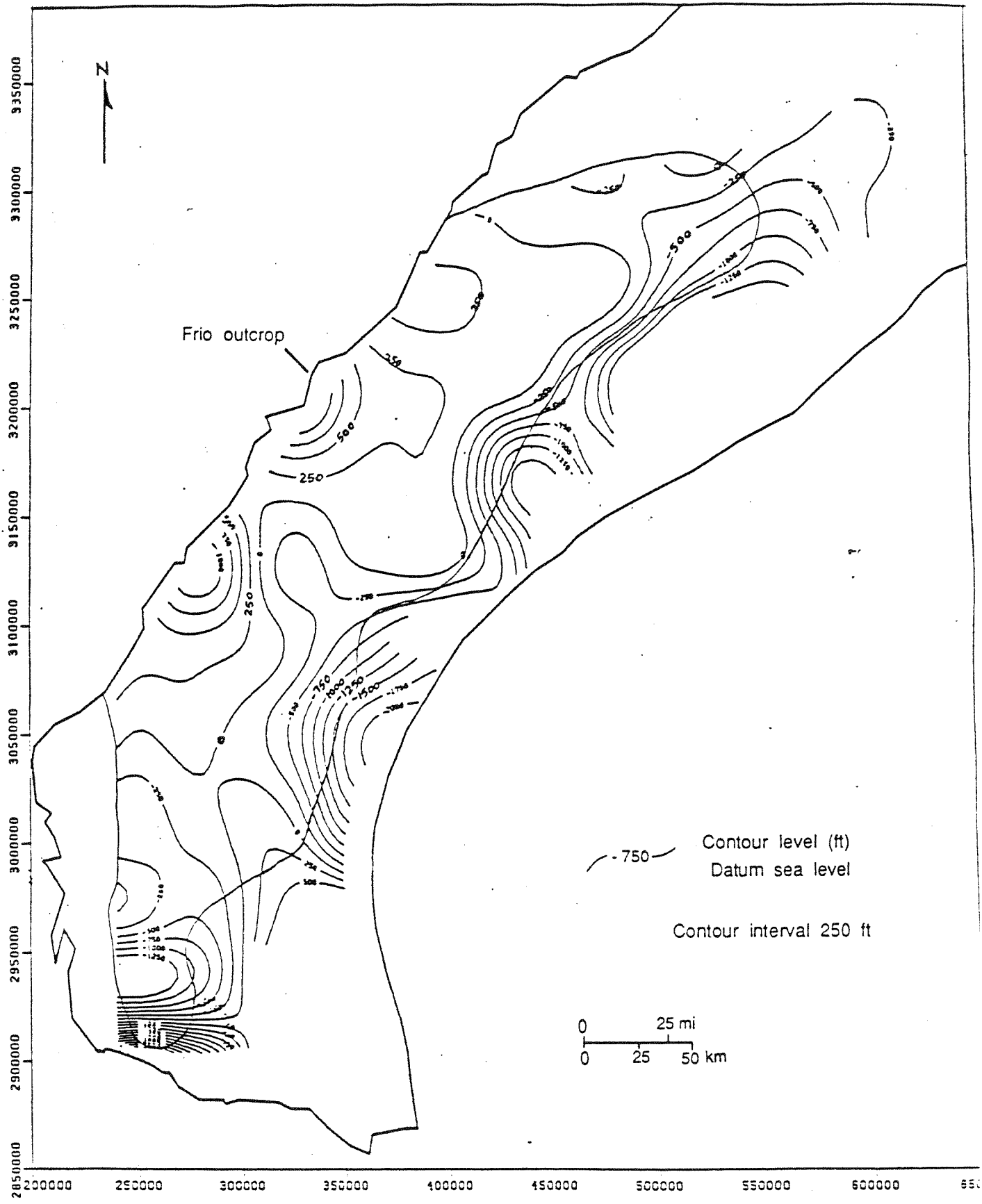


Figure 22. Regional potentiometric surface, Frio regions A-B-C, all class data, years 1975-84, 2,000-4,000 ft horizontal slice. Equivalent fresh-water heads.

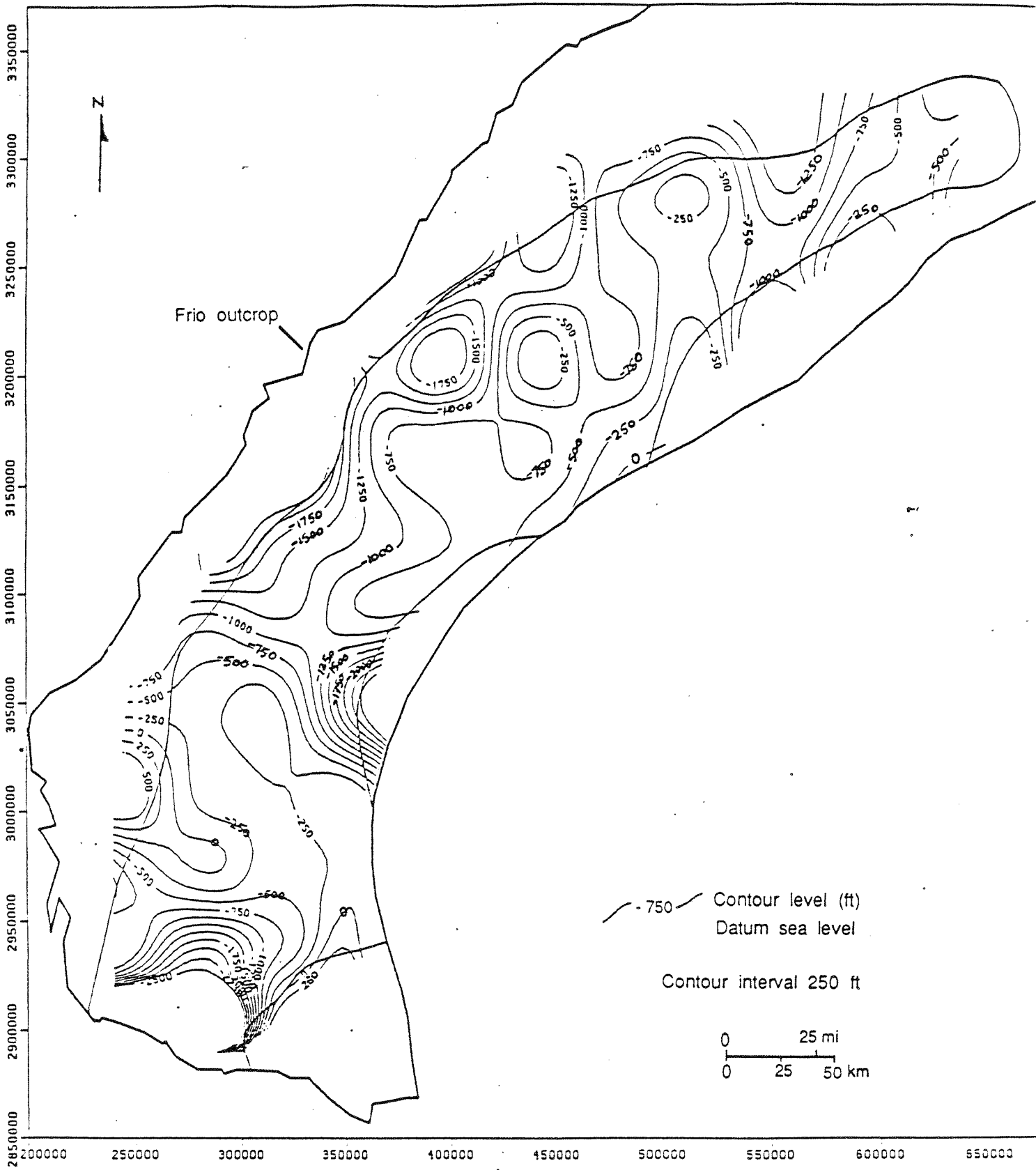


Figure 23. Regional potentiometric surface, Frio regions A-B-C, all class data, years 1975-84, 4,000-6,000 ft horizontal slice. Equivalent brine heads.

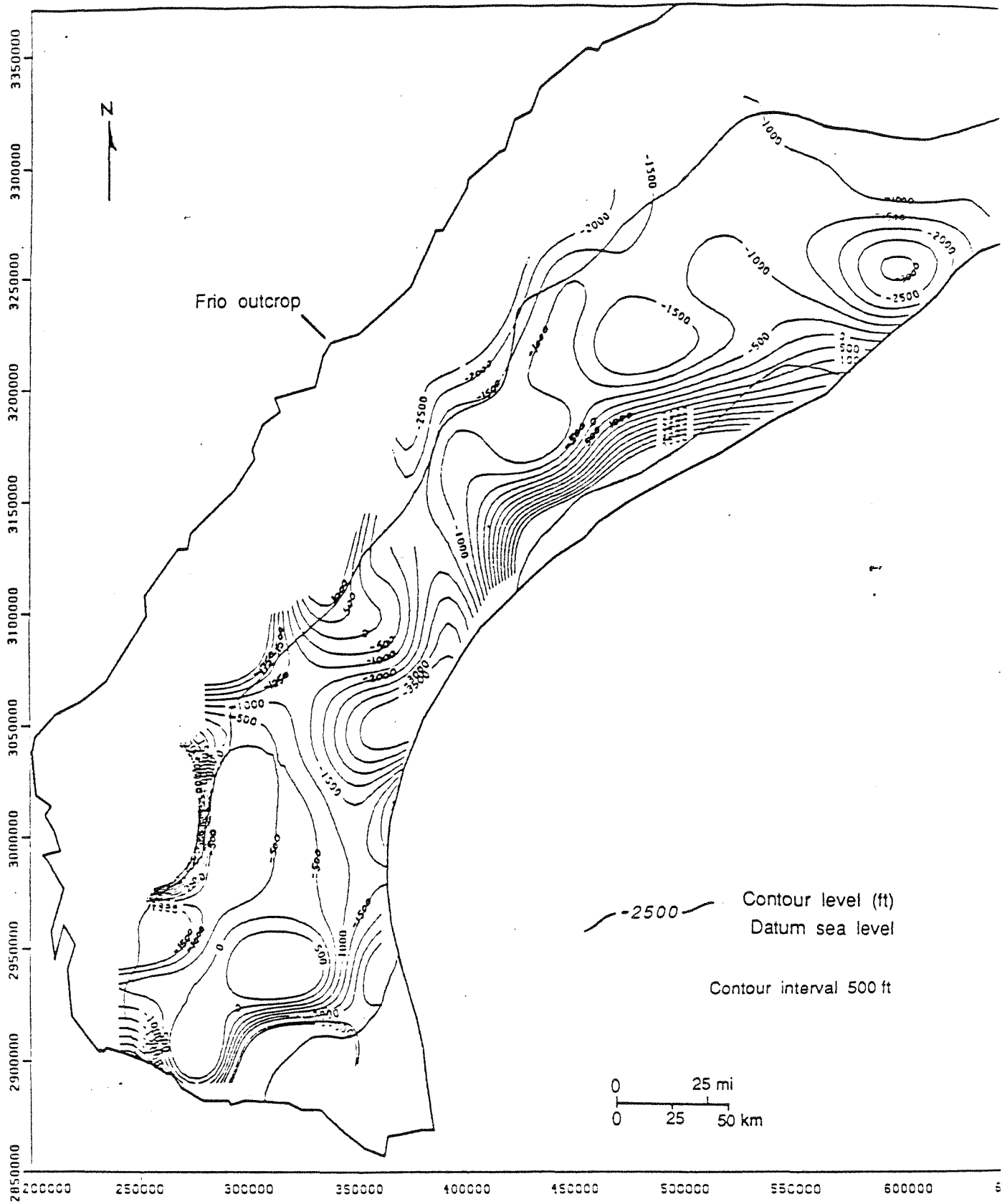


Figure 24. Regional potentiometric surface, Frio regions A-B-C, all class data, years 1975-84, 6,000-8,000 ft horizontal slice. Equivalent brine heads.

(e). 8,000-10,000 ft interval (fig. 25): A large part of the surface is encompassed by positive contours, especially closer to the coast line. This reflects a transition to overpressured gradients in the predominantly gas wells in this slice.

(f). 10,000-12,000 ft interval (fig. 26): The hydraulic heads in this surface are all positive, ranging from 2,000 to 10,000 ft above sea level. All the pressure gradients are above 0.465 psi/ft and reflect overpressured conditions.

The geographic position of these discrete thickness slices moves toward the coast-line with each successively lower interval. Thus, each structurally lower horizon dips toward the Gulf Coast and thickens. There is sufficient lateral heterogeneity within each slice of the hydrologic system for it to exhibit a complex potentiometric surface. Hydraulic communication is inferred in the central part of each slice, where pressures seem to have uniformly declined due to oil and gas exploration.

Furthermore, residual surfaces that compare the potentiometric surfaces in the shallow and deeper intervals were created for better definition of vertical flow potential. Figures 27 through 32 are the residual surfaces between depth intervals 0-2,000, 2,000-4,000, 4,000-6,000, and 6,000-8,000 ft. Constructing a residual potential surface involves subtracting the potentiometric surface for one (shallower) depth interval from the other (deeper) depth interval. The shallow potentiometric surfaces (down to 4,000 ft) were constructed with fresh-water equivalent heads (0.433 psi/ft gradient), whereas deeper surfaces were generated by using brine hydrostatic gradient (0.465 psi/ft). This is considered more logical for evaluating the vertical flow gradient in view of the predominantly brine densities encountered in the deep Frio sediments.

(a). 4K-2K Residual Surface (fig. 27): This surface results from subtracting the potentiometric surface for the 0-2,000-ft slice from the surface for the 2,000-4,000-ft slice. In the center of the map, a large area defined by positive contours represents potential for upflow from the deeper to the shallower horizon, whereas the negative contours in the upper and lower flanks outline potential for downward flow toward the deeper zone. Quantitatively, except in the center of the map (area of Jim Wells County), no extreme vertical gradient exists in either direction, given the fact that both slices are predominantly in the fresh to moderately saline hydrostatic environment. The negative contours in the lower section of the map confirm the depressured part of the 2,000-4,000-ft slice.

(b). 6K-4K Residual Surface (fig. 28): This surface is generated by subtracting the 2,000-4,000-ft slice potentiometric surface from the 4,000-6,000-ft slice potentiometric

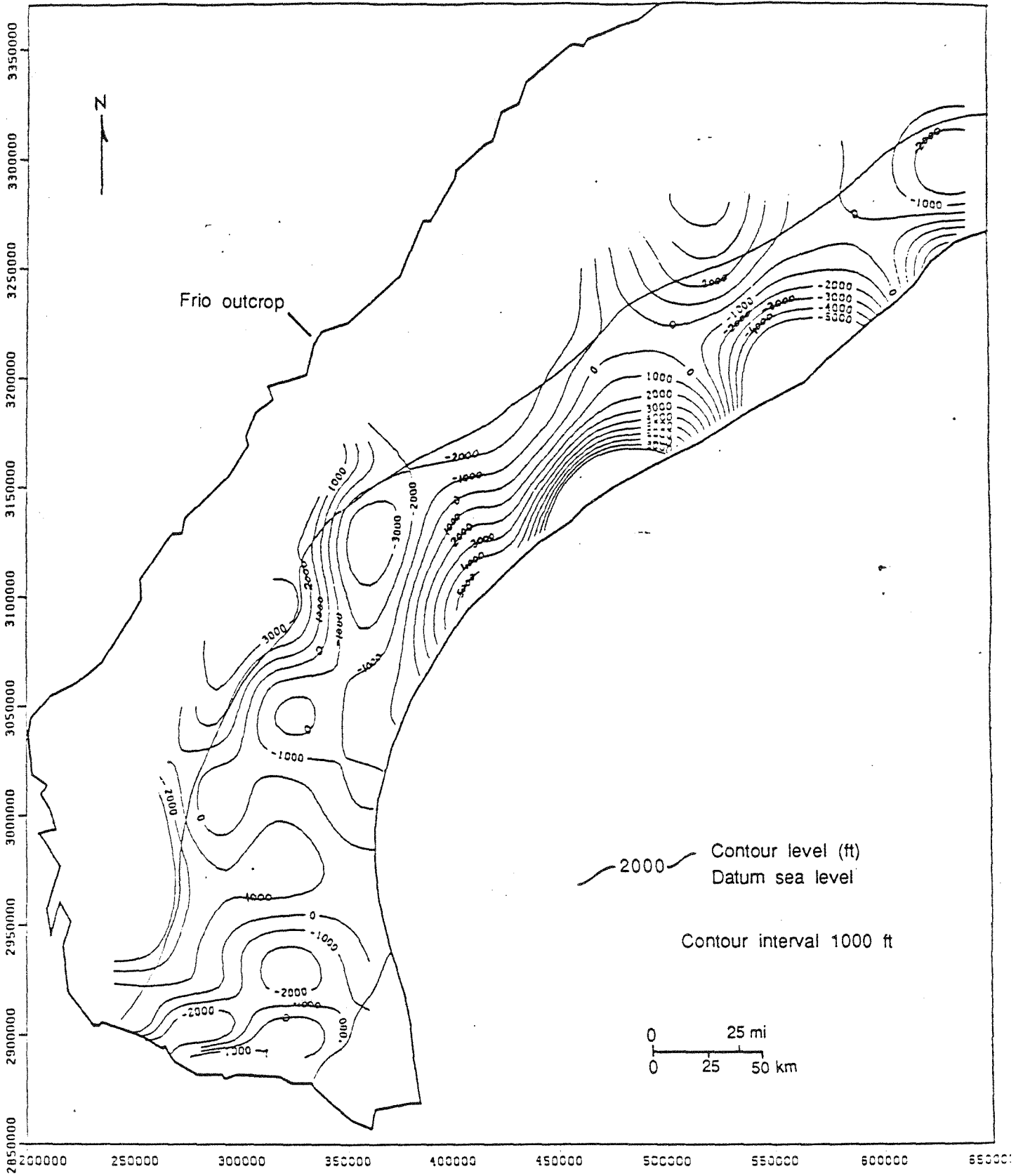


Figure 25. Regional potentiometric surface, Frio regions A-B-C, all class data, years 1975-84, 8,000-10,000 ft horizontal slice. Equivalent brine heads.

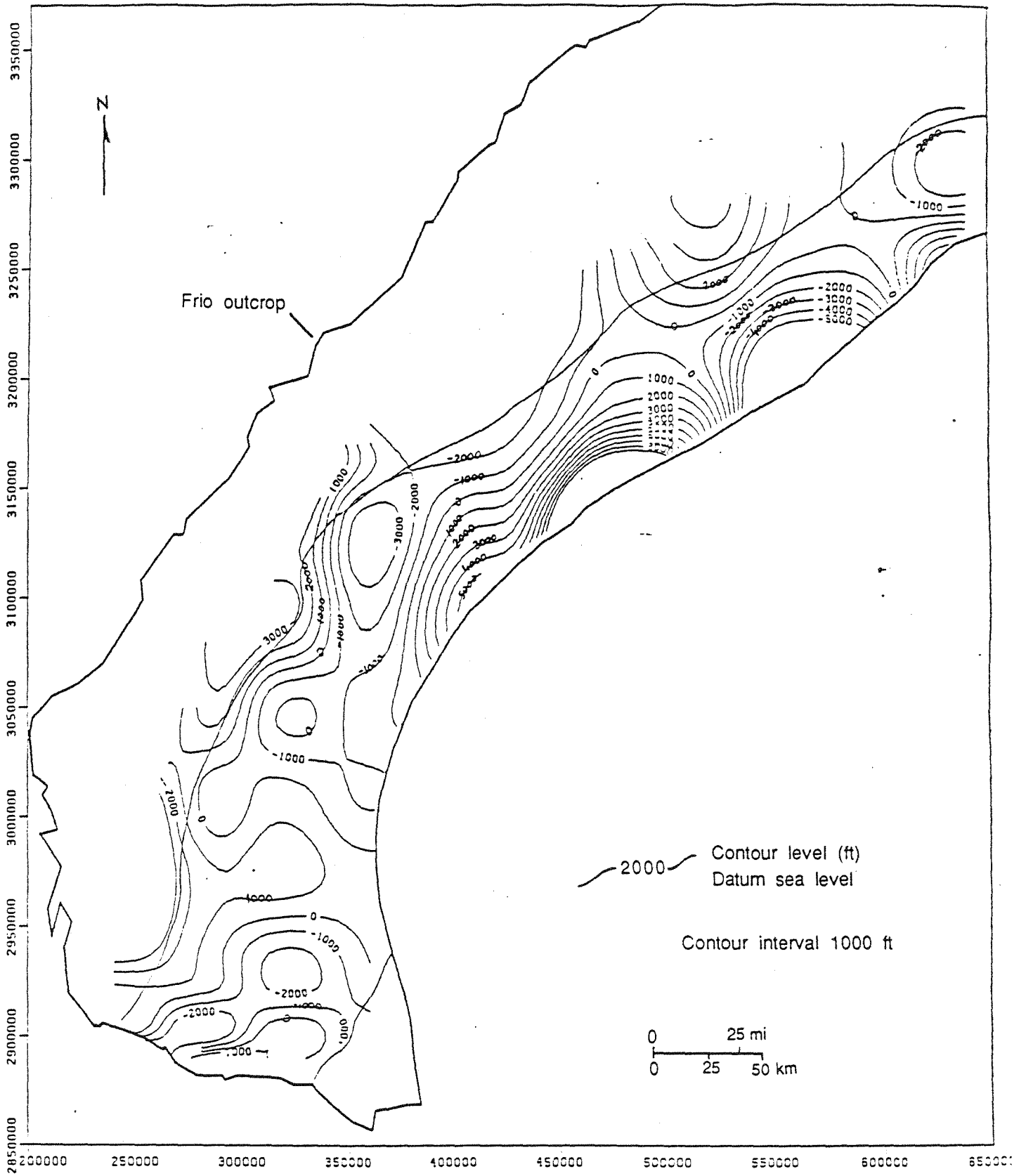


Figure 25. Regional potentiometric surface, Frio regions A-B-C, all class data, years 1975-84, 8,000-10,000 ft horizontal slice. Equivalent brine heads.

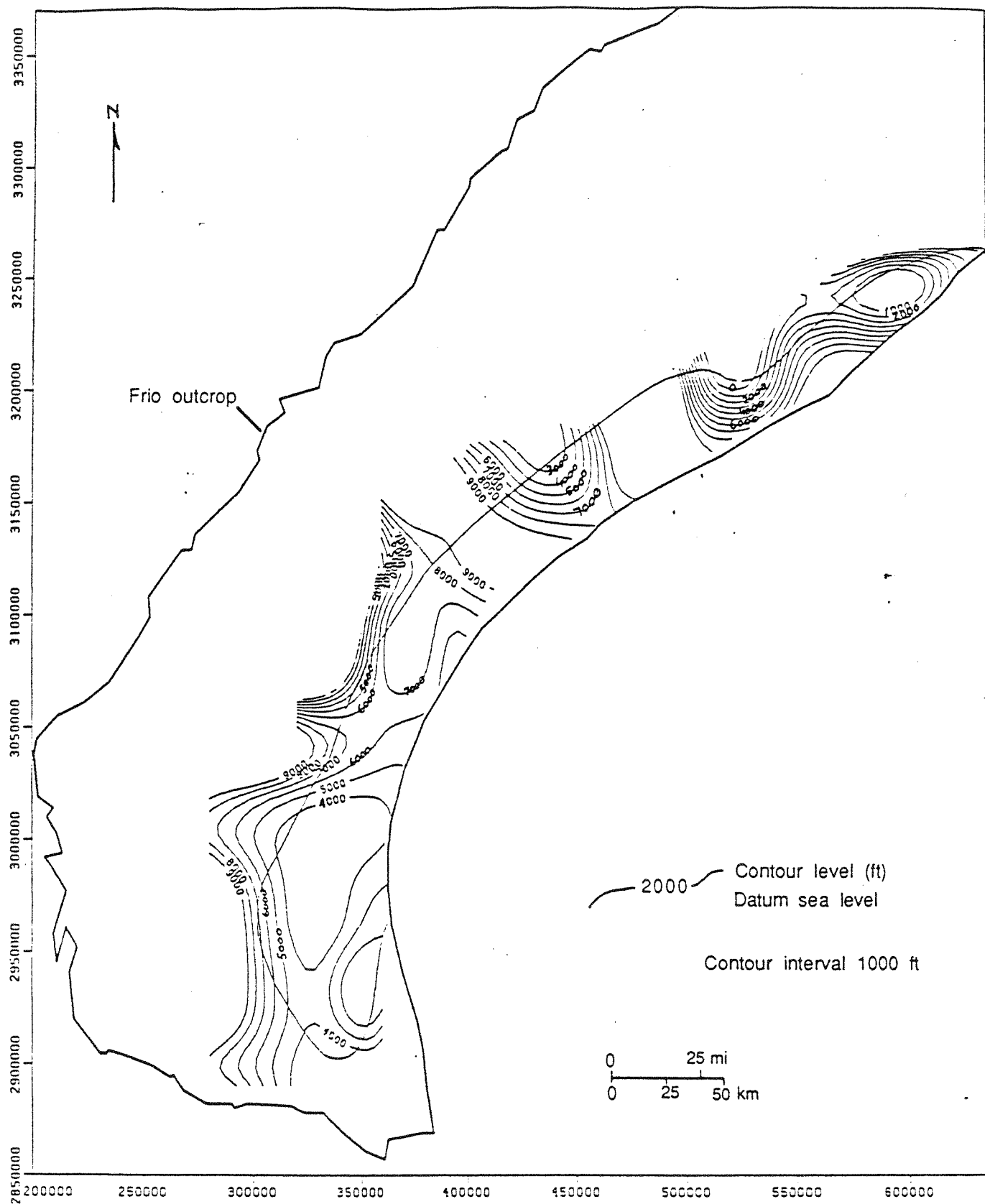


Figure 26. Regional potentiometric surface, Frio regions A-B-C, all class data, years 1975-84, 10,000-12,000 ft horizontal slice. Equivalent brine heads.

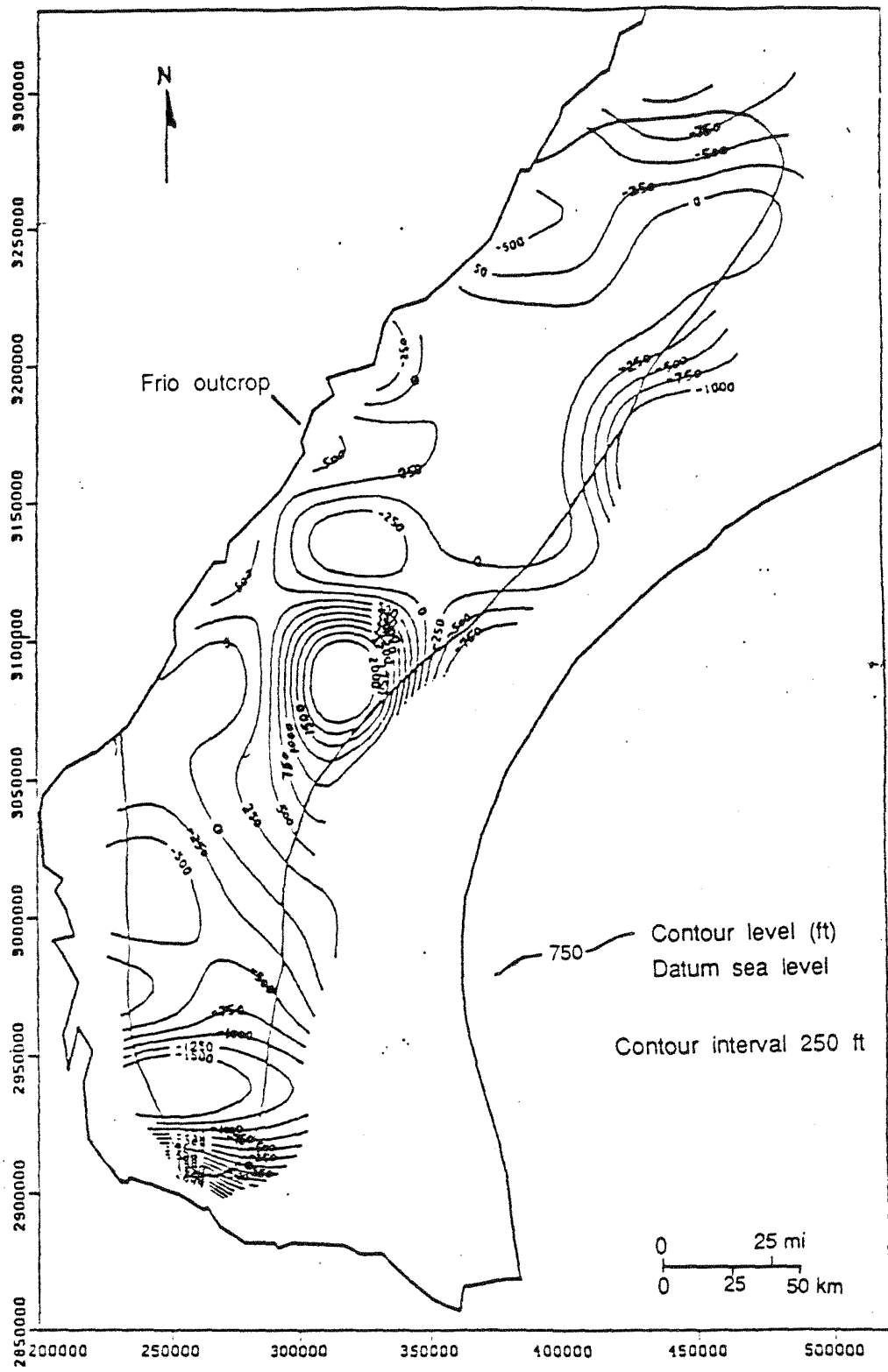


Figure 27. Frio residual potential surface, 2,000-4,000 ft minus 0-2,000 ft slice (4K-2K), all classes, 1975-84 data. Positive contours indicate upward flow, and negative contours indicate downward flow. Heads for both surfaces computed with fresh water gradient.

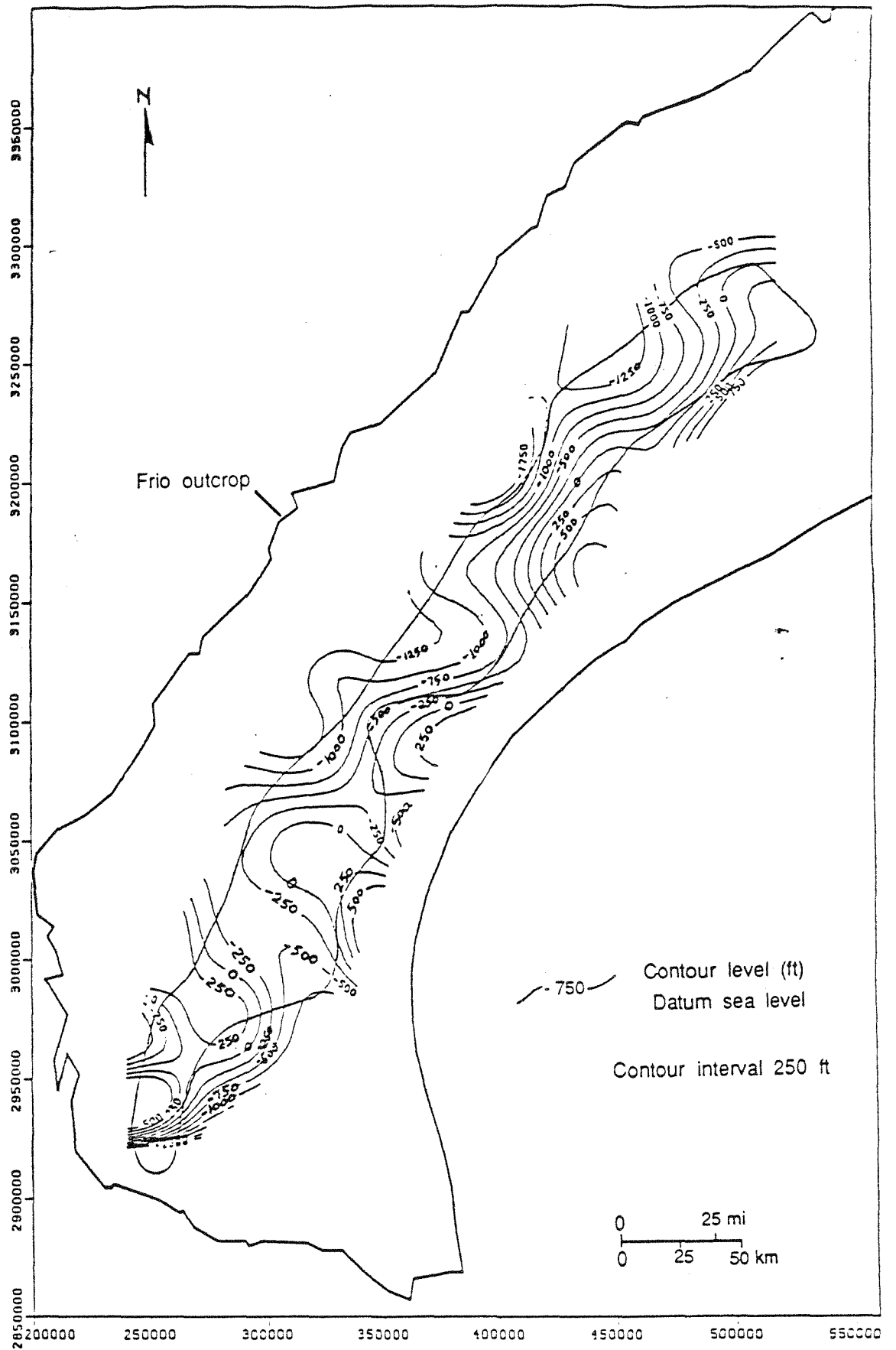


Figure 28. Frio residual potential surface, 4,000-6,000 ft minus 2,000-4,000 ft slice (6K-4K), all classes, 1975-84 data. Positive contours indicate upward flow, and negative contours indicate downward flow. Heads for 6K surface computed with environmental brine gradier

surface. The residual surface is characterized by negative contours in most of the regions, except positive contours in the east flanks and southern area. This reflects a large area of downflow potential. The steep downward gradient results from a great degree of depressurization that has occurred in the 4,000-6,000-ft slice.

(c). 6K-2K Residual Surface (fig. 29): Due to the relative lateral displacement of these two slices, only a narrow section of the two surfaces overlaps. Most of the residual surface exhibits potential downflow (negative contours) due to the depressured condition in the deeper slice. The objective of mapping this surface is to determine whether fluid from a deeper slice could bypass the intermediate horizon and still rise to the topmost zone.

(d). 8K-2K Residual Surface (fig. 30): A very narrow band of overlapping sections from the two surfaces results in residuals that are bunched together and exhibit reversals of flow direction. The maximum residual head is about -2,000 feet in the downward direction.

(e). 8K-4K Residual Surface (fig. 31): The dominating trend in the central and southern part is upflow to the shallower (2,000-4,000 ft) slice, and in the rest of the region is downward to the deeper (6,000-8,000 ft) slice.

(f). 8K-6K Residual Surface (fig. 32): The configuration of this residual surface is similar to the previous surface. Low residual values suggest good hydrologic continuity and pressure equilibrium between the two slices (6,000-8,000 ft and 4,000-6,000 ft).

A common characteristic of the residual surfaces is an upward flow trend through all the slices in the south-central part (confluence of Nueces, San Patricio, Jim Wells Counties). In other regions, the gradient is a function of the depressurization in the slice.

It must be reiterated that these horizontal slices are merely a qualitative interpretation of the variability in pressure and the resulting fluid flow potential in the different layers of the extremely heterogeneous Frio Formation. In reality, no discrete 2,000-ft thick slices exist, and the hydrologic continuity within the Frio is very difficult to map on a large (regional) scale.

This regional approach provides fundamental information on the hydrology of the Frio Formation. Incorporating so much data from a large area into a single map, however, smooths trends and prevents a detailed picture of smaller areas. To understand the "regional" flow and its interaction with an injection facility, county-size maps are needed. The next section describes the detailed mapping of the hydrologic system in Victoria County.

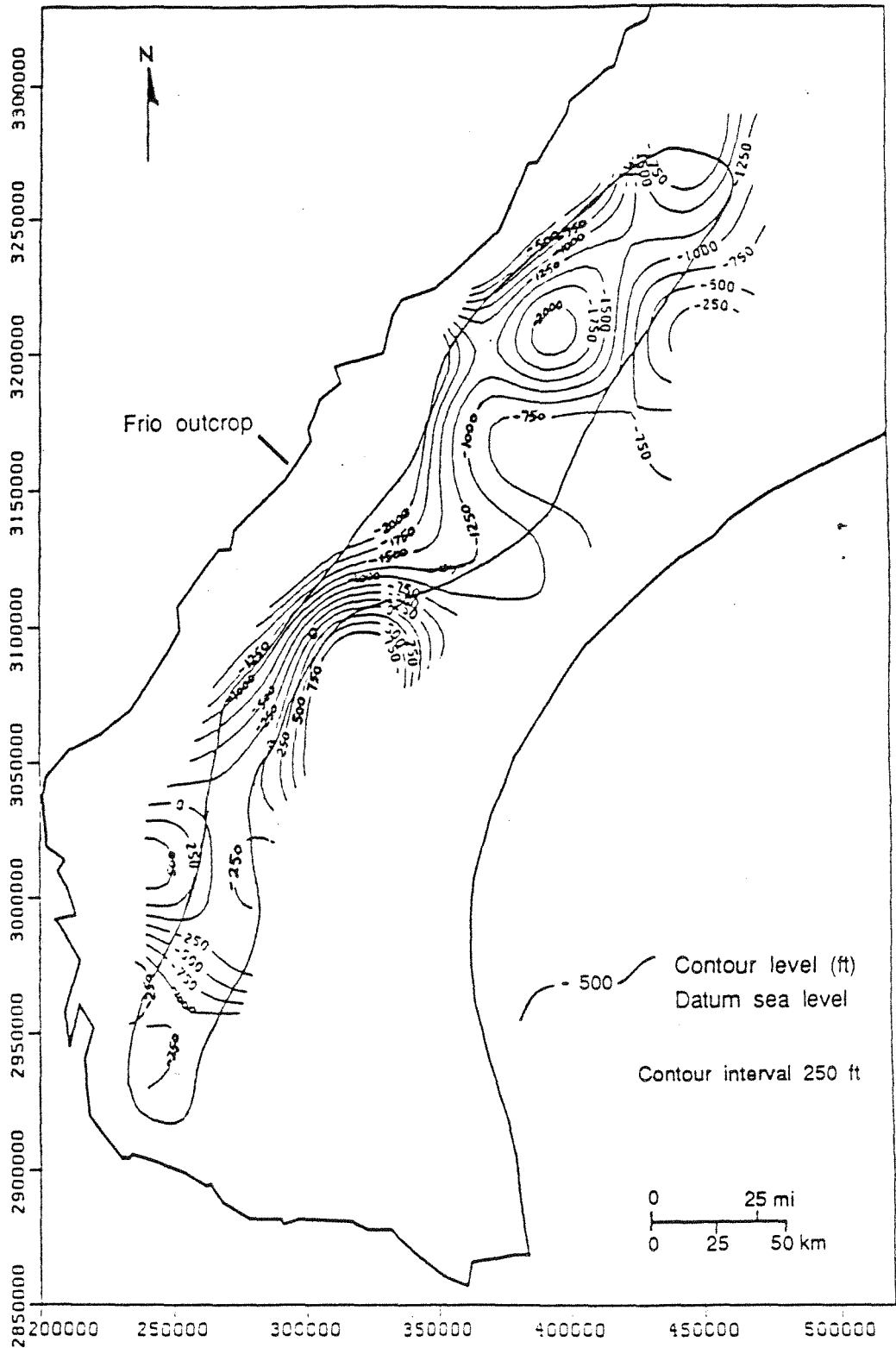


Figure 29. Frio residual potential surface, 4,000-6,000 ft minus 0-2,000 ft slice (6K-2K), all classes, 1975-84 data. Positive contours indicate upward flow, and negative contours indicate downward flow. Heads for 6K surface computed with environmental brine gradient.

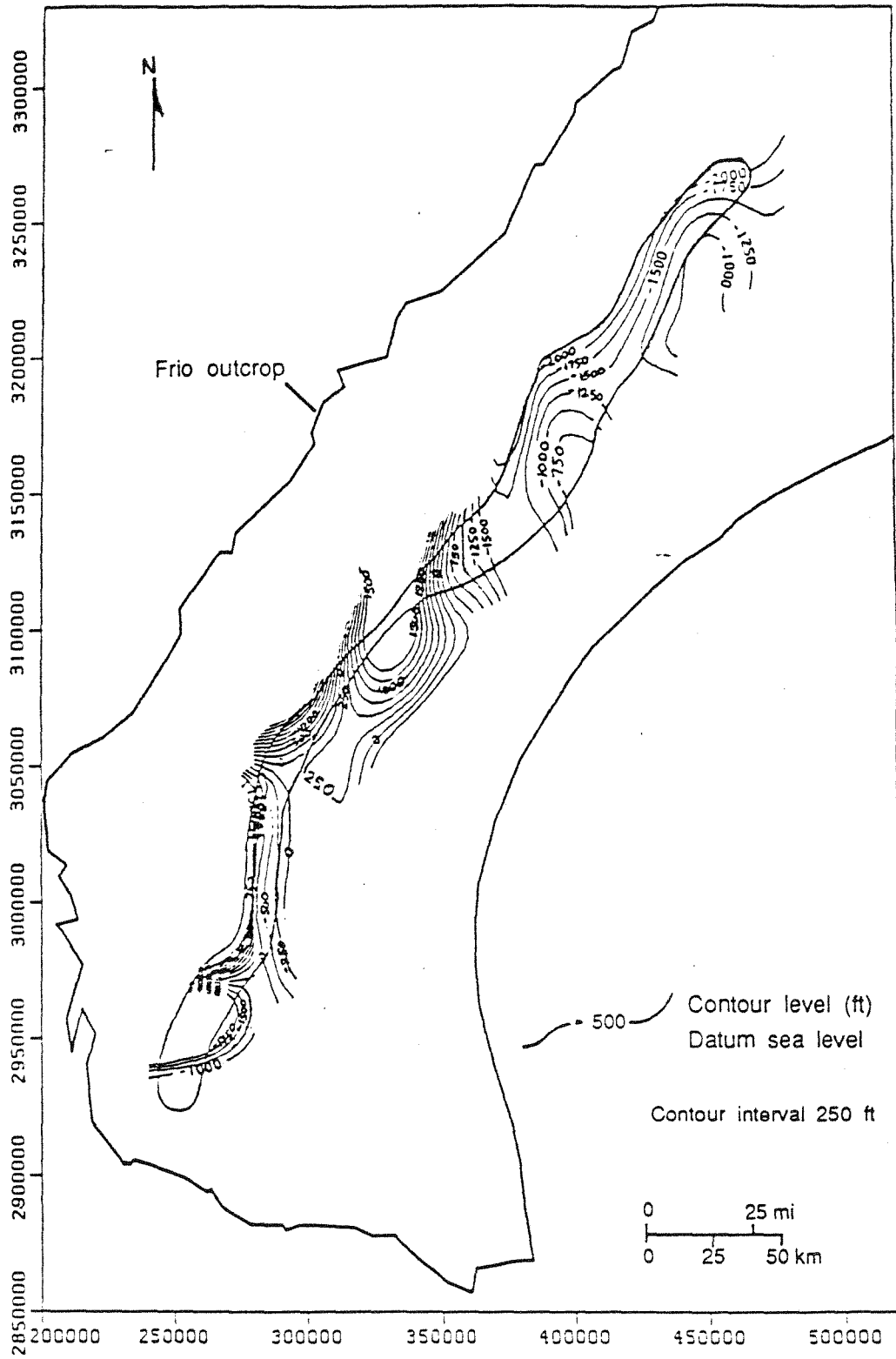


Figure 30. Frio residual potential surface, 6,000-8,000 ft minus 0-2,000 ft slice (8K-2K), all classes, 1975-84 data. Positive contours indicate upward flow, and negative contours indicate downward flow. Heads for 8K surface computed with environmental brine gradient.

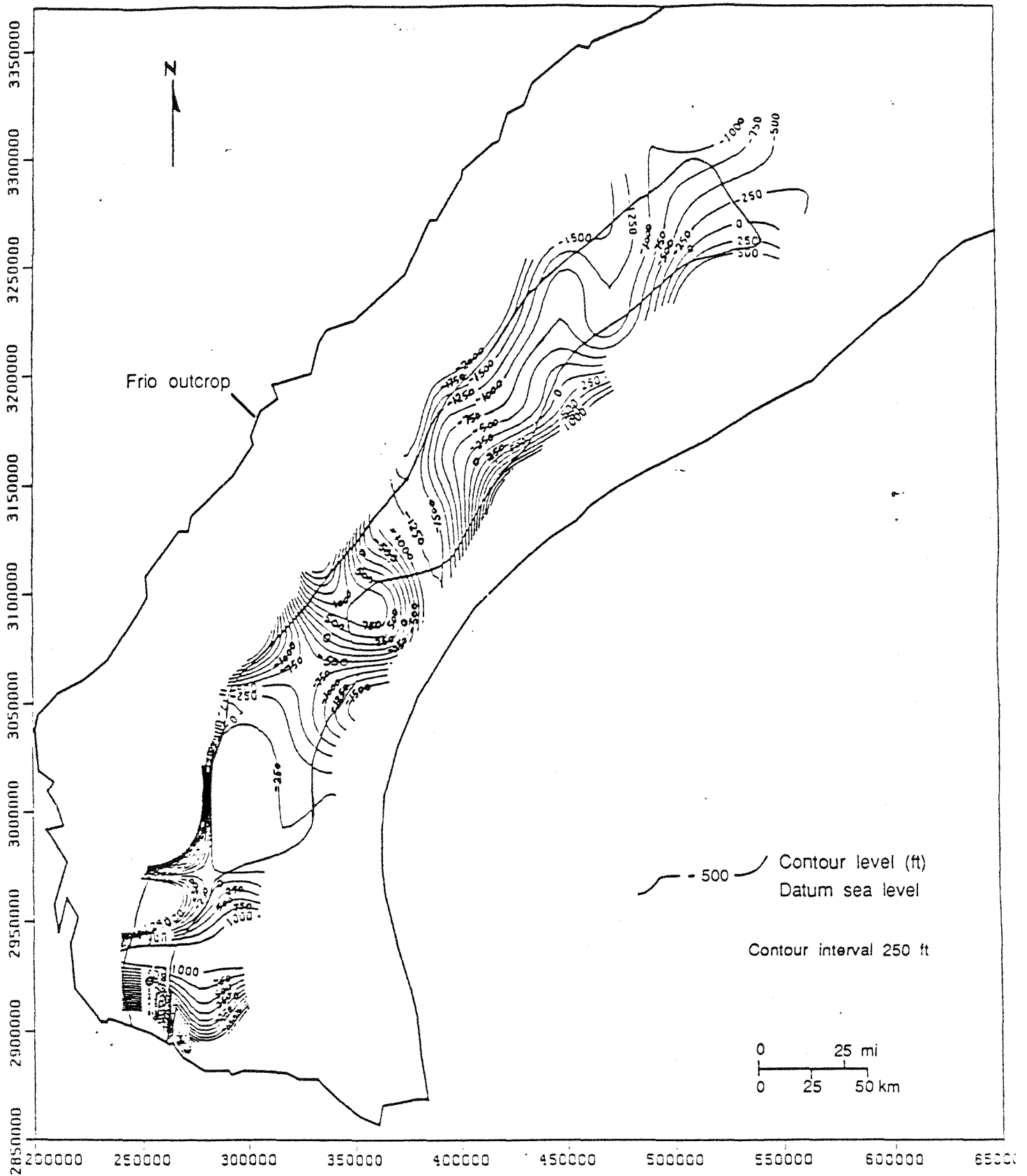


Figure 31. Frio residual potential surface, 6,000-8,000 ft minus 2,000-4,000 ft slice (8K-4K), all classes, 1975-84 data. Positive contours indicate upward flow, and negative contours indicate downward flow. Heads for 8K surface computed with environmental brine gradient.

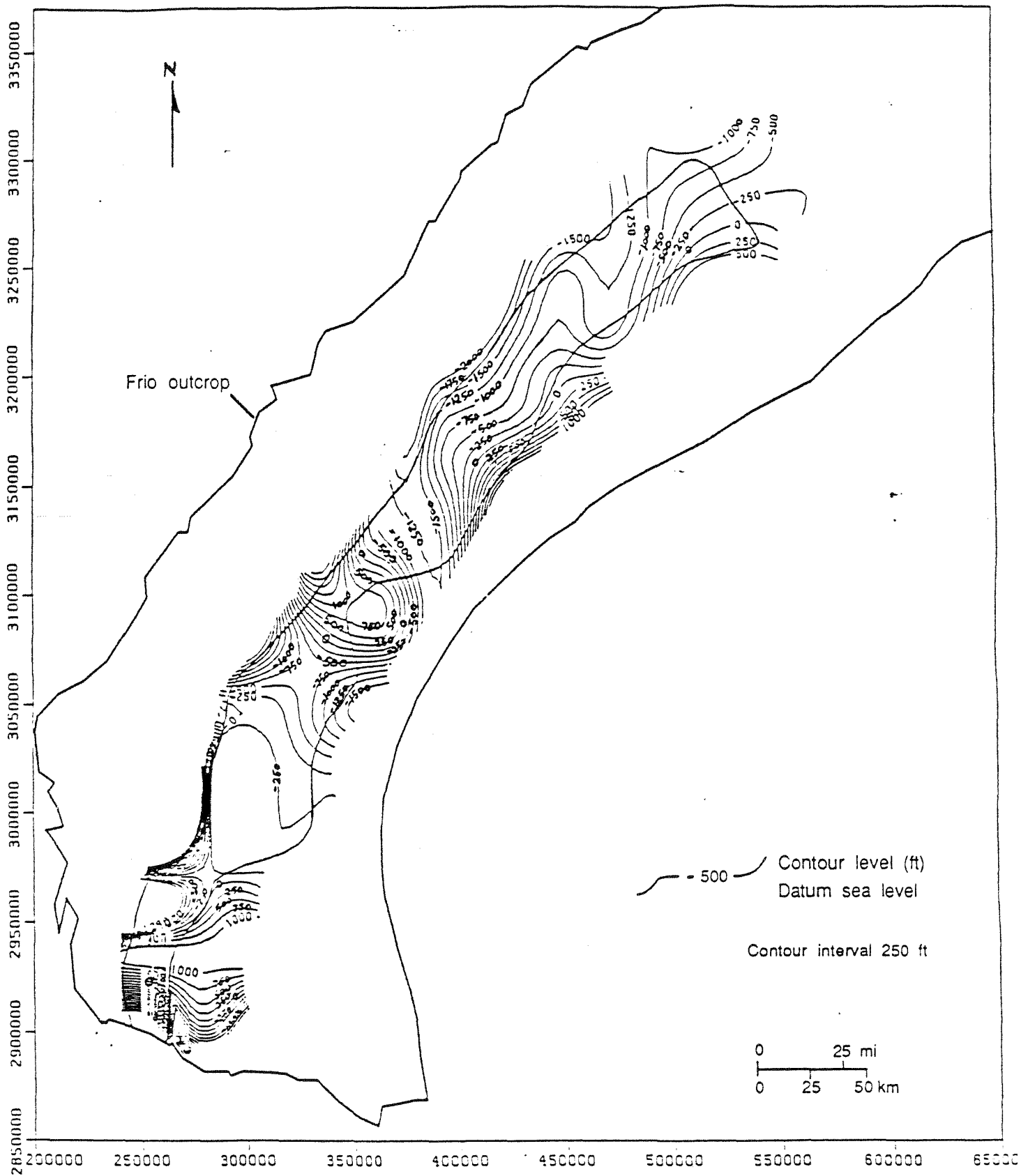


Figure 31. Frio residual potential surface, 6,000-8,000 ft minus 2,000-4,000 ft slice (8K-4K), all classes, 1975-84 data. Positive contours indicate upward flow, and negative contours indicate downward flow. Heads for 8K surface computed with environmental brine gradient.

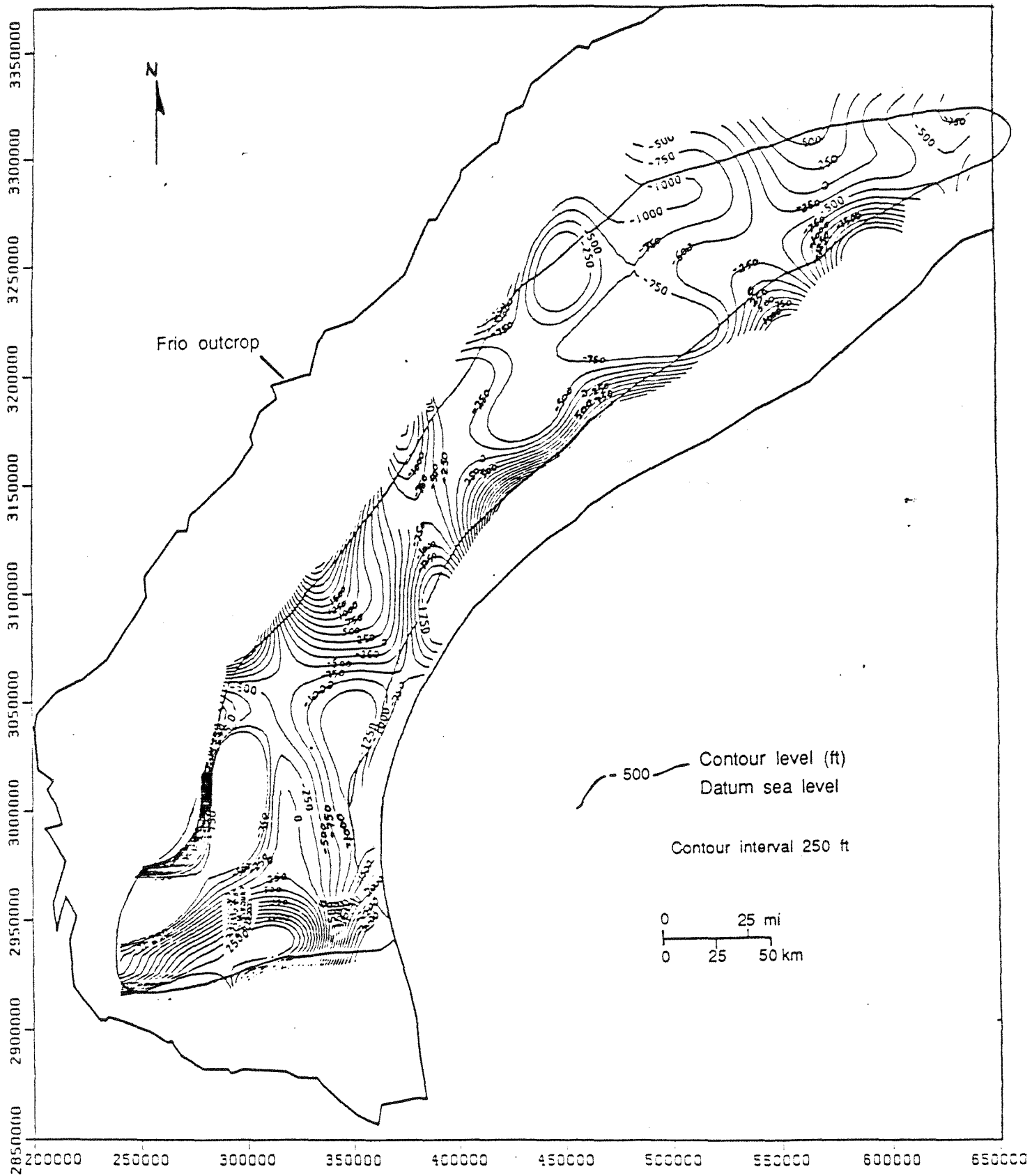


Figure 32. Frio residual potential surface, 6,000-8,000 ft minus 4,000-6,000 ft slice (8K-6K), all classes, 1975-84 data. Positive contours indicate upward flow, and negative contours indicate downward flow. Heads for 8K surface computed with environmental brine gradient.

5. CASE ANALYSIS, VICTORIA COUNTY, TEXAS

As a representative study on a county scale, the pressure data in Victoria County were used for developing pressure-depth plot and potentiometric surfaces.

5.1 Pressure-Depth Plot

All the available pressures in Victoria County were plotted on a pressure-depth plot. The resulting profile in figure 33 is similar in character to the integrated Frio pressure-depth profile (fig. 11). Two trend lines, one for 0.433 psi/ft fresh-water gradient and the other for 0.465 psi/ft brine (with 80,000 ppm salinity), are drawn on the Victoria County plot. Additionally, a scatter of overpressured data and an extended area of depressed conditions are visible on the plot. Figure 34 is a formation brine salinity-depth plot for Victoria County based on data from Kreitler and Richter (1986). It indicates relatively consistent salinities between 60,000 and 80,000 ppm below 4,000 ft. Although salinities from depths shallower than 4,000 ft in Victoria County are not directly available, other data from the middle Gulf Coast Frio Formation reflect values closer to fresh-water environments (Kreitler and Richter, 1986). This observation is also confirmed by the gradient (psi/ft) values computed from individual bottomhole pressures in the PI pressure file. Thus, a correlation of pressure-depth and salinity-depth profiles formed the basis for use of fresh-water gradient in shallow depths and brine gradient in deeper intervals for calculation of equivalent hydraulic heads.

5.2 Potentiometric Surfaces

An integrated potentiometric surface of the entire Frio thickness in Victoria County would presumably be too complex due to the steep gulfward dip of the various components of the Tertiary system. Figure 35 is a simplified isometric view of the structure tops of the Frio, Vicksburg-Jackson, Claiborne, and Wilcox Formations. Analogous to the regional Frio surfaces, horizontal slices were used for constructing potentiometric surfaces in Victoria County. Figures 36 and 37 consist of the posted hydraulic-head values and the resulting potentiometric surface in the 0-2,000-ft depth interval. Pressure data from all Tertiary formations through the years 1965-84 were included in this surface. Relative paucity of Frio data and a need to maintain integrity of the surface necessitated use of the other Tertiary data. Moreover, available formation brine salinity data in this depth interval for all formations suggest a predominantly fresh-water environment; hence, pooling all the pressures and using a 0.433 psi/ft pressure gradient for hydraulic head conversion were considered justifiable.

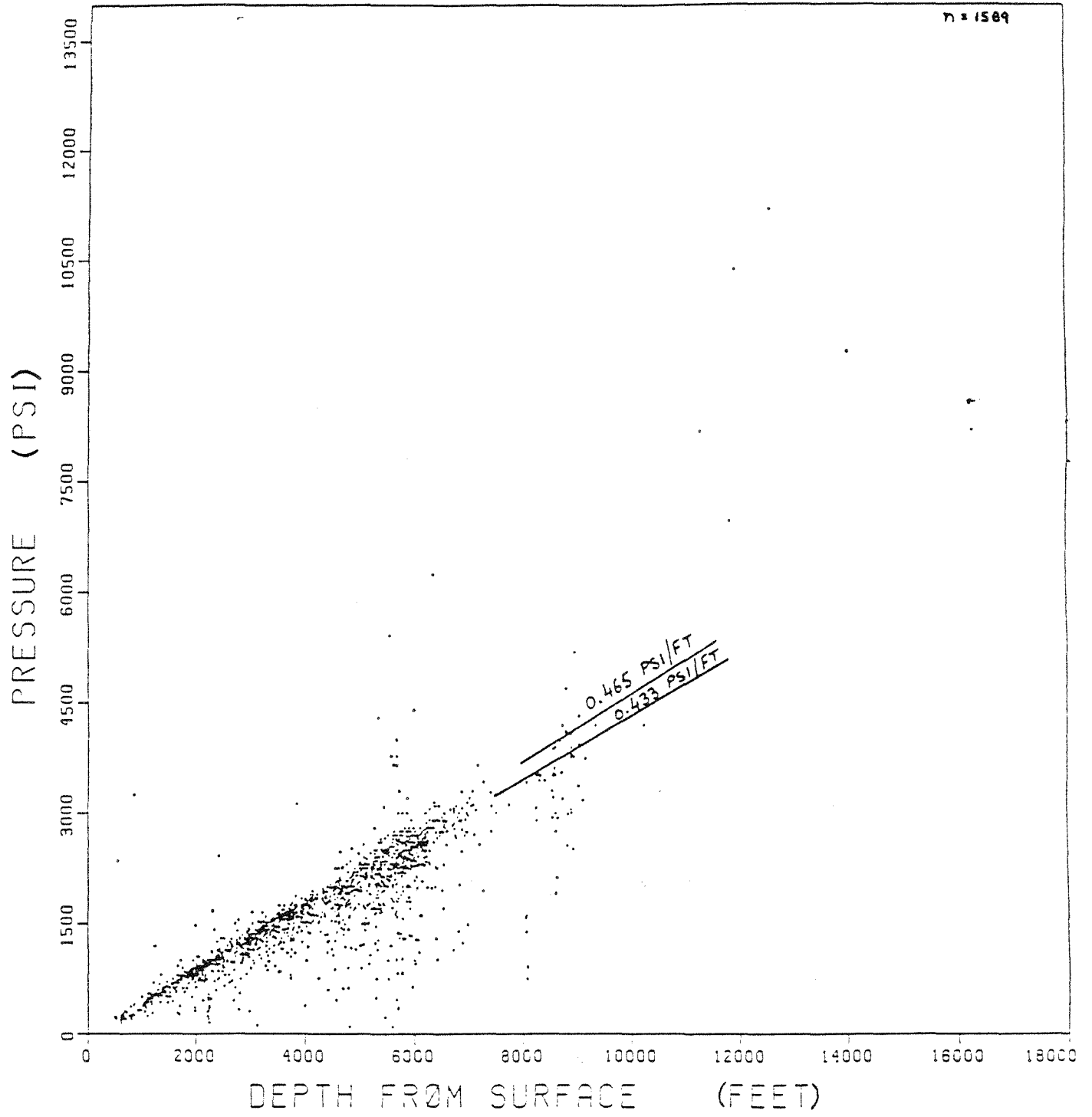


Figure 33. Pressure-depth diagram, Victoria County data.

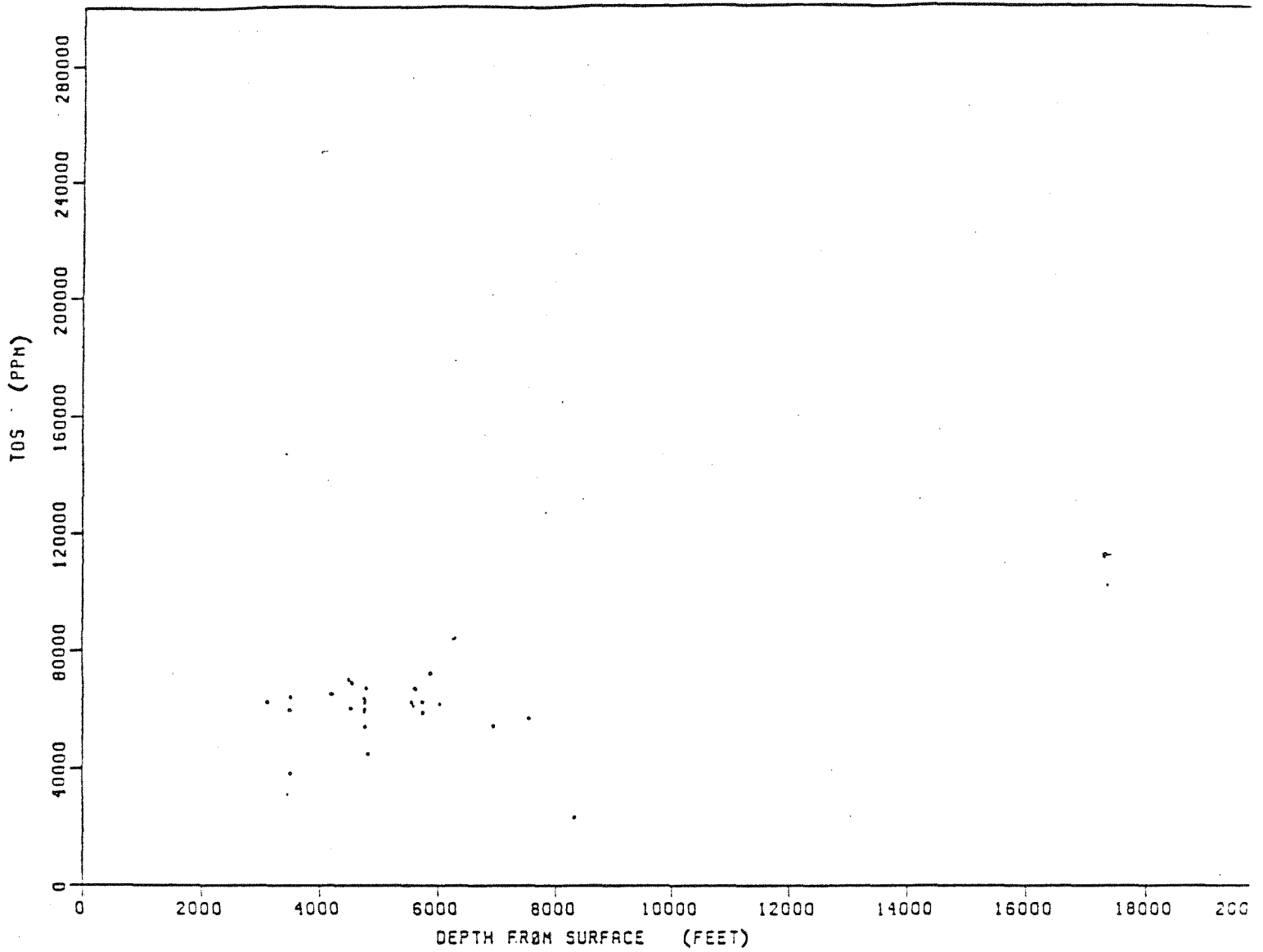


Figure 34. Salinity (total dissolved solids)-depth plot for Tertiary formations in Victoria County (from Kreitler and Richter, 1986).

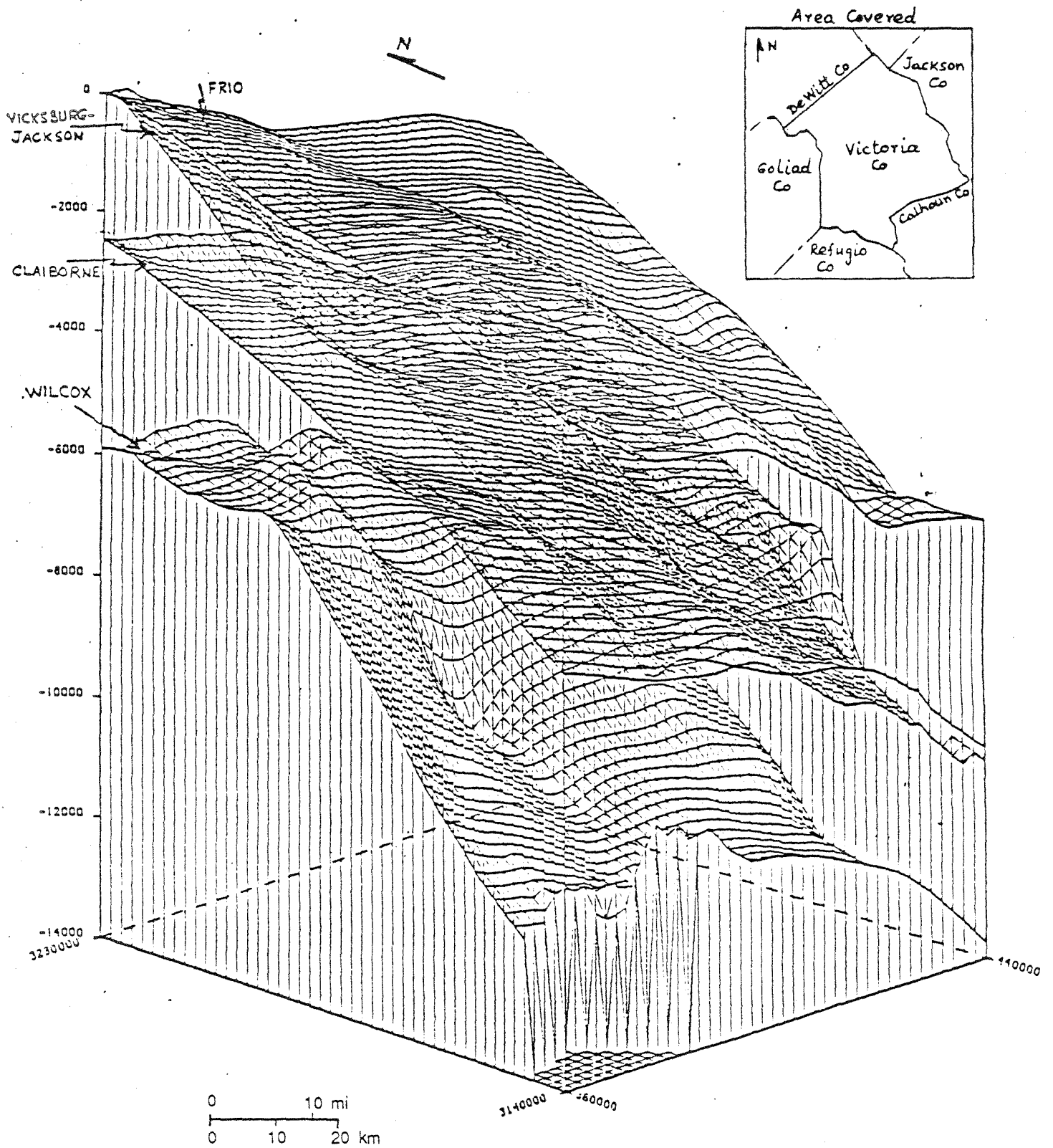


Figure 35. Isometric view of structure tops, Tertiary system, Victoria County. Tops of Frio, Vicksburg-Jackson, Claiborne, and Wilcox Formations (after Dodge and Posey, 1981).

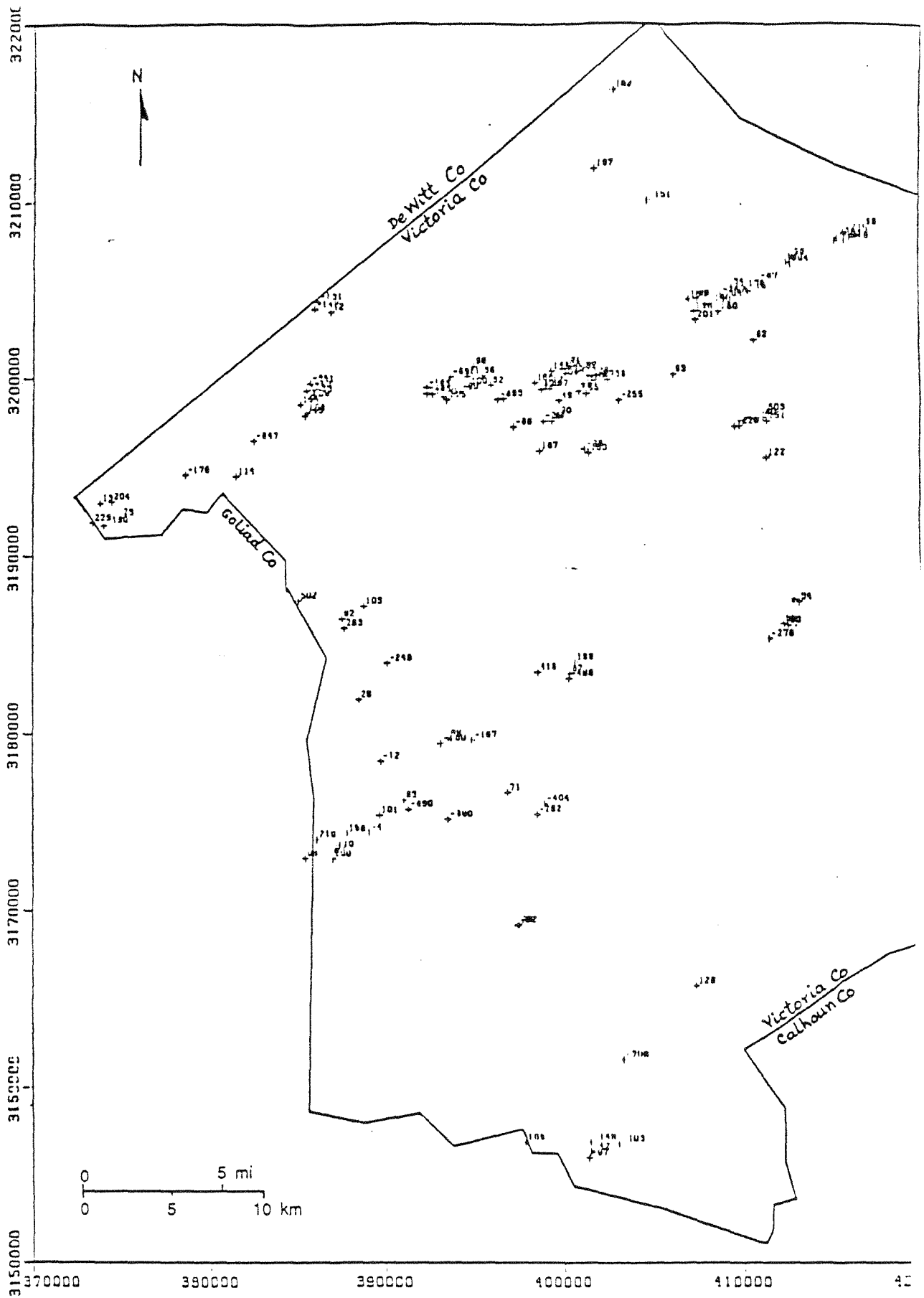


Figure 36. Hydraulic head values, 0-2000 ft horizontal slice, Victoria Co., all formations, all classes, 1965-84 data. Equivalent fresh-water heads.

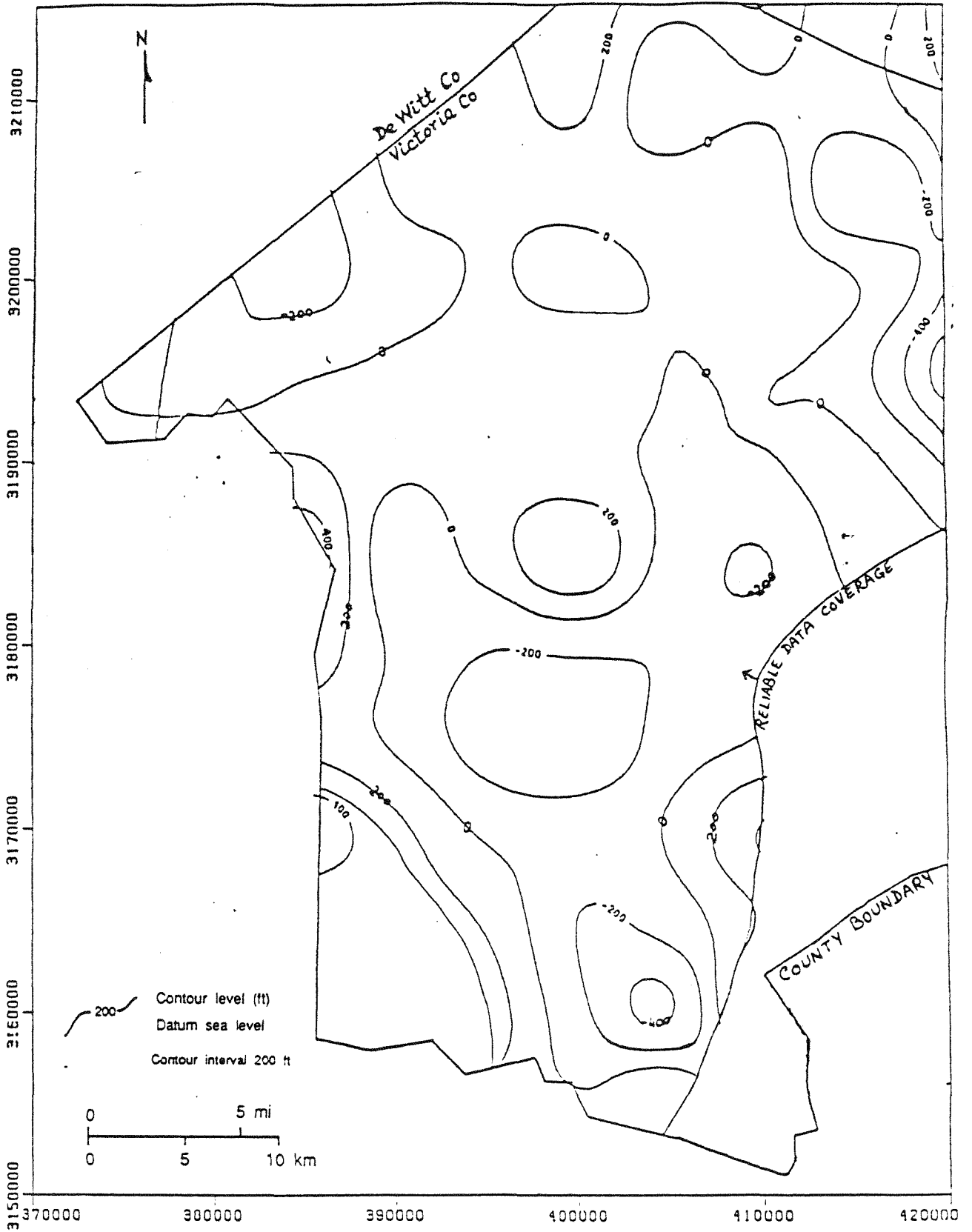


Figure 37. Potentiometric surface, 0-2000 ft slice, Victoria Co., all formations, all classes, 1965-84 data. Equivalent fresh-water heads.

The potentiometric surface for this slice is quite flat, with near-land-surface head values. The county boundary (thick border) and confines of reliable data coverage (thin inner line) are marked in figure 37.

Figures 38 and 39 represent, respectively, the hydraulic head values and the potentiometric surface for the 2,000-4,000-ft depth interval. Pressures from Frio and its updip equivalent, the Catahoula Formation, were screened from the time interval 1965-84, and converted to fresh-water equivalent hydraulic heads. The head values are near land surface, although some depressurization is observed in the central part of the county.

Figure 40 reflects the posted head values for the horizontal slice through the 4,000-6,000-ft depth interval. The corresponding potentiometric surface for this dataset is plotted in figure 41. This dataset encompasses pressures in Frio and Catahoula Formations in 1965-84. A general feature of this plot is the mostly negative contours reflecting depressed conditions. The negative depression is slightly enhanced toward the southeast. Pressure data from the injection wells operated by Du Pont de Nemours (Frank, 1986) were included in this dataset for constructing the potentiometric surface.

Figures 42 and 43 consist of the posted hydraulic-head values and the corresponding potentiometric surface in the 4,000-4,900-ft depth interval, a more restrictive depth range that encompasses the depths of injection by Du Pont. For greater areal coverage this dataset was expanded to include pressures in the Frio and Catahoula Formations in the Tertiary for the years 1945-84. Negative contours are more enhanced in the lower half of this surface. The outline of major oil and gas fields producing from the 4,000-5,000-ft depth range and the location of Du Pont's major deep well injection facility are marked in figure 43. A regional flow trend toward the south and southwest is indicated on this figure. Flow from the injection facility would be south or southwest. Inadequate data control in the immediate vicinity of the injection facility makes it difficult to better define the potentiometric surface in that area. An isometric view of this surface from the southeast is presented in figure 44. This dataset includes the injection formation pressure at Du Pont's facility.

5.3 Residual Surface

For a qualitative definition of vertical flow potential, residual surfaces were created whereby the potentiometric surface in the uppermost interval (0-2,000-ft) was subtracted from the average potentiometric surface in the deeper (4,000-6,000-ft) interval. The 0-2,000-ft potentiometric surface was generated with fresh-water (0.433 psi/ft) equivalent heads, and the 4,000-6,000-ft surface was based on

The potentiometric surface for this slice is quite flat, with near-land-surface head values. The county boundary (thick border) and confines of reliable data coverage (thin inner line) are marked in figure 37.

Figures 38 and 39 represent, respectively, the hydraulic head values and the potentiometric surface for the 2,000-4,000-ft depth interval. Pressures from Frio and its updip equivalent, the Catahoula Formation, were screened from the time interval 1965-84, and converted to fresh-water equivalent hydraulic heads. The head values are near land surface, although some depressurization is observed in the central part of the county.

Figure 40 reflects the posted head values for the horizontal slice through the 4,000-6,000-ft depth interval. The corresponding potentiometric surface for this dataset is plotted in figure 41. This dataset encompasses pressures in Frio and Catahoula Formations in 1965-84. A general feature of this plot is the mostly negative contours reflecting depressured conditions. The negative depression is slightly enhanced toward the southeast. Pressure data from the injection wells operated by Du Pont de Nemours (Frank, 1986) were included in this dataset for constructing the potentiometric surface.

Figures 42 and 43 consist of the posted hydraulic-head values and the corresponding potentiometric surface in the 4,000-4,900-ft depth interval, a more restrictive depth range that encompasses the depths of injection by Du Pont. For greater areal coverage this dataset was expanded to include pressures in the Frio and Catahoula Formations in the Tertiary for the years 1945-84. Negative contours are more enhanced in the lower half of this surface. The outline of major oil and gas fields producing from the 4,000-5,000-ft depth range and the location of Du Pont's major deep well injection facility are marked in figure 43. A regional flow trend toward the south and southwest is indicated on this figure. Flow from the injection facility would be south or southwest. Inadequate data control in the immediate vicinity of the injection facility makes it difficult to better define the potentiometric surface in that area. An isometric view of this surface from the southeast is presented in figure 44. This dataset includes the injection formation pressure at Du Pont's facility.

5.3 Residual Surface

For a qualitative definition of vertical flow potential, residual surfaces were created whereby the potentiometric surface in the uppermost interval (0-2,000-ft) was subtracted from the average potentiometric surface in the deeper (4,000-6,000-ft) interval. The 0-2,000-ft potentiometric surface was generated with fresh-water (0.433 psi/ft) equivalent heads, and the 4,000-6,000-ft surface was based on

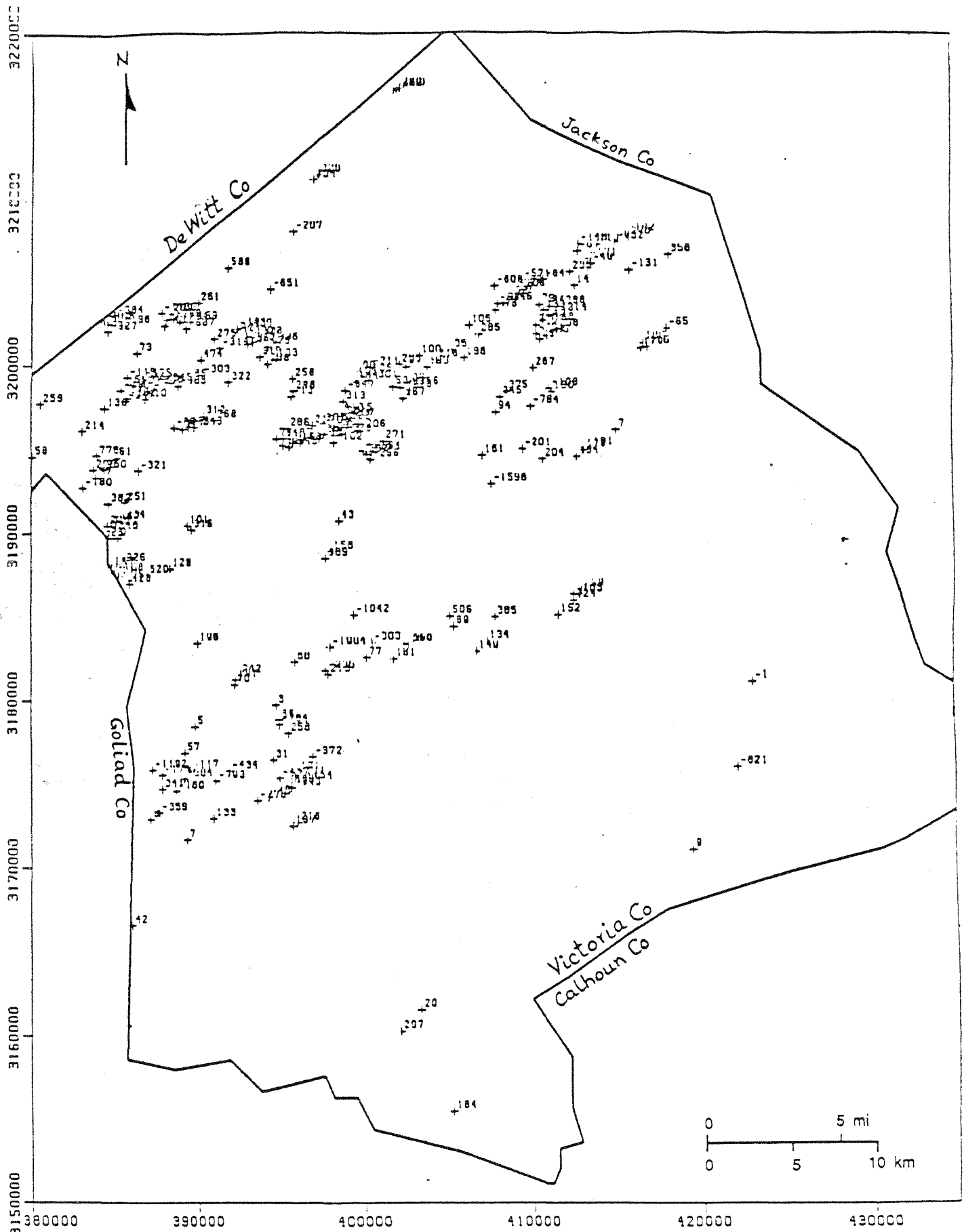


Figure 38. Hydraulic head values, 2,000-4,000 ft horizontal slice, Victoria Co., Frio and Catahoula, all classes, 1965-84 data. equivalent fresh-water heads.

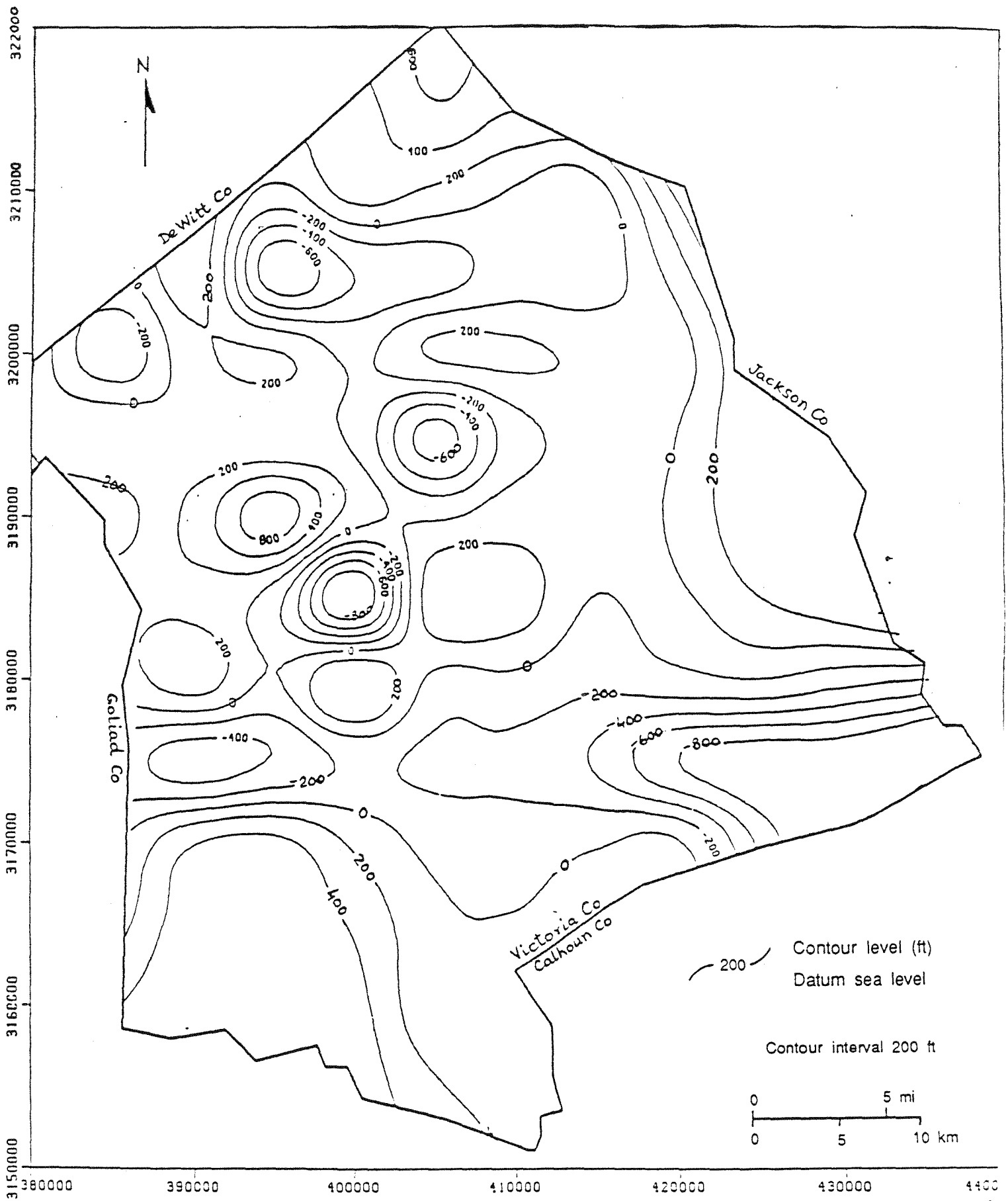


Figure 39. Potentiometric surface, 2,000-4,000 ft horizontal slice, Victoria Co., Frio and Catahoula, all classes, 1965-84 data. Equivalent fresh-water heads.

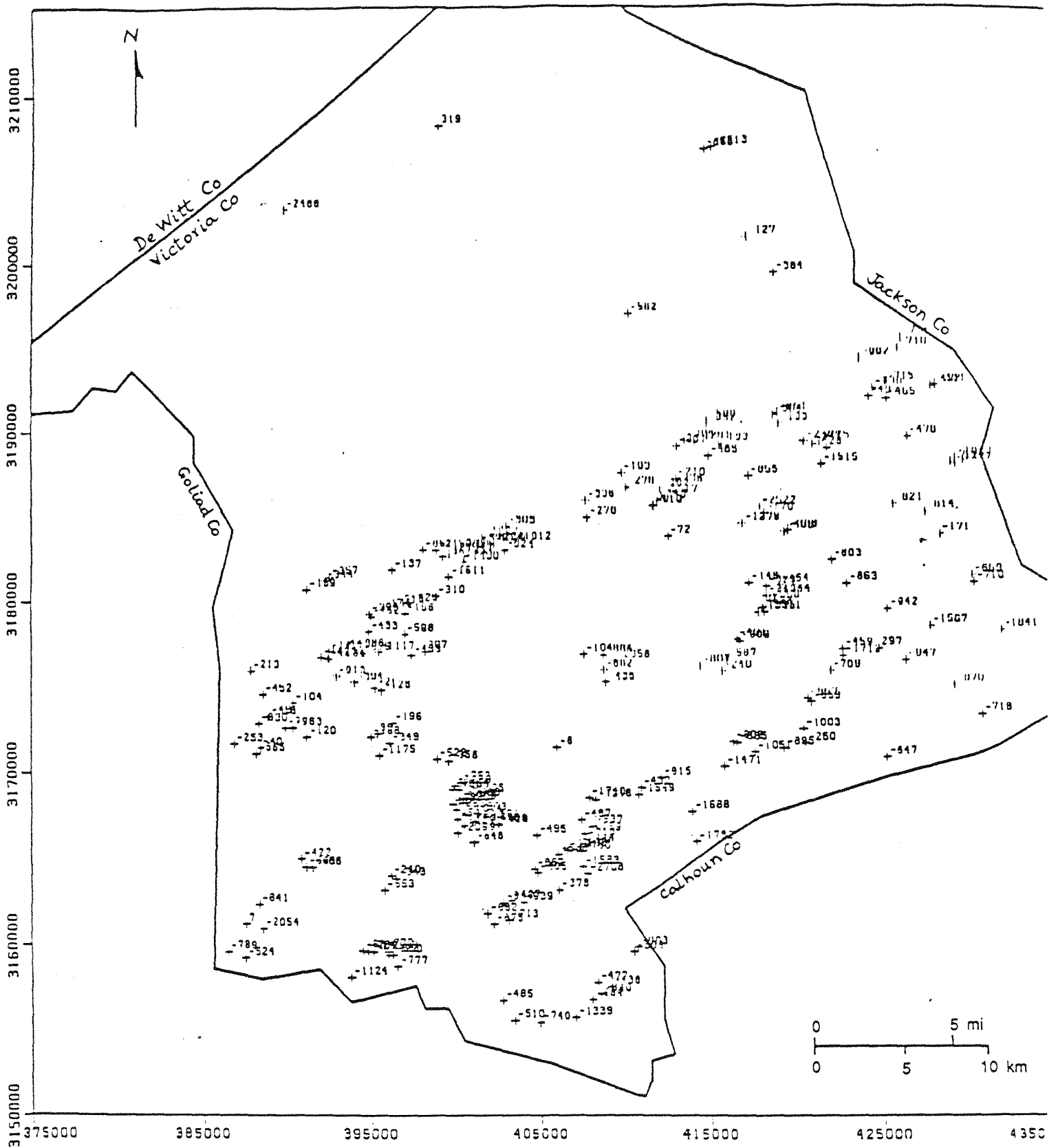


Figure 40. Hydraulic head values, 4,000-6,000 ft horizontal slice, Victoria Co., Frio Formation, all classes, 1965-84 data. Include formation pressure at Du Pont facility. Equivalent brine heads.

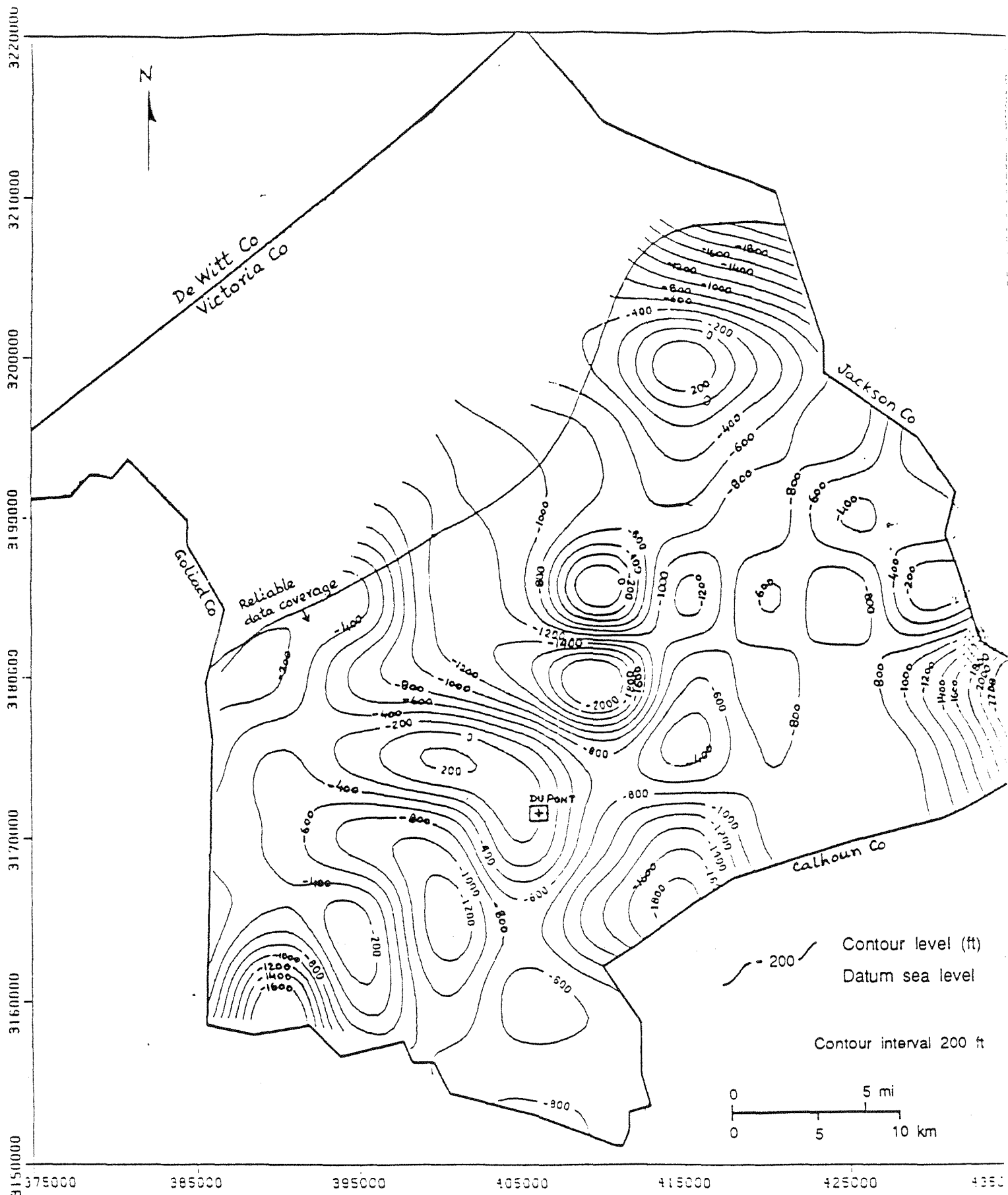


Figure 41. Potentiometric surface, 4,000-6,000 ft slice, Victoria Co., Frio Formation, all classes, 1965-84 data. Includes formation pressure at Du Pont facility. Equivalent brine heads.

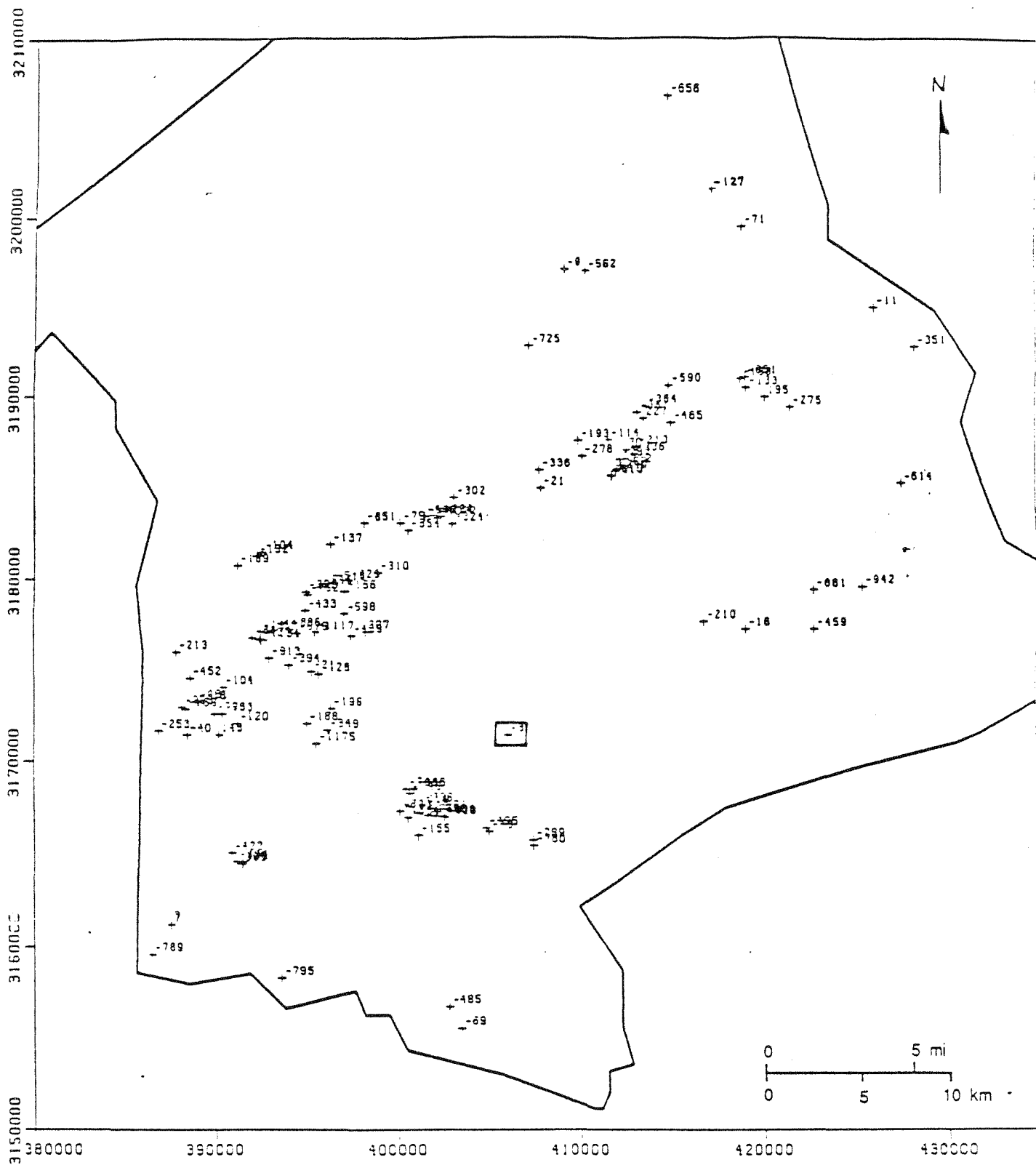


Figure 42. Hydraulic head values, 4,000-4,900 ft slice, Victoria Co., Frio and Catahoula, all classes, 1945-84 data. Includes formation pressure at Du Pont facility. Equivalent brine heads.

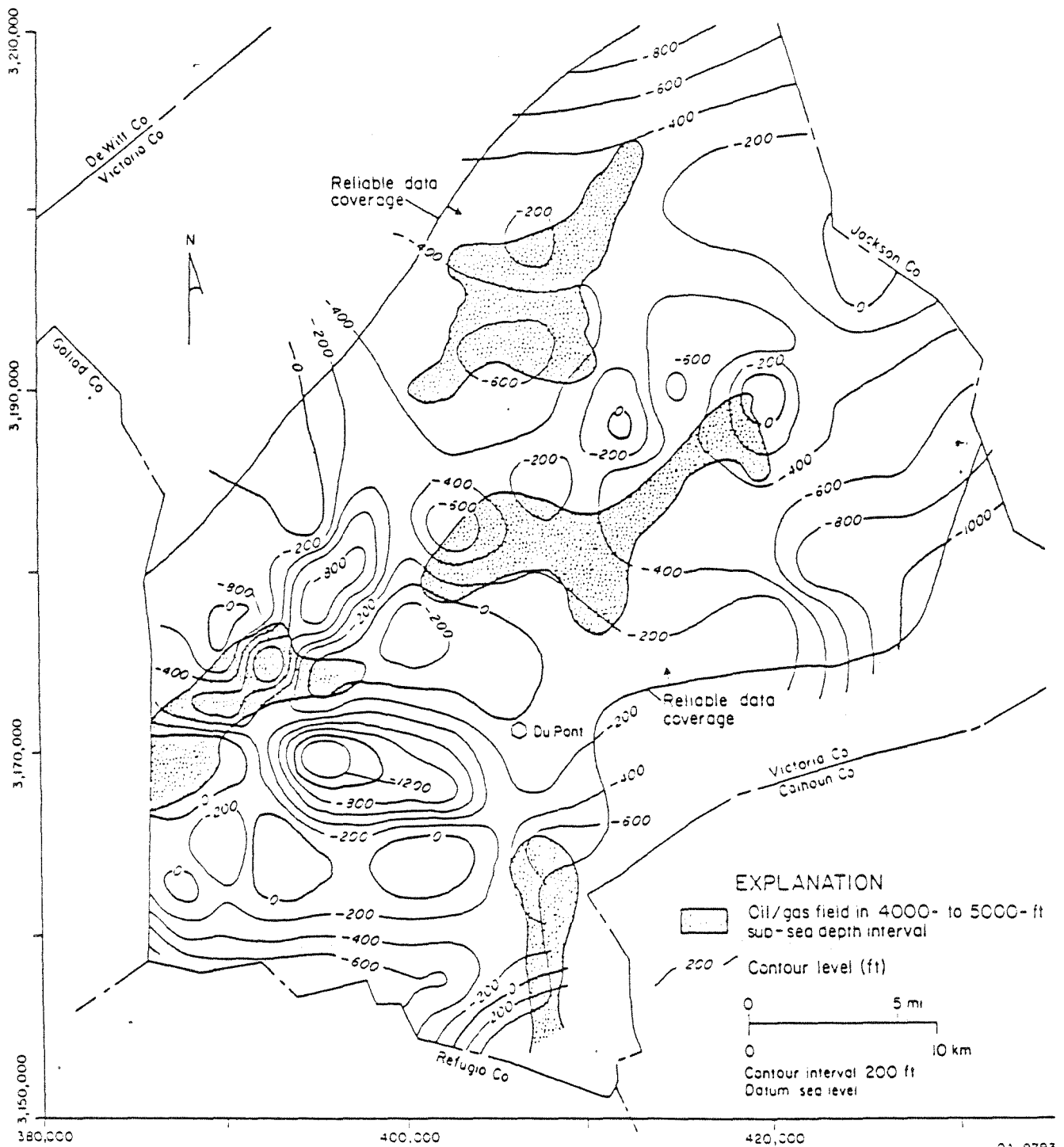


Figure 43. Potentiometric surface, 4,000-4,900 ft slice, Victoria Co., Frio and Catahoula, all classes, 1945-84 data. Includes formation pressure at Du Pont facility. Equivalent brine heads.

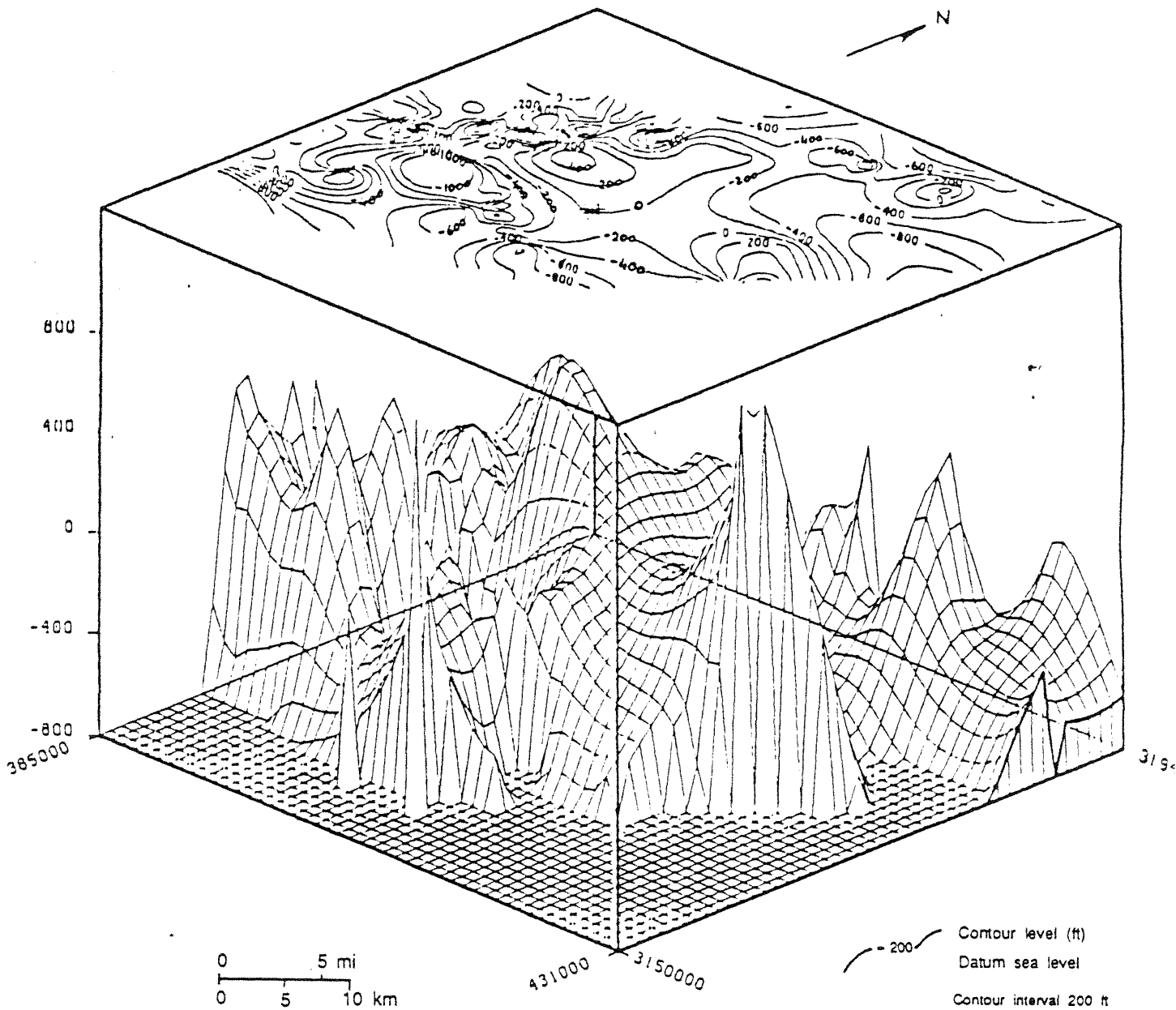


Figure 44. Isometric view of potentiometric surface, 4,000-4,900 ft slice, Victoria Co., Frio and Catahoula, all classes, 1945-84 data. Includes formation pressure at Du Pont facility. Equivalent brine heads.

equivalent brine heads (0.465 psi/ft). This residual surface is plotted in figure 45 in the plan view and in figure 46 in an isometric view. The residuals are all negative, implying a flow potential in the downward direction, that is, toward the deeper interval. This logically follows from the underpressured environment in the deeper zone. The 4,000-6,000-ft interval has historically been the target of the most oil and gas development.

6. DISCUSSION--PHYSICAL HYDROLOGY

6.1 Regional Trends

The pressure-depth profiles reflect the existence of two hydrologic systems in the Frio. Hydrostatic and subhydrostatic pressures exist in the depth interval above 10,000 ft. This is overlapped by an overpressured system observed as shallow as 6,000 ft. Extensive oil and gas development seems to have caused large-scale depressurization and resulted in subhydrostatic pressures within the productive plays of the Frio. The overpressures at shallow depths indicate two possibilities: (1) there is compactional disequilibrium in an environment of restricted drainage in the shallow depth range of the hydrostatic system, and/or (2) brines from deeper geopressed zones are leaking upward into the shallower hydrostatic section.

Grossly overpressured and underpressured aberrant data that did not match surrounding values were culled to refine the potentiometric surfaces. Still, within regional context there are numerous depressured areas and frequent reversals of flow direction to make definition of regional flow trends very difficult. Identifying flow potential on a local scale with better definition of pressures in the vicinity of injection sites is made possible by using the county maps.

6.2 Victoria County Hydrologic Trends

The potentiometric surfaces in the predominantly fresh to moderately saline environment (0-4,000-ft interval) are quite flat. Effect of depressurization is felt in the deeper intervals. In the context of chemical waste injection, this implies that injected fluids in the deep subsurface under existing hydrologic regimes would be constrained from migrating upward, but they possess a greater potential for lateral migration. Alteration of hydrologic conditions, however, could change this scenario. For example, massive localized fluid injection could raise the formation pressures and hydraulic heads sharply and develop vertically upward potential gradients.

The Victoria County residual surface map needs to be integrated with a structure map that locates faults and salt domes, and with a deep-well/abandoned-borehole

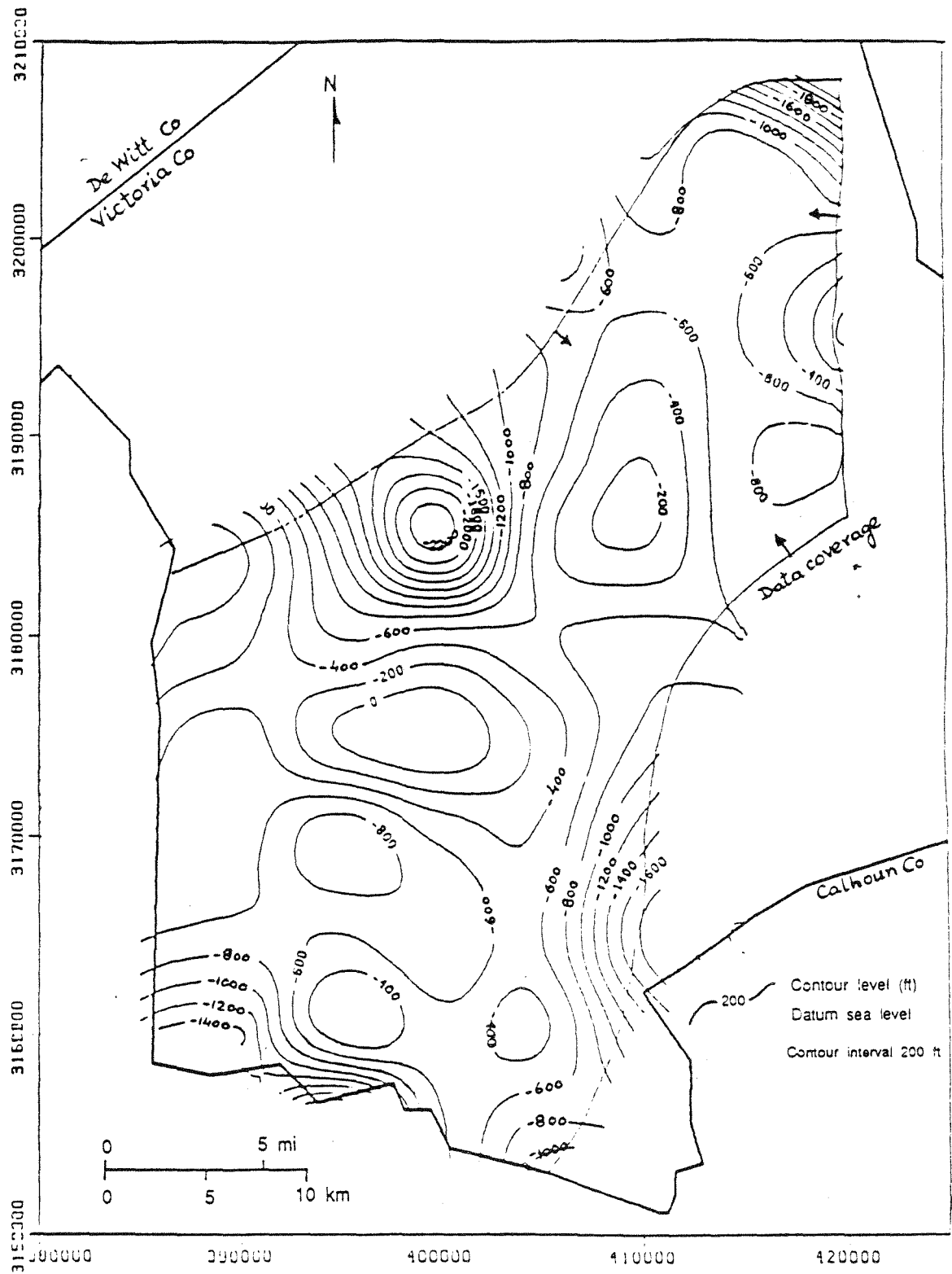


Figure 45. Residual potential surface, 4,000-6,000 ft (Frio) minus 0-2,000 ft (Miocene) slice, Victoria Co., all classes, 1965-84 data. Negative contours indicate downward flow. The 4,000-6,000 ft surface generated with equivalent brine heads.

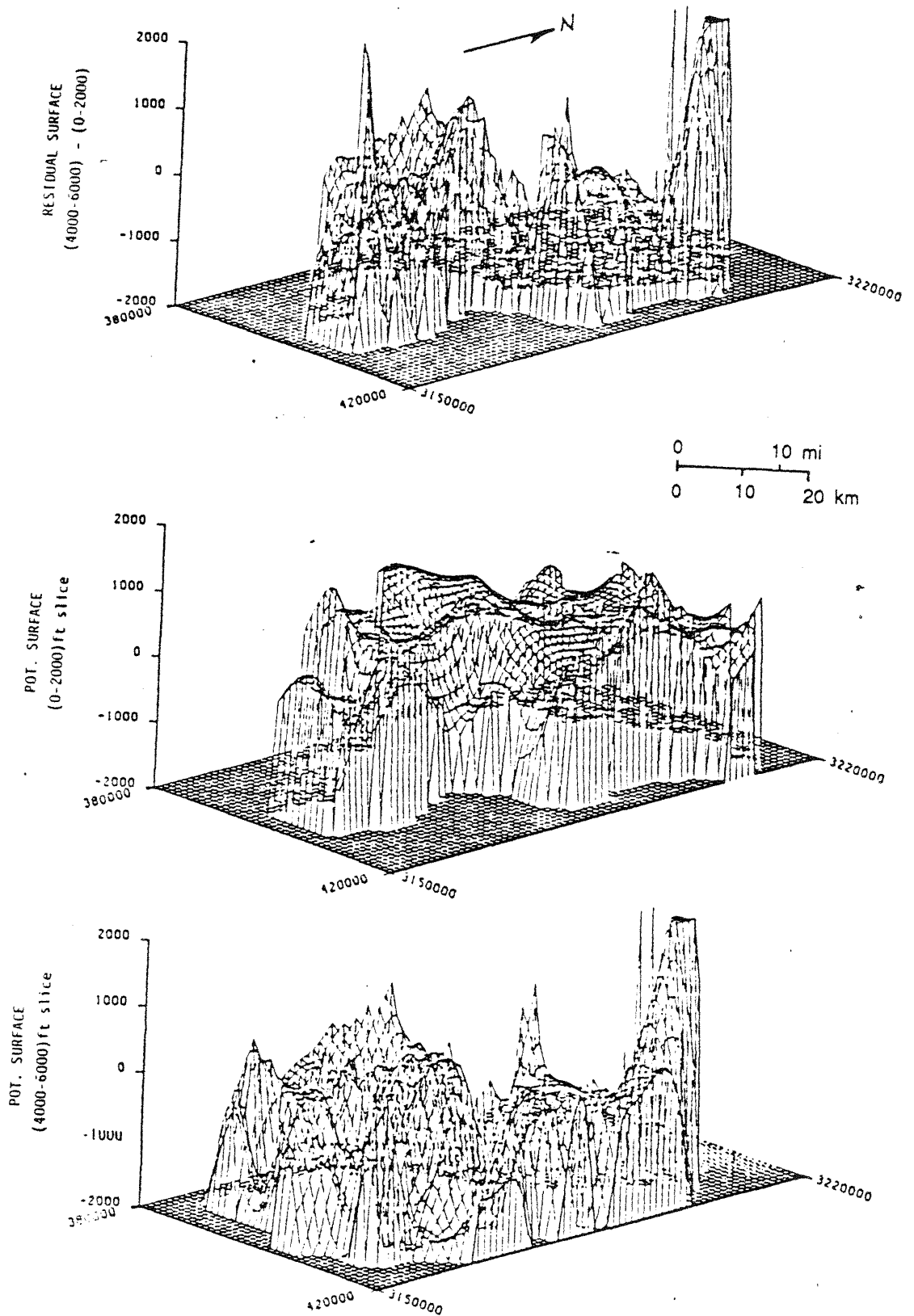


Figure 46. Isometric view of residual potential surface, 4,000-6,000 ft minus 0-2,000 ft slice, Victoria Co., all formations, all classes, 1965-85 data. Positive contours indicate upward flow, and negative contours indicate downward flow. The 4,000-6,000 ft surface generated with equivalent brine heads.

map. Such integrated maps will present a comprehensive picture of permeability pathways as well as the direction for potential flow.

6.3 Reservoir Parameters and Fluid Velocities

Table 1 summarizes some of the hydrologic parameters of the Texas Gulf Coast Tertiary formations, retrieved from various hydrologic reports submitted by injectors of hazardous chemical wastes to regulatory authorities during the permitting process.

Table 1: Hydrologic properties of Tertiary formations in injection zones (from Knape, 1984; PI Corp. data).

| Aquifer | Average injection depth (ft) | Average porosity (%) | Permeability (md) |
|----------------------|------------------------------|----------------------|-------------------|
| Undifferent. Miocene | 5,100 | 31 | 300-1,800 |
| Frio | 6,700 | 31 | 200-1,200 |
| Yegua | 4,200 | 26 | 200-500 |
| Catahoula | 4,450 | 30 | 400-800 |
| Oakville | 3,850 | 30 | 500-1,300 |
| Wilcox | 6,500 | 25 | 100-600 |

Figure 47 represents the permeability distribution in the 4,000-6,000-ft-depth interval for Texas Gulf Coast Tertiary formations. These values (included in square brackets) reflect results of core analyses or pressure tests conducted by well operators in the injection intervals, and mostly lie in the 200-2000 millidarcy (md) range. Other values marked on figure 47 were computed from drillstem test pressure data retrieved from the PI file, and are predominantly from the oil and gas bearing sands. Figure 48 locates flow gradients in the 4000-6000-ft Frio interval in different regions used for calculating fluid flow velocities. The average linear flow velocities in horizontal direction (product of average permeability and flow gradient, divided by average porosity) were computed in three different regions (A, B, and C) in the 4000-6000-ft interval and are summarized in table 2.

map. Such integrated maps will present a comprehensive picture of permeability pathways as well as the direction for potential flow.

6.3 Reservoir Parameters and Fluid Velocities

Table 1 summarizes some of the hydrologic parameters of the Texas Gulf Coast Tertiary formations, retrieved from various hydrologic reports submitted by injectors of hazardous chemical wastes to regulatory authorities during the permitting process.

Table 1: Hydrologic properties of Tertiary formations in injection zones (from Knape, 1984; PI Corp. data).

| Aquifer | Average injection depth (ft) | Average porosity (%) | Permeability (md) |
|----------------------|------------------------------|----------------------|-------------------|
| Undifferent. Miocene | 5,100 | 31 | 300-1,800 |
| Frio | 6,700 | 31 | 200-1,200 |
| Yegua | 4,200 | 26 | 200-500 |
| Catahoula | 4,450 | 30 | 400-800 |
| Oakville | 3,850 | 30 | 500-1,300 |
| Wilcox | 6,500 | 25 | 100-600 |

Figure 47 represents the permeability distribution in the 4,000-6,000-ft-depth interval for Texas Gulf Coast Tertiary formations. These values (included in square brackets) reflect results of core analyses or pressure tests conducted by well operators in the injection intervals, and mostly lie in the 200-2000 millidarcy (md) range. Other values marked on figure 47 were computed from drillstem test pressure data retrieved from the PI file, and are predominantly from the oil and gas bearing sands. Figure 48 locates flow gradients in the 4000-6000-ft Frio interval in different regions used for calculating fluid flow velocities. The average linear flow velocities in horizontal direction (product of average permeability and flow gradient, divided by average porosity) were computed in three different regions (A, B, and C) in the 4000-6000-ft interval and are summarized in table 2.

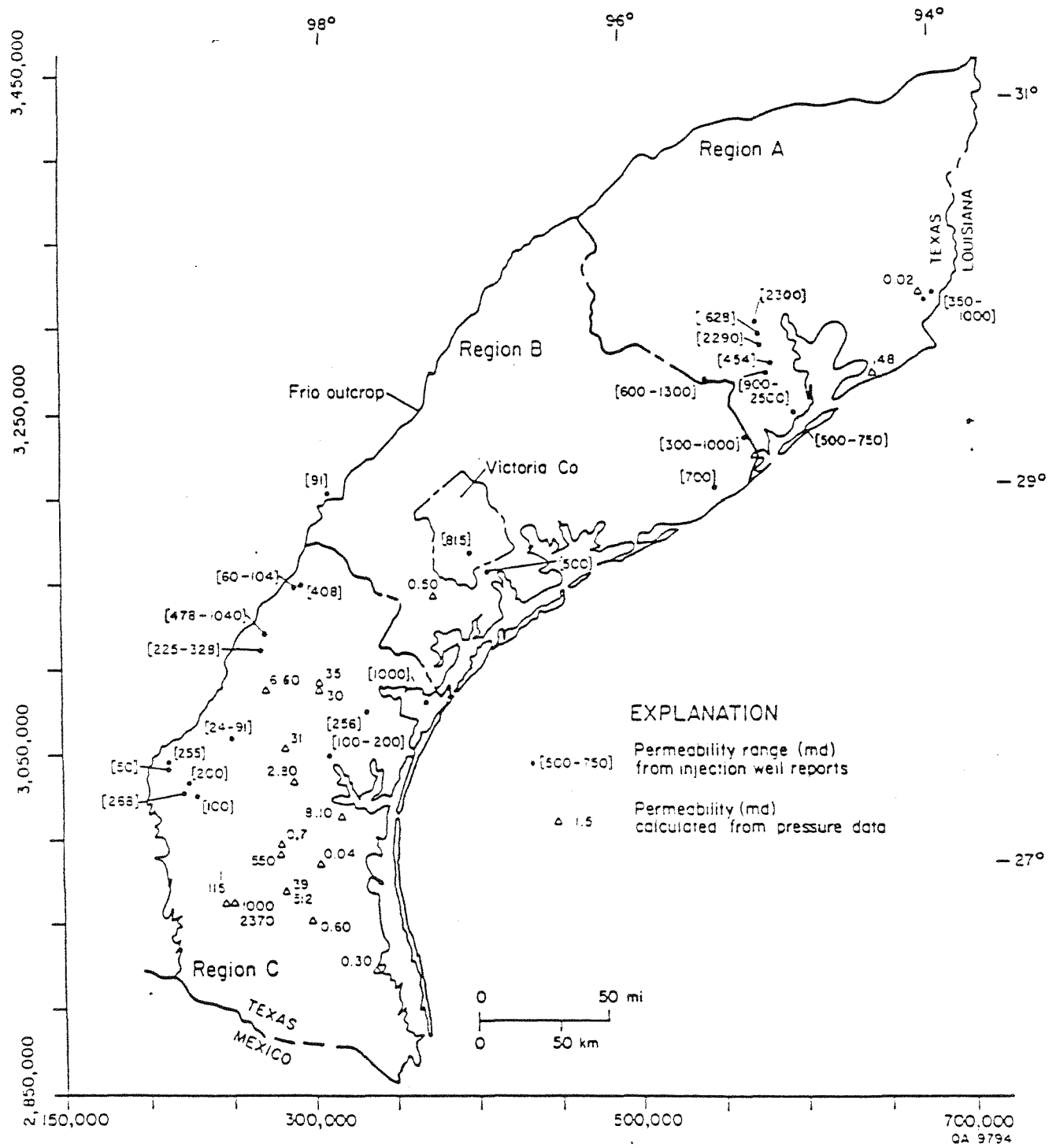


Figure 47. Permeability distribution in Texas Gulf Coast Tertiary formations, 4,000-6,000 ft interval, summarized from injection-well completion reports and computed from PI Corp. pressure data.

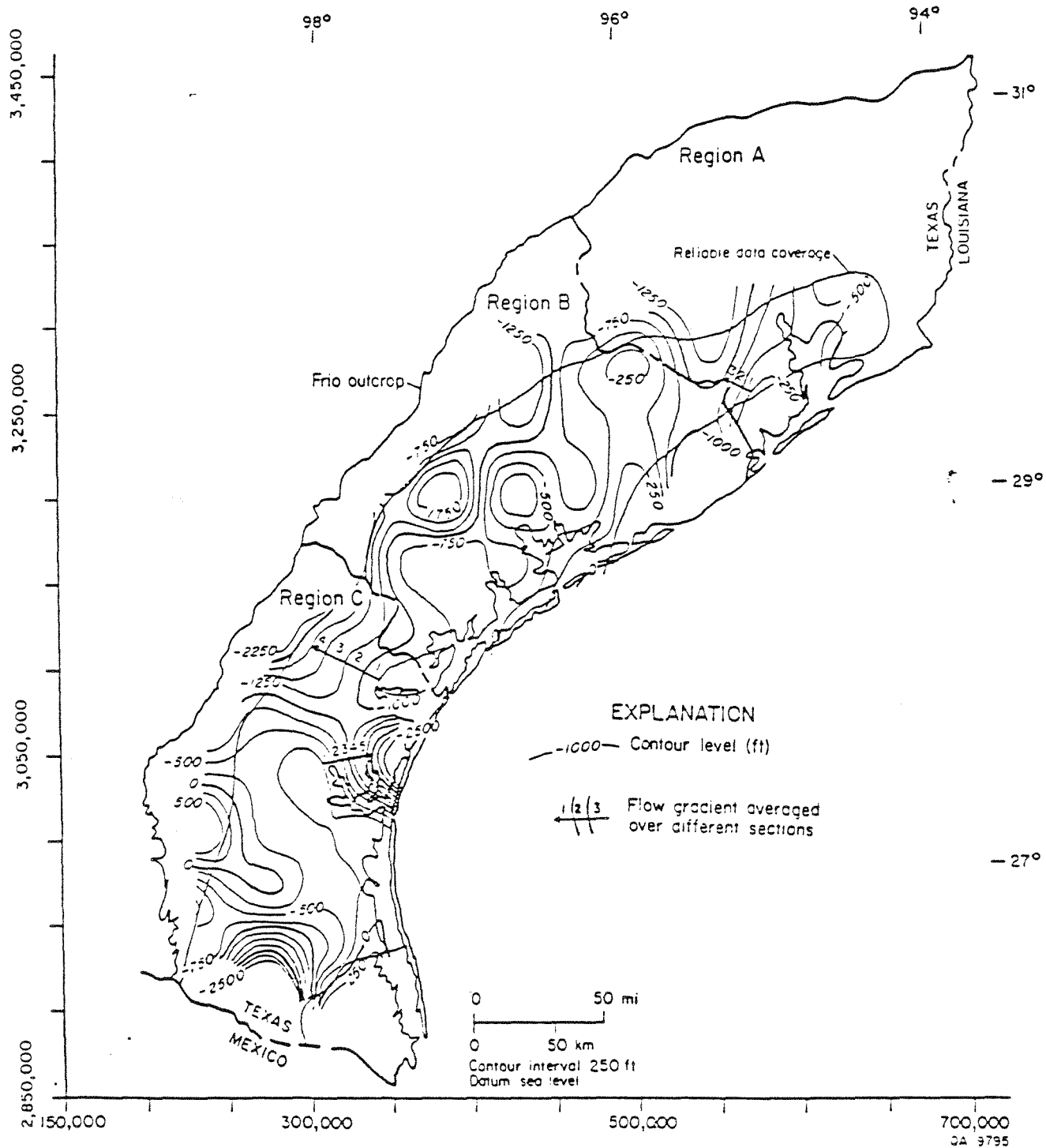


Figure 48. Location of average flow gradients in the 4,000-6,000 ft interval, Frio Formation, Texas Gulf Coast. Potentiometric surface generated with equivalent brine heads.

Table 2. Average horizontal linear velocities in 4,000-6,000-ft depth interval.

| Region | Flow gradient (dimensionless) | Porosity (%) | Permeability (ft/yr) | Avg. linear velocity (ft/yr) |
|--------|----------------------------------|-----------------|-------------------------|---------------------------------|
| A | 0.0141 | 31 | 300 | 13.7 |
| | 0.0141 | 31 | 2300 | 104.6 |
| B | 0.0063 | 31 | 0.5 | 0.01 |
| | 0.0063 | 31 | 800 | 16.3 |
| C | 0.0167 | 31 | 3.0 | 0.2 |
| | 0.0167 | 31 | 1000 | 53.9 |

Thus, the average horizontal linear velocities range from 0.01 ft/yr to 105 ft/yr in regions with moderate flow gradients. These values are based on oil and gas formation pressures and reflect more realistically the flow potential toward moderately depressurized fields. In instances of extreme depressurization, these velocities can be several times higher. For a better estimate of flow velocities from an injection zone toward an oil field, additional pressure distribution in the injection area is required.

6.4 Sensitivity of Potentiometric Surfaces to Data Selection and Fluid Density

The classification and screening system applied to the dataset allowed a more objective evaluation of the potentiometric surfaces. Surfaces were constructed with the highest confidence data (classes A, B, and Z) and were compared with surfaces for the same depth range and area resulting from all the pooled data (classes A, B, C, and D). The differences in these surfaces were analyzed and attributed to intra-class variance for a better explanation of some of the local variations in flow trends. This was helpful in culling some aberrant data from the dataset. Depressured and overpressured data introduce localized reversals in flow direction that do not fit a smooth regional trend but that must be considered a realistic reflection of existing conditions. Elimination of exceptionally high or low hydraulic heads relative to the surrounding values from the dataset resulted in more realistic regional surfaces. In instances of multiple head values for the same well location, the highest class and highest head value were retained. Averaging of data values is an artifact of the contouring software CPS-1, and the resultant contours reflect the dominating trend from a group of high and low values within a selected grid cell. The potentiometric surfaces for horizontal slices are considered representative of the regional trends because, on the one hand, they are not complicated by the extremes of highs and

lows resulting from a mixing of depressured and overpressured data from different depths, and on the other hand they preserve the local variations in flow directions and hydraulic gradients.

A good example of the sensitivity of potentiometric surfaces to data screening is the 4,000-4,900-ft slice in Victoria County. The surface in figure 43 was constructed after eliminating some extreme high and low heads and including data for only the Frio and Catahoula Formations. This surface is mostly flat and has near-land-surface head values, except in the south and southwest parts where cones of depression exist. The data in figure 49 include these extreme head values (identified within circled areas) and also include heads for other Tertiary formations. The resulting potentiometric surface in figure 50 exhibits greater localized highs and lows. Both these surfaces were constructed with brine equivalent heads (0.465 psi/ft gradient) and include an estimated pressure at Du Pont's injection site (Frank, 1986). Inclusion of non-Frio data is not as critical as the extreme values that are aberrant to local pressures. These extremes represent localized conditions without extensive lateral and vertical equilibration, and their exclusion results in a more average representative potentiometric surface.

Sensitivity of the potentiometric surface to fluid density is demonstrated in figure 51 in the 4,000-4,900-ft slice, Victoria County. This surface is based on equivalent hydraulic heads computed with a fluid gradient of 0.433 psi/ft (fresh water). The surface in figure 51 exhibits characteristics similar to those of the surface in figure 43 (both are for the 4,000-4,900-ft slice), except that the contours in the 0.433 gradient surface (fig. 51) are higher by 150-200 ft than the corresponding contours in the 0.465 gradient surface (fig. 43). Use of correct gradient (0.433 or 0.465) is critical to mapping potentiometric and residual surfaces and is based on availability of formation-brine-chemistry data.

This discussion of the sensitivity of the potentiometric surfaces highlights the need to examine the dataset very carefully, bearing in mind all the local variations possible within the context of the various pressure regimes.

6.5 Implications of Depressurization

The Frio Formation in the Gulf Coast has produced over 20 billion boe (barrels of oil equivalent) of hydrocarbons in the past 50 years of exploration and development. This appears to have led to extensive depressurization. In the 4,000-8,000-ft-depth interval, pressures have declined in some areas by as much as 1,000 psi from the original hydrostatic level. This is equivalent to a decline of more than 2,000 ft in the hydraulic heads. Depressurization may be beneficial in that the leakage of injected fluids up faults into shallow aquifers may be impeded. However,

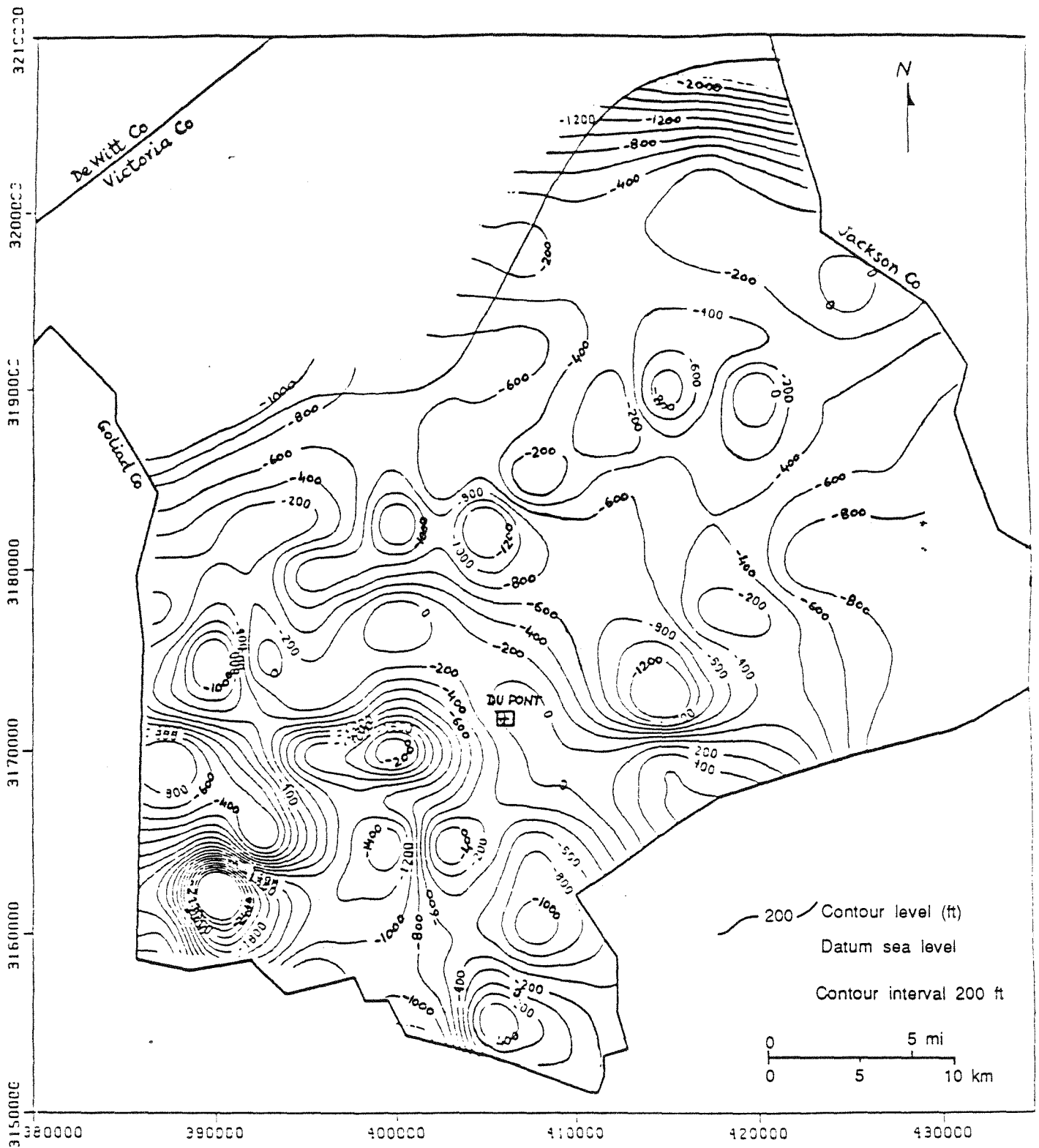


Figure 50. Potentiometric surface, 4,000-4,900 ft slice, Victoria Co., with 0.465 gradient, includes extreme heads, all classes, all formations, 1945-84 data. Includes formation pressure at Du Pont facility.

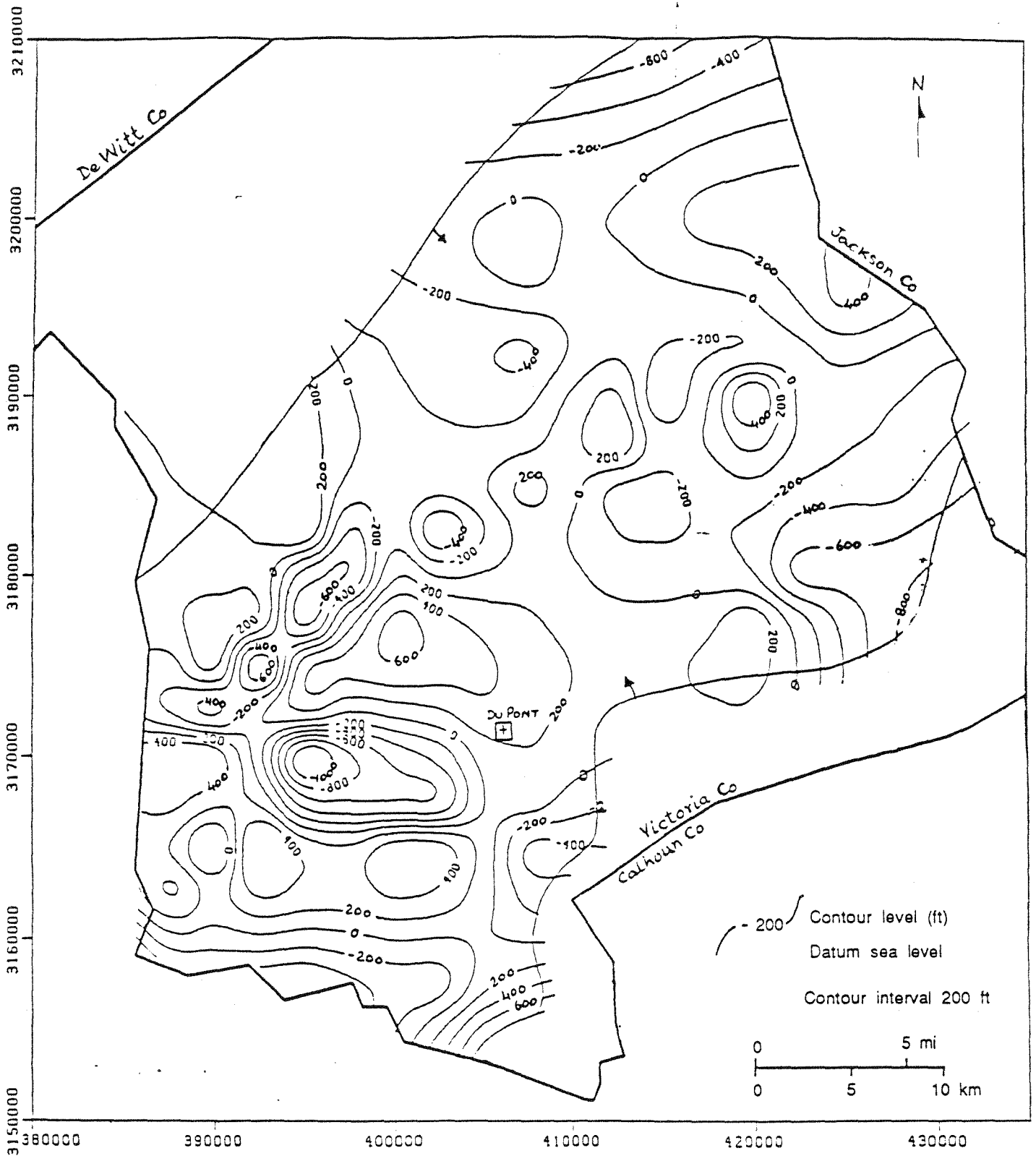


Figure 51. Potentiometric surface, 4,000-4,900 ft slice, Victoria Co., with 0.433 gradient, Frio and Catahoula, all classes, 1945-84 data. Includes formation pressure at Du Pont facility.

the negative effect could be that oil fields may become the ultimate sinks for these wastes. This problem could be compounded by the presence of numerous improperly abandoned wells in old depleted fields. The steep hydraulic gradients and high permeability of Frio sands may enable the migration of injected fluids to an oil field within a time period significantly less than the 10,000 years stipulated by EPA regulations. Fluid velocities (between 0.01 and 100 ft/yr) could accelerate by an order of magnitude owing to the presence of high-permeability streaks in the injected formations.

The depressurization phenomenon is reflected in localized depressions and negative contours on the potentiometric surfaces. Although some of these depressions may be temporal, they have serious implications for the regional trend in flow potential, in that the possibility for fluid flow toward the oil and gas fields is enhanced. A reasonable degree of hydraulic continuity, high permeability, and a steep hydraulic gradient could result in the flow of injected chemical wastes toward a depressured abandoned or producing field. At present we do not know how far the depressurized zone from an oil field may migrate laterally. Pressure declines may only be confined within a field, or they may migrate significantly far from the field, depending upon permeability, storativity, and presence of hydrologic barriers. Attempts to correlate potentiometric cones of depression to location of oil and gas fields reveal that not all depressions center on such fields. Reasons for this mismatch could be (1) factors other than hydrocarbon production contributing to depressuring, (2) contouring of potentiometric surfaces with localized temporal depressured data skewing the potential gradients and offsetting the cones of depression. The areal extent of depressurization is better determined by means of transient pressure analyses. This requires formation injectivity and productivity tests. More detailed investigations of the depressurization phenomenon are needed.

6.6 Implications of Overpressurization

Pressure-depth profiles have helped identify the top of geopressured sediments as significantly shallower than previously recognized. Top of geopressure in the Frio and Wilcox may be as shallow as 6,000 to 8,000 ft. The hydrostatic regime may bottom out at about 10,000 ft. Formation pressures from the PI data base were used with 0.465 psi/ft gradient as the marker to contour and delineate the hydrostatic and geopressured hydrologic regimes. Figure 52 represents the structure contours at the base of the saline hydrostatic section mapped for the deepest occurrence of fluid gradients less than or equal to 0.465 psi/ft. Shallowest occurrences of gradients greater than 0.465 psi/ft were used to delineate the top of geopressure structure in

the negative effect could be that oil fields may become the ultimate sinks for these wastes. This problem could be compounded by the presence of numerous improperly abandoned wells in old depleted fields. The steep hydraulic gradients and high permeability of Frio sands may enable the migration of injected fluids to an oil field within a time period significantly less than the 10,000 years stipulated by EPA regulations. Fluid velocities (between 0.01 and 100 ft/yr) could accelerate by an order of magnitude owing to the presence of high-permeability streaks in the injected formations.

The depressurization phenomenon is reflected in localized depressions and negative contours on the potentiometric surfaces. Although some of these depressions may be temporal, they have serious implications for the regional trend in flow potential, in that the possibility for fluid flow toward the oil and gas fields is enhanced. A reasonable degree of hydraulic continuity, high permeability, and a steep hydraulic gradient could result in the flow of injected chemical wastes toward a depressured abandoned or producing field. At present we do not know how far the depressurized zone from an oil field may migrate laterally. Pressure declines may only be confined within a field, or they may migrate significantly far from the field, depending upon permeability, storativity, and presence of hydrologic barriers. Attempts to correlate potentiometric cones of depression to location of oil and gas fields reveal that not all depressions center on such fields. Reasons for this mismatch could be (1) factors other than hydrocarbon production contributing to depressuring, (2) contouring of potentiometric surfaces with localized temporal depressured data skewing the potential gradients and offsetting the cones of depression. The areal extent of depressurization is better determined by means of transient pressure analyses. This requires formation injectivity and productivity tests. More detailed investigations of the depressurization phenomenon are needed.

6.6 Implications of Overpressurization

Pressure-depth profiles have helped identify the top of geopressed sediments as significantly shallower than previously recognized. Top of geopressure in the Frio and Wilcox may be as shallow as 6,000 to 8,000 ft. The hydrostatic regime may bottom out at about 10,000 ft. Formation pressures from the PI data base were used with 0.465 psi/ft gradient as the marker to contour and delineate the hydrostatic and geopressed hydrologic regimes. Figure 52 represents the structure contours at the base of the saline hydrostatic section mapped for the deepest occurrence of fluid gradients less than or equal to 0.465 psi/ft. Shallowest occurrences of gradients greater than 0.465 psi/ft were used to delineate the top of geopressure structure in

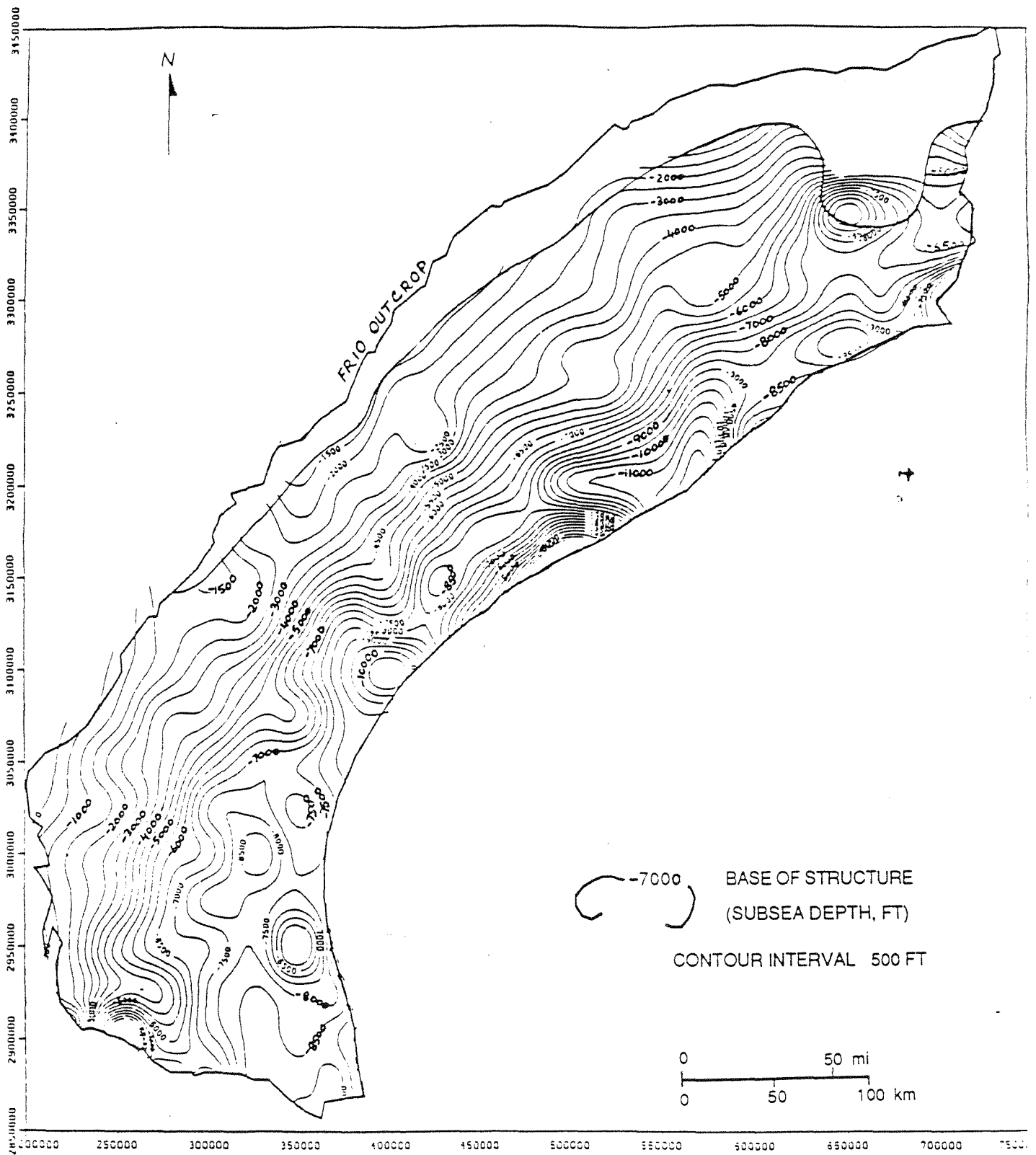


Figure 52. Base of saline hydrostatic section along the Texas Gulf Coast (mapped for deepest occurrence of ≤ 0.465 psi/ft fluid gradient).

figure 53. The outlined areas in figure 53 identify counties where the hydrostatic and overpressured surfaces may overlap. The overlap of top of geopressure (fig. 53) and base of hydrostatic (fig. 52), both contoured with 0.465 psi/ft gradient marker, is shown in figure 54. Contours in figure 54 reflect the interval thickness in which geopressed sediments either overlie or are interspersed within normally pressured sands; there are only isolated pockets of overlap. Pressure-depth profiles of counties (Kenedy, Brazoria, and parts of Brooks and Refugio) (figs. 55 through 58) within the overlapping segments are included in the appendix, and they confirm the shallow transition to overpressures. The apparent overlap of normally pressured and geopressed regimes, as seen in pressure-depth plot (fig. 11), is exaggerated due to the pooling of all data from different geographical areas. When individual counties are examined, it can be seen that the overlap is much smaller and is more a reflection of some overpressured sands interspersed in the hydrostatically pressured formations. Top of geopressure from the shallowest occurrence of 0.7 psi/ft gradient is contoured in figure 59. The fluid pressure gradient of 0.7 psi/ft is traditionally considered to be the marker for top of geopressed sediments (Powers, 1967; Jones, 1975). The difference between top of geopressure based on > 0.7 gradient and top of geopressure based on > 0.465 gradient is mapped in figure 60. This figure indicates how much shallower top of geopressure is encountered if it is delineated using the 0.465 gradient marker. Correct identification of top of geopressure may be important for safe siting of hazardous waste facilities.

Figures 61 and 62 are the pressure-depth profiles for the middle-Wilcox and the undifferentiated Miocene formations. The transition to overpressured sediments is observed on both plots and bears strong resemblance to Frio pressure-depth profiles. Similar processes may control formation of geopressing in all Tertiary formations. Most of the overpressured Miocene data lie offshore. Since offshore pressure data were not available for this study, relatively few overpressured values are included in the Miocene data.

The phenomenon of overpressured conditions existing at relatively shallow depths is complex and is linked to occurrence of shales and faults (Dickey and others, 1968). The presence of hydrostatic and overpressured conditions in the same depth range suggests compartmentalization that may be fault controlled. This compartmentalization may be important in locating future injection facilities. If faults indeed act as barriers to flow, then they may be advantageous to confinement of injected chemical wastes. Conversely, if they act as pathways for upward migration of deep overpressured brines, injection wells should be drilled away from such locations.

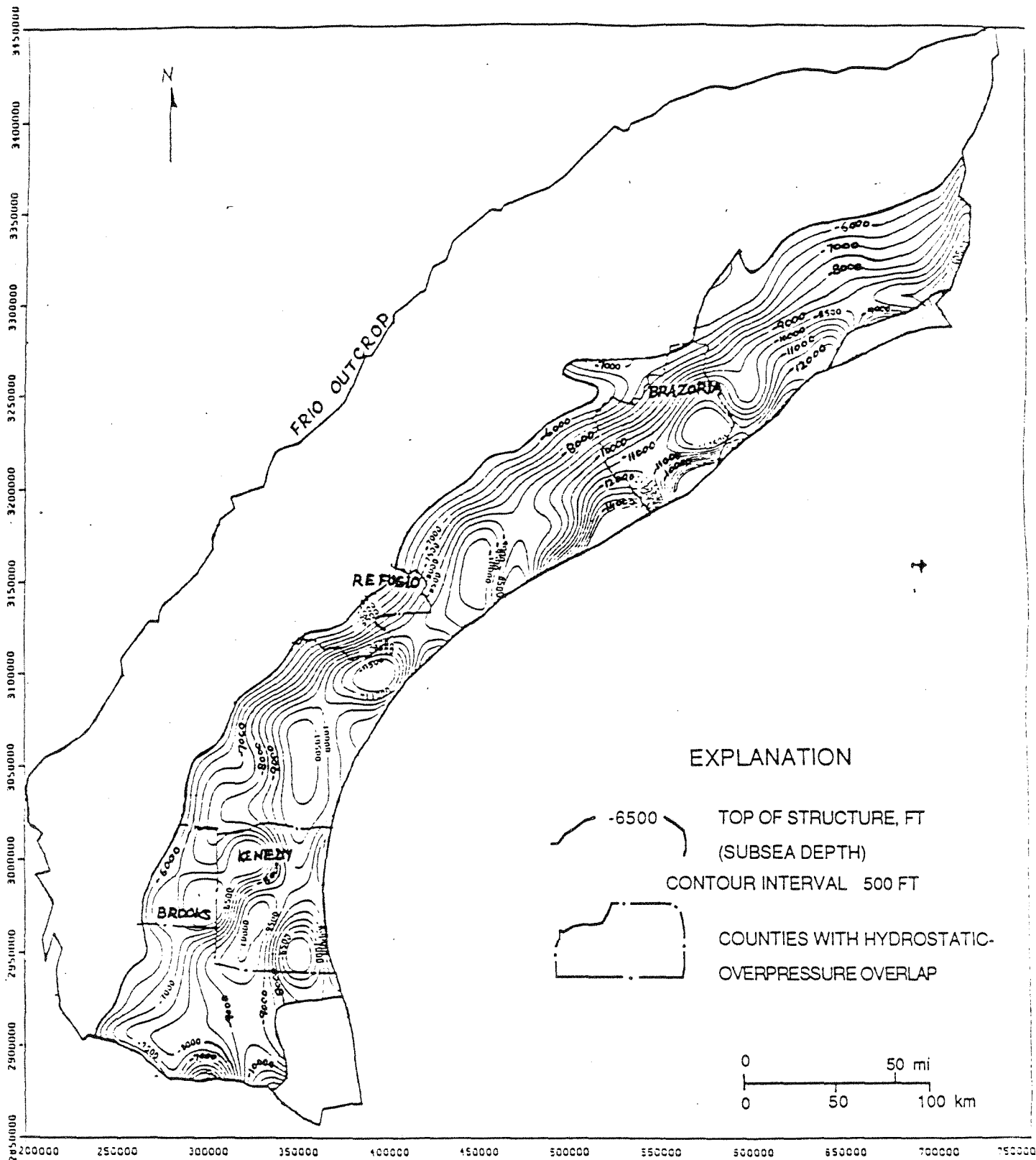


Figure 53. Top of geopressured section along the Texas Gulf Coast (mapped for shallowest occurrence of > 0.465 psi/ft fluid gradient).

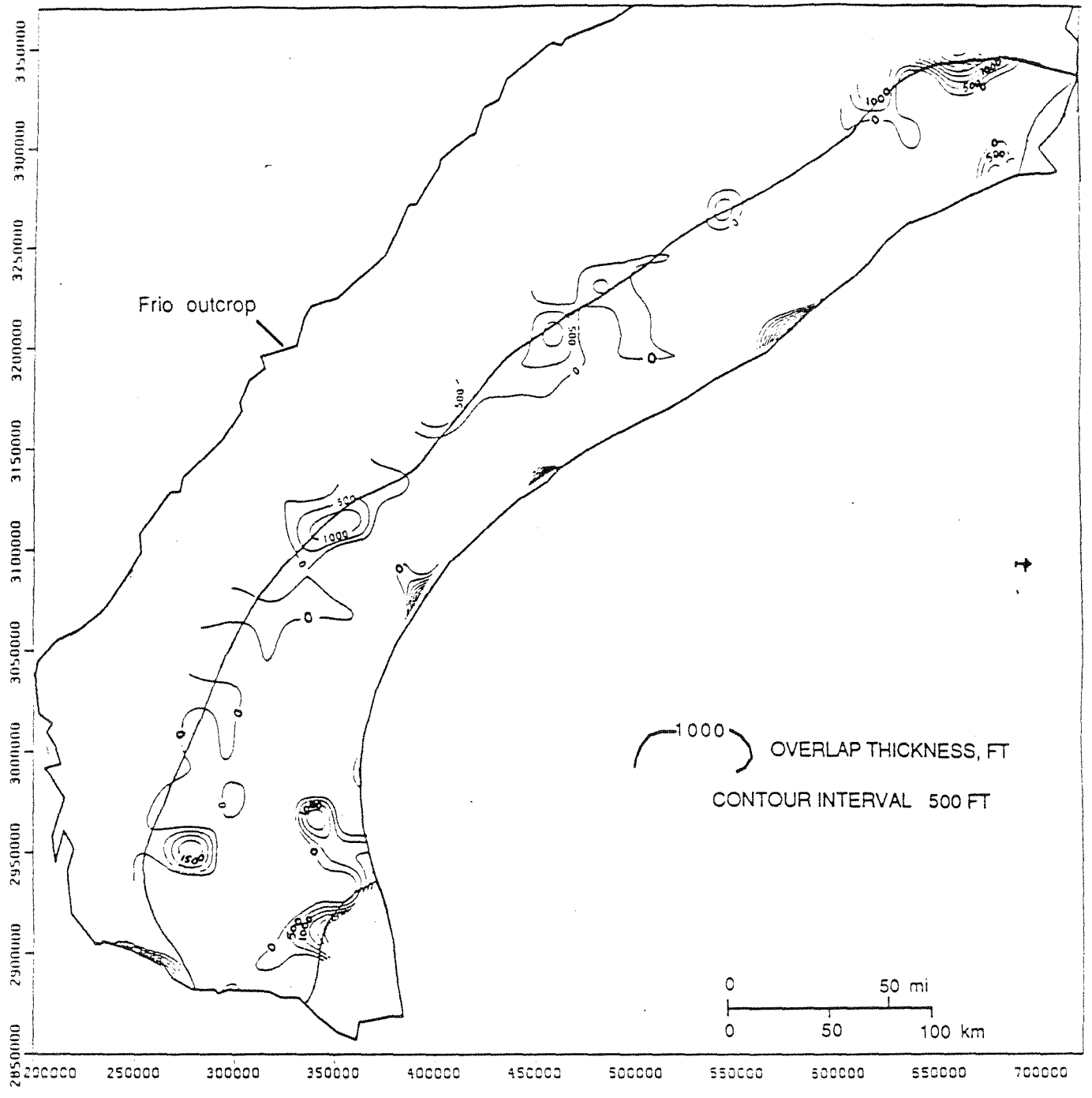


Figure 54. Overlap between base of hydrostatic and top of geopressured sections (figs. 53 and 52). Base of hydrostatic contoured for deepest occurrence of ≤ 0.465 psi/ft gradient, and top of geopressured contoured for shallowest occurrence of > 0.465 psi/ft gradient.

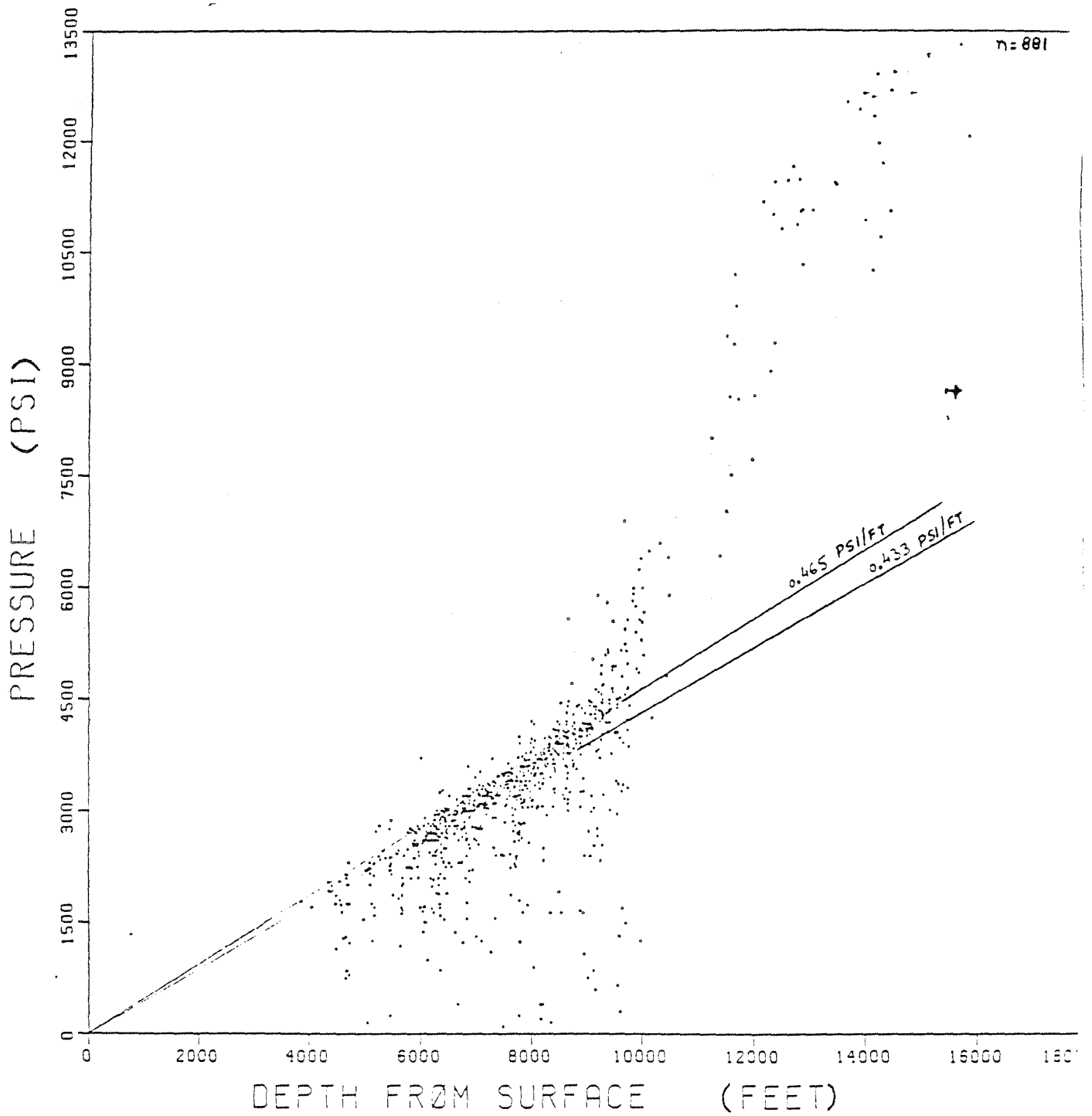


Figure 55. Pressure-depth diagram, Kenedy County data.

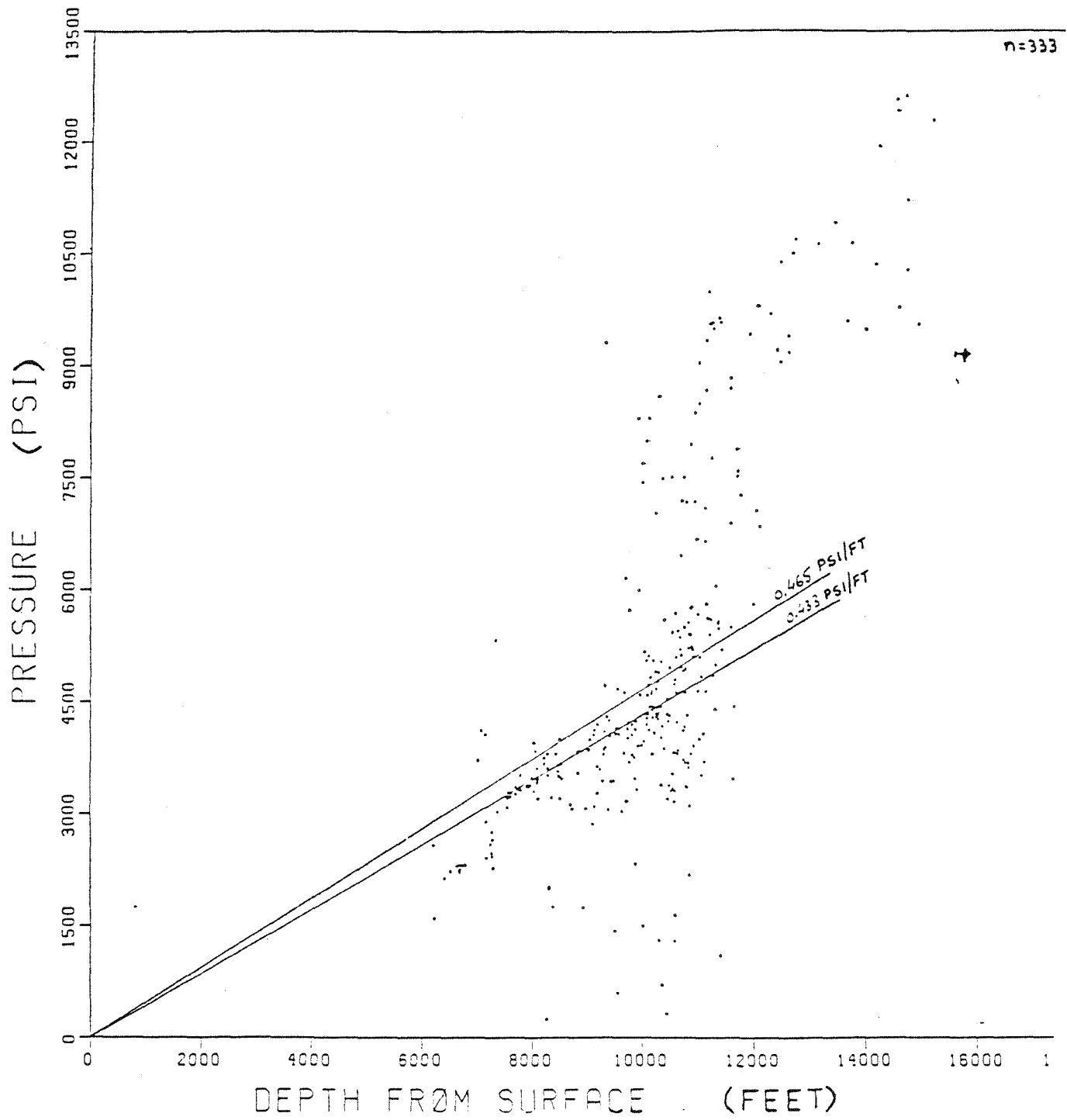


Figure 56. Pressure-depth diagram, Brazoria County data.

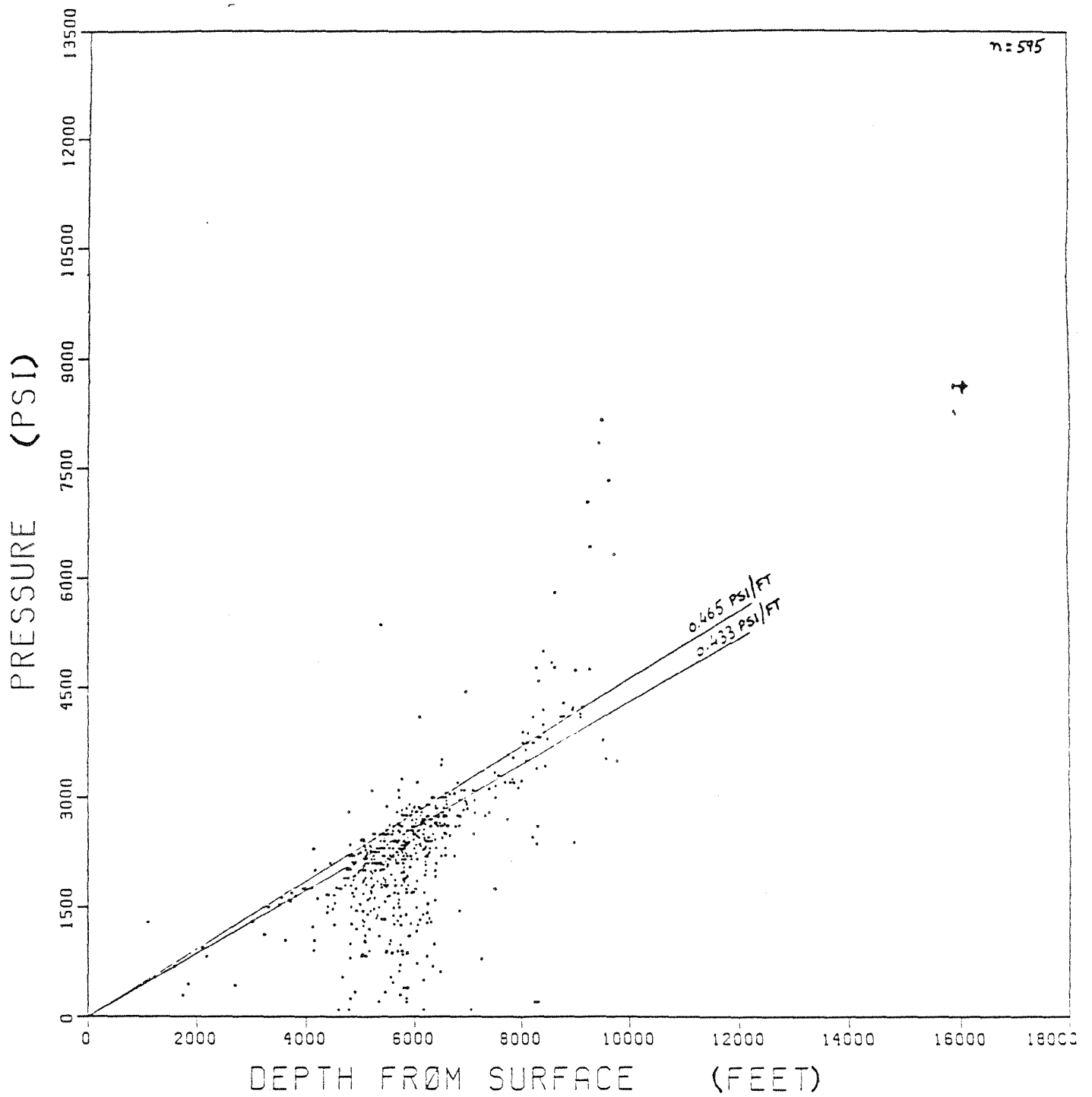


Figure 58. Pressure-depth diagram, Refugio County data.

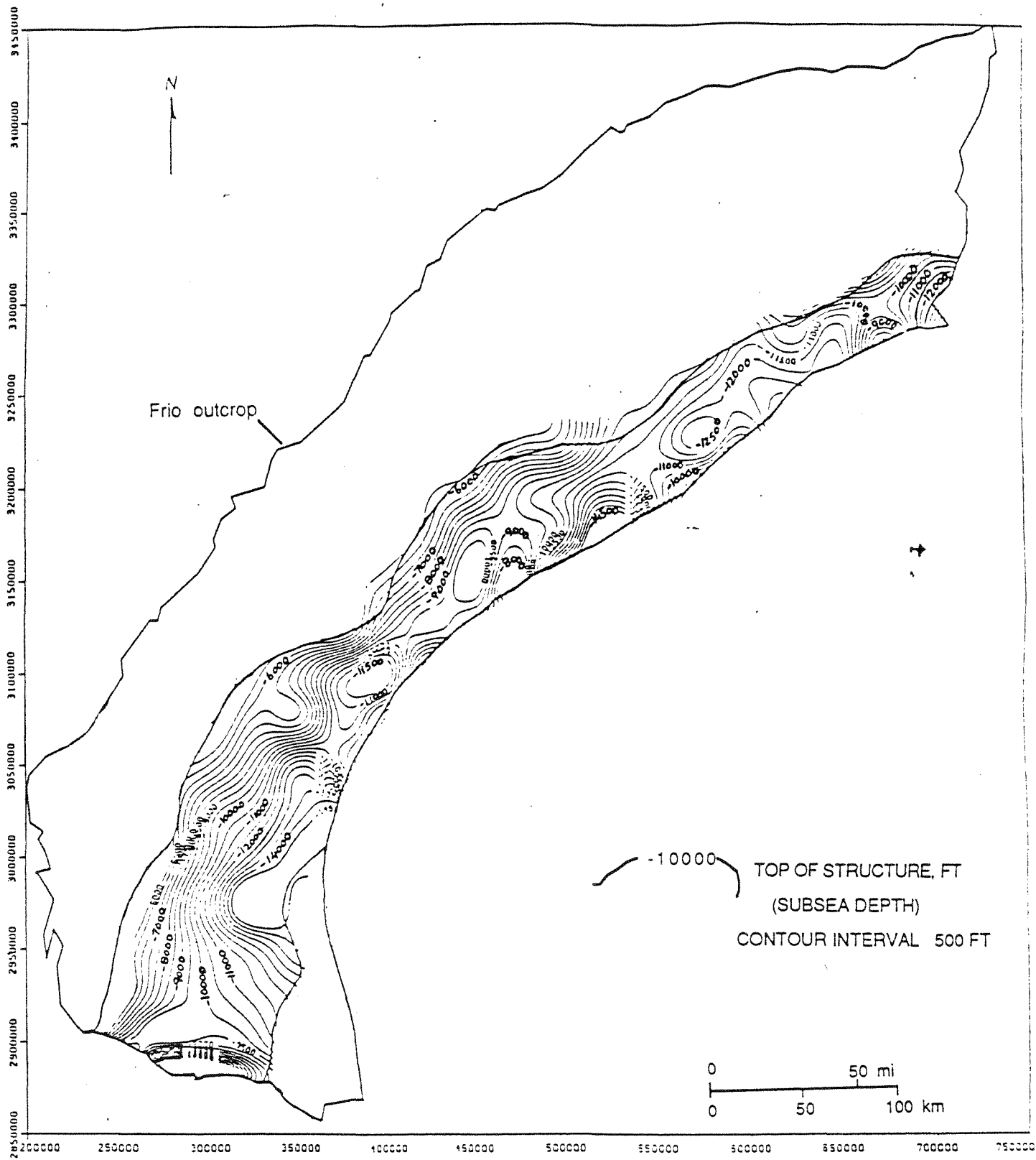


Figure 59. Top of geopressed section along the Texas Gulf Coast (mapped for shallowest occurrence of > 0.7 psi/ft fluid gradient).

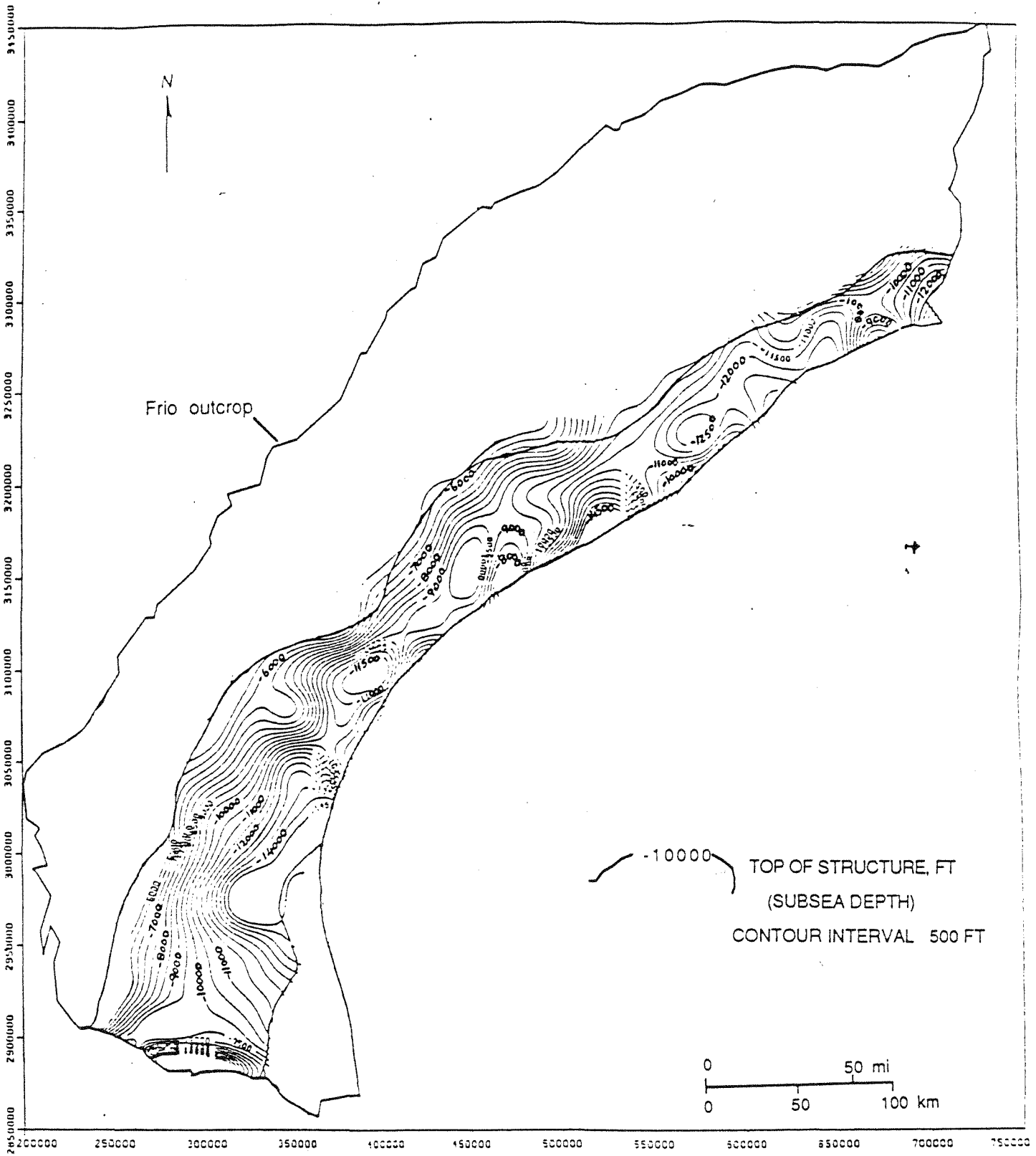


Figure 59. Top of geopressured section along the Texas Gulf Coast (mapped for shallowest occurrence of > 0.7 psi/ft fluid gradient).

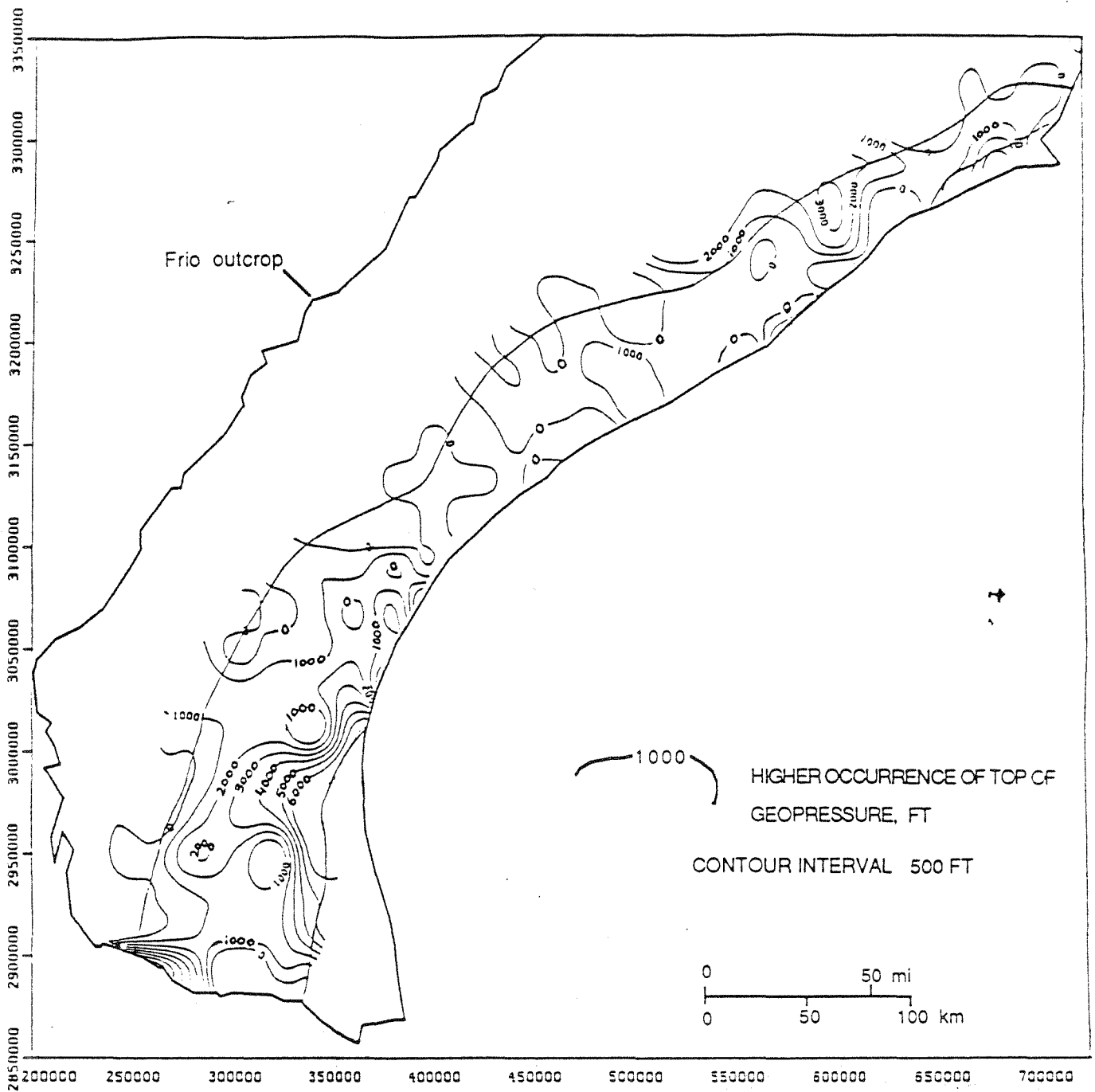


Figure 60. Difference between structure top of geopressure based on > 0.465 gradient and top of geopressure based on > 0.7 gradient (figs. 53 and 54).

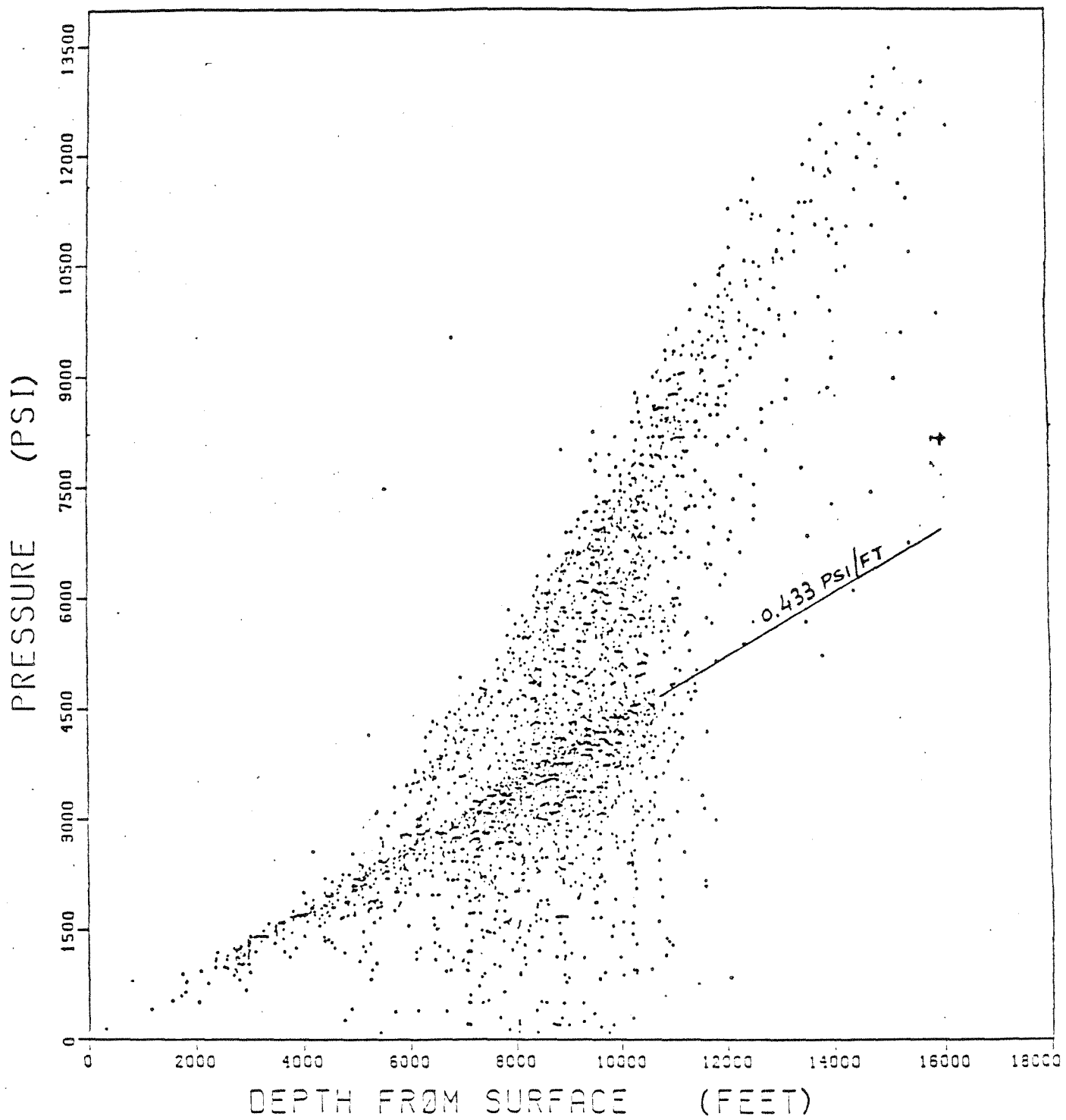


Figure 61. Pressure-depth diagram for middle Wilcox Formation, regions A-B-C data.

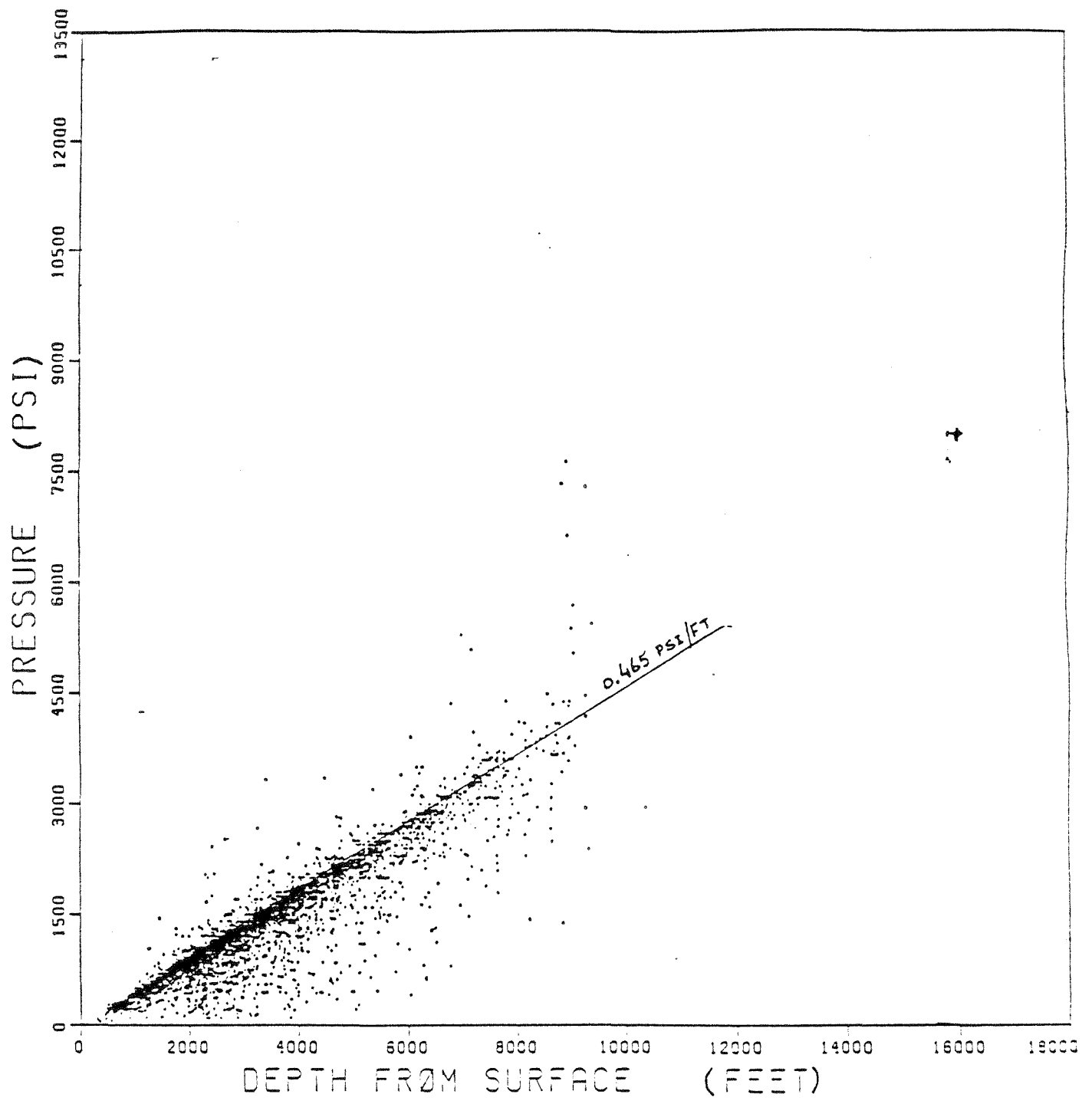


Figure 62. Pressure-depth diagram for undifferentiated Miocene Formation, regions A-B-C data.

7. WATER CHEMISTRY - INTRODUCTION

The chemical composition of saline Frio Formation waters provides additional information for understanding the process of deep-well injection of chemical wastes into deep saline formations in the Texas Gulf Coast, in three ways: (1) Chemical composition helps define the geochemical environment into which wastes are injected; (2) Fluid density is needed for the construction of potentiometric-surface maps based on DST pressure data; (3) Water chemistry, in conjunction with pressure data, helps define the regional hydrogeology of these saline formations.

7.1 Hydrochemical Environment

Kreitler and Richter (1986) previously characterized the geochemical environment of disposal horizons used in Gulf Coast saline formations as having varying salinities, predominantly NaCl in chemical composition, warm ($<100^{\circ}\text{C}$), and possibly high in organic acids. The injection zone typically was a permeable argillaceous-arkosic, unconsolidated sandstone. To better characterize the geochemical conditions of injection zones, additional information was needed primarily on actual organic acid concentrations. The presence or absence of organic acids may indicate biologically mediated reactions (Carothers and Kharaka, 1978). The acids may also function as ligands for metal transport (Drez, 1988). The presence of organic acids generally has only been inferred from measurements of total alkalinity because the titration for total alkalinity measures bicarbonate, borate and sulfide as well as organic acids. Total alkalinity, not the concentrations of individual acids, is typically measured in routine oil-field brine analyses.

7.2 Construction of Potentiometric Surfaces

Construction of potentiometric surfaces in saline aquifers presents inherent problems because of the variability of water salinity within a formation and between formations (Luszczynski, 1961). To investigate ground-water flow in the horizontal direction, fresh-water equivalent head maps are often constructed. Head values are calculated from drill-stem-test pressure data as if the sampled waters were fresh. To investigate vertical flow between formations containing waters of differing salinities, potentiometric surfaces need to be adjusted to account for the varying densities (and salinities). For this second type of mapping the density of the waters is important. These maps are called environmental or point source head maps.

7.3 Hydrochemical Interpretation of the Hydrogeology of Saline Formations

The waters in the hydrostatic section of the Frio Formation may have been derived from three different origins: (1) continental meteoric waters that have penetrated deep beneath the fresh-water section, (2) original waters that were emplaced at the time of sediment deposition, and (3) waters that have migrated up from the overpressured section or are a mixture of these different water sources. If the waters are original formation waters, a stagnant hydrologic system is implied. If the waters originated as geopressured waters, upward migration of deeper waters into shallower horizons is implied. If the waters are meteoric in origin, deep penetration of contaminated water and a relatively active hydrodynamic system may be inferred. These three hypotheses for the origin of the waters in the Frio hydrostatic can be tested by evaluation of the water chemistry.

- A. Deep penetration of meteoric waters. Four observations, based on previously collected geochemical data, suggest deep penetration of meteoric waters into the Frio Formation.
1. Many waters in the Gulf Coast saline formations, including the Frio Formation, have chlorinities less than sea water chlorinity (Kreitler and Richter, 1986).
 2. The $\delta^{18}\text{O}$ values of waters from the hydrostatic section of the Wilcox Formation (stratigraphically beneath the Frio) are isotopically light and not in isotopic equilibrium for their depth and temperature of occurrence (Fisher, 1982). Waters from the hydrostatic section of the Frio might show a similar meteoric influence. A limited number of Frio waters showed enriched $\delta^{18}\text{O}$ values (Lundegard, 1985) and appeared to be in isotopic equilibrium; these samples, however, were collected from deeper in the geopressured section of the Frio. It was unknown whether the hydrostatic sections of the Frio may also contain isotopically light meteoric water.
 3. Many oils from the hydrostatic section of the Frio Formation have high gravities (low API numbers) and high sulfur contents, suggesting biodegradation (Galloway and Hobday, 1983). Previous authors investigating biodegradation (for example, Bailey and others, 1973a) have suggested that meteoric waters have been the cause of biodegradation.
 4. Kreitler and Richter (1986) observed an inverse correlation between total alkalinity and chlorinity. Deep formation waters often have high concentrations of aliphatic acids. Kerogen has been altered by thermal maturation to natural gas and organic acids. Shallow formation waters were expected to have low concentrations of

organic acids, because of biologic consumption of the short-chained, easily-degraded organics (Carothers and Kharaka, 1978). The observed inverse correlation between total alkalinity and chlorinity suggests a source of the organic acids other than thermal maturation. The low chlorinities suggest deep penetration of meteoric water, and the high alkalinities suggest biodegradation of hydrocarbons by these brackish waters and subsequent formation of organic acids as a resulting product.

These observations are tentative. The measurement of total alkalinity represents field titrated alkalinity and is not specific to organic acids. API gravity and sulfur content only imply degradation of oil. The presence of specific organic acids and degraded oils is confirmed by gas chromatograph analysis. The isotopic composition of waters in the Wilcox is known, but the isotopic composition of Frio waters in the hydrostatic section is not.

If there has been deep penetration of meteoric water in the Frio, one might expect low TDS waters, light oxygen and hydrogen isotopic values suggestive of meteoric recharge, and heavy oils indicating biodegradation and/or water washing. If these waters are meteoric in origin, is it also possible to date this process of penetration?

B. Original formation waters. If the waters in the Frio are the original waters trapped during sediment deposition, TDS concentrations should range from brackish to seawater, and concentration of select ions should be similar to that of seawater. Rock/water reactions may have altered the original seawater composition. Salt dome dissolution is considered to have an important control on the water chemistry in the geopressured section (Morton and Land, 1987). These waters may have isotopic compositions similar to that of seawater or have become isotopically enriched through reaction with the rock matrix or mixing with deeper upward migrating geopressured waters. Degraded oils would not be expected. The hydrocarbons have migrated to their present traps after sedimentation and burial (Galloway and others, 1982). If degradation has occurred, a mechanism is needed to explain either how bacteria can migrate to depths of at least 6,000 ft or how bacteria can survive from the time of initial sediment deposition to the time of oil migration, which may be millions of years later.

C. Upward migration of geopressured waters. The concept that waters that have migrated from deeper geopressured horizons up faults or along the flanks of salt domes into shallower hydrostatic horizons is based on four observations.

1. Many oil fields in the Gulf Coast occur at depths above the "oil window," the temperature/pressure regime where oil maturation occurs (Young and others, 1977), and may have temperature and salinity anomalies associated with them (Tyler and others, 1985).
2. Lead-zinc mineralization associated with salt dome caprocks must have resulted when metal-rich brines migrated from deeper in the sedimentary basin (Ulrich and others, 1984).
3. The low-TDS Na-acetate waters at the top of the geopressure sediments suggest thermal convection of low-density waters and that the high-Ca water in the Frio geopressured section may result from leakage of waters from deeper Mesozoic formations that are being metamorphosed (Morton and Land, 1987). They conclude that because of the large volumes of relatively insoluble cements that have been precipitated, large volumes of waters must have discharged through the geopressured section.
4. Sulfide alteration found in uranium deposits has sulfur isotope compositions that can only be attributed to fluid migration from Mesozoic rocks deep within the basin (Galloway, 1982; Morton and Land, 1987), and indicates that fluid migration has been into the fresh-water aquifers. This upward migration process is not limited to the saline section.

Thirty-two water samples collected from the Frio Formation were analyzed for pH, total alkalinity, and inorganic and organic composition of the dissolved species. Oils associated with the sampled waters were also collected. Gas chromatographic analyses of 11 samples were run to determine if the oils were biodegraded. These data along with the larger, but less complete data base of previously published and unpublished data were investigated to address the questions of geochemical environment, fluid density and variability, and hydrogeology.

8. WATER CHEMISTRY - METHODOLOGY

Chemical data used in this report are from Kreitler and Richter (1986). Approximately 850 Frio analyses are used, the majority of which contain only major cation and anion data from oil field operators and constitute a very good source of major ion data from the Texas Gulf Coast. These data are subdivided geographically into Northgulf, Northcentral, Southcentral and Southgulf (table 3a through d). A second data set (table 4), which contains approximately 150 analyses, includes major and minor ions and is based on minor element analyses from Kreitler and Richter (1986) and Morton and Land (1987). Thirty-two additional waters sampled by the Bureau of

Table 3a. Major ion chemistry from Frio Formation, Northgulf region. Ionic concentrations in mg/L. Data from Kreitler and Richter, 1986.

| County | Latitude | Longitude | Ca | Mg | Na | K | Alkalinity | SO4 | Cl | TDS | Depth (feet) |
|-----------|----------|-----------|-------|------|-------|-----|------------|------|-------|--------|--------------|
| Newton | 30.71 | 93.65 | 5800 | 2120 | 24500 | 0 | 220 | 8 | 42000 | 69018 | 2900 |
| Newton | 30.47 | 93.80 | 10000 | 3490 | 33900 | 0 | 186 | 4 | 59500 | 97507 | 3000- 3100 |
| Fort Bend | 29.47 | 95.25 | 5100 | 628 | 40307 | 0 | 193 | 8 | 73000 | 119236 | 3644 |
| Fort Bend | 29.47 | 95.25 | 3480 | 484 | 34856 | 0 | 169 | 3 | 61300 | 100292 | 3788 |
| Fort Bend | 29.47 | 95.25 | 3880 | 472 | 37145 | 0 | 181 | 6 | 65500 | 107184 | 4126 |
| Fort Bend | 29.55 | 95.05 | 2781 | 508 | 30980 | 0 | 311 | 1 | 54000 | 88581 | 3717 |
| Fort Bend | 29.47 | 95.57 | 2040 | 322 | 37937 | 0 | 195 | 1 | 63000 | 103495 | 5385 |
| Fort Bend | 29.47 | 95.57 | 2280 | 1160 | 32700 | 0 | 122 | 1 | 57784 | 94047 | 5400 |
| Harris | 29.75 | 95.10 | 2320 | 437 | 41415 | 0 | 61 | 0 | 69255 | 113375 | 6865-6875 |
| Harris | 25.97 | 95.05 | 2476 | 403 | 44214 | 0 | 111 | 98 | 73609 | 120924 | 6000-6700 |
| Harris | 29.75 | 95.10 | 2740 | 340 | 39200 | 0 | 115 | 5 | 70000 | 112400 | 4900-7200 |
| Harris | 29.75 | 95.10 | 1850 | 440 | 34500 | 0 | 150 | 11 | 60140 | 124900 | 6800-7650 |
| Harris | 29.72 | 95.09 | 2200 | 457 | 39400 | 0 | 0 | 0 | 70000 | 113400 | 6600-7535 |
| Harris | 29.72 | 95.09 | 2160 | 453 | 41200 | 0 | 0 | 0 | 70000 | 115400 | 6600-7535 |
| Harris | 29.75 | 95.10 | 5100 | 1150 | 76916 | 0 | 160 | 425 | 82639 | 166408 | 6340-6640 |
| Harris | 29.75 | 95.10 | 5700 | 1800 | 62982 | 0 | 127 | 23 | 70446 | 141192 | 6490-6550 |
| Harris | 29.75 | 95.10 | 6400 | 1400 | 55664 | 0 | 99 | 12 | 63548 | 127318 | 6590-6650 |
| Harris | 29.74 | 95.09 | 2400 | 480 | 43000 | 0 | 463 | 0 | 19018 | 704000 | 6800-7300 |
| Harris | 29.73 | 95.13 | 10 | 5 | 25000 | 0 | 1400 | 1600 | 65000 | 60140 | 6800-7650 |
| Harris | 29.72 | 95.09 | 2775 | 462 | 14700 | 0 | 148 | 150 | 0 | 66900 | |
| Harris | 29.67 | 95.33 | 4740 | 1007 | 27931 | 0 | 140 | 1 | 54400 | 88219 | 4495 |
| Harris | 29.67 | 95.33 | 2552 | 402 | 40600 | 0 | 170 | 1 | 67300 | 111025 | 4828 |
| Harris | 30.12 | 95.63 | 1540 | 122 | 14610 | 0 | 189 | 1 | 25500 | 41962 | 3695 |
| Harris | 29.62 | 95.27 | 1849 | 303 | 39120 | 0 | 116 | 1 | 64400 | 105789 | 4873 |
| Harris | 29.55 | 95.17 | 3050 | 397 | 35997 | 0 | 220 | 1 | 62000 | 101665 | 6048 |
| Harris | 29.62 | 95.02 | 2744 | 337 | 37720 | 0 | 122 | 1 | 64000 | 104924 | 5925 |
| Harris | 29.42 | 95.17 | 8350 | 710 | 44000 | 624 | 88 | 2 | 83600 | 139000 | 11398-11408 |
| Harris | 29.42 | 95.17 | 8580 | 670 | 42400 | 643 | 94 | 3 | 80900 | 133000 | 11472-11499 |
| Galveston | 29.30 | 95.13 | 2000 | 220 | 26500 | 400 | 333 | 3 | 42700 | 73300 | 11299 |
| Galveston | 29.30 | 95.13 | 380 | 70 | 16250 | 140 | 361 | 43 | 24000 | 42800 | 8609 |
| Galveston | 29.30 | 95.13 | 180 | 40 | 15750 | 110 | 525 | 42 | 22400 | 40000 | 8845 |
| Galveston | 29.30 | 95.13 | 130 | 30 | 16500 | 120 | 582 | 25 | 23800 | 42000 | 8796 |
| Galveston | 29.30 | 95.13 | 290 | 60 | 16500 | 110 | 397 | 39 | 16500 | 42100 | 8615 |
| Galveston | 29.30 | 95.13 | 2000 | 235 | 24000 | 300 | 317 | 1 | 40500 | 68600 | 11725 |
| Galveston | 29.30 | 95.14 | 140 | 30 | 14000 | 100 | 596 | 17 | 20400 | 36600 | 9278 |
| Galveston | 29.30 | 95.14 | 425 | 98 | 15165 | 0 | 1596 | 58 | 24181 | 41405 | 8675- 8680 |
| Galveston | 29.30 | 95.14 | 302 | 81 | 15124 | 0 | 1635 | 46 | 23151 | 40339 | 8755- 8770 |
| Galveston | 29.30 | 95.14 | 292 | 72 | 16467 | 0 | 1437 | 78 | 25234 | 43580 | 9158- 9163 |
| Galveston | 29.30 | 95.14 | 827 | 138 | 18043 | 0 | 655 | 39 | 29289 | 48991 | 10895-10905 |
| Galveston | 29.30 | 95.14 | 1600 | 185 | 20400 | 0 | 394 | 38 | 34625 | 57322 | 11422-11461 |
| Galveston | 29.30 | 95.14 | 302 | 81 | 15124 | 0 | 1635 | 46 | 23151 | 40339 | 8755- 8770 |
| Galveston | 29.30 | 95.14 | 292 | 72 | 16467 | 0 | 1437 | 78 | 25234 | 43580 | 9158- 9163 |
| Galveston | 29.30 | 95.14 | 827 | 138 | 18043 | 0 | 655 | 39 | 29289 | 48991 | 10895-10905 |

Table 3a (continued)

| County | Latitude | Longitude | Ca | Mg | Na | K | Alkalinity | SO4 | Cl | TDS | Depth (feet) |
|-----------|----------|-----------|------|------|-------|-----|------------|-----|-------|--------|--------------|
| Galveston | 29.30 | 95.14 | 1600 | 185 | 20400 | 0 | 394 | 38 | 34625 | 57322 | 11422-11461 |
| Galveston | 29.30 | 95.14 | 441 | 101 | 13843 | 0 | 1630 | 24 | 21459 | 37498 | 8822- 8832 |
| Galveston | 29.30 | 95.14 | 582 | 101 | 18306 | 0 | 1093 | 24 | 28934 | 49091 | 9374- 9386 |
| Galveston | 29.31 | 95.14 | 1104 | 168 | 23994 | 0 | 649 | 34 | 39102 | 65147 | 11056-11068 |
| Galveston | 29.31 | 95.14 | 4319 | 595 | 27820 | 0 | 369 | 1 | 52600 | 86685 | 12238-12248 |
| Galveston | 29.31 | 95.14 | 8980 | 625 | 42100 | 570 | 0 | 14 | 78500 | 129600 | 14650 |
| Galveston | 29.52 | 95.20 | 4260 | 660 | 49300 | 371 | 219 | 12 | 59500 | 98500 | 9767- 9784 |
| Galveston | 29.33 | 95.10 | 1490 | 151 | 29800 | 230 | 536 | 18 | 46300 | 79900 | 12270-12280 |
| Galveston | 29.33 | 95.10 | 783 | 95 | 22700 | 192 | 628 | 7 | 35200 | 58900 | 11250-11254 |
| Galveston | 29.33 | 95.10 | 606 | 88 | 24900 | 180 | 848 | 6 | 36700 | 62500 | 10800- |
| Galveston | 29.33 | 95.07 | 480 | 98 | 15680 | 0 | 1122 | 0 | 24650 | 42085 | 9090- 9110 |
| Galveston | 29.50 | 95.05 | 4320 | 708 | 41030 | 0 | 793 | 1 | 72700 | 119339 | 8663- 8675 |
| Galveston | 29.33 | 95.10 | 880 | 183 | 15200 | 0 | 673 | 13 | 25180 | 42223 | 13014-13022 |
| Galveston | 29.33 | 95.10 | 660 | 134 | 18170 | 0 | 630 | 7 | 29260 | 49034 | 11150-11210 |
| Galveston | 29.47 | 95.10 | 2374 | 486 | 39996 | 0 | 453 | 40 | 67012 | 110361 | 9257 |
| Galveston | 29.47 | 95.10 | 1886 | 400 | 37432 | 0 | 450 | 25 | 61921 | 102114 | 9117 |
| Galveston | 29.45 | 94.95 | 512 | 235 | 20435 | 0 | 616 | 1 | 32750 | 54549 | 9078 |
| Galveston | 29.45 | 94.95 | 2852 | 496 | 27106 | 0 | 488 | 1 | 48100 | 79043 | 8031 |
| Galveston | 29.45 | 94.95 | 746 | 68 | 16542 | 0 | 561 | 1 | 26700 | 44618 | 8570 |
| Galveston | 29.45 | 94.95 | 2910 | 380 | 34170 | 0 | 458 | 1 | 58750 | 96669 | 8050 |
| Galveston | 29.45 | 94.95 | 2288 | 265 | 23783 | 0 | 561 | 1 | 41000 | 67898 | 8095 |
| Galveston | 29.45 | 94.95 | 1880 | 41 | 19056 | 0 | 885 | 25 | 32300 | 54187 | 8464 |
| Galveston | 29.33 | 95.10 | 418 | 81 | 17120 | 0 | 1089 | 103 | 26684 | 45495 | 9300 |
| Galveston | 29.33 | 95.10 | 629 | 163 | 23446 | 0 | 854 | 52 | 37233 | 62377 | 10360 |
| Galveston | 29.37 | 95.13 | 380 | 70 | 15250 | 140 | 414 | 31 | 23400 | 41300 | 8795 |
| Galveston | 29.37 | 95.13 | 400 | 75 | 16000 | 120 | 312 | 32 | 23800 | 42500 | 8828 |
| Galveston | 29.35 | 94.97 | 550 | 95 | 19000 | 180 | 334 | 31 | 26400 | 47600 | 8933 |
| Galveston | 29.35 | 94.97 | 470 | 85 | 17000 | 160 | 643 | 34 | 25200 | 44600 | 8933 |
| Galveston | 29.33 | 95.10 | 700 | 90 | 19500 | 190 | 787 | 11 | 31000 | 53100 | 11080 |
| Galveston | 29.33 | 95.10 | 1230 | 170 | 18250 | 190 | 506 | 8 | 29300 | 50400 | 12992 |
| Chambers | 29.63 | 94.90 | 1764 | 420 | 38472 | 265 | 244 | 373 | 63900 | 105789 | 5806- 5890 |
| Chambers | 29.63 | 94.90 | 2095 | 613 | 38878 | 226 | 195 | 186 | 63900 | 106498 | 5822- 5858 |
| Chambers | 29.63 | 94.90 | 1849 | 458 | 37482 | 262 | 231 | 230 | 63900 | 104776 | 5814- 5836 |
| Chambers | 29.63 | 94.90 | 2050 | 511 | 39672 | 240 | 207 | 360 | 65675 | 109142 | 5952- 5964 |
| Chambers | 29.67 | 94.50 | 4830 | 1010 | 41700 | 0 | 269 | 2 | 75700 | 123655 | 8300- 8335 |
| Chambers | 29.67 | 94.50 | 3420 | 1160 | 30100 | 0 | 162 | 0 | 56000 | 91072 | 8254- 8264 |
| Chambers | 29.67 | 94.50 | 4840 | 1330 | 47100 | 0 | 245 | 2 | 84900 | 138553 | 8236- 8246 |
| Chambers | 29.53 | 94.83 | 392 | 29 | 17991 | 0 | 898 | 20 | 28045 | 47728 | 9200 |
| Chambers | 29.80 | 94.40 | 2914 | 1770 | 33900 | 0 | 222 | 15 | 62150 | 100355 | |
| Chambers | 29.80 | 94.40 | 2320 | 732 | 37240 | 0 | 500 | 3 | 63480 | 104406 | 7610- 7612 |
| Chambers | 29.80 | 94.40 | 2240 | 561 | 37197 | 0 | 383 | 6 | 62770 | 103223 | 7820- 7826 |
| Chambers | 29.53 | 94.83 | 1020 | 197 | 16900 | 0 | 590 | 36 | 28200 | 46992 | 10098-10128 |
| Chambers | 29.53 | 94.83 | 1010 | 343 | 32900 | 0 | 485 | 0 | 53200 | 87982 | 9730- 9742 |

Table 3a (continued)

| County | Latitude | Longitude | Ca | Mg | Na | K | Alkalinity | SO4 | Cl | TDS | Depth (feet) |
|-----------|----------|-----------|-------|------|-------|-----|------------|-----|--------|--------|--------------|
| Chambers | 29.53 | 94.83 | 1500 | 343 | 34600 | 0 | 554 | 0 | 56600 | 93652 | 10440-10450 |
| Chambers | 29.53 | 94.83 | 887 | 218 | 23700 | 0 | 546 | 0 | 38600 | 64000 | 10836-10846 |
| Chambers | 29.53 | 94.83 | 4870 | 9450 | 27200 | 0 | 179 | 0 | 78000 | 119819 | 8166- 8170 |
| Chambers | 29.54 | 94.84 | 7590 | 766 | 46300 | 0 | 185 | 0 | 87100 | 142203 | 9334- 9347 |
| Chambers | 29.77 | 94.38 | 4230 | 550 | 27900 | 0 | 0 | 0 | 52100 | 84800 | 10465-10469 |
| Chambers | 29.77 | 94.38 | 2190 | 953 | 27700 | 0 | 237 | 13 | 49400 | 80576 | 8396 |
| Chambers | 29.78 | 94.58 | 2608 | 312 | 42472 | 0 | 159 | 1 | 71000 | 116552 | 7127 |
| Chambers | 29.78 | 94.58 | 4310 | 517 | 31116 | 0 | 146 | 50 | 57000 | 93139 | 7126 |
| Chambers | 29.53 | 94.82 | 1286 | 220 | 37368 | 0 | 854 | 1 | 60100 | 99829 | 9767 |
| Chambers | 29.63 | 94.92 | 4350 | 450 | 34965 | 0 | 98 | 101 | 62800 | 102764 | 6095 |
| Chambers | 29.63 | 94.92 | 4130 | 347 | 28786 | 0 | 232 | 378 | 52300 | 86173 | 6096 |
| Chambers | 29.85 | 94.67 | 1725 | 483 | 25267 | 0 | 171 | 103 | 43261 | 71010 | 6643 |
| Brazoria | 29.22 | 95.15 | 15912 | 1000 | 36700 | 434 | 88 | 0 | 90800 | 144934 | 14894 |
| Brazoria | 29.22 | 95.15 | 19176 | 1137 | 40500 | 490 | 113 | 0 | 103500 | 164916 | 14622 |
| Brazoria | 29.22 | 95.15 | 61 | 9 | 5200 | 58 | 743 | 0 | 7000 | 13071 | 12362 |
| Brazoria | 29.40 | 95.28 | 1010 | 180 | 37900 | 292 | 600 | 12 | 59500 | 98500 | 10497-10574 |
| Brazoria | 29.27 | 95.30 | 2600 | 535 | 69700 | 218 | 30 | 16 | 52000 | 35000 | 12558-12568 |
| Brazoria | 29.37 | 95.25 | 330 | 60 | 22700 | 171 | 1280 | 21 | 34000 | 56600 | 10858-10864 |
| Brazoria | 29.32 | 95.20 | 380 | 70 | 16250 | 140 | 361 | 43 | 24000 | 42800 | 8610 |
| Brazoria | 29.32 | 95.20 | 280 | 60 | 15250 | 120 | 427 | 43 | 22500 | 40200 | 8615 |
| Brazoria | 29.32 | 95.20 | 180 | 40 | 15750 | 110 | 525 | 42 | 22400 | 40000 | 8845 |
| Brazoria | 29.32 | 95.20 | 290 | 60 | 16500 | 130 | 397 | 39 | 23200 | 42100 | 8615 |
| Brazoria | 29.32 | 95.20 | 130 | 30 | 16500 | 120 | 582 | 25 | 23800 | 42000 | 9780 |
| Brazoria | 29.32 | 95.20 | 2000 | 220 | 26500 | 400 | 333 | 3 | 42700 | 73300 | 11360 |
| Brazoria | 29.32 | 95.20 | 710 | 90 | 25000 | 280 | 269 | 11 | 36300 | 63700 | 10690 |
| Brazoria | 29.32 | 95.20 | 1700 | 200 | 22000 | 270 | 262 | 5 | 37500 | 63000 | 11164 |
| Brazoria | 29.32 | 95.20 | 130 | 25 | 13000 | 90 | 562 | 57 | 18100 | 33400 | 9255 |
| Brazoria | 29.32 | 95.20 | 160 | 35 | 14000 | 90 | 632 | 59 | 19600 | 35800 | 9285 |
| Brazoria | 29.32 | 95.20 | 610 | 95 | 23250 | 220 | 302 | 11 | 35200 | 60700 | 11286 |
| Brazoria | 29.32 | 95.20 | 2000 | 235 | 24000 | 300 | 317 | 1 | 40500 | 68600 | 11725 |
| Brazoria | 29.32 | 95.20 | 140 | 30 | 14000 | 100 | 596 | 17 | 20400 | 36600 | 9278 |
| Brazoria | 29.32 | 95.20 | 170 | 30 | 12500 | 100 | 484 | 59 | 19600 | 34300 | 9281 |
| Galveston | 29.37 | 95.13 | 380 | 70 | 15250 | 140 | 414 | 31 | 23400 | 41300 | 8795 |
| Galveston | 29.37 | 95.13 | 400 | 75 | 16000 | 120 | 312 | 32 | 23800 | 42500 | 8828 |
| Brazoria | 29.28 | 95.13 | 1800 | 170 | 20500 | 180 | 356 | 16 | 34500 | 58000 | 13650 |
| Brazoria | 29.28 | 95.13 | 1600 | 185 | 17750 | 240 | 400 | 6 | 29300 | 50200 | 12770 |
| Brazoria | 29.07 | 95.67 | 333 | 21 | 10750 | 0 | 1348 | 1 | 16450 | 28903 | 10115 |
| Brazoria | 29.07 | 95.67 | 98 | 21 | 10779 | 0 | 1815 | 60 | 15769 | 28542 | 9726 |
| Brazoria | 29.07 | 95.67 | 137 | 64 | 14155 | 0 | 1507 | 151 | 21276 | 37290 | 10137 |
| Brazoria | 29.07 | 95.67 | 24 | 17 | 7180 | 0 | 1808 | 256 | 9928 | 19213 | 10100 |
| Brazoria | 29.32 | 95.17 | 2244 | 360 | 29170 | 0 | 580 | 37 | 49951 | 82342 | 11407 |
| Brazoria | 29.27 | 95.33 | 638 | 112 | 16625 | 0 | 976 | 75 | 26500 | 44926 | 6617 |
| Brazoria | 29.27 | 95.33 | 1104 | 29 | 27400 | 0 | 921 | 1 | 43800 | 73255 | 5670 |

Table 3a (continued)

| County | Latitude | Longitude | Ca | Mg | Na | K | Alkalinity | SO4 | Cl | TDS | Depth (feet) |
|-----------|----------|-----------|------|-----|-------|-----|------------|-----|-------|--------|--------------|
| Brazoria | 29.20 | 95.42 | 1688 | 68 | 17581 | 0 | 854 | 1 | 29800 | 49992 | 10582 |
| Brazoria | 29.50 | 95.25 | 1804 | 322 | 38852 | 0 | 183 | 1 | 64000 | 105162 | 6118 |
| Brazoria | 29.17 | 95.80 | 253 | 72 | 6890 | 0 | 665 | 1 | 10900 | 18781 | 6800 |
| Brazoria | 29.40 | 95.42 | 1808 | 338 | 36262 | 0 | 244 | 69 | 59927 | 98648 | 6497 |
| Brazoria | 29.40 | 95.42 | 2005 | 368 | 38899 | 0 | 104 | 37 | 64537 | 105950 | 6495 |
| Brazoria | 29.02 | 95.75 | 384 | 78 | 15467 | 0 | 781 | 16 | 24300 | 410260 | 10776 |
| Brazoria | 29.03 | 95.77 | 344 | 64 | 17520 | 0 | 878 | 14 | 27300 | 461200 | 10433 |
| Brazoria | 29.04 | 95.68 | 432 | 68 | 17046 | 0 | 695 | 72 | 26800 | 45113 | 10740 10766 |
| Brazoria | 29.04 | 95.69 | 184 | 31 | 12370 | 0 | 1720 | 69 | 18450 | 32849 | 10122 10140 |
| Brazoria | 29.06 | 95.68 | 90 | 18 | 9145 | 0 | 2180 | 68 | 13000 | 24512 | 10104 10122 |
| Brazoria | 29.06 | 95.69 | 144 | 39 | 14258 | 0 | 1270 | 32 | 21600 | 37343 | 10096 10142 |
| Brazoria | 29.06 | 95.73 | 120 | 44 | 9361 | 0 | 2310 | 50 | 13400 | 25285 | 10270 10280 |
| Brazoria | 29.06 | 96.59 | 1180 | 223 | 21822 | 0 | 140 | 4 | 36200 | 60000 | 4051 |
| Brazoria | 29.06 | 95.73 | 160 | 49 | 14480 | 0 | 1270 | 32 | 22000 | 37991 | 10350 10354 |
| Brazoria | 29.06 | 95.74 | 96 | 39 | 13152 | 0 | 1440 | 46 | 19700 | 34473 | 10165 10170 |
| Brazoria | 29.09 | 95.56 | 731 | 148 | 17553 | 0 | 850 | 578 | 27900 | 47760 | 12232 12244 |
| Brazoria | 29.09 | 95.56 | 1547 | 206 | 24338 | 0 | 468 | 730 | 40100 | 67389 | 11970 11992 |
| Matagorda | 28.97 | 95.49 | 450 | 80 | 4911 | 0 | 171 | 20 | 8510 | 14142 | 11302- 11329 |
| Matagorda | 28.97 | 95.49 | 847 | 188 | 13954 | 0 | 488 | 0 | 23290 | 38767 | 11302-11329 |
| Matagorda | 28.97 | 95.48 | 1660 | 259 | 20881 | 0 | 769 | 2 | 35460 | 59031 | 11306- 11348 |
| Matagorda | 29.01 | 96.13 | 3520 | 183 | 26300 | 0 | 241 | 0 | 47300 | 77613 | 3711-3719 |
| Matagorda | 28.97 | 95.92 | 4350 | 450 | 34965 | 0 | 98 | 101 | 62800 | 102764 | 8207 |
| Matagorda | 28.90 | 96.05 | 896 | 174 | 19780 | 0 | 1647 | 50 | 31636 | 54183 | 7926 |
| Matagorda | 28.97 | 96.03 | 244 | 59 | 16968 | 0 | 1198 | 51 | 26053 | 44573 | 8558 |
| Matagorda | 28.97 | 96.03 | 64 | 28 | 4616 | 0 | 1159 | 112 | 6560 | 12539 | 8938 |
| Matagorda | 28.97 | 96.03 | 52 | 51 | 6424 | 0 | 1824 | 66 | 9042 | 17459 | 9402 |
| Matagorda | 29.08 | 95.87 | 874 | 153 | 27000 | 306 | 230 | 0 | 45700 | 74263 | 9299 |
| Matagorda | 29.08 | 95.87 | 1583 | 289 | 34200 | 358 | 156 | 0 | 61000 | 97586 | 8984 |
| Matagorda | 29.08 | 95.87 | 1750 | 285 | 33700 | 431 | 338 | 0 | 60000 | 96504 | 8971 |
| Matagorda | 28.77 | 96.28 | 85 | 14 | 9100 | 81 | 629 | 0 | 12600 | 22509 | 10191 |
| Matagorda | 28.88 | 96.10 | 29 | 90 | 15431 | 0 | 1785 | 35 | 23000 | 40435 | 9800 |
| Matagorda | 28.95 | 95.17 | 25 | 4 | 5540 | 0 | 3510 | 670 | 6060 | 15813 | 10430-10458 |
| Matagorda | 28.78 | 96.30 | 83 | 12 | 9810 | 65 | 1790 | 0 | 13120 | 25390 | 10190-10268 |
| Matagorda | 28.78 | 96.30 | 100 | 9 | 5840 | 61 | 806 | 0 | 8470 | 15380 | 11655- 1171 |
| Matagorda | 29.07 | 95.90 | 1620 | 286 | 37400 | 310 | 230 | 15 | 61000 | 100000 | 8940- 8945 |
| Matagorda | 29.07 | 95.90 | 1660 | 277 | 36000 | 359 | 242 | 6 | 59100 | 98800 | 8996- 9000 |
| Matagorda | 29.07 | 95.90 | 1070 | 225 | 35900 | 260 | 257 | 7 | 56900 | 93700 | 8708- 8712 |
| Matagorda | 28.98 | 95.92 | 118 | 26 | 15040 | 110 | 1251 | 11 | 22480 | 39048 | 8893- 8899 |
| Matagorda | 28.95 | 96.17 | 1230 | 356 | 30900 | 0 | 171 | 6 | 50800 | 83540 | 8322- 8331 |
| Matagorda | 28.95 | 96.17 | 671 | 153 | 21500 | 0 | 469 | 18 | 34500 | 57341 | 8348- 8352 |
| Matagorda | 29.07 | 95.90 | 2006 | 648 | 27061 | 0 | 854 | 0 | 46718 | 78600 | 9195 |
| Matagorda | 29.07 | 95.90 | 1040 | 187 | 39146 | 0 | 511 | 45 | 62481 | 103600 | 9195 |
| Matagorda | 29.07 | 95.90 | 2890 | 401 | 35000 | 0 | 279 | 0 | 60200 | 98836 | 8897- 8902 |

Table 3a (continued)

| County | Latitude | Longitude | Ca | Mg | Na | K | Alkalinity | SO4 | Cl | TDS | Depth (feet) |
|-----------|----------|-----------|------|-----|-------|-----|------------|-----|-------|--------|--------------|
| Matagorda | 29.07 | 95.90 | 2380 | 23 | 33000 | 0 | 263 | 360 | 54800 | 90938 | 8980-8992 |
| Matagorda | 29.07 | 95.90 | 1710 | 349 | 40600 | 0 | 260 | 78 | 66600 | 109673 | 8920-8928 |
| Jefferson | 30.01 | 94.41 | 2044 | 48 | 36568 | 0 | 244 | 0 | 59929 | 99585 | 7266-7280 |
| Jefferson | 29.97 | 94.13 | 426 | 79 | 11903 | 0 | 537 | 62 | 19000 | 32007 | 7788 |
| Jefferson | 29.97 | 94.13 | 816 | 136 | 16290 | 0 | 287 | 1 | 26800 | 44330 | 7723 |
| Jefferson | 29.97 | 94.13 | 348 | 152 | 11869 | 0 | 659 | 80 | 18900 | 32008 | 7835 |
| Jefferson | 30.07 | 94.13 | 2756 | 606 | 35540 | 0 | 79 | 1 | 61400 | 100382 | 6778 |
| Jefferson | 30.07 | 94.13 | 1475 | 192 | 17670 | 0 | 43 | 1 | 30400 | 49781 | 6779 |
| Jefferson | 30.07 | 94.13 | 1568 | 238 | 20290 | 0 | 98 | 1 | 34700 | 56895 | 6778 |
| Jefferson | 30.02 | 94.40 | 2835 | 764 | 40100 | 0 | 27 | 11 | 69100 | 112837 | 6055 |
| Jefferson | 30.02 | 94.40 | 2970 | 611 | 38232 | 0 | 221 | 103 | 65794 | 107931 | 6038 |
| Jefferson | 29.80 | 94.28 | 4655 | 906 | 38383 | 0 | 908 | 96 | 69502 | 114450 | 8521 |
| Jefferson | 29.80 | 94.28 | 2658 | 211 | 30692 | 0 | 605 | 79 | 52268 | 86513 | 8825 |
| Jefferson | 29.60 | 94.42 | 480 | 100 | 22600 | 146 | 1130 | 14 | 33800 | 57200 | 10421-10434 |
| Jefferson | 28.00 | 97.25 | 190 | 31 | 10500 | 80 | 880 | 75 | 15500 | 27900 | 10906-10914 |
| Jefferson | 29.95 | 94.00 | 2248 | 272 | 28200 | 0 | 6751 | 250 | 45200 | 83131 | 10606-10616 |
| Jefferson | 29.95 | 94.00 | 2685 | 216 | 30080 | 0 | 158 | 134 | 48800 | 82258 | 10642-10650 |
| Jefferson | 29.92 | 94.00 | 2455 | 233 | 23860 | 0 | 660 | 48 | 41400 | 68790 | 11276-11286 |
| Jefferson | 29.92 | 94.00 | 1288 | 160 | 14496 | 0 | 530 | 19 | 25115 | 41878 | 10946-10956 |

Table 3b. Major ion chemistry from Frio Formation, Northcentral region. Ionic concentrations in mg/L. Data from Kreitler and Richter, 1986.

| County | Latitude | Longitude | Ca | Mg | Na | K | Alkalinity | SO4 | Cl | TDS | Depth (feet) |
|----------|----------|-----------|------|-----|-------|-----|------------|-----|-------|--------|--------------|
| Wharton | 29.15 | 96.05 | 2124 | 607 | 29890 | 0 | 390 | 0 | 51420 | 84621 | 5542-5546 |
| Wharton | 29.15 | 96.05 | 1470 | 638 | 32490 | 0 | 425 | 0 | 54340 | 89613 | 5543-5548 |
| Wharton | 29.17 | 96.08 | 2352 | 376 | 30583 | 0 | 817 | 1 | 52000 | 86129 | 5535 |
| Wharton | 29.08 | 96.37 | 870 | 109 | 19957 | 0 | 390 | 1 | 32400 | 53727 | 5814 |
| Wharton | 29.25 | 96.20 | 2660 | 220 | 23100 | 0 | 290 | 1 | 41000 | 67271 | 5500 |
| Jackson | 28.78 | 96.57 | 987 | 193 | 23200 | 212 | 245 | 0 | 41100 | 65937 | 6419 |
| Jackson | 28.78 | 96.57 | 956 | 187 | 24500 | 219 | 240 | 0 | 42400 | 68502 | 6412 |
| Jackson | 28.78 | 96.57 | 1023 | 178 | 23700 | 226 | 215 | 0 | 42400 | 67742 | 6258 |
| Jackson | 29.13 | 96.67 | 8260 | 730 | 33500 | 767 | 59 | 4 | 68100 | 114000 | 9246-9268 |
| Jackson | 29.02 | 96.50 | 652 | 123 | 23319 | 0 | 442 | 1 | 37250 | 61787 | 6633 |
| Jackson | 29.03 | 96.50 | 934 | 232 | 23290 | 0 | 488 | 15 | 38000 | 62959 | 5483 |
| Jackson | 28.92 | 96.42 | 1314 | 307 | 23616 | 0 | 305 | 1 | 39500 | 65043 | 5237 |
| Jackson | 28.88 | 96.50 | 1680 | 119 | 21598 | 0 | 183 | 1 | 38000 | 61581 | 5228 |
| Jackson | 28.83 | 96.50 | 900 | 170 | 25643 | 0 | 293 | 12 | 41500 | 68518 | 6398 |
| Jackson | 28.92 | 96.73 | 1832 | 93 | 21271 | 0 | 262 | 1 | 36200 | 59659 | 4602 |
| Jackson | 28.92 | 96.73 | 1052 | 68 | 18229 | 0 | 344 | 6 | 30000 | 49699 | 5451 |
| Jackson | 28.76 | 96.65 | 1150 | 192 | 22900 | 0 | 207 | 0 | 37800 | 63268 | 5731-5763 |
| Jackson | 28.76 | 96.65 | 1300 | 190 | 23300 | 0 | 182 | 0 | 38700 | 63700 | 5737-5753 |
| Jackson | 28.77 | 96.64 | 1200 | 210 | 21220 | 0 | 187 | 0 | 35420 | 58354 | 5592-5596 |
| Jackson | 28.77 | 96.64 | 1200 | 275 | 21590 | 0 | 189 | 6 | 36680 | 60000 | 5592-5602 |
| Jackson | 28.77 | 96.65 | 1200 | 319 | 9547 | 0 | 74 | 7 | 17731 | 28884 | 5590-5593 |
| Jackson | 28.77 | 96.65 | 1049 | 376 | 9602 | 0 | 48 | 5 | 17731 | 28821 | 5756-5757 |
| Jackson | 28.77 | 96.64 | 1096 | 271 | 21849 | 0 | 184 | 6 | 36314 | 59723 | 5583-5593 |
| Jackson | 28.77 | 96.64 | 1080 | 250 | 20780 | 0 | 209 | 6 | 35260 | 57669 | 5583-5593 |
| Jackson | 28.77 | 96.65 | 2890 | 464 | 13660 | 0 | 64 | 4 | 27830 | 45030 | 5593-5760 |
| Jackson | 28.84 | 96.53 | 1090 | 325 | 21780 | 0 | 255 | 0 | 36830 | 60333 | 5245-5279 |
| Jackson | 28.89 | 96.48 | 710 | 153 | 24334 | 0 | 415 | 123 | 38800 | 67500 | 6796-6798 |
| Jackson | 28.89 | 96.48 | 850 | 158 | 22425 | 0 | 329 | 41 | 36200 | 63500 | 5675-5678 |
| Jackson | 28.91 | 96.66 | 1100 | 203 | 22954 | 0 | 244 | 129 | 37600 | 53000 | 4715-4740 |
| Jackson | 28.95 | 96.61 | 1060 | 21 | 22236 | 0 | 201 | 4 | 36000 | 62500 | 4985-5005 |
| Jackson | 29.02 | 96.47 | 1400 | 235 | 16200 | 0 | 142 | 10 | 50500 | 66700 | 4833-4860 |
| Victoria | 28.63 | 96.87 | 1482 | 277 | 24112 | 144 | 208 | 0 | 40800 | 67234 | 4790-4810 |
| Victoria | 28.63 | 96.86 | 1120 | 170 | 22917 | 140 | 232 | 0 | 37850 | 62484 | 5558-5562 |
| Victoria | 28.58 | 96.95 | 1680 | 230 | 24900 | 0 | 249 | 20 | 41800 | 68918 | 4548-4553 |
| Victoria | 28.58 | 96.95 | 814 | 246 | 22400 | 0 | 755 | 43 | 36200 | 60467 | 4536-4556 |
| Victoria | 28.58 | 96.95 | 754 | 280 | 26300 | 0 | 293 | 0 | 42500 | 70141 | 4489-4492 |
| Victoria | 28.58 | 96.95 | 2260 | 327 | 22300 | 0 | 145 | 0 | 39200 | 64248 | 3500-3512 |
| Victoria | 28.62 | 96.89 | 1112 | 180 | 23125 | 0 | 390 | 0 | 31942 | 56749 | 5484-5494 |
| Victoria | 28.62 | 96.89 | 1280 | 170 | 22943 | 0 | 292 | 60 | 37942 | 62687 | 5478-5493 |
| Victoria | 28.62 | 96.87 | 1202 | 204 | 22955 | 0 | 330 | 0 | 37926 | 62617 | 5734-5738 |
| Victoria | 28.62 | 96.87 | 2035 | 266 | 23262 | 0 | 188 | 0 | 39411 | 65162 | 4204-4208 |
| Victoria | 28.62 | 96.88 | 1302 | 170 | 22391 | 0 | 2183 | 0 | 37220 | 61266 | 5589-5591 |

Table 3b (continued)

| County | Latitude | Longitude | Ca | Mg | Na | K | Alkalinity | SO4 | Cl | TDS | Depth (feet) |
|----------|----------|-----------|------|-----|-------|---|------------|-----|-------|-------|--------------|
| Victoria | 28.63 | 96.87 | 132 | 19 | 8960 | 0 | 519 | 97 | 13730 | 23457 | 8322-8328 |
| Victoria | 28.63 | 96.87 | 1165 | 145 | 20895 | 0 | 293 | 5 | 34527 | 57030 | 7545-7548 |
| Victoria | 28.63 | 96.87 | 1425 | 168 | 19540 | 0 | 235 | 25 | 32980 | 54373 | 6940-6950 |
| Victoria | 28.63 | 96.87 | 1186 | 365 | 22752 | 0 | 209 | 20 | 38106 | 62638 | 4768-4773 |
| Victoria | 28.63 | 96.87 | 1150 | 333 | 22648 | 0 | 140 | 14 | 37833 | 62118 | 4768-4773 |
| Victoria | 28.63 | 96.87 | 1200 | 435 | 19280 | 0 | 245 | 8 | 32970 | 54138 | 4767-4772 |
| Victoria | 28.63 | 96.87 | 1530 | 395 | 21340 | 0 | 115 | 10 | 36690 | 60080 | 4768-4773 |
| Victoria | 28.63 | 96.87 | 1170 | 216 | 21600 | 0 | 462 | 0 | 35747 | 59195 | 5745-5747 |
| Victoria | 28.63 | 96.87 | 1300 | 206 | 22748 | 0 | 391 | 0 | 37750 | 62395 | 5745-5748 |
| Victoria | 28.63 | 96.87 | 2692 | 447 | 19858 | 0 | 125 | 0 | 36624 | 59746 | 3495-3505 |
| Victoria | 28.63 | 96.87 | 1305 | 390 | 21275 | 0 | 210 | 5 | 36120 | 59305 | 4760-4775 |
| Victoria | 28.63 | 96.87 | 1312 | 208 | 22720 | 0 | 354 | 0 | 37750 | 62344 | 5742-5744 |
| Victoria | 28.63 | 96.87 | 1288 | 206 | 21428 | 0 | 298 | 0 | 35758 | 58978 | 5742-5744 |
| Victoria | 28.63 | 96.87 | 1466 | 186 | 22403 | 0 | 214 | 0 | 37557 | 61826 | 6029-6041 |
| Victoria | 28.63 | 96.88 | 1456 | 194 | 22703 | 0 | 244 | 115 | 37942 | 62654 | 6139-6144 |
| Victoria | 28.63 | 96.87 | 1260 | 0 | 23316 | 0 | 439 | 5 | 37942 | 62962 | 5474-5486 |
| Victoria | 28.64 | 96.87 | 1305 | 206 | 21393 | 0 | 240 | 0 | 35768 | 58912 | 5743-5746 |
| Victoria | 28.68 | 96.82 | 1671 | 272 | 22801 | 0 | 237 | 0 | 38766 | 63510 | 4767-4774 |
| Victoria | 28.69 | 96.83 | 1705 | 275 | 22771 | 0 | 269 | 0 | 38770 | 63810 | 4754-4778 |
| Victoria | 28.69 | 97.13 | 770 | 160 | 16610 | 0 | 230 | 0 | 27300 | 45060 | 4821-4825 |
| Victoria | 28.73 | 97.08 | 1638 | 313 | 22294 | 0 | 219 | 5 | 38100 | 62569 | 3116-3126 |
| Victoria | 28.75 | 96.83 | 2324 | 329 | 25750 | 0 | 0 | 26 | 43890 | 72319 | 5874-5878 |
| Victoria | 28.75 | 96.83 | 1980 | 224 | 23880 | 0 | 103 | 11 | 40910 | 67108 | 5614-5619 |
| Victoria | 28.89 | 97.06 | 1338 | 188 | 13320 | 0 | 94 | 48 | 23360 | 38348 | 3515 |

Table 3c. Major ion chemistry from Frio Formation, Southcentral region. Ionic concentrations in mg/L.
Data from Kreitler and Richter, 1986.

| County | Latitude | Longitude | Ca | Mg | Na | K | Alkalinity | SO4 | Cl | TDS | Depth (feet) |
|-----------|----------|-----------|-------|-----|-------|-----|------------|------|-------|--------|--------------|
| Jim Wells | 27.87 | 98.00 | 133 | 15 | 4828 | 0 | 409 | 263 | 7300 | 12984 | 4449-4480 |
| Jim Wells | 27.68 | 97.95 | 10643 | 698 | 23687 | 0 | 153 | 0 | 57400 | 92581 | 6133-6141 |
| Jim Wells | 27.68 | 97.95 | 45 | 19 | 7713 | 0 | 1274 | 0 | 11150 | 20387 | 4061-4094 |
| Jim Wells | 27.66 | 97.95 | 8168 | 234 | 25549 | 0 | 201 | 0 | 54499 | 88649 | 6196-6221 |
| Goliad | 28.56 | 97.37 | 740 | 122 | 12757 | 0 | 720 | 30 | 20900 | 35269 | 3513-3522 |
| Goliad | 28.56 | 97.37 | 860 | 134 | 12938 | 0 | 625 | 6 | 21500 | 36063 | 3456-3470 |
| Goliad | 28.56 | 97.37 | 40 | 5 | 2754 | 0 | 1490 | 220 | 3190 | 7795 | 3193-3199 |
| Goliad | 28.57 | 97.29 | 100 | 12 | 5367 | 0 | 1560 | 136 | 7480 | 14655 | 5592-5597 |
| Goliad | 28.57 | 97.29 | 96 | 18 | 5439 | 0 | 1600 | 120 | 7590 | 14863 | 5592-5597 |
| Goliad | 28.57 | 97.29 | 376 | 146 | 13969 | 0 | 720 | 24 | 22200 | 37435 | 5088-5093 |
| Goliad | 28.62 | 97.29 | 580 | 159 | 15225 | 0 | 537 | 82 | 24600 | 41183 | 4527-4532 |
| Goliad | 28.62 | 97.29 | 700 | 172 | 16143 | 0 | 395 | 15 | 26400 | 43825 | 4516-4521 |
| Goliad | 28.74 | 97.41 | 490 | 195 | 9205 | 0 | 220 | 0 | 15500 | 25610 | 3042-3047 |
| Goliad | 28.74 | 97.41 | 650 | 210 | 10586 | 0 | 317 | 0 | 17900 | 29663 | 3336-3350 |
| Goliad | 28.74 | 97.41 | 629 | 230 | 11333 | 0 | 323 | 0 | 19100 | 31615 | 3678-3692 |
| Bee | 28.38 | 97.45 | 210 | 290 | 23500 | 0 | 0 | 0 | 37500 | 61500 | 5032 |
| Aransas | 28.10 | 96.98 | 460 | 50 | 10500 | 112 | 490 | 7 | 17150 | 28400 | 11204-11250 |
| Aransas | 28.08 | 97.13 | 6320 | 482 | 30544 | 0 | 409 | 1 | 59720 | 98081 | 8352-8362 |
| Aransas | 28.27 | 96.87 | 130 | 2 | 6700 | 47 | 1 | 5 | 24300 | 40500 | 9506-9518 |
| Aransas | 27.78 | 97.45 | 315 | 17 | 8400 | 122 | 580 | 17 | 13050 | 22400 | 10904-10960 |
| Aransas | 27.78 | 97.45 | 330 | 29 | 8400 | 130 | 540 | 49 | 13400 | 22900 | 11697-11712 |
| Aransas | 28.23 | 96.83 | 30 | 5 | 7050 | 49 | 2040 | 86 | 8700 | 16600 | 9203-9240 |
| Calhoun | 28.20 | 96.53 | 450 | 111 | 27200 | 171 | 574 | 24 | 41500 | 70100 | 9293-9309 |
| Calhoun | 28.28 | 96.67 | 2100 | 170 | 22600 | 130 | 120 | 5 | 42050 | 59800 | 8882-8892 |
| Calhoun | 28.28 | 96.67 | 740 | 105 | 17100 | 110 | 710 | 23 | 27800 | 49100 | 8780-8790 |
| Calhoun | 28.28 | 96.67 | 185 | 31 | 11200 | 85 | 1300 | 45 | 17050 | 31000 | 8796-8802 |
| Calhoun | 28.63 | 96.82 | 984 | 225 | 24154 | 0 | 311 | 1 | 39500 | 65175 | 5450 |
| Calhoun | 28.57 | 96.84 | 1320 | 163 | 22379 | 0 | 138 | 105 | 63847 | 39671 | 6750-8250 |
| Calhoun | 28.57 | 96.84 | 2000 | 100 | 80000 | 0 | 0 | 1000 | 99400 | 175700 | 6750-7500 |
| Calhoun | 28.56 | 96.87 | 2558 | 194 | 25404 | 0 | 113 | 0 | 44250 | 72519 | 5067-5072 |
| Calhoun | 28.56 | 96.87 | 3549 | 116 | 24889 | 0 | 120 | 0 | 45000 | 73683 | 7412-7419 |
| Calhoun | 28.57 | 96.52 | 80 | 60 | 4120 | 0 | 1705 | 135 | 5580 | 11680 | 8721-8727 |
| Calhoun | 28.57 | 96.53 | 30 | 8 | 3505 | 32 | 1438 | 62 | 4630 | 9705 | 8754-8804 |
| Calhoun | 28.58 | 96.73 | 59 | 39 | 6245 | 0 | 3739 | 245 | 7500 | 17827 | 8988-9002 |
| Calhoun | 28.58 | 96.73 | 62 | 39 | 5872 | 0 | 2392 | 330 | 7650 | 16345 | 8968-8970 |
| Calhoun | 28.58 | 96.73 | 55 | 52 | 5597 | 0 | 2778 | 230 | 7100 | 15812 | 8989-9002 |
| Calhoun | 28.58 | 96.73 | 22 | 19 | 5296 | 0 | 2814 | 150 | 6520 | 14821 | 8996-8999 |
| Calhoun | 28.58 | 96.73 | 22 | 19 | 5675 | 0 | 3092 | 170 | 6930 | 15908 | 9004-9011 |
| Calhoun | 28.59 | 96.73 | 172 | 73 | 5573 | 0 | 311 | 350 | 8680 | 15159 | 5640-5649 |
| Calhoun | 28.59 | 96.73 | 154 | 36 | 5054 | 0 | 476 | 500 | 7380 | 13600 | 5688-5697 |
| Calhoun | 28.59 | 96.73 | 1911 | 304 | 23804 | 0 | 115 | 102 | 40200 | 66436 | 5710-5720 |
| Calhoun | 28.61 | 96.86 | 2549 | 380 | 21669 | 0 | 135 | 0 | 39000 | 63733 | 5459-5466 |

↓

Table 3c (continued)

| County | Latitude | Longitude | Ca | Mg | Na | K | Alkalinity | SO4 | Cl | TDS | Depth (feet) |
|--------------|----------|-----------|------|-----|-------|-----|------------|-----|-------|-------|--------------|
| Calhoun | 28.61 | 96.86 | 1275 | 160 | 22380 | 0 | 207 | 23 | 37100 | 61145 | 5462-5470 |
| Calhoun | 28.61 | 96.86 | 2060 | 182 | 21045 | 0 | 397 | 0 | 36400 | 60084 | 5425 |
| Calhoun | 28.62 | 96.88 | 911 | 238 | 22930 | 0 | 173 | 6 | 37600 | 61858 | 5435-7536 |
| Calhoun | 28.62 | 96.88 | 913 | 177 | 23230 | 0 | 321 | 6 | 37800 | 62447 | 5435-7536 |
| Calhoun | 28.62 | 96.88 | 921 | 192 | 23581 | 0 | 321 | 6 | 38400 | 63421 | 5435-7536 |
| Calhoun | 28.62 | 96.87 | 962 | 167 | 24146 | 0 | 272 | 6 | 39300 | 64853 | 4769-5499 |
| Calhoun | 28.62 | 96.66 | 212 | 26 | 5743 | 0 | 1793 | 452 | 7940 | 16166 | 7945-7951 |
| Calhoun | 28.62 | 96.66 | 126 | 21 | 6304 | 0 | 1952 | 406 | 8580 | 17389 | 7896-7902 |
| Calhoun | 28.63 | 96.71 | 1041 | 140 | 15973 | 0 | 702 | 0 | 26500 | 44318 | 7932-7938 |
| Calhoun | 28.63 | 96.71 | 57 | 90 | 5707 | 0 | 2790 | 0 | 7550 | 16194 | 8390-8401 |
| Calhoun | 28.63 | 96.71 | 72 | 164 | 7396 | 0 | 3185 | 260 | 9975 | 21052 | 8613-8619 |
| Calhoun | 28.63 | 96.71 | 206 | 109 | 11353 | 0 | 1074 | 112 | 17500 | 30354 | 9421-9434 |
| Calhoun | 28.63 | 96.68 | 52 | 30 | 2307 | 0 | 2980 | 456 | 1670 | 7495 | 8924-8938 |
| Calhoun | 28.63 | 96.69 | 18 | 2 | 2259 | 0 | 2603 | 200 | 1620 | 6905 | 9036-9048 |
| Calhoun | 28.63 | 96.69 | 2728 | 963 | 8720 | 0 | 328 | 300 | 20700 | 33739 | 9224-9284 |
| Calhoun | 28.64 | 96.68 | 127 | 17 | 11707 | 0 | 1279 | 135 | 17500 | 30765 | 8858-8890 |
| Calhoun | 28.64 | 96.68 | 678 | 109 | 21312 | 0 | 514 | 24 | 34100 | 56737 | 8966-8971 |
| Calhoun | 28.67 | 96.41 | 26 | 8 | 4330 | 109 | 1871 | 128 | 5660 | 12132 | 7806-7810 |
| Calhoun | 28.67 | 96.41 | 280 | 55 | 4460 | 75 | 968 | 136 | 6935 | 12909 | 7806-7810 |
| San Patricio | 28.02 | 97.25 | 42 | 9 | 5650 | 33 | 800 | 66 | 7600 | 15900 | 10965-10983 |
| San Patricio | 28.02 | 97.25 | 45 | 8 | 7170 | 32 | 1720 | 64 | 9400 | 18600 | 10521-10535 |
| San Patricio | 27.90 | 97.37 | 2925 | 580 | 29282 | 0 | 148 | 1 | 51783 | 84719 | 5670 |
| San Patricio | 27.90 | 97.42 | 101 | 21 | 10000 | 62 | 915 | 40 | 15100 | 27500 | 10728 |
| San Patricio | 27.90 | 97.42 | 134 | 22 | 9000 | 59 | 939 | 46 | 13400 | 24600 | 10670 |
| San Patricio | 27.90 | 97.42 | 89 | 15 | 6500 | 68 | 1040 | 110 | 9270 | 17900 | 11528 |
| San Patricio | 27.90 | 97.42 | 101 | 18 | 7500 | 62 | 932 | 59 | 10700 | 20300 | 11050 |
| San Patricio | 27.90 | 97.42 | 54 | 9 | 5375 | 43 | 775 | 75 | 7400 | 14700 | 11480 |
| San Patricio | 27.90 | 97.42 | 47 | 9 | 6250 | 46 | 1213 | 67 | 8200 | 16600 | 11180 |
| San Patricio | 28.00 | 97.22 | 42 | 9 | 6500 | 51 | 858 | 54 | 8700 | 17500 | 10550 |
| San Patricio | 27.97 | 97.33 | 370 | 56 | 11750 | 44 | 575 | 26 | 18700 | 32400 | 12120 |
| San Patricio | 27.97 | 97.33 | 330 | 48 | 13250 | 72 | 200 | 42 | 21000 | 36300 | 11880 |
| San Patricio | 27.90 | 97.42 | 2500 | 455 | 29500 | 215 | 270 | 13 | 51700 | 85400 | 4900 |
| San Patricio | 27.90 | 97.42 | 3040 | 475 | 22750 | 77 | 97 | 67 | 42800 | 69800 | 3350 |
| San Patricio | 27.90 | 97.42 | 2500 | 590 | 28500 | 152 | 189 | 15 | 50600 | 83300 | 4600 |
| San Patricio | 27.90 | 97.42 | 2880 | 340 | 25250 | 125 | 113 | 50 | 45100 | 74600 | 5790 |
| San Patricio | 27.90 | 97.42 | 200 | 31 | 9250 | 70 | 278 | 22 | 14000 | 24800 | 10320 |
| San Patricio | 28.02 | 97.25 | 42 | 9 | 5650 | 33 | 800 | 66 | 7600 | 15900 | 10965-10983 |
| San Patricio | 28.02 | 97.25 | 45 | 8 | 7170 | 32 | 1720 | 64 | 9400 | 18600 | 10521-10535 |
| San Patricio | 27.98 | 97.30 | 484 | 29 | 31300 | 173 | 237 | 270 | 46100 | 77800 | 9656- 9695 |
| San Patricio | 27.98 | 97.30 | 24 | 12 | 8100 | 41 | 1220 | 9 | 10900 | 19900 | 9660- 9702 |
| San Patricio | 27.98 | 97.30 | 282 | 22 | 7550 | 73 | 687 | 15 | 12150 | 20700 | 10693-11134 |
| San Patricio | 27.98 | 97.30 | 398 | 46 | 12690 | 92 | 820 | 9 | 19000 | 32500 | 11074-13162 |

99

↓

Table 3c (continued)

| County | Latitude | Longitude | Ca | Mg | Na | K | Alkalinity | SO4 | Cl | TDS | Depth (feet) |
|--------------|----------|-----------|------|-----|-------|-----|------------|------|-------|--------|--------------|
| San Patricio | 27.98 | 97.30 | 392 | 136 | 8924 | 89 | 1708 | 365 | 13500 | 25015 | 11962-11994 |
| San Patricio | 27.98 | 97.30 | 270 | 31 | 7500 | 0 | 970 | 60 | 11600 | 20465 | 12572-12582 |
| San Patricio | 27.99 | 97.30 | 330 | 48 | 13250 | 72 | 200 | 42 | 21000 | 36300 | 11880 |
| San Patricio | 27.99 | 97.30 | 370 | 56 | 11750 | 44 | 575 | 26 | 18700 | 32400 | 12001 |
| San Patricio | 27.87 | 97.30 | 156 | 23 | 10500 | 78 | 1120 | 52 | 15200 | 27400 | 10665-10745 |
| San Patricio | 27.87 | 97.30 | 48 | 8 | 7330 | 40 | 2760 | 37 | 8900 | 16900 | 9715- 9724 |
| San Patricio | 27.87 | 97.30 | 31 | 8 | 7860 | 55 | 1720 | 4 | 10200 | 19400 | 9480- 9490 |
| San Patricio | 27.87 | 97.30 | 64 | 37 | 4763 | 0 | 2013 | 260 | 6300 | 13485 | 12246-12263 |
| San Patricio | 27.87 | 97.30 | 60 | 37 | 9895 | 0 | 1574 | 45 | 14700 | 26360 | 10720-10735 |
| San Patricio | 27.87 | 97.30 | 88 | 24 | 7367 | 0 | 1488 | 109 | 10700 | 19805 | 11020-11080 |
| San Patricio | 27.87 | 97.30 | 3480 | 464 | 23541 | 0 | 506 | 10 | 43600 | 71625 | 9049- 9051 |
| San Patricio | 27.87 | 97.30 | 3760 | 293 | 29976 | 0 | 37 | 123 | 53800 | 88050 | 8848- 8857 |
| San Patricio | 27.87 | 97.30 | 3200 | 0 | 34592 | 0 | 0 | 1 | 64800 | 105595 | 8713- 8726 |
| San Patricio | 27.87 | 97.30 | 72 | 5 | 6010 | 0 | 1403 | 47 | 8600 | 16155 | 11444-11486 |
| San Patricio | 27.87 | 97.30 | 70 | 37 | 6366 | 0 | 1513 | 204 | 9100 | 17325 | 11520-11537 |
| San Patricio | 27.87 | 97.30 | 420 | 98 | 14469 | 0 | 586 | 56 | 23100 | 38790 | 10079-10306 |
| San Patricio | 27.87 | 97.30 | 120 | 32 | 8259 | 0 | 1427 | 73 | 12400 | 22430 | 10821-10844 |
| San Patricio | 27.87 | 97.30 | 100 | 18 | 5550 | 0 | 2111 | 104 | 7500 | 15390 | 11135-11220 |
| San Patricio | 27.87 | 97.30 | 101 | 21 | 10000 | 62 | 915 | 40 | 15100 | 27500 | 10667 |
| San Patricio | 27.87 | 97.30 | 134 | 22 | 9000 | 59 | 939 | 46 | 13400 | 24600 | 10667 |
| San Patricio | 27.87 | 97.30 | 89 | 15 | 6500 | 68 | 1104 | 110 | 9270 | 17900 | 11526 |
| San Patricio | 27.87 | 97.30 | 101 | 18 | 7500 | 62 | 932 | 59 | 10700 | 20300 | 11047 |
| San Patricio | 27.87 | 97.31 | 54 | 9 | 5375 | 43 | 775 | 75 | 7400 | 14700 | 11477 |
| San Patricio | 27.87 | 97.31 | 47 | 9 | 6250 | 46 | 1213 | 67 | 8200 | 16600 | 11175 |
| San Patricio | 27.99 | 97.30 | 159 | 4 | 5360 | 233 | 1678 | 1130 | 5380 | 14000 | 13365-13500 |
| San Patricio | 27.99 | 97.30 | 296 | 24 | 9340 | 198 | 737 | 172 | 14710 | 25480 | 13365-13500 |
| San Patricio | 25.97 | 97.23 | 27 | 9 | 7900 | 36 | 1750 | 58 | 10300 | 21000 | 10475-10490 |
| San Patricio | 28.03 | 97.38 | 2232 | 452 | 27010 | 0 | 123 | 1 | 46900 | 76718 | 4889- 4934 |
| San Patricio | 27.88 | 97.43 | 3170 | 370 | 29100 | 0 | 239 | 1 | 51400 | 84360 | 5008- 5016 |
| San Patricio | 27.88 | 97.44 | 1239 | 586 | 29790 | 0 | 197 | 6 | 49730 | 81550 | 5640- 5647 |
| San Patricio | 27.88 | 97.44 | 2360 | 393 | 29500 | 0 | 200 | 0 | 50600 | 83074 | 5612- 5655 |
| San Patricio | 27.88 | 97.44 | 1184 | 599 | 30294 | 0 | 191 | 6 | 50450 | 82727 | 5581- 5636 |
| San Patricio | 27.88 | 97.44 | 1156 | 500 | 30195 | 0 | 230 | 5 | 50041 | 82145 | 5603- 5624 |
| San Patricio | 27.88 | 97.44 | 3420 | 247 | 20800 | 0 | 434 | 60 | 38700 | 63728 | 6382- 6384 |
| San Patricio | 27.88 | 97.44 | 2870 | 281 | 25500 | 0 | 575 | 1 | 45100 | 74564 | 5942- 5944 |
| San Patricio | 27.88 | 97.44 | 1175 | 737 | 30742 | 0 | 129 | 6 | 51576 | 84379 | 6736- 6740 |
| San Patricio | 27.88 | 97.44 | 3184 | 475 | 29464 | 0 | 136 | 0 | 52380 | 85707 | 4987- 4992 |
| San Patricio | 27.88 | 97.44 | 1165 | 464 | 28544 | 0 | 448 | 6 | 47175 | 77803 | 5865- 5867 |
| San Patricio | 27.88 | 97.44 | 1175 | 562 | 26743 | 0 | 230 | 13 | 44822 | 73574 | 5939- 5942 |
| San Patricio | 27.88 | 97.44 | 2401 | 571 | 27405 | 0 | 274 | 0 | 48015 | 78741 | 5939- 5942 |
| San Patricio | 28.03 | 97.38 | 2232 | 485 | 27273 | 0 | 123 | 1 | 47400 | 77514 | 4366- 4371 |
| San Patricio | 28.03 | 97.38 | 2199 | 435 | 27276 | 0 | 123 | 0 | 47200 | 77233 | 4350- 4357 |

Table 3c (continued)

| County | Latitude | Longitude | Ca | Mg | Na | K | Alkalinity | SO4 | Cl | TDS | Depth (feet) |
|--------------|----------|-----------|------|------|-------|-----|------------|-----|-------|-------|--------------|
| San Patricio | 28.04 | 97.38 | 2202 | 381 | 26787 | 0 | 111 | 1 | 46300 | 75782 | 5595- 5745 |
| San Patricio | 27.90 | 97.27 | 760 | 68 | 2814 | 0 | 49 | 433 | 5500 | 9660 | 8060- 8080 |
| San Patricio | 27.90 | 97.27 | 1712 | 95 | 13931 | 0 | 354 | 287 | 24400 | 40779 | 8120- 8140 |
| San Patricio | 27.90 | 97.27 | 526 | 12 | 5550 | 0 | 183 | 300 | 9100 | 15645 | 7967- 7980 |
| San Patricio | 27.90 | 97.27 | 232 | 18 | 2751 | 0 | 37 | 280 | 4420 | 7792 | 8020- 8040 |
| San Patricio | 27.90 | 97.27 | 2404 | 58 | 7004 | 0 | 214 | 370 | 14850 | 24900 | 9120- 9140 |
| San Patricio | 27.90 | 97.27 | 8088 | 201 | 19918 | 0 | 146 | 0 | 45600 | 73953 | 9120- 9140 |
| San Patricio | 27.91 | 97.27 | 1190 | 122 | 17984 | 0 | 988 | 70 | 29600 | 49954 | 6736- 6746 |
| San Patricio | 27.92 | 97.27 | 608 | 302 | 24888 | 0 | 470 | 0 | 40100 | 66368 | 6017- 6022 |
| San Patricio | 27.98 | 97.27 | 1884 | 170 | 14645 | 0 | 231 | 80 | 26250 | 43260 | 8386- 8391 |
| San Patricio | 27.98 | 97.27 | 97 | 77 | 9392 | 0 | 2097 | 235 | 13400 | 25383 | 9978- 9984 |
| San Patricio | 27.88 | 97.43 | 2571 | 588 | 29918 | 0 | 265 | 7 | 52300 | 85649 | 5644- 5647 |
| San Patricio | 27.88 | 97.43 | 1732 | 387 | 28983 | 0 | 495 | 0 | 48650 | 80247 | 5652- 5674 |
| San Patricio | 27.88 | 97.44 | 2657 | 503 | 30084 | 0 | 365 | 7 | 52400 | 86016 | 5652- 5674 |
| San Patricio | 27.88 | 97.43 | 891 | 0 | 20872 | 0 | 0 | 198 | 33645 | 55737 | 5587- 5607 |
| San Patricio | 27.88 | 97.43 | 3060 | 359 | 29400 | 0 | 134 | 0 | 51800 | 84769 | 3310- 5655 |
| San Patricio | 27.88 | 97.43 | 2427 | 586 | 26566 | 0 | 221 | 0 | 46851 | 76726 | 4987- 4992 |
| San Patricio | 27.88 | 97.43 | 2767 | 729 | 30027 | 0 | 143 | 0 | 53253 | 73000 | 5627- 5630 |
| San Patricio | 27.88 | 97.44 | 2310 | 399 | 29800 | 0 | 138 | 0 | 51200 | 83865 | 5620- 5624 |
| San Patricio | 27.88 | 97.44 | 2870 | 464 | 32000 | 0 | 97 | 70 | 50700 | 86383 | 5608- 5664 |
| San Patricio | 27.88 | 97.44 | 1221 | 1562 | 29144 | 0 | 127 | 6 | 51576 | 83639 | 4996- 5002 |
| San Patricio | 27.88 | 97.43 | 2890 | 503 | 27500 | 0 | 199 | 0 | 48600 | 79993 | 4991- 4995 |
| Refugio | 28.53 | 97.10 | 2345 | 410 | 24402 | 0 | 110 | 1 | 42900 | 70168 | 4720 |
| Refugio | 28.53 | 97.10 | 2022 | 253 | 24812 | 0 | 122 | 1 | 42500 | 69710 | 4487 |
| Refugio | 28.53 | 97.10 | 1034 | 115 | 25900 | 0 | 256 | 1 | 42000 | 69306 | 5000 |
| Refugio | 28.53 | 97.10 | 1454 | 218 | 25217 | 0 | 211 | 1 | 42000 | 69101 | 5015 |
| Refugio | 28.42 | 97.17 | 626 | 195 | 27758 | 0 | 519 | 1 | 44000 | 73099 | 5459 |
| Refugio | 28.45 | 96.97 | 560 | 112 | 19500 | 177 | 753 | 3 | 31580 | 52731 | 7924- 7926 |
| Refugio | 28.53 | 97.04 | 1084 | 232 | 17173 | 0 | 122 | 0 | 29000 | 47611 | 4525- 4541 |
| Refugio | 28.53 | 97.05 | 2210 | 378 | 25510 | 0 | 244 | 0 | 44200 | 72542 | 5301- 5309 |
| Refugio | 28.49 | 97.00 | 2620 | 175 | 23284 | 0 | 256 | 0 | 40900 | 67235 | 5895- 5898 |
| Refugio | 28.37 | 97.17 | 1126 | 300 | 25473 | 0 | 673 | 0 | 41800 | 69372 | 5502- 5508 |
| Refugio | 28.37 | 97.17 | 1126 | 300 | 22266 | 0 | 417 | 0 | 37000 | 61109 | 5154- 5158 |
| Refugio | 28.38 | 97.18 | 626 | 195 | 27758 | 0 | 519 | 0 | 44000 | 73098 | 5459 |
| Refugio | 28.39 | 97.26 | 2020 | 212 | 21800 | 0 | 292 | 0 | 37700 | 62031 | 6204- 6212 |
| Refugio | 28.42 | 97.26 | 1980 | 174 | 22700 | 0 | 206 | 0 | 38900 | 64023 | 6177- 6192 |
| Refugio | 28.35 | 97.15 | 518 | 43 | 25217 | 0 | 335 | 0 | 42000 | 69133 | 5881 |
| Refugio | 28.35 | 97.15 | 1034 | 115 | 25900 | 0 | 256 | 0 | 42000 | 69305 | 5015 |
| Refugio | 28.29 | 97.22 | 2540 | 97 | 25775 | 0 | 121 | 5 | 44500 | 73038 | 5516- 5876 |
| Refugio | 28.27 | 97.23 | 2657 | 180 | 23293 | 0 | 138 | 19 | 41100 | 67387 | 5911- 5919 |
| Refugio | 28.27 | 97.23 | 2380 | 255 | 25679 | 0 | 174 | 3 | 44500 | 72991 | 4093- 5942 |
| Refugio | 28.28 | 97.23 | 1097 | 218 | 24206 | 0 | 555 | 31 | 39600 | 65707 | 5314- 5316 |

Table 3c (continued)

| County | Latitude | Longitude | Ca | Mg | Na | K | Alkalinity | SO4 | Cl | TDS | Depth (feet) |
|--------------|----------|-----------|------|------|-------|-----|------------|-----|-------|-------|--------------|
| San Patricio | 28.04 | 97.38 | 2202 | 381 | 26787 | 0 | 111 | 1 | 46300 | 75782 | 5595- 5745 |
| San Patricio | 27.90 | 97.27 | 760 | 68 | 2814 | 0 | 49 | 433 | 5500 | 9660 | 8060- 8080 |
| San Patricio | 27.90 | 97.27 | 1712 | 95 | 13931 | 0 | 354 | 287 | 24400 | 40779 | 8120- 8140 |
| San Patricio | 27.90 | 97.27 | 526 | 12 | 5550 | 0 | 183 | 300 | 9100 | 15645 | 7967- 7980 |
| San Patricio | 27.90 | 97.27 | 232 | 18 | 2751 | 0 | 37 | 280 | 4420 | 7792 | 8020- 8040 |
| San Patricio | 27.90 | 97.27 | 2404 | 58 | 7004 | 0 | 214 | 370 | 14850 | 24900 | 9120- 9140 |
| San Patricio | 27.90 | 97.27 | 8088 | 201 | 19918 | 0 | 146 | 0 | 45600 | 73953 | 9120- 9140 |
| San Patricio | 27.91 | 97.27 | 1190 | 122 | 17984 | 0 | 988 | 70 | 29600 | 49954 | 6736- 6746 |
| San Patricio | 27.92 | 97.27 | 608 | 302 | 24888 | 0 | 470 | 0 | 40100 | 66368 | 6017- 6022 |
| San Patricio | 27.98 | 97.27 | 1884 | 170 | 14645 | 0 | 231 | 80 | 26250 | 43260 | 8386- 8391 |
| San Patricio | 27.98 | 97.27 | 97 | 77 | 9392 | 0 | 2097 | 235 | 13400 | 25383 | 9978- 9984 |
| San Patricio | 27.88 | 97.43 | 2571 | 588 | 29918 | 0 | 265 | 7 | 52300 | 85649 | 5644- 5647 |
| San Patricio | 27.88 | 97.43 | 1732 | 387 | 28983 | 0 | 495 | 0 | 48650 | 80247 | 5652- 5674 |
| San Patricio | 27.88 | 97.44 | 2657 | 503 | 30084 | 0 | 365 | 7 | 52400 | 86016 | 5652- 5674 |
| San Patricio | 27.88 | 97.43 | 891 | 0 | 20872 | 0 | 0 | 198 | 33645 | 55737 | 5587- 5607 |
| San Patricio | 27.88 | 97.43 | 3060 | 359 | 29400 | 0 | 134 | 0 | 51800 | 84769 | 3310- 5655 |
| San Patricio | 27.88 | 97.43 | 2427 | 586 | 26566 | 0 | 221 | 0 | 46851 | 76726 | 4987- 4992 |
| San Patricio | 27.88 | 97.43 | 2767 | 729 | 30027 | 0 | 143 | 0 | 53253 | 73000 | 5627- 5630 |
| San Patricio | 27.88 | 97.44 | 2310 | 399 | 29800 | 0 | 138 | 0 | 51200 | 83865 | 5620- 5624 |
| San Patricio | 27.88 | 97.44 | 2870 | 464 | 32000 | 0 | 97 | 70 | 50700 | 86383 | 5608- 5664 |
| San Patricio | 27.88 | 97.44 | 1221 | 1562 | 29144 | 0 | 127 | 6 | 51576 | 83639 | 4996- 5002 |
| San Patricio | 27.88 | 97.43 | 2890 | 503 | 27500 | 0 | 199 | 0 | 48600 | 79993 | 4991- 4995 |
| Refugio | 28.53 | 97.10 | 2345 | 410 | 24402 | 0 | 110 | 1 | 42900 | 70168 | 4720 |
| Refugio | 28.53 | 97.10 | 2022 | 253 | 24812 | 0 | 122 | 1 | 42500 | 69710 | 4487 |
| Refugio | 28.53 | 97.10 | 1034 | 115 | 25900 | 0 | 256 | 1 | 42000 | 69306 | 5000 |
| Refugio | 28.53 | 97.10 | 1454 | 218 | 25217 | 0 | 211 | 1 | 42000 | 69101 | 5015 |
| Refugio | 28.42 | 97.17 | 626 | 195 | 27758 | 0 | 519 | 1 | 44000 | 73099 | 5459 |
| Refugio | 28.45 | 96.97 | 560 | 112 | 19500 | 177 | 753 | 3 | 31580 | 52731 | 7924- 7926 |
| Refugio | 28.53 | 97.04 | 1084 | 232 | 17173 | 0 | 122 | 0 | 29000 | 47611 | 4525- 4541 |
| Refugio | 28.53 | 97.05 | 2210 | 378 | 25510 | 0 | 244 | 0 | 44200 | 72542 | 5301- 5309 |
| Refugio | 28.49 | 97.00 | 2620 | 175 | 23284 | 0 | 256 | 0 | 40900 | 67235 | 5895- 5898 |
| Refugio | 28.37 | 97.17 | 1126 | 300 | 25473 | 0 | 673 | 0 | 41800 | 69372 | 5502- 5508 |
| Refugio | 28.37 | 97.17 | 1126 | 300 | 22266 | 0 | 417 | 0 | 37000 | 61109 | 5154- 5158 |
| Refugio | 28.38 | 97.18 | 626 | 195 | 27758 | 0 | 519 | 0 | 44000 | 73098 | 5459 |
| Refugio | 28.39 | 97.26 | 2020 | 212 | 21800 | 0 | 292 | 0 | 37700 | 62031 | 6204- 6212 |
| Refugio | 28.42 | 97.26 | 1980 | 174 | 22700 | 0 | 206 | 0 | 38900 | 64023 | 6177- 6192 |
| Refugio | 28.35 | 97.15 | 518 | 43 | 25217 | 0 | 335 | 0 | 42000 | 69133 | 5881 |
| Refugio | 28.35 | 97.15 | 1034 | 115 | 25900 | 0 | 256 | 0 | 42000 | 69305 | 5015 |
| Refugio | 28.29 | 97.22 | 2540 | 97 | 25775 | 0 | 121 | 5 | 44500 | 73038 | 5516- 5876 |
| Refugio | 28.27 | 97.23 | 2657 | 180 | 23293 | 0 | 138 | 19 | 41100 | 67387 | 5911- 5919 |
| Refugio | 28.27 | 97.23 | 2380 | 255 | 25679 | 0 | 174 | 3 | 44500 | 72991 | 4093- 5942 |
| Refugio | 28.28 | 97.23 | 1097 | 218 | 24206 | 0 | 555 | 31 | 39600 | 65707 | 5314- 5316 |

↓

Table 3c (continued)

| County | Latitude | Longitude | Ca | Mg | Na | K | Alkalinity | SO4 | Cl | TDS | Depth (feet) |
|---------|----------|-----------|-------|------|-------|-----|------------|-----|--------|--------|--------------|
| Refugio | 28.29 | 97.23 | 189 | 24 | 9051 | 0 | 3529 | 97 | 12250 | 25140 | 8592- 8602 |
| Refugio | 28.29 | 97.23 | 143 | 24 | 8916 | 0 | 3554 | 110 | 11950 | 24702 | 8674- 8682 |
| Refugio | 28.27 | 97.24 | 2457 | 244 | 24632 | 0 | 151 | 6 | 43000 | 70490 | 5870- 5879 |
| Refugio | 28.27 | 97.24 | 2426 | 255 | 25474 | 0 | 117 | 3 | 44300 | 72575 | 5854- 5858 |
| Refugio | 28.27 | 97.24 | 2216 | 269 | 25608 | 0 | 247 | 3 | 44100 | 72443 | 5694- 5702 |
| Refugio | 28.27 | 97.24 | 2657 | 205 | 25306 | 0 | 120 | 6 | 44300 | 72594 | 5872- 5882 |
| Refugio | 28.24 | 97.26 | 491 | 47 | 12673 | 0 | 825 | 460 | 19750 | 34246 | 5446- 5550 |
| Refugio | 28.20 | 97.27 | 1183 | 141 | 18736 | 0 | 725 | 13 | 31000 | 51798 | 8122- 8148 |
| Refugio | 28.20 | 97.26 | 2171 | 467 | 26629 | 0 | 542 | 6 | 46000 | 75815 | 4556- 4560 |
| Refugio | 28.20 | 97.26 | 2500 | 480 | 25191 | 0 | 378 | 0 | 44500 | 73049 | 4494- 4583 |
| Refugio | 28.20 | 97.26 | 2409 | 508 | 26462 | 0 | 176 | 0 | 46500 | 76055 | 4570- 4581 |
| Refugio | 28.53 | 97.06 | 2345 | 410 | 24402 | 0 | 116 | 0 | 42900 | 70173 | 4720- 4738 |
| Refugio | 28.53 | 97.06 | 1737 | 360 | 19311 | 0 | 165 | 0 | 33800 | 55793 | 4716- 4732 |
| Refugio | 28.53 | 97.06 | 2436 | 505 | 23537 | 0 | 122 | 0 | 42000 | 68600 | 4825- 4830 |
| Refugio | 28.53 | 97.06 | 2244 | 460 | 23383 | 0 | 122 | 0 | 41300 | 67509 | 4995- 5018 |
| Nueces | 27.87 | 97.35 | 3700 | 375 | 26000 | 260 | 162 | 18 | 48200 | 80100 | 9000 |
| Nueces | 27.83 | 97.70 | 2148 | 91 | 19481 | 0 | 140 | 30 | 34050 | 55940 | 5974 |
| Nueces | 27.67 | 97.30 | 1026 | 241 | 25716 | 0 | 805 | 20 | 41700 | 69508 | 6680 |
| Nueces | 27.67 | 97.73 | 2090 | 493 | 23237 | 0 | 97 | 1 | 40892 | 66810 | 4700 |
| Nueces | 27.83 | 97.92 | 6 | 43 | 3808 | 0 | 1122 | 109 | 5274 | 10362 | 5586 |
| Nueces | 27.75 | 97.55 | 166 | 28 | 14400 | 76 | 1550 | 28 | 20600 | 37900 | 10460-10482 |
| Nueces | 27.75 | 97.55 | 181 | 30 | 13300 | 105 | 990 | 18 | 20000 | 34200 | 9340- 9346 |
| Nueces | 27.75 | 97.55 | 491 | 45 | 10600 | 264 | 570 | 46 | 16700 | 29900 | 10879-10898 |
| Nueces | 27.75 | 97.55 | 375 | 26 | 8860 | 375 | 400 | 5 | 14000 | 24500 | 12538-12586 |
| Nueces | 27.75 | 97.55 | 87 | 38 | 15200 | 211 | 1070 | 3 | 22000 | 38900 | 11658-11670 |
| Nueces | 27.78 | 97.25 | 21000 | 715 | 53600 | 485 | 114 | 8 | 125600 | 213000 | 10942-10993 |
| Nueces | 27.77 | 97.18 | 689 | 117 | 21988 | 0 | 846 | 75 | 34959 | 58674 | 8698- 8726 |
| Nueces | 27.77 | 97.18 | 498 | 125 | 20893 | 0 | 1292 | 21 | 32734 | 55563 | 9367- 9387 |
| Nueces | 27.77 | 97.18 | 2050 | 74 | 21036 | 0 | 317 | 12 | 36125 | 60183 | 10700 |
| Nueces | 27.77 | 97.18 | 532 | 105 | 20344 | 0 | 842 | 0 | 32117 | 53950 | 10200 |
| Nueces | 27.85 | 97.45 | 4200 | 120 | 21896 | 0 | 354 | 0 | 41180 | 67750 | 6800 |
| Nueces | 27.85 | 97.45 | 106 | 58 | 9075 | 0 | 1545 | 6 | 13453 | 24243 | 8831 |
| Nueces | 27.87 | 97.15 | 83 | 16 | 8000 | 4 | 740 | 25 | 11600 | 21200 | 10682 |
| Nueces | 27.87 | 97.15 | 3700 | 375 | 26000 | 260 | 162 | 18 | 48200 | 80100 | 9000 |
| Nueces | 27.87 | 97.15 | 1640 | 15 | 10500 | 95 | 115 | 47 | 18900 | 31800 | 8784 |
| Nueces | 27.78 | 97.25 | 36020 | 1664 | 42138 | 0 | 237 | 1 | 133680 | 214524 | 10942- 10969 |
| Nueces | 27.78 | 97.25 | 29640 | 1791 | 53051 | 0 | 41 | 1 | 139700 | 226262 | 9983- 9996 |
| Nueces | 27.78 | 97.25 | 31190 | 1640 | 57732 | 0 | 123 | 1 | 149460 | 241606 | 12490-12496 |
| Nueces | 27.75 | 97.54 | 1331 | 2233 | 23640 | 0 | 340 | 9 | 45130 | 72700 | 7606- 7616 |
| Nueces | 27.75 | 97.54 | 4727 | 351 | 21220 | 0 | 352 | 6 | 41940 | 68600 | 8140- 8150 |
| Nueces | 27.75 | 97.53 | 207 | 0 | 8730 | 0 | 1360 | 44 | 13000 | 23411 | 9062- 9100 |
| Nueces | 27.76 | 97.53 | 7450 | 513 | 31700 | 0 | 92 | 0 | 63400 | 103200 | 6050- 6054 |

↓

Table 3c (continued)

| County | Latitude | Longitude | Ca | Mg | Na | K | Alkalinity | SO4 | Cl | TDS | Depth (feet) |
|---------|----------|-----------|------|------|-------|---|------------|------|-------|--------|--------------|
| Nueces | 27.76 | 97.53 | 5580 | 181 | 25400 | 0 | 350 | 0 | 49400 | 80908 | 7135- 7139 |
| Nueces | 27.82 | 97.20 | 684 | 80 | 17396 | 0 | 868 | 244 | 27666 | 47060 | 8980- 8986 |
| Nueces | 27.82 | 97.20 | 473 | 0 | 17295 | 0 | 618 | 136 | 26950 | 45554 | 8270- 8276 |
| Nueces | 27.80 | 97.16 | 826 | 289 | 23450 | 0 | 640 | 15 | 38100 | 63320 | 7957- 7976 |
| Nueces | 27.80 | 97.15 | 799 | 315 | 23590 | 0 | 615 | 44 | 38360 | 63730 | 7940- 7954 |
| Nueces | 27.80 | 97.16 | 1220 | 255 | 26000 | 0 | 814 | 28 | 42500 | 70848 | 7441- 7467 |
| Nueces | 27.80 | 97.16 | 907 | 178 | 22700 | 0 | 935 | 35 | 35000 | 61269 | 7819- 7836 |
| Nueces | 27.81 | 97.18 | 464 | 168 | 18756 | 0 | 1202 | 8 | 29522 | 50120 | 7946- 7995 |
| Nueces | 27.84 | 97.18 | 6496 | 896 | 33560 | 0 | 65 | 160 | 65696 | 106900 | 5600 |
| Nueces | 27.83 | 97.17 | 534 | 224 | 19172 | 0 | 1123 | 16 | 30492 | 51561 | 7972- 7986 |
| Nueces | 27.82 | 97.16 | 664 | 0 | 18200 | 0 | 0 | 0 | 27900 | 47537 | 8689- 8702 |
| Nueces | 27.82 | 97.15 | 154 | 61 | 10190 | 0 | 1175 | 590 | 15050 | 27220 | 8135 |
| Nueces | 27.80 | 97.15 | 534 | 321 | 20272 | 0 | 579 | 53 | 32657 | 54598 | 7912- 7934 |
| Nueces | 27.84 | 97.15 | 288 | 148 | 17200 | 0 | 1200 | 144 | 26700 | 45687 | 8712- 8714 |
| Nueces | 27.84 | 97.15 | 252 | 148 | 15100 | 0 | 1540 | 217 | 23100 | 40371 | 8432- 8450 |
| Nueces | 27.84 | 97.15 | 294 | 156 | 18800 | 0 | 1310 | 10 | 29200 | 49798 | 8332- 8339 |
| Nueces | 27.84 | 97.15 | 548 | 146 | 22300 | 0 | 1340 | 70 | 35000 | 59462 | 8047- 8055 |
| Nueces | 27.84 | 97.16 | 480 | 216 | 21700 | 0 | 1220 | 0 | 34200 | 57854 | 7970- 7980 |
| Nueces | 27.84 | 97.16 | 844 | 231 | 22300 | 0 | 966 | 98 | 36000 | 60491 | 8440- 8447 |
| Nueces | 27.84 | 97.15 | 287 | 88 | 19400 | 0 | 1220 | 0 | 30000 | 51012 | 8726- 8728 |
| Nueces | 27.73 | 97.19 | 872 | 488 | 24810 | 0 | 777 | 29 | 40740 | 67720 | 7312- 7332 |
| Nueces | 27.73 | 97.19 | 1260 | 300 | 25634 | 0 | 1176 | 25 | 42540 | 71058 | 7381- 7406 |
| Nueces | 27.68 | 97.31 | 1404 | 419 | 29947 | 0 | 0 | 567 | 49600 | 81945 | 6729- 6735 |
| Nueces | 27.66 | 97.29 | 296 | 71 | 9483 | 0 | 408 | 20 | 15100 | 25370 | 6640- 6655 |
| Nueces | 27.67 | 97.29 | 733 | 183 | 22000 | 0 | 641 | 0 | 35400 | 58950 | 6645- 6660 |
| Nueces | 27.66 | 97.29 | 1150 | 207 | 25590 | 0 | 763 | 1 | 41650 | 69360 | 6633- 6657 |
| Nueces | 27.67 | 97.30 | 2472 | 159 | 25340 | 0 | 781 | 23 | 43500 | 72280 | 6645- 6660 |
| Nueces | 27.80 | 97.63 | 2148 | 91 | 19480 | 0 | 140 | 30 | 34050 | 55940 | 5968- 5984 |
| Nueces | 27.75 | 97.54 | 1313 | 2308 | 24520 | 0 | 342 | 10 | 46660 | 75160 | 7888- 7898 |
| Nueces | 27.68 | 97.28 | 498 | 138 | 12620 | 0 | 756 | 276 | 20100 | 34380 | 6668- 6680 |
| Nueces | 27.68 | 97.28 | 1026 | 241 | 25710 | 0 | 805 | 1 | 41700 | 69480 | 6671- 6679 |
| Nueces | 27.68 | 97.28 | 1364 | 319 | 25620 | 0 | 756 | 0 | 42400 | 70460 | 6665- 6678 |
| Nueces | 27.68 | 97.27 | 6279 | 452 | 28600 | 0 | 42 | 1200 | 55700 | 92270 | 6601- 6605 |
| Nueces | 27.68 | 97.27 | 1427 | 181 | 25770 | 0 | 852 | 0 | 42350 | 70580 | 6617- 6628 |
| Nueces | 27.67 | 97.28 | 680 | 104 | 8202 | 0 | 616 | 267 | 13600 | 23470 | 6670- 6680 |
| Nueces | 27.65 | 97.28 | 1880 | 300 | 24400 | 0 | 610 | 27 | 41500 | 68720 | 6640- 6651 |
| Nueces | 27.68 | 97.26 | 1483 | 451 | 26580 | 0 | 813 | 9 | 44500 | 73840 | 6638- 6646 |
| Nueces | 27.75 | 97.53 | 211 | 14 | 8723 | 0 | 1352 | 48 | 13072 | 23467 | 8954- 8958 |
| Nueces | 27.82 | 97.15 | 835 | 143 | 14641 | 0 | 731 | 0 | 24153 | 40785 | 12410-12600 |
| Nueces | 27.66 | 97.14 | 1509 | 307 | 22850 | 0 | 833 | 145 | 38230 | 63920 | 7644- 7653 |
| Kleberg | 27.44 | 97.57 | 7678 | 196 | 25028 | 0 | 87 | 110 | 52700 | 85799 | 7234- 7235 |
| Kleberg | 27.44 | 97.57 | 7476 | 712 | 35961 | 0 | 87 | 6 | 70800 | 115000 | 5665- 5668 |

Table 3c (continued)

| County | Latitude | Longitude | Ca | Mg | Na | K | Alkalinity | SO4 | Cl | TDS | Depth (feet) |
|---------|----------|-----------|-------|-----|-------|---|------------|-----|-------|--------|--------------|
| Kleberg | 27.44 | 97.57 | 11241 | 307 | 18036 | 0 | 55 | 6 | 48650 | 78295 | 7215 |
| Kleberg | 27.44 | 97.57 | 10099 | 258 | 17530 | 0 | 49 | 10 | 45700 | 73646 | 7885 |
| Kleberg | 27.44 | 97.57 | 10789 | 355 | 19337 | 0 | 49 | 7 | 50000 | 80537 | 8290 |
| Kleberg | 27.44 | 97.57 | 8365 | 270 | 22856 | 0 | 49 | 115 | 50800 | 82455 | 7237- 7243 |
| Kleberg | 27.44 | 97.57 | 11436 | 73 | 17187 | 0 | 62 | 6 | 47000 | 75764 | 7890- 7893 |
| Kleberg | 27.47 | 97.58 | 7961 | 761 | 33800 | 0 | 25 | 11 | 68500 | 111100 | 5392- 5394 |
| Kleberg | 27.45 | 97.58 | 9092 | 73 | 20595 | 0 | 68 | 3 | 48100 | 77931 | 7565- 7568 |
| Kleberg | 27.45 | 97.59 | 9456 | 98 | 19610 | 0 | 62 | 3 | 47300 | 76529 | 7280- 7284 |
| Kleberg | 27.45 | 97.60 | 9335 | 49 | 21203 | 0 | 62 | 3 | 49400 | 80088 | 7526- 7529 |
| Kleberg | 27.45 | 97.58 | 7557 | 393 | 32638 | 0 | 43 | 15 | 64900 | 105500 | 6355- 6356 |
| Kleberg | 27.45 | 97.59 | 8082 | 245 | 24437 | 0 | 62 | 60 | 52700 | 85586 | 7113- 7117 |
| Kleberg | 27.44 | 97.59 | 8809 | 73 | 22103 | 0 | 105 | 7 | 49900 | 80997 | 7470- 7473 |
| Kleberg | 27.44 | 97.59 | 8283 | 614 | 30537 | 0 | 49 | 27 | 63500 | 103000 | 7080 |
| Kleberg | 27.44 | 97.59 | 8122 | 147 | 24725 | 0 | 93 | 76 | 52900 | 86063 | 7114- 7117 |
| Kleberg | 27.40 | 97.56 | 3686 | 10 | 11917 | 0 | 290 | 62 | 24750 | 40715 | 10069-10118 |

Table 3d. Major ion chemistry from Frio Formation, Southgulf region. Ionic concentrations in mg/L. Data from Kreitler and Richter, 1986.

| County | Latitude | Longitude | Ca | Mg | Na | K | Alkalinity | SO4 | Cl | TDS | Depth (feet) |
|-----------|----------|-----------|-------|-----|-------|---|------------|------|-------|--------|--------------|
| Jim Wells | 27.38 | 98.08 | 1016 | 220 | 11100 | 0 | 718 | 0 | 19200 | 32267 | 5930- 5933 |
| Jim Wells | 27.38 | 98.09 | 907 | 166 | 10790 | 0 | 724 | 0 | 18300 | 30910 | 6050- 6055 |
| Jim Wells | 27.37 | 98.13 | 615 | 617 | 10370 | 0 | 460 | 16 | 18600 | 30709 | 5536-5556 |
| Jim Wells | 27.37 | 98.11 | 542 | 129 | 8542 | 0 | 968 | 15 | 13930 | 24139 | 6117-6123 |
| Jim Wells | 27.37 | 98.12 | 1294 | 404 | 10620 | 0 | 187 | 31 | 19720 | 32259 | 5244-5288 |
| Jim Wells | 27.38 | 98.12 | 606 | 326 | 3004 | 0 | 296 | 5 | 6508 | 10820 | 6922-6942 |
| Jim Wells | 27.38 | 98.12 | 450 | 76 | 7194 | 0 | 149 | 7 | 12040 | 19920 | 6097-6137 |
| Jim Wells | 27.71 | 98.06 | 275 | 80 | 8105 | 0 | 194 | 74 | 13040 | 21769 | 5329-5343 |
| Duval | 27.64 | 98.30 | 90 | 182 | 4958 | 0 | 77 | 500 | 7840 | 13722 | 2984- 2996 |
| Duval | 27.64 | 98.30 | 112 | 6 | 4022 | 0 | 171 | 12 | 6290 | 10636 | 3768- 3791 |
| Duval | 27.64 | 98.30 | 359 | 90 | 6684 | 0 | 91 | 80 | 11050 | 18341 | 3450- 3454 |
| Hidalgo | 26.17 | 98.07 | 2128 | 36 | 5711 | 0 | 293 | 175 | 12375 | 20968 | 8125- 8265 |
| Hidalgo | 26.17 | 98.07 | 328 | 15 | 6081 | 0 | 315 | 327 | 9585 | 16649 | 7100 |
| Hidalgo | 26.17 | 98.07 | 512 | 58 | 10459 | 1 | 366 | 1812 | 15672 | 28904 | 6556- 6621 |
| Hidalgo | 26.17 | 98.07 | 733 | 36 | 7353 | 0 | 182 | 120 | 12544 | 21450 | 7780 |
| Hidalgo | 26.23 | 98.53 | 95 | 48 | 10321 | 0 | 84 | 83 | 16062 | 26693 | 2556 |
| Hidalgo | 26.23 | 98.53 | 173 | 44 | 6933 | 0 | 367 | 1 | 10912 | 18430 | 2775 |
| Hidalgo | 26.23 | 98.53 | 130 | 47 | 12048 | 0 | 809 | 4 | 18470 | 31508 | 3095 |
| Hidalgo | 26.27 | 98.42 | 1096 | 162 | 17028 | 0 | 182 | 10 | 28555 | 47033 | 4002 |
| Hidalgo | 26.27 | 98.42 | 1640 | 270 | 15251 | 0 | 157 | 3672 | 24297 | 45287 | 7505 |
| Hidalgo | 26.27 | 98.42 | 762 | 126 | 15548 | 0 | 194 | 1 | 25578 | 42209 | 4016 |
| Hidalgo | 26.27 | 98.42 | 925 | 96 | 11564 | 0 | 73 | 987 | 18963 | 32608 | 4666 |
| Hidalgo | 26.50 | 98.42 | 727 | 0 | 9045 | 0 | 0 | 1250 | 11234 | 24770 | 4785- 4792 |
| Hidalgo | 26.36 | 98.33 | 2801 | 168 | 12263 | 0 | 186 | 24 | 24319 | 39901 | 6490- 6498 |
| Hidalgo | 26.36 | 98.33 | 5497 | 207 | 23330 | 0 | 292 | 12 | 46137 | 75498 | 6490- 6498 |
| Hidalgo | 26.36 | 98.33 | 2290 | 170 | 12500 | 0 | 304 | 131 | 23100 | 38511 | 7920- 7935 |
| Hidalgo | 26.78 | 98.10 | 8018 | 172 | 20442 | 0 | 290 | 80 | 46000 | 75053 | 6627- 6637 |
| Hidalgo | 26.78 | 98.10 | 799 | 25 | 6667 | 0 | 0 | 1000 | 10300 | 19348 | 6766- 6776 |
| Hidalgo | 26.78 | 98.10 | 2387 | 148 | 13187 | 0 | 32 | 840 | 24000 | 40916 | 6827- 6836 |
| Hidalgo | 26.78 | 98.10 | 9181 | 387 | 29817 | 0 | 227 | 20 | 63300 | 102900 | 7231- 7238 |
| Hidalgo | 26.78 | 98.10 | 7706 | 161 | 28425 | 0 | 138 | 150 | 57600 | 94375 | 7350- 7365 |
| Hidalgo | 26.78 | 98.10 | 11088 | 387 | 35652 | 0 | 239 | 0 | 75700 | 123100 | 7795- 7809 |
| Hidalgo | 26.66 | 98.30 | 1070 | 0 | 7716 | 0 | 122 | 4000 | 10767 | 23700 | 2663- 2749 |
| Brooks | 26.83 | 98.40 | 2460 | 60 | 13502 | 0 | 66 | 32 | 25286 | 41406 | 4744 |
| Brooks | 26.97 | 98.25 | 3032 | 170 | 18941 | 0 | 610 | 12 | 34700 | 57465 | 4900 |
| Brooks | 26.82 | 98.39 | 2173 | 3 | 16507 | 0 | 1257 | 16 | 28600 | 48556 | 4970- 6551 |
| Brooks | 26.82 | 98.40 | 3200 | 90 | 14777 | 0 | 69 | 13 | 28700 | 46849 | 4710- 4719 |
| Brooks | 26.82 | 98.40 | 2599 | 7 | 11480 | 0 | 85 | 138 | 22200 | 36509 | 4462- 4508 |
| Brooks | 26.81 | 98.40 | 2914 | 148 | 14144 | 0 | 44 | 13 | 27400 | 44663 | 4718- 4728 |
| Brooks | 26.81 | 98.40 | 2800 | 151 | 13884 | 0 | 44 | 20 | 26800 | 43699 | 4487- 4494 |
| Brooks | 26.79 | 98.40 | 444 | 3 | 2476 | 0 | 165 | 4250 | 1300 | 8718 | 3368- 3400 |
| Brooks | 26.79 | 98.40 | 1946 | 33 | 15851 | 0 | 1025 | 26 | 27400 | 46281 | 6100- 6110 |
| Brooks | 26.79 | 98.40 | 595 | 0 | 4162 | 0 | 451 | 22 | 7200 | 12430 | 5661- 5669 |

Table 3d (continued)

| County | Latitude | Longitude | Ca | Mg | Na | K | AlkalInlty | SO4 | Cl | TDS | Depth (feet) |
|--------|----------|-----------|-------|------|-------|---|------------|------|--------|--------|--------------|
| Brooks | 26.78 | 98.40 | 4567 | 214 | 25888 | 0 | 220 | 14 | 48550 | 79453 | 6721- 6729 |
| Brooks | 26.94 | 98.18 | 7688 | 1034 | 25924 | 0 | 262 | 32 | 56500 | 91440 | 6661- 6668 |
| Brooks | 26.94 | 98.17 | 6827 | 681 | 19788 | 0 | 104 | 120 | 44500 | 72020 | 5828- 5838 |
| Brooks | 26.94 | 98.17 | 7751 | 559 | 24852 | 0 | 232 | 18 | 53600 | 87012 | 6230- 6240 |
| Brooks | 26.93 | 98.17 | 4571 | 331 | 18294 | 0 | 470 | 124 | 36950 | 60740 | 6425- 6445 |
| Brooks | 26.85 | 98.08 | 9833 | 291 | 28801 | 0 | 160 | 1030 | 61900 | 102000 | 8205- 8219 |
| Brooks | 26.84 | 98.11 | 5678 | 1445 | 17042 | 0 | 231 | 50 | 40250 | 64846 | 6998- 7010 |
| Brooks | 26.84 | 98.11 | 912 | 73 | 9145 | 0 | 0 | 450 | 14600 | 25780 | 4411- 4429 |
| Brooks | 26.84 | 98.11 | 3853 | 36 | 16942 | 0 | 0 | 130 | 32400 | 53700 | 4674- 4688 |
| Brooks | 26.84 | 98.11 | 8619 | 273 | 24261 | 0 | 259 | 0 | 53350 | 86797 | 6167- 6174 |
| Brooks | 26.83 | 98.10 | 11466 | 516 | 28399 | 0 | 37 | 38 | 65600 | 106100 | 6903- 6914 |
| Brooks | 27.07 | 98.02 | 21284 | 242 | 26816 | 0 | 134 | 0 | 79800 | 128300 | 8222- 8229 |
| Brooks | 27.07 | 98.02 | 3881 | 121 | 12358 | 0 | 317 | 180 | 26000 | 42857 | 7191- 7198 |
| Brooks | 27.07 | 98.03 | 2619 | 299 | 10302 | 0 | 487 | 1000 | 20400 | 35107 | 6246- 6259 |
| Brooks | 27.07 | 98.03 | 5228 | 320 | 17900 | 0 | 407 | 10 | 37650 | 61545 | 7342- 7352 |
| Brooks | 27.07 | 98.03 | 4266 | 973 | 18377 | 0 | 418 | 180 | 38400 | 62614 | 8033- 8043 |
| Brooks | 27.07 | 98.03 | 2410 | 438 | 7961 | 0 | 531 | 180 | 17400 | 28920 | 7326- 7332 |
| Brooks | 27.07 | 98.03 | 7831 | 948 | 17847 | 0 | 232 | 110 | 44000 | 70968 | 6235- 6240 |
| Brooks | 27.06 | 98.03 | 121 | 268 | 2848 | 0 | 438 | 578 | 4695 | 8940 | 8085- 8087 |
| Brooks | 27.06 | 98.03 | 289 | 97 | 5959 | 0 | 590 | 1645 | 9160 | 17740 | 8575- 8582 |
| Brooks | 27.06 | 98.03 | 404 | 61 | 4744 | 0 | 420 | 480 | 7650 | 13759 | 8125- 8142 |
| Brooks | 27.02 | 98.12 | 30258 | 3190 | 50891 | 0 | 121 | 0 | 141500 | 226000 | 5836- 5854 |
| Brooks | 27.14 | 98.38 | 19600 | 1986 | 62633 | 0 | 61 | 4 | 137000 | 221300 | 4769- 4775 |
| Brooks | 27.00 | 98.28 | 4563 | 340 | 13750 | 0 | 639 | 20 | 30000 | 49312 | 6545- 6555 |
| Brooks | 27.00 | 98.28 | 3414 | 1520 | 14861 | 0 | 573 | 90 | 32800 | 53258 | 6552- 6578 |
| Brooks | 26.99 | 98.28 | 105 | 128 | 3962 | 0 | 328 | 80 | 6425 | 11028 | 6550- 6573 |
| Brooks | 26.98 | 98.28 | 4067 | 851 | 13930 | 0 | 342 | 10 | 31000 | 50200 | 6544- 6560 |
| Brooks | 26.83 | 98.38 | 2906 | 243 | 18242 | 0 | 1061 | 8 | 33400 | 55860 | 6141- 6144 |
| Brooks | 26.84 | 98.39 | 1946 | 289 | 21134 | 0 | 778 | 51 | 36400 | 60589 | 6169- 6176 |
| Brooks | 26.84 | 98.39 | 1875 | 122 | 15844 | 0 | 1165 | 80 | 27400 | 46486 | 5592- 5599 |
| Brooks | 26.84 | 98.39 | 1934 | 912 | 15415 | 0 | 1501 | 20 | 29000 | 48782 | 5783- 5791 |
| Brooks | 26.84 | 98.39 | 2460 | 821 | 22074 | 0 | 744 | 0 | 40400 | 66499 | 6167- 6173 |
| Brooks | 26.84 | 98.38 | 2480 | 547 | 16352 | 0 | 883 | 18 | 30700 | 50980 | 5626- 5632 |
| Brooks | 26.84 | 98.39 | 2000 | 1 | 16188 | 0 | 1366 | 22 | 27725 | 47301 | 5520- 5530 |
| Brooks | 26.84 | 98.39 | 1606 | 292 | 17968 | 0 | 903 | 14 | 30900 | 51683 | 6141- 6148 |
| Brooks | 26.84 | 98.39 | 2117 | 135 | 15560 | 0 | 1437 | 44 | 27300 | 46593 | 5570- 5577 |
| Brooks | 26.84 | 98.38 | 2053 | 71 | 16735 | 0 | 1708 | 130 | 27700 | 48397 | 5794- 5804 |
| Brooks | 26.83 | 98.39 | 1946 | 66 | 14882 | 0 | 1635 | 20 | 25650 | 44199 | 5582- 5593 |
| Brooks | 26.83 | 98.38 | 2594 | 1 | 18183 | 0 | 268 | 20 | 32500 | 53565 | 6108- 6125 |
| Brooks | 26.83 | 98.39 | 2811 | 328 | 17666 | 0 | 885 | 0 | 32700 | 54390 | 6231- 6241 |
| Brooks | 26.83 | 98.39 | 1861 | 109 | 17532 | 0 | 1122 | 40 | 30000 | 50664 | 6140- 6144 |
| Brooks | 26.83 | 98.40 | 2675 | 17 | 15191 | 0 | 122 | 100 | 28100 | 46205 | 4981- 4986 |
| Brooks | 26.83 | 98.41 | 4919 | 17 | 17175 | 0 | 55 | 8 | 35250 | 57424 | 4725- 4734 |

Table 3d (continued)

| County | Latitude | Longitude | Ca | Mg | Na | K | Alkalinity | SO4 | Cl | TDS | Depth (feet) |
|--------|----------|-----------|-------|------|-------|---|------------|------|-------|-------|--------------|
| Brooks | 26.83 | 98.40 | 676 | 1 | 9492 | 0 | 1427 | 26 | 15000 | 26621 | 5460- 5470 |
| Brooks | 26.83 | 98.40 | 2123 | 62 | 15157 | 0 | 171 | 60 | 27200 | 44773 | 5136- 5144 |
| Brooks | 26.82 | 98.39 | 2173 | 3 | 16061 | 0 | 1251 | 36 | 27900 | 47424 | 4970- 6551 |
| Brooks | 27.14 | 98.04 | 3373 | 255 | 7741 | 0 | 287 | 20 | 18500 | 30176 | 7502- 7524 |
| Brooks | 27.14 | 98.04 | 1673 | 121 | 16067 | 0 | 537 | 16 | 27800 | 46214 | 7584- 7591 |
| Brooks | 27.08 | 98.01 | 7904 | 696 | 18692 | 0 | 331 | 28 | 44600 | 72335 | 6789- 6794 |
| Brooks | 27.08 | 98.01 | 7904 | 127 | 19784 | 0 | 92 | 190 | 44400 | 72702 | 6280- 6292 |
| Brooks | 27.08 | 98.01 | 8052 | 190 | 20572 | 0 | 379 | 68 | 46300 | 75585 | 6615- 6652 |
| Brooks | 27.08 | 98.01 | 7825 | 443 | 20628 | 0 | 355 | 20 | 46800 | 76071 | 6809- 6818 |
| Brooks | 27.08 | 98.01 | 6876 | 443 | 20320 | 0 | 490 | 106 | 44400 | 72719 | 7110- 7120 |
| Brooks | 27.08 | 98.02 | 5434 | 411 | 16806 | 0 | 588 | 60 | 36400 | 59699 | 7374- 7389 |
| Brooks | 27.08 | 98.02 | 8200 | 570 | 20932 | 0 | 526 | 24 | 48200 | 78452 | 7774- 7751 |
| Brooks | 27.08 | 98.02 | 7212 | 506 | 19611 | 0 | 239 | 120 | 44200 | 71990 | 7792- 7801 |
| Brooks | 27.08 | 98.02 | 6547 | 963 | 16314 | 0 | 367 | 0 | 39400 | 63591 | 7118- 7123 |
| Brooks | 27.08 | 98.03 | 7114 | 1125 | 17218 | 0 | 318 | 100 | 42200 | 68099 | 6757- 6764 |
| Brooks | 27.07 | 98.02 | 11603 | 158 | 23746 | 0 | 183 | 0 | 57600 | 93290 | 7912- 7918 |
| Brooks | 27.07 | 98.02 | 9016 | 377 | 20471 | 0 | 159 | 12 | 48600 | 78635 | 6643- 6650 |
| Brooks | 27.07 | 98.02 | 5040 | 328 | 13463 | 0 | 165 | 120 | 30500 | 49616 | 6733- 6740 |
| Brooks | 27.07 | 98.02 | 5743 | 304 | 17644 | 0 | 317 | 40 | 38100 | 62148 | 7416- 7422 |
| Starr | 26.70 | 98.50 | 1656 | 73 | 13802 | 0 | 214 | 18 | 24244 | 40007 | 4140 |
| Starr | 26.77 | 98.47 | 2444 | 58 | 13819 | 0 | 116 | 53 | 25896 | 42386 | 4653 |
| Starr | 26.42 | 98.67 | 344 | 90 | 11921 | 0 | 842 | 1 | 18764 | 31962 | 2585 |
| Starr | 26.60 | 98.57 | 1268 | 50 | 7395 | 0 | 110 | 1400 | 12696 | 22919 | 3483 |
| Starr | 26.60 | 98.57 | 933 | 78 | 10707 | 0 | 78 | 445 | 17923 | 30164 | 4617 |
| Starr | 26.38 | 98.07 | 455 | 90 | 14583 | 0 | 288 | 37 | 23356 | 38809 | 3731 |
| Starr | 26.38 | 98.07 | 360 | 102 | 13714 | 0 | 433 | 112 | 21746 | 36467 | 3887 |
| Starr | 26.38 | 98.07 | 480 | 131 | 15606 | 0 | 444 | 78 | 24980 | 41719 | 3970 |
| Starr | 26.70 | 98.50 | 923 | 98 | 11008 | 0 | 1781 | 25 | 17839 | 31674 | 4932 |
| Starr | 26.60 | 98.57 | 801 | 96 | 14823 | 0 | 212 | 37 | 24400 | 40369 | 4395 |
| Starr | 26.60 | 98.57 | 192 | 46 | 6882 | 0 | 689 | 362 | 10418 | 18589 | 4377 |
| Starr | 26.38 | 98.12 | 190 | 55 | 8300 | 0 | 464 | 1 | 13023 | 22033 | 3775 |
| Starr | 26.70 | 98.57 | 690 | 87 | 10351 | 0 | 1060 | 91 | 16750 | 29029 | 4590 |
| Starr | 26.77 | 98.47 | 1096 | 88 | 12938 | 0 | 1647 | 1 | 21189 | 36959 | 5332 |
| Starr | 26.43 | 98.27 | 480 | 116 | 14085 | 0 | 350 | 1 | 22700 | 37732 | 1774 |
| Starr | 26.43 | 98.27 | 356 | 78 | 12189 | 0 | 562 | 1 | 19326 | 32512 | 1544 |
| Starr | 26.77 | 98.47 | 1786 | 76 | 13536 | 0 | 226 | 49 | 24084 | 39757 | 4350 |
| Starr | 26.77 | 98.47 | 4160 | 274 | 22074 | 0 | 368 | 1 | 41983 | 68860 | 5812 |
| Starr | 26.61 | 98.53 | 112 | 0 | 5710 | 0 | 1070 | 3080 | 6040 | 16078 | 4378- 4390 |
| Starr | 26.61 | 98.53 | 772 | 0 | 10045 | 0 | 395 | 1110 | 15700 | 28104 | 4582- 4588 |
| Starr | 26.60 | 98.54 | 7797 | 221 | 15717 | 0 | 376 | 0 | 38497 | 62668 | 6040- 6050 |
| Starr | 26.61 | 98.53 | 11701 | 266 | 15209 | 0 | 435 | 0 | 44697 | 72336 | 6465- 6469 |
| Starr | 26.61 | 98.53 | 1692 | 109 | 12534 | 0 | 565 | 44 | 22278 | 37222 | 5805- 5809 |
| Starr | 26.58 | 98.51 | 1996 | 78 | 15522 | 0 | 785 | 480 | 26883 | 45754 | 4676- 4685 |

Table 3d (continued)

| County | Latitude | Longitude | Ca | Mg | Na | K | Alkalinity | SO4 | Cl | TDS | Depth (feet) |
|--------|----------|-----------|-------|------|-------|---|------------|------|-------|-------|--------------|
| Brooks | 26.83 | 98.40 | 676 | 1 | 9492 | 0 | 1427 | 26 | 15000 | 26621 | 5460- 5470 |
| Brooks | 26.83 | 98.40 | 2123 | 62 | 15157 | 0 | 171 | 60 | 27200 | 44773 | 5136- 5144 |
| Brooks | 26.82 | 98.39 | 2173 | 3 | 16061 | 0 | 1251 | 36 | 27900 | 47424 | 4970- 6551 |
| Brooks | 27.14 | 98.04 | 3373 | 255 | 7741 | 0 | 287 | 20 | 18500 | 30176 | 7502- 7524 |
| Brooks | 27.14 | 98.04 | 1673 | 121 | 16067 | 0 | 537 | 16 | 27800 | 46214 | 7584- 7591 |
| Brooks | 27.08 | 98.01 | 7904 | 696 | 18692 | 0 | 331 | 28 | 44600 | 72335 | 6789- 6794 |
| Brooks | 27.08 | 98.01 | 7904 | 127 | 19784 | 0 | 92 | 190 | 44400 | 72702 | 6280- 6292 |
| Brooks | 27.08 | 98.01 | 8052 | 190 | 20572 | 0 | 379 | 68 | 46300 | 75585 | 6615- 6652 |
| Brooks | 27.08 | 98.01 | 7825 | 443 | 20628 | 0 | 355 | 20 | 46800 | 76071 | 6809- 6818 |
| Brooks | 27.08 | 98.01 | 6876 | 443 | 20320 | 0 | 490 | 106 | 44400 | 72719 | 7110- 7120 |
| Brooks | 27.08 | 98.02 | 5434 | 411 | 16806 | 0 | 588 | 60 | 36400 | 59699 | 7374- 7389 |
| Brooks | 27.08 | 98.02 | 8200 | 570 | 20932 | 0 | 526 | 24 | 48200 | 78452 | 7774- 7751 |
| Brooks | 27.08 | 98.02 | 7212 | 506 | 19611 | 0 | 239 | 120 | 44200 | 71990 | 7792- 7801 |
| Brooks | 27.08 | 98.02 | 6547 | 963 | 16314 | 0 | 367 | 0 | 39400 | 63591 | 7118- 7123 |
| Brooks | 27.08 | 98.03 | 7114 | 1125 | 17218 | 0 | 318 | 100 | 42200 | 68099 | 6757- 6764 |
| Brooks | 27.07 | 98.02 | 11603 | 158 | 23746 | 0 | 183 | 0 | 57600 | 93290 | 7912- 7918 |
| Brooks | 27.07 | 98.02 | 9016 | 377 | 20471 | 0 | 159 | 12 | 48600 | 78635 | 6643- 6650 |
| Brooks | 27.07 | 98.02 | 5040 | 328 | 13463 | 0 | 165 | 120 | 30500 | 49616 | 6733- 6740 |
| Brooks | 27.07 | 98.02 | 5743 | 304 | 17644 | 0 | 317 | 40 | 38100 | 62148 | 7416- 7422 |
| Starr | 26.70 | 98.50 | 1656 | 73 | 13802 | 0 | 214 | 18 | 24244 | 40007 | 4140 |
| Starr | 26.77 | 98.47 | 2444 | 58 | 13819 | 0 | 116 | 53 | 25896 | 42386 | 4653 |
| Starr | 26.42 | 98.67 | 344 | 90 | 11921 | 0 | 842 | 1 | 18764 | 31962 | 2585 |
| Starr | 26.60 | 98.57 | 1268 | 50 | 7395 | 0 | 110 | 1400 | 12696 | 22919 | 3483 |
| Starr | 26.60 | 98.57 | 933 | 78 | 10707 | 0 | 78 | 445 | 17923 | 30164 | 4617 |
| Starr | 26.38 | 98.07 | 455 | 90 | 14583 | 0 | 288 | 37 | 23356 | 38809 | 3731 |
| Starr | 26.38 | 98.07 | 360 | 102 | 13714 | 0 | 433 | 112 | 21746 | 36467 | 3887 |
| Starr | 26.38 | 98.07 | 480 | 131 | 15606 | 0 | 444 | 78 | 24980 | 41719 | 3970 |
| Starr | 26.70 | 98.50 | 923 | 98 | 11008 | 0 | 1781 | 25 | 17839 | 31674 | 4932 |
| Starr | 26.60 | 98.57 | 801 | 96 | 14823 | 0 | 212 | 37 | 24400 | 40369 | 4395 |
| Starr | 26.60 | 98.57 | 192 | 46 | 6882 | 0 | 689 | 362 | 10418 | 18589 | 4377 |
| Starr | 26.38 | 98.12 | 190 | 55 | 8300 | 0 | 464 | 1 | 13023 | 22033 | 3775 |
| Starr | 26.70 | 98.57 | 690 | 87 | 10351 | 0 | 1060 | 91 | 16750 | 29029 | 4590 |
| Starr | 26.77 | 98.47 | 1096 | 88 | 12938 | 0 | 1647 | 1 | 21189 | 36959 | 5332 |
| Starr | 26.43 | 98.27 | 480 | 116 | 14085 | 0 | 350 | 1 | 22700 | 37732 | 1774 |
| Starr | 26.43 | 98.27 | 356 | 78 | 12189 | 0 | 562 | 1 | 19326 | 32512 | 1544 |
| Starr | 26.77 | 98.47 | 1786 | 76 | 13536 | 0 | 226 | 49 | 24084 | 39757 | 4350 |
| Starr | 26.77 | 98.47 | 4160 | 274 | 22074 | 0 | 368 | 1 | 41983 | 68860 | 5812 |
| Starr | 26.61 | 98.53 | 112 | 0 | 5710 | 0 | 1070 | 3080 | 6040 | 16078 | 4378- 4390 |
| Starr | 26.61 | 98.53 | 772 | 0 | 10045 | 0 | 395 | 1110 | 15700 | 28104 | 4582- 4588 |
| Starr | 26.60 | 98.54 | 7797 | 221 | 15717 | 0 | 376 | 0 | 38497 | 62668 | 6040- 6050 |
| Starr | 26.61 | 98.53 | 11701 | 266 | 15209 | 0 | 435 | 0 | 44697 | 72336 | 6465- 6469 |
| Starr | 26.61 | 98.53 | 1692 | 109 | 12534 | 0 | 565 | 44 | 22278 | 37222 | 5805- 5809 |
| Starr | 26.58 | 98.51 | 1996 | 78 | 15522 | 0 | 785 | 480 | 26883 | 45754 | 4676- 4685 |

Table 3d (continued)

| County | Latitude | Longitude | Ca | Mg | Na | K | Alkalinity | SO4 | Cl | TDS | Depth (feet) |
|---------|----------|-----------|------|-----|-------|---|------------|------|-------|-------|--------------|
| Starr | 26.77 | 98.83 | 37 | 2 | 1175 | 0 | 150 | 376 | 1394 | 3262 | 1504- 1518 |
| Starr | 26.77 | 98.83 | 42 | 2 | 1212 | 0 | 110 | 360 | 1558 | 3365 | 1474- 1496 |
| Starr | 26.78 | 98.41 | 1986 | 28 | 10911 | 0 | 116 | 103 | 20250 | 33376 | 4749- 4752 |
| Starr | 26.78 | 98.42 | 1513 | 1 | 12842 | 0 | 641 | 48 | 22100 | 37144 | 5124- 5130 |
| Starr | 26.78 | 98.42 | 4432 | 230 | 25158 | 0 | 268 | 18 | 47200 | 77306 | 6506- 6516 |
| Starr | 26.77 | 98.39 | 509 | 12 | 2930 | 0 | 82 | 6750 | 420 | 10703 | 2114- 2152 |
| Starr | 26.77 | 98.39 | 589 | 20 | 4288 | 0 | 88 | 7840 | 1870 | 14695 | 2630- 2657 |
| Starr | 26.77 | 98.39 | 1177 | 6 | 6298 | 0 | 50 | 2430 | 10000 | 19961 | 3798- 3842 |
| Starr | 26.77 | 98.43 | 2594 | 33 | 13979 | 0 | 61 | 58 | 26200 | 42925 | 4747- 4759 |
| Starr | 26.69 | 98.37 | 2500 | 210 | 17336 | 0 | 656 | 64 | 31341 | 52108 | 5696- 5800 |
| Starr | 26.57 | 98.51 | 2359 | 280 | 18208 | 0 | 400 | 40 | 32810 | 54097 | 4770- 4773 |
| Starr | 26.58 | 98.51 | 2745 | 178 | 9936 | 0 | 442 | 17 | 20410 | 33728 | 4846- 4854 |
| Starr | 26.52 | 98.63 | 704 | 67 | 10140 | 0 | 128 | 30 | 17000 | 28069 | 3954- 3963 |
| Starr | 26.52 | 98.63 | 404 | 41 | 7973 | 0 | 268 | 930 | 12300 | 21916 | 3885- 3895 |
| Starr | 26.52 | 98.63 | 334 | 10 | 4142 | 0 | 311 | 3140 | 4500 | 12446 | 3646- 3655 |
| Starr | 26.52 | 98.63 | 658 | 34 | 10415 | 0 | 226 | 151 | 17100 | 28584 | 3898- 3907 |
| Starr | 26.52 | 98.63 | 300 | 61 | 6651 | 0 | 183 | 93 | 10800 | 18088 | 3892- 3912 |
| Starr | 26.43 | 98.76 | 526 | 64 | 12559 | 0 | 538 | 0 | 20176 | 33868 | 1432- 1437 |
| Starr | 26.43 | 98.77 | 500 | 64 | 11651 | 0 | 543 | 0 | 18724 | 31488 | 1417- 1425 |
| Kleberg | 27.43 | 98.03 | 738 | 35 | 8257 | 0 | 128 | 111 | 14000 | 23269 | 4695 |
| Kleberg | 27.43 | 98.03 | 1500 | 10 | 10634 | 0 | 384 | 54 | 19000 | 31582 | 5695 |
| Kleberg | 27.60 | 97.92 | 195 | 18 | 5800 | 0 | 1068 | 1 | 8750 | 15832 | 6669 |
| Kleberg | 27.60 | 97.92 | 8168 | 234 | 25551 | 0 | 201 | 1 | 54500 | 88655 | 6200 |
| Kleberg | 27.48 | 97.47 | 2400 | 24 | 13756 | 0 | 201 | 160 | 25300 | 41841 | 5233 |
| Kleberg | 27.50 | 98.02 | 754 | 17 | 11178 | 0 | 397 | 11 | 18400 | 30757 | 5754- 5757 |
| Kleberg | 27.50 | 98.03 | 1536 | 25 | 11175 | 0 | 253 | 268 | 19700 | 32957 | 4392- 4398 |
| Kleberg | 27.61 | 97.88 | 248 | 67 | 6028 | 0 | 1061 | 300 | 9100 | 16804 | 6654- 6663 |
| Kleberg | 27.60 | 97.88 | 126 | 7 | 6301 | 0 | 958 | 18 | 9400 | 16810 | 6645- 6655 |
| Kleberg | 27.60 | 97.88 | 164 | 7 | 6456 | 0 | 644 | 1 | 9900 | 17172 | 6633- 6655 |
| Kleberg | 27.60 | 97.88 | 195 | 18 | 5809 | 0 | 1068 | 0 | 8750 | 15840 | 6665- 6669 |
| Kleberg | 27.60 | 97.90 | 210 | 31 | 4282 | 0 | 647 | 262 | 6500 | 11932 | 6453- 6464 |
| Kleberg | 27.59 | 97.88 | 118 | 38 | 6457 | 0 | 943 | 50 | 9700 | 17306 | 6653- 6659 |
| Kleberg | 27.59 | 97.89 | 16 | 34 | 4313 | 0 | 1683 | 1110 | 4685 | 12094 | 6545- 6552 |
| Kleberg | 27.59 | 97.89 | 1567 | 250 | 5520 | 0 | 641 | 80 | 11600 | 19658 | 6614- 6624 |
| Kleberg | 27.59 | 97.95 | 445 | 194 | 5661 | 0 | 915 | 28 | 9550 | 16793 | 6393- 6399 |
| Kleberg | 27.58 | 97.95 | 284 | 61 | 5700 | 0 | 967 | 156 | 8800 | 15968 | 6368- 6374 |
| Kleberg | 27.55 | 98.06 | 79 | 45 | 6865 | 0 | 514 | 305 | 10300 | 18144 | 5958- 5967 |
| Kleberg | 27.53 | 98.01 | 436 | 15 | 9298 | 0 | 618 | 12 | 14800 | 25179 | 6097- 6100 |
| Kleberg | 27.53 | 98.01 | 139 | 16 | 8470 | 0 | 1666 | 173 | 11800 | 22264 | 6147- 6154 |
| Kleberg | 27.53 | 98.01 | 1386 | 7 | 10114 | 0 | 223 | 85 | 17900 | 29715 | 6209- 6213 |
| Kleberg | 27.51 | 98.03 | 1344 | 145 | 8573 | 0 | 85 | 400 | 15700 | 26247 | 4874- 4880 |
| Kleberg | 27.51 | 98.03 | 1265 | 230 | 8391 | 0 | 183 | 220 | 15600 | 25889 | 5121- 5127 |
| Kleberg | 27.51 | 98.03 | 165 | 79 | 9476 | 0 | 3346 | 0 | 13200 | 26266 | 6545- 6551 |

Table 3d (continued)

| County | Latitude | Longitude | Ca | Mg | Na | K | Alkalinity | SO4 | Cl | TDS | Depth (feet) |
|---------|----------|-----------|------|-----|-------|---|------------|-----|-------|-------|--------------|
| Kleberg | 27.51 | 98.00 | 70 | 15 | 9774 | 0 | 1779 | 22 | 14200 | 25860 | 7140- 7146 |
| Kleberg | 27.50 | 98.00 | 152 | 22 | 9347 | 0 | 1372 | 15 | 13950 | 24858 | 6423- 6427 |
| Kleberg | 27.48 | 98.00 | 769 | 123 | 11906 | 0 | 677 | 8 | 19700 | 33183 | 6065- 6073 |
| Kleberg | 27.48 | 98.00 | 454 | 110 | 10703 | 0 | 907 | 28 | 17100 | 29302 | 6257- 6263 |
| Kleberg | 27.48 | 98.00 | 116 | 74 | 11102 | 0 | 1787 | 20 | 16500 | 29599 | 7043- 7055 |
| Kleberg | 27.51 | 98.00 | 103 | 20 | 10329 | 0 | 2034 | 0 | 15000 | 27486 | 7112- 7120 |
| Kleberg | 27.48 | 98.00 | 194 | 22 | 9938 | 0 | 1036 | 263 | 14950 | 26403 | 7311- 7322 |
| Kleberg | 27.50 | 98.00 | 703 | 25 | 11273 | 0 | 513 | 29 | 18400 | 30943 | 4872- 4877 |
| Kleberg | 27.50 | 98.03 | 544 | 31 | 10500 | 0 | 781 | 11 | 16800 | 28667 | 4402- 4408 |
| Kleberg | 27.50 | 98.03 | 1556 | 25 | 11100 | 0 | 266 | 286 | 19600 | 32833 | 4365- 4369 |
| Kleberg | 27.50 | 98.03 | 2442 | 31 | 12174 | 0 | 157 | 370 | 22850 | 38024 | 4434- 4442 |
| Kleberg | 27.50 | 98.03 | 1192 | 43 | 11159 | 0 | 297 | 125 | 19200 | 32016 | 4434- 4442 |
| Kleberg | 27.49 | 98.03 | 445 | 250 | 11059 | 0 | 1231 | 40 | 17800 | 30861 | 6129- 6135 |
| Kleberg | 27.49 | 98.01 | 213 | 49 | 4001 | 0 | 232 | 760 | 6000 | 11255 | 5116- 5126 |
| Kleberg | 27.49 | 98.01 | 803 | 145 | 7951 | 0 | 586 | 270 | 13600 | 23355 | 5463- 5473 |
| Kleberg | 27.49 | 98.01 | 285 | 158 | 9280 | 0 | 988 | 20 | 14700 | 25431 | 6171- 6179 |
| Kleberg | 27.49 | 98.01 | 122 | 44 | 10416 | 0 | 1587 | 0 | 15500 | 27669 | 6978- 6984 |
| Kleberg | 27.48 | 98.01 | 115 | 15 | 10288 | 0 | 1396 | 19 | 15300 | 27133 | 7104- 7109 |
| Kleberg | 27.48 | 98.01 | 93 | 21 | 10649 | 0 | 1459 | 19 | 15800 | 18041 | 7131- 7133 |
| Kleberg | 27.48 | 98.06 | 736 | 49 | 15129 | 0 | 420 | 7 | 24550 | 40891 | 6366- 6375 |
| Kleberg | 27.48 | 98.06 | 800 | 54 | 12543 | 0 | 407 | 1 | 20700 | 34505 | 6070- 6082 |
| Kleberg | 27.48 | 98.05 | 784 | 39 | 11055 | 0 | 445 | 14 | 18300 | 30637 | 6042- 6045 |
| Kleberg | 27.48 | 98.02 | 877 | 25 | 9364 | 0 | 482 | 1 | 15800 | 26594 | 5683- 5693 |
| Kleberg | 27.47 | 98.02 | 321 | 63 | 7163 | 0 | 759 | 495 | 11000 | 19801 | 6070- 6084 |
| Kleberg | 27.47 | 98.02 | 719 | 20 | 11238 | 0 | 383 | 9 | 18450 | 30819 | 6071- 6073 |
| Kleberg | 27.47 | 98.00 | 119 | 181 | 10339 | 0 | 2530 | 0 | 15500 | 28195 | 7117- 7137 |
| Kleberg | 27.47 | 98.02 | 150 | 101 | 10284 | 0 | 1421 | 12 | 15600 | 27568 | 6980- 6985 |
| Kleberg | 27.46 | 98.01 | 261 | 13 | 12079 | 0 | 1293 | 24 | 18375 | 32045 | 7099- 7113 |
| Kleberg | 27.46 | 98.02 | 439 | 75 | 9873 | 0 | 1041 | 40 | 15600 | 27068 | 6506- 6520 |
| Kleberg | 27.45 | 98.04 | 159 | 44 | 8864 | 0 | 1884 | 130 | 12900 | 23981 | 6962- 6969 |
| Kleberg | 27.44 | 98.02 | 759 | 39 | 10131 | 0 | 1012 | 30 | 16400 | 28443 | 6765- 6788 |
| Kleberg | 27.45 | 98.05 | 694 | 109 | 10347 | 0 | 691 | 24 | 17100 | 28965 | 5613- 5619 |
| Kleberg | 27.44 | 98.05 | 116 | 69 | 9312 | 0 | 1787 | 140 | 13600 | 25024 | 6762- 6768 |
| Kleberg | 27.44 | 98.05 | 100 | 59 | 10109 | 0 | 1932 | 38 | 14800 | 27038 | 6792- 6822 |
| Kleberg | 27.44 | 98.05 | 416 | 32 | 9323 | 0 | 721 | 3 | 14800 | 25295 | 6031- 6340 |
| Kleberg | 27.44 | 98.05 | 850 | 26 | 10176 | 0 | 411 | 3 | 17050 | 28516 | 6268- 6278 |
| Kleberg | 27.44 | 98.05 | 260 | 19 | 9934 | 0 | 1274 | 11 | 15100 | 26598 | 6268- 6278 |
| Kleberg | 27.45 | 98.06 | 747 | 29 | 10672 | 0 | 256 | 46 | 17700 | 29450 | 4876- 4890 |
| Kleberg | 27.45 | 98.06 | 402 | 28 | 9885 | 0 | 685 | 76 | 15600 | 26676 | 4000- 6699 |
| Kleberg | 27.45 | 98.06 | 695 | 44 | 9327 | 0 | 1607 | 32 | 14800 | 26505 | 4000- 6699 |
| Kleberg | 27.45 | 98.06 | 263 | 17 | 7542 | 0 | 803 | 63 | 11600 | 20325 | 4000- 6699 |
| Kleberg | 27.42 | 98.05 | 573 | 97 | 9418 | 0 | 1840 | 105 | 14650 | 26683 | 6143- 6150 |
| Kleberg | 27.42 | 98.05 | 158 | 18 | 6785 | 0 | 1801 | 40 | 9725 | 18527 | 7008- 7016 |

Table 3d (continued)

| County | Latitude | Longitude | Ca | Mg | Na | K | Alkalinity | SO4 | Cl | TDS | Depth (feet) |
|---------|----------|-----------|------|-----|-------|---|------------|------|-------|-------|--------------|
| Kleberg | 27.42 | 98.05 | 844 | 29 | 8764 | 0 | 110 | 63 | 15000 | 24810 | 4686- 4695 |
| Kleberg | 27.41 | 98.06 | 1404 | 177 | 9561 | 0 | 331 | 100 | 17500 | 29073 | 5258- 5268 |
| Kleberg | 27.41 | 98.06 | 474 | 177 | 8764 | 0 | 919 | 70 | 14300 | 24704 | 6140- 6147 |
| Kleberg | 27.41 | 98.06 | 115 | 193 | 9537 | 0 | 1800 | 40 | 14400 | 26058 | 7087- 7098 |
| Kleberg | 27.40 | 98.06 | 1526 | 34 | 9042 | 0 | 1372 | 101 | 16600 | 28675 | 5294- 5302 |
| Kleberg | 27.40 | 98.06 | 1590 | 10 | 10634 | 0 | 384 | 54 | 19000 | 31672 | 5692- 5699 |
| Kleberg | 27.40 | 98.05 | 334 | 48 | 6108 | 0 | 173 | 1 | 10060 | 16724 | 6902- 6921 |
| Kleberg | 27.57 | 97.93 | 140 | 44 | 9230 | 0 | 1734 | 52 | 13575 | 24775 | 6970- 6975 |
| Kleberg | 27.56 | 97.93 | 873 | 15 | 10579 | 0 | 371 | 7 | 17700 | 29545 | 6168- 6174 |
| Kleberg | 27.58 | 97.91 | 108 | 10 | 5844 | 0 | 1343 | 12 | 8450 | 15767 | 6631- 6638 |
| Kleberg | 27.57 | 97.90 | 1938 | 38 | 9924 | 0 | 411 | 39 | 18600 | 30950 | 6395- 6400 |
| Kleberg | 27.57 | 97.90 | 444 | 19 | 6626 | 0 | 425 | 3140 | 8500 | 19154 | 4000- 6699 |
| Kleberg | 27.57 | 97.90 | 707 | 14 | 6221 | 0 | 76 | 4400 | 7600 | 19018 | 6323- 6328 |
| Kleberg | 27.57 | 97.93 | 226 | 18 | 9884 | 0 | 1041 | 5 | 15100 | 26274 | 6323- 6526 |
| Kleberg | 27.57 | 97.91 | 614 | 24 | 8116 | 0 | 678 | 24 | 13725 | 22731 | 6175- 6183 |
| Kleberg | 27.56 | 97.92 | 198 | 15 | 9645 | 0 | 982 | 12 | 14700 | 25552 | 6985- 6988 |
| Kleberg | 27.54 | 97.99 | 154 | 35 | 9223 | 0 | 2254 | 0 | 13300 | 24966 | 6475- 6491 |
| Kleberg | 27.54 | 97.99 | 117 | 205 | 8578 | 0 | 2141 | 0 | 12800 | 23841 | 6949- 6957 |
| Kleberg | 27.53 | 97.99 | 1495 | 12 | 10134 | 0 | 173 | 42 | 18200 | 30056 | 5214- 5218 |
| Kleberg | 27.53 | 97.98 | 1394 | 11 | 7527 | 0 | 232 | 120 | 13900 | 23184 | 5222- 5229 |
| Kleberg | 27.53 | 97.98 | 103 | 12 | 6647 | 0 | 1676 | 260 | 9310 | 18008 | 6975- 6988 |
| Kleberg | 27.53 | 97.98 | 228 | 14 | 7846 | 0 | 1261 | 32 | 11800 | 21181 | 6335- 6343 |
| Kleberg | 27.53 | 97.98 | 103 | 14 | 5467 | 0 | 1826 | 0 | 14700 | 22110 | 7002- 7008 |
| Kleberg | 27.53 | 97.98 | 87 | 14 | 9543 | 0 | 1977 | 0 | 13775 | 25396 | 7024- 7031 |
| Kleberg | 27.53 | 97.98 | 323 | 29 | 7420 | 0 | 954 | 8 | 11550 | 20284 | 6291- 6298 |
| Kleberg | 27.53 | 97.98 | 77 | 5 | 9093 | 0 | 2456 | 77 | 12700 | 24408 | 4950- 4958 |
| Kleberg | 27.53 | 97.98 | 1 | 1 | 7741 | 0 | 1396 | 572 | 10200 | 19910 | 7131- 7141 |
| Kleberg | 27.53 | 98.00 | 82 | 25 | 9210 | 0 | 2237 | 43 | 13100 | 24697 | 6864- 6873 |
| Kleberg | 27.53 | 98.00 | 83 | 64 | 7754 | 0 | 2138 | 215 | 10900 | 21154 | 6951- 6957 |
| Kleberg | 27.53 | 98.00 | 65 | 3 | 7825 | 0 | 2272 | 40 | 10850 | 21055 | 7100- 7106 |
| Kleberg | 27.53 | 98.00 | 79 | 24 | 8437 | 0 | 2643 | 28 | 11675 | 22886 | 7209- 7216 |
| Kleberg | 27.53 | 97.99 | 1228 | 20 | 10093 | 0 | 346 | 21 | 17600 | 29308 | 6932- 6942 |
| Kleberg | 27.52 | 97.98 | 68 | 18 | 9532 | 0 | 2168 | 32 | 13600 | 25418 | 6932- 6942 |
| Kleberg | 27.51 | 97.99 | 291 | 17 | 9346 | 0 | 1080 | 16 | 14350 | 25100 | 6274- 6285 |
| Kleberg | 27.51 | 97.99 | 61 | 13 | 8973 | 0 | 1842 | 32 | 12900 | 23821 | 7151- 7155 |
| Kleberg | 27.51 | 97.99 | 156 | 16 | 9061 | 0 | 1557 | 3 | 13400 | 24193 | 6355- 6359 |
| Kleberg | 27.51 | 97.99 | 876 | 172 | 7514 | 0 | 459 | 700 | 12800 | 22580 | 5472- 5478 |
| Kleberg | 27.51 | 97.99 | 184 | 48 | 10607 | 0 | 1784 | 0 | 15800 | 28423 | 6467- 6473 |
| Kleberg | 27.51 | 97.99 | 754 | 121 | 8727 | 0 | 540 | 200 | 14700 | 25042 | 5808- 5817 |
| Kleberg | 27.51 | 97.99 | 1517 | 84 | 10576 | 0 | 641 | 120 | 18800 | 31738 | 5483- 5491 |
| Kleberg | 27.51 | 97.99 | 120 | 121 | 11509 | 0 | 1571 | 20 | 17400 | 30741 | 6936- 6948 |
| Kleberg | 27.51 | 97.99 | 104 | 109 | 10110 | 0 | 2010 | 50 | 14900 | 33155 | 4876- 4881 |
| Kleberg | 27.50 | 97.99 | 1788 | 43 | 11002 | 0 | 62 | 60 | 20200 | 33155 | 4876- 4881 |

Table 3d (continued)

| County | Latitude | Longitude | Ca | Mg | Na | K | Alkalinity | SO4 | Cl | TDS | Depth (feet) |
|---------|----------|-----------|-------|------|-------|------|------------|-----|--------|--------|--------------|
| Kleberg | 27.50 | 97.99 | 1818 | 37 | 10919 | 0 | 74 | 60 | 20100 | 33008 | 5156-5180 |
| Kleberg | 27.45 | 98.03 | 155 | 93 | 11032 | 0 | 1474 | 24 | 16700 | 29478 | 7020-7029 |
| Kleberg | 27.45 | 98.03 | 399 | 172 | 9661 | 0 | 845 | 40 | 15600 | 26717 | 6476-6486 |
| Kleberg | 27.48 | 97.79 | 2400 | 24 | 13756 | 0 | 201 | 160 | 25300 | 41841 | 5222-5243 |
| Kleberg | 27.50 | 97.98 | 20 | 26 | 10994 | 0 | 555 | 597 | 16000 | 28192 | 7664-7693 |
| Kleberg | 27.50 | 97.99 | 453 | 29 | 10444 | 0 | 816 | 47 | 16500 | 28289 | 5184 |
| Kleberg | 27.48 | 98.00 | 1629 | 172 | 10578 | 0 | 483 | 52 | 19400 | 32314 | 5143-5151 |
| Kenedy | 26.79 | 97.96 | 1638 | 97 | 13430 | 0 | 362 | 8 | 23699 | 39229 | 8292-8304 |
| Kenedy | 26.88 | 97.84 | 9600 | 88 | 18880 | 0 | 353 | 320 | 45999 | 75239 | 8580-8588 |
| Kenedy | 26.89 | 97.85 | 8771 | 63 | 17570 | 0 | 107 | 752 | 42249 | 69509 | 6277-6291 |
| Kenedy | 26.90 | 97.17 | 5287 | 114 | 26119 | 0 | 233 | 3 | 49899 | 81659 | 17530-17580 |
| Kenedy | 26.96 | 97.76 | 6800 | 3 | 14060 | 0 | 25 | 128 | 33499 | 54659 | 8650-8663 |
| Kenedy | 27.24 | 97.73 | 7557 | 221 | 29169 | 0 | 0 | 62 | 58899 | 95909 | 5963-5967 |
| Kenedy | 27.25 | 97.72 | 8163 | 172 | 26369 | 0 | 111 | 175 | 55499 | 90489 | 6258-6260 |
| Kenedy | 27.26 | 97.74 | 9485 | 419 | 37498 | 0 | 176 | 0 | 60400 | 108000 | 7080-7090 |
| Kenedy | 27.25 | 97.75 | 7554 | 1250 | 25819 | 0 | 61 | 370 | 56600 | 91654 | 6226-6234 |
| Kenedy | 27.25 | 97.75 | 6859 | 1125 | 23226 | 0 | 147 | 300 | 51000 | 82657 | 6383-6390 |
| Kenedy | 27.25 | 97.75 | 9534 | 1375 | 24509 | 0 | 245 | 32 | 58600 | 94295 | 6919-6928 |
| Kenedy | 27.25 | 97.75 | 10078 | 1375 | 25442 | 0 | 270 | 20 | 61000 | 98185 | 7051-7058 |
| Kenedy | 27.25 | 97.75 | 10621 | 1375 | 26867 | 0 | 233 | 0 | 64200 | 103300 | 7081-7089 |
| Kenedy | 27.25 | 97.75 | 10433 | 625 | 20852 | 0 | 220 | 0 | 52400 | 84530 | 7704-7712 |
| Kenedy | 27.25 | 97.75 | 3162 | 1000 | 6535 | 0 | 196 | 122 | 18400 | 29427 | 7777-7785 |
| Kenedy | 27.00 | 97.87 | 16762 | 39 | 20284 | 0 | 0 | 48 | 60200 | 97510 | 8133-8140 |
| Kenedy | 27.00 | 97.87 | 4365 | 542 | 12563 | 0 | 0 | 200 | 28400 | 46205 | 5982-5991 |
| Kenedy | 27.00 | 97.87 | 4412 | 152 | 13875 | 0 | 0 | 460 | 29150 | 48186 | 6194-6204 |
| Kenedy | 27.00 | 97.88 | 12648 | 602 | 16673 | 0 | 208 | 28 | 49800 | 79959 | 7333-7343 |
| Kenedy | 27.00 | 97.88 | 6046 | 455 | 8815 | 0 | 300 | 800 | 24900 | 41316 | 8337-8351 |
| Kenedy | 27.00 | 97.88 | 7577 | 485 | 7240 | 0 | 98 | 355 | 25550 | 41450 | 8176-8188 |
| Kenedy | 27.38 | 97.55 | 8100 | 95 | 25600 | 150 | 84 | 25 | 53850 | 91200 | 7262-7340 |
| Kenedy | 26.67 | 97.45 | 5939 | 241 | 38300 | 1066 | 173 | 22 | 61500 | 132573 | 15728-15775 |
| Kenedy | 26.67 | 97.45 | 15400 | 26 | 19750 | 143 | 59 | 5 | 56300 | 96300 | 8604-8608 |
| Kenedy | 26.67 | 97.45 | 2440 | 8 | 1370 | 34 | 26 | 1 | 6530 | 10600 | 15728-15828 |
| Kenedy | 26.67 | 97.45 | 32240 | 220 | 39900 | 2900 | 47 | 12 | 129400 | 245600 | 12781-12870 |
| Kenedy | 26.67 | 97.45 | 34000 | 12 | 11300 | 200 | 70 | 2 | 76650 | 125200 | 10028-10040 |
| Kenedy | 26.67 | 97.45 | 35800 | 177 | 46000 | 3200 | 53 | 7 | 141000 | 252000 | 12781-12870 |
| Kenedy | 26.67 | 97.45 | 27500 | 46 | 14200 | 135 | 43 | 1 | 70000 | 111400 | 9304-9316 |
| Kenedy | 26.67 | 97.45 | 22260 | 117 | 17870 | 140 | 48 | 2 | 65400 | 102600 | 9476-9484 |
| Kenedy | 27.00 | 97.88 | 15800 | 70 | 13900 | 145 | 21 | 10 | 50150 | 81800 | 8801-8836 |
| Kenedy | 27.00 | 97.88 | 14100 | 74 | 23400 | 148 | 120 | 10 | 59300 | 94600 | 7492-7496 |
| Kenedy | 27.00 | 97.88 | 28700 | 98 | 33300 | 1870 | 127 | 2 | 105300 | 171000 | 12939-12946 |
| Kenedy | 27.27 | 97.73 | 6675 | 287 | 29000 | 142 | 51 | 5 | 57800 | 97700 | 7321-7328 |
| Kenedy | 27.27 | 97.73 | 7670 | 112 | 25950 | 137 | 143 | 3 | 55900 | 95900 | 7439-7443 |
| Kenedy | 27.27 | 97.73 | 5350 | 319 | 23350 | 225 | 135 | 100 | 47150 | 79100 | 13837-14667 |

Table 3d (continued)

| County | Latitude | Longitude | Ca | Mg | Na | K | Alkalinity | SO4 | Cl | TDS | Depth (feet) |
|--------|----------|-----------|-------|-----|-------|------|------------|-----|-------|--------|--------------|
| Kenedy | 27.27 | 97.73 | 25400 | 111 | 23850 | 1250 | 89 | 3 | 81400 | 146200 | 14302-14599 |
| Kenedy | 27.23 | 98.93 | 2045 | 65 | 19800 | 264 | 411 | 1 | 35000 | 57685 | 9364- 9370 |
| Kenedy | 27.00 | 97.88 | 9721 | 153 | 21500 | 1040 | 216 | 0 | 53300 | 85930 | 14304 |
| Kenedy | 27.00 | 97.88 | 12036 | 134 | 26200 | 1263 | 14 | 0 | 64600 | 104247 | 12687 |
| Kenedy | 27.15 | 97.73 | 23970 | 139 | 19300 | 1112 | 147 | 0 | 73200 | 117868 | 14304 |
| Kenedy | 27.00 | 97.88 | 2540 | 25 | 3800 | 219 | 227 | 0 | 10700 | 17511 | 12936 |
| Kenedy | 27.00 | 97.88 | 27438 | 138 | 27700 | 1773 | 271 | 0 | 95500 | 152820 | 12769 |

Table 4. Major and minor ion chemistry from Frio Formation. Ionic concentrations in mg/L. Data from Kreitler and Richter (1986), and Morton and Land (1987).

| No. | County | Latitude | Longitude | Depth (ft) | TDS | Ca | Mg | Na | K | Alkalinity | SO4 | Cl | Fe | SiO2 | Sr | Ba | B | Br |
|-----|--------------|----------|-----------|------------|--------|------|-----|-------|-----|------------|-----|-------|-----|------|-----|-----|----|-----|
| 1 | Aransas | 28.00 | 97.00 | 10932 | 25472 | 2234 | 120 | 6946 | 238 | 979 | 0 | 14955 | 0 | 478 | 35 | 0 | 1 | 1 |
| 2 | Aransas | 28.00 | 97.00 | 9509 | 17441 | 130 | 3 | 6700 | 48 | 1428 | 82 | 9050 | 0 | 149 | 10 | 0 | 0 | 0 |
| 3 | Aransas | 27.47 | 97.27 | 11697 | 22900 | 330 | 29 | 8400 | 130 | 540 | 49 | 13400 | 2.6 | 87 | 28 | 0 | 41 | 78 |
| 4 | Aransas | 28.14 | 96.50 | 9203 | 16600 | 30 | 5 | 7050 | 49 | 2040 | 86 | 8700 | 2 | 97 | 5 | 0 | 39 | 49 |
| 5 | San Patricio | 28.01 | 97.15 | 10965 | 15900 | 42 | 9 | 5650 | 33 | 800 | 66 | 7600 | 117 | 51 | 5 | 0 | 38 | 19 |
| 6 | San Patricio | 28.01 | 97.15 | 10521 | 18600 | 45 | 8 | 7170 | 32 | 1720 | 64 | 9400 | 36 | 82 | 4 | 0 | 51 | 34 |
| 7 | San Patricio | 27.54 | 97.25 | 10670 | 24600 | 134 | 22 | 9000 | 59 | 939 | 46 | 13400 | 8 | 80 | 9 | 3.8 | 54 | 34 |
| 8 | San Patricio | 27.54 | 97.25 | 11528 | 17900 | 89 | 15 | 6500 | 68 | 1040 | 110 | 9270 | 2 | 93 | 7 | 1.4 | 62 | 19 |
| 9 | San Patricio | 27.54 | 97.25 | 11050 | 20300 | 101 | 18 | 7500 | 62 | 932 | 59 | 10700 | 34 | 73 | 7 | 3.7 | 54 | 30 |
| 10 | San Patricio | 27.54 | 97.25 | 11480 | 14700 | 54 | 9 | 5375 | 43 | 775 | 75 | 7400 | 17 | 79 | 4 | 1.5 | 54 | 0 |
| 11 | San Patricio | 27.54 | 97.25 | 11180 | 16600 | 47 | 9 | 6250 | 46 | 1213 | 67 | 8200 | 5 | 86 | 4 | 1.4 | 55 | 21 |
| 12 | San Patricio | 28.00 | 97.13 | 10550 | 17500 | 42 | 9 | 6500 | 51 | 858 | 54 | 8700 | 0.1 | 85 | 5 | 1 | 58 | 24 |
| 13 | San Patricio | 27.58 | 97.20 | 12120 | 32400 | 370 | 56 | 11750 | 44 | 575 | 26 | 18700 | 6 | 92 | 28 | 11 | 41 | 29 |
| 14 | San Patricio | 27.58 | 97.20 | 11880 | 36300 | 330 | 48 | 13250 | 72 | 200 | 42 | 21000 | 2 | 132 | 23 | 13 | 35 | 45 |
| 15 | San Patricio | 27.54 | 97.25 | 4900 | 85400 | 2500 | 455 | 29500 | 215 | 270 | 13 | 51700 | 14 | 32 | 275 | 115 | 53 | 260 |
| 16 | San Patricio | 27.54 | 97.25 | 3350 | 69800 | 3040 | 475 | 22750 | 77 | 97 | 67 | 42800 | 17 | 18 | 155 | 61 | 35 | 200 |
| 17 | San Patricio | 27.54 | 97.25 | 4600 | 83300 | 2500 | 590 | 28500 | 152 | 189 | 15 | 50600 | 8 | 26 | 265 | 160 | 61 | 240 |
| 18 | San Patricio | 27.54 | 97.25 | 5790 | 74600 | 2880 | 340 | 25250 | 125 | 113 | 50 | 45100 | 9 | 35 | 275 | 140 | 55 | 210 |
| 19 | San Patricio | 27.54 | 97.25 | 10320 | 24800 | 200 | 31 | 9250 | 70 | 278 | 22 | 14000 | 70 | 34 | 25 | 12 | 24 | 37 |
| 20 | San Patricio | 28.01 | 97.15 | 10965 | 15900 | 42 | 9 | 5650 | 33 | 800 | 66 | 7600 | 117 | 51 | 5 | 0 | 38 | 19 |
| 21 | San Patricio | 28.01 | 97.15 | 10521 | 18600 | 45 | 8 | 7170 | 32 | 1720 | 64 | 9400 | 36 | 82 | 4 | 0 | 51 | 34 |
| 22 | San Patricio | 27.59 | 97.18 | 9656 | 77800 | 484 | 29 | 31300 | 173 | 237 | 270 | 46100 | 317 | 33 | 16 | 0 | 33 | 45 |
| 23 | San Patricio | 27.59 | 97.18 | 9660 | 19900 | 24 | 12 | 8100 | 41 | 1220 | 9 | 10900 | 0.8 | 53 | 10 | 0 | 37 | 45 |
| 24 | San Patricio | 27.59 | 97.18 | 10693 | 20700 | 282 | 22 | 7550 | 73 | 687 | 15 | 12150 | 1.6 | 134 | 22 | 0 | 40 | 40 |
| 25 | San Patricio | 27.59 | 97.18 | 11074 | 32500 | 398 | 46 | 12690 | 92 | 820 | 9 | 19000 | 3.4 | 124 | 34 | 0 | 48 | 54 |
| 26 | San Patricio | 27.52 | 97.18 | 10665 | 27400 | 156 | 23 | 10500 | 78 | 1120 | 52 | 15200 | 0.2 | 83 | 18 | 0 | 74 | 43 |
| 27 | San Patricio | 27.52 | 97.18 | 9715 | 16900 | 48 | 8 | 7330 | 40 | 2760 | 37 | 8900 | 0.4 | 111 | 5 | 0 | 56 | 40 |
| 28 | San Patricio | 27.52 | 97.18 | 9480 | 19400 | 31 | 8 | 7860 | 55 | 1720 | 4 | 10200 | 0.2 | 126 | 9 | 0 | 44 | 36 |
| 29 | San Patricio | 25.58 | 97.14 | 10475 | 21000 | 27 | 9 | 7900 | 36 | 1750 | 58 | 10300 | 1.9 | 88 | 5 | 0 | 41 | 36 |
| 30 | San Patricio | 27.52 | 97.18 | 10667 | 27500 | 101 | 21 | 10000 | 62 | 915 | 40 | 15100 | 32 | 70 | 11 | 0 | 49 | 38 |
| 31 | San Patricio | 27.50 | 97.00 | 10978 | 23875 | 158 | 26 | 9400 | 71 | 0 | 120 | 14100 | 0 | 122 | 11 | 0 | 1 | 0 |
| 32 | San Patricio | 27.50 | 97.00 | 10739 | 31203 | 207 | 34 | 11900 | 81 | 1143 | 38 | 17800 | 13 | 190 | 18 | 0 | 1 | 0 |
| 33 | San Patricio | 27.50 | 97.00 | 10535 | 17045 | 56 | 10 | 7230 | 45 | 0 | 4 | 9700 | 0 | 179 | 6 | 0 | 1 | 0 |
| 34 | San Patricio | 27.50 | 97.00 | 10906 | 26376 | 190 | 31 | 10500 | 80 | 0 | 75 | 15500 | 8 | 144 | 16 | 0 | 1 | 0 |
| 35 | San Patricio | 27.50 | 97.00 | 10653 | 35335 | 748 | 84 | 13300 | 156 | 0 | 47 | 21000 | 182 | 205 | 34 | 0 | 0 | 0 |
| 36 | Nueces | 27.50 | 97.30 | 11218 | 77481 | 7660 | 200 | 21600 | 270 | 0 | 1 | 47750 | 85 | 52 | 508 | 0 | 1 | 0 |
| 37 | Nueces | 27.50 | 97.30 | 9912 | 46618 | 6450 | 93 | 11400 | 124 | 0 | 1 | 28550 | 200 | 29 | 350 | 0 | 0 | 0 |
| 38 | Nueces | 27.50 | 97.30 | 8869 | 101815 | 9100 | 240 | 30200 | 300 | 0 | 5 | 61970 | 7 | 98 | 680 | 0 | 0 | 0 |
| 39 | Nueces | 27.50 | 97.30 | 10444 | 43770 | 298 | 48 | 17700 | 91 | 0 | 33 | 25600 | 0 | 128 | 31 | 0 | 0 | 0 |
| 40 | Nueces | 27.50 | 97.30 | 11119 | 44787 | 590 | 70 | 17140 | 177 | 0 | 10 | 26800 | 0 | 138 | 54 | 0 | 1 | 0 |
| 41 | Nueces | 27.50 | 97.30 | 32797 | 30181 | 2490 | 9 | 8830 | 845 | 407 | 0 | 17600 | 0 | 8 | 93 | 0 | 1 | 1 |

Table 4 (continued)

| No. | County | Latitude | Longitude | Depth (ft) | TDS | Ca | Mg | Na | K | Alkalinity | SO4 | Cl | Fe | SiO2 | Sr | Ba | B | Br |
|-----|-----------|----------|-----------|------------|--------|-------|------|-------|------|------------|-----|--------|------|------|------|-----|-----|-----|
| 42 | Nueces | 27.50 | 97.30 | 11329 | 24286 | 459 | 48 | 8850 | 328 | 800 | 1 | 13800 | 38 | 227 | 40 | 0 | 1 | 1 |
| 43 | Nueces | 27.50 | 97.30 | 32797 | 19311 | 430 | 395 | 6910 | 102 | 574 | 0 | 10900 | 0 | 114 | 46 | 0 | 1 | 1 |
| 44 | Nueces | 27.52 | 97.21 | 9000 | 80100 | 3700 | 375 | 26000 | 260 | 162 | 18 | 48200 | 14 | 55 | 440 | 92 | 33 | 267 |
| 45 | Nueces | 27.45 | 97.33 | 10460 | 37900 | 166 | 28 | 14400 | 76 | 1550 | 28 | 20600 | 4.8 | 114 | 20 | 0 | 44 | 127 |
| 46 | Nueces | 27.45 | 97.33 | 9340 | 34200 | 181 | 30 | 13300 | 105 | 990 | 18 | 20000 | 4.3 | 90 | 51 | 0 | 36 | 92 |
| 47 | Nueces | 27.45 | 97.33 | 10879 | 29900 | 491 | 45 | 10600 | 264 | 570 | 46 | 16700 | 2.6 | 108 | 46 | 0 | 47 | 63 |
| 48 | Nueces | 27.45 | 97.33 | 12538 | 24500 | 375 | 26 | 8860 | 375 | 400 | 5 | 14000 | 21.2 | 192 | 31 | 0 | 67 | 56 |
| 49 | Nueces | 27.45 | 97.33 | 11658 | 38900 | 87 | 38 | 15200 | 211 | 1070 | 3 | 22000 | 0.1 | 271 | 58 | 0 | 43 | 104 |
| 50 | Nueces | 27.47 | 97.15 | 10942 | 213000 | 21000 | 715 | 53600 | 485 | 114 | 8 | 125600 | 38 | 33 | 1300 | 0 | 34 | 580 |
| 51 | Nueces | 27.52 | 97.09 | 10682 | 21200 | 83 | 16 | 8000 | 4 | 740 | 25 | 11600 | 3 | 72 | 11 | 0 | 59 | 31 |
| 52 | Nueces | 27.52 | 97.09 | 8784 | 31800 | 1640 | 15 | 10500 | 95 | 115 | 47 | 18900 | 140 | 16 | 100 | 0 | 4 | 71 |
| 53 | Nueces | 27.47 | 97.15 | 10942 | 214524 | 36020 | 1664 | 42138 | 0 | 237 | 1 | 133680 | 220 | 17 | 0 | 548 | 0 | 0 |
| 54 | Nueces | 27.47 | 97.15 | 9983 | 226262 | 29640 | 1791 | 53051 | 0 | 41 | 1 | 139700 | 486 | 20 | 0 | 533 | 0 | 0 |
| 55 | Nueces | 27.47 | 97.15 | 12490 | 241606 | 31190 | 1640 | 57732 | 0 | 123 | 1 | 149460 | 280 | 78 | 0 | 103 | 0 | 0 |
| 56 | Kenedy | 27.23 | 97.33 | 7262 | 91200 | 8100 | 95 | 25600 | 150 | 84 | 25 | 53850 | 1.4 | 44 | 500 | 0 | 69 | 245 |
| 57 | Kenedy | 26.40 | 97.27 | 8604 | 96300 | 15400 | 26 | 19750 | 143 | 59 | 5 | 56300 | 2.8 | 54 | 800 | 0 | 64 | 225 |
| 58 | Kenedy | 26.40 | 97.27 | 15728 | 10600 | 2440 | 8 | 1370 | 34 | 26 | 1 | 6530 | 75 | 23 | 110 | 0 | 7 | 25 |
| 59 | Kenedy | 26.40 | 97.27 | 12781 | 245600 | 32240 | 220 | 39900 | 2900 | 47 | 12 | 129400 | 35 | 56 | 1670 | 0 | 100 | 800 |
| 60 | Kenedy | 26.40 | 97.27 | 10028 | 125200 | 34000 | 12 | 11300 | 200 | 70 | 2 | 76650 | 0.5 | 82 | 1180 | 0 | 36 | 353 |
| 61 | Kenedy | 26.40 | 97.27 | 12781 | 252000 | 35800 | 177 | 46000 | 3200 | 53 | 7 | 141000 | 81.5 | 88 | 1970 | 0 | 111 | 710 |
| 62 | Kenedy | 26.40 | 97.27 | 9304 | 111400 | 27500 | 46 | 14200 | 135 | 43 | 1 | 70000 | 8.5 | 73 | 1280 | 0 | 37 | 287 |
| 63 | Kenedy | 26.40 | 97.27 | 9476 | 102600 | 22260 | 117 | 17870 | 140 | 48 | 2 | 65400 | 24.6 | 144 | 1220 | 0 | 47 | 299 |
| 64 | Kenedy | 27.00 | 97.53 | 8801 | 81800 | 15800 | 70 | 13900 | 145 | 21 | 10 | 50150 | 50 | 41 | 740 | 0 | 34 | 220 |
| 65 | Kenedy | 27.00 | 97.53 | 7492 | 94600 | 14100 | 74 | 23400 | 148 | 120 | 10 | 59300 | 6.6 | 55 | 860 | 0 | 66 | 237 |
| 66 | Kenedy | 27.00 | 97.53 | 12939 | 171000 | 28700 | 98 | 33300 | 1870 | 127 | 2 | 105300 | 21.6 | 103 | 2120 | 0 | 122 | 567 |
| 67 | Kenedy | 27.16 | 97.44 | 7321 | 97700 | 6675 | 287 | 29000 | 142 | 51 | 5 | 57800 | 6.7 | 33 | 290 | 0 | 41 | 220 |
| 68 | Kenedy | 27.16 | 97.44 | 7439 | 95900 | 7670 | 112 | 25950 | 137 | 143 | 3 | 55900 | 0.6 | 56 | 643 | 0 | 76 | 239 |
| 69 | Kenedy | 27.16 | 97.44 | 13837 | 79100 | 5350 | 319 | 23350 | 225 | 135 | 100 | 47150 | 4.5 | 26 | 281 | 0 | 40 | 178 |
| 70 | Kenedy | 27.16 | 97.44 | 14302 | 146200 | 25400 | 111 | 23850 | 1250 | 89 | 3 | 81400 | 23.5 | 82 | 1100 | 0 | 78 | 215 |
| 71 | Kenedy | 27.00 | 97.50 | 6199 | 101749 | 3670 | 427 | 36300 | 217 | 85 | 350 | 60700 | 7 | 62 | 285 | 0.7 | 1 | 0 |
| 72 | Kenedy | 27.00 | 97.50 | 6098 | 94925 | 3140 | 360 | 32900 | 195 | 120 | 840 | 57370 | 20 | 68 | 214 | 0.7 | 1 | 0 |
| 73 | Kenedy | 27.00 | 97.50 | 6199 | 92522 | 2900 | 333 | 33050 | 184 | 65 | 260 | 55730 | 36 | 4 | 206 | 0.8 | 1 | 0 |
| 74 | Kenedy | 27.00 | 97.50 | 14248 | 91360 | 6510 | 178 | 27190 | 1160 | 0 | 22 | 56300 | 65 | 122 | 500 | 0 | 1 | 0 |
| 75 | Jefferson | 29.36 | 94.25 | 10421 | 57200 | 480 | 100 | 22600 | 146 | 1130 | 14 | 33800 | 0.1 | 58 | 70 | 0 | 65 | 67 |
| 76 | Jefferson | 28.00 | 97.15 | 10906 | 27900 | 190 | 31 | 10500 | 80 | 880 | 75 | 15500 | 8 | 90 | 15 | 0 | 96 | 42 |
| 77 | Jefferson | 29.48 | 94.10 | 6300 | 120067 | 3800 | 779 | 41800 | 0 | 80 | 15 | 73500 | 12 | 0 | 0 | 92 | 0 | 0 |
| 78 | Jefferson | 29.48 | 94.10 | 6900 | 121611 | 2930 | 1020 | 43000 | 0 | 89 | 1 | 74500 | 26 | 0 | 0 | 58 | 0 | 0 |
| 79 | Jefferson | 29.50 | 94.00 | 9489 | 42468 | 204 | 55 | 17250 | 99 | 0 | 460 | 24400 | 0 | 106 | 45 | 0 | 1 | 1 |
| 80 | Chambers | 29.38 | 94.54 | 5806 | 105789 | 1764 | 420 | 38472 | 265 | 244 | 373 | 63900 | 10.6 | 47 | 166 | 0 | 53 | 68 |
| 81 | Chambers | 29.38 | 94.54 | 5822 | 106498 | 2095 | 613 | 38878 | 226 | 195 | 186 | 63900 | 45.7 | 36 | 193 | 0 | 39 | 68 |
| 82 | Chambers | 29.38 | 94.54 | 5814 | 104776 | 1849 | 458 | 37482 | 262 | 231 | 230 | 63900 | 16.8 | 44 | 204 | 0 | 35 | 55 |

Table 4 (continued)

| No. | County | Latitude | Longitude | Depth (ft) | TDS | Ca | Mg | Na | K | Alkalinity | SO4 | Cl | Fe | SiO2 | Sr | Ba | B | Br |
|-----|-----------|----------|-----------|------------|--------|-------|------|-------|------|------------|------|--------|-----|------|-----|-----|----|-----|
| 83 | Chambers | 29.38 | 94.54 | 5952 | 109142 | 2050 | 511 | 39672 | 240 | 207 | 360 | 65675 | 9.3 | 34 | 245 | 0 | 49 | 68 |
| 84 | Chambers | 29.32 | 94.50 | 10098 | 46992 | 1020 | 197 | 16900 | 0 | 590 | 36 | 28200 | 272 | 0 | 0 | 15 | 0 | 0 |
| 85 | Chambers | 29.32 | 94.50 | 9730 | 87982 | 1010 | 343 | 32900 | 0 | 485 | 1 | 53200 | 6 | 0 | 0 | 40 | 0 | 0 |
| 86 | Chambers | 29.32 | 94.50 | 10440 | 93652 | 1500 | 343 | 34600 | 0 | 554 | 1 | 56600 | 20 | 0 | 0 | 53 | 0 | 0 |
| 87 | Chambers | 29.32 | 94.50 | 10836 | 64000 | 887 | 218 | 23700 | 0 | 546 | 1 | 38600 | 2 | 0 | 0 | 37 | 0 | 0 |
| 88 | Chambers | 29.32 | 94.50 | 8166 | 119819 | 4870 | 9450 | 27200 | 0 | 179 | 1 | 78000 | 11 | 0 | 0 | 115 | 0 | 0 |
| 89 | Chambers | 29.32 | 94.50 | 9334 | 142203 | 7590 | 766 | 46300 | 0 | 185 | 1 | 87100 | 30 | 0 | 0 | 224 | 0 | 0 |
| 90 | Chambers | 29.46 | 94.23 | 10465 | 84800 | 4230 | 550 | 27900 | 0 | 1 | 1 | 52100 | 185 | 0 | 0 | 6 | 0 | 0 |
| 91 | Chambers | 29.46 | 94.23 | 8396 | 80576 | 2190 | 953 | 27700 | 0 | 237 | 13 | 49400 | 12 | 0 | 0 | 83 | 0 | 0 |
| 92 | Chambers | 29.40 | 94.20 | 12149 | 122095 | 4280 | 465 | 43600 | 450 | 0 | 0 | 73300 | 0 | 117 | 415 | 0 | 0 | 1 |
| 93 | Chambers | 29.40 | 94.20 | 11598 | 78125 | 2485 | 430 | 27450 | 340 | 0 | 720 | 46700 | 0 | 101 | 230 | 0 | 0 | 1 |
| 94 | Harris | 29.45 | 95.06 | 6865 | 113375 | 2320 | 437 | 41415 | 0 | 61 | 1 | 69255 | 0 | 0 | 0 | 85 | 0 | 0 |
| 95 | Harris | 29.45 | 95.06 | 7650 | 124900 | 1850 | 440 | 34500 | 0 | 150 | 11 | 60140 | 13 | 29 | 130 | 43 | 25 | 0 |
| 96 | Harris | 29.43 | 95.07 | 7650 | 65000 | 10 | 5 | 25000 | 0 | 1400 | 1600 | 36800 | 3 | 0 | 0 | 0 | 0 | 0 |
| 97 | Harris | 29.25 | 95.10 | 11398 | 139000 | 8350 | 710 | 44000 | 624 | 88 | 2 | 83600 | 0.1 | 25 | 350 | 0 | 68 | 81 |
| 98 | Harris | 29.25 | 95.10 | 11472 | 133000 | 8580 | 670 | 42400 | 643 | 94 | 3 | 80900 | 0.1 | 22 | 380 | 0 | 64 | 80 |
| 99 | Galveston | 29.20 | 95.00 | 11401 | 137286 | 8350 | 710 | 44000 | 624 | 0 | 2 | 83600 | 0 | 40 | 350 | 0 | 1 | 1 |
| 100 | Galveston | 29.20 | 95.00 | 11483 | 133196 | 8580 | 670 | 42400 | 643 | 0 | 3 | 80900 | 0 | 35 | 380 | 0 | 1 | 1 |
| 101 | Galveston | 29.20 | 95.00 | 11277 | 55529 | 1190 | 153 | 20900 | 185 | 0 | 1 | 33100 | 5 | 71 | 143 | 0 | 0 | 0 |
| 102 | Galveston | 29.20 | 95.00 | 9774 | 138242 | 4260 | 660 | 49300 | 371 | 0 | 51 | 83600 | 0 | 14 | 381 | 0 | 1 | 1 |
| 103 | Galveston | 29.18 | 95.08 | 8615 | 42100 | 290 | 60 | 16500 | 110 | 397 | 39 | 23200 | 0.1 | 70 | 22 | 0 | 42 | 60 |
| 104 | Galveston | 29.20 | 95.06 | 12270 | 79900 | 1490 | 151 | 29800 | 230 | 536 | 18 | 46300 | 3.9 | 83 | 272 | 0 | 53 | 57 |
| 105 | Galveston | 29.20 | 95.06 | 11250 | 58900 | 783 | 95 | 22700 | 192 | 628 | 7 | 35200 | 0.1 | 114 | 145 | 0 | 39 | 43 |
| 106 | Galveston | 29.20 | 95.06 | 10800 | 62500 | 606 | 88 | 24900 | 180 | 848 | 6 | 36700 | 0.1 | 102 | 116 | 0 | 44 | 48 |
| 107 | Galveston | 29.30 | 95.03 | 8663 | 119339 | 4320 | 708 | 41030 | 0 | 793 | 1 | 72700 | 13 | 0 | 0 | 323 | 0 | 0 |
| 108 | Galveston | 29.20 | 95.06 | 13014 | 42223 | 880 | 183 | 15200 | 0 | 673 | 13 | 25180 | 0 | 0 | 0 | 94 | 0 | 0 |
| 109 | Galveston | 29.20 | 95.06 | 11150 | 49034 | 660 | 134 | 18170 | 0 | 630 | 7 | 29260 | 89 | 0 | 0 | 84 | 0 | 0 |
| 110 | Galveston | 29.22 | 95.08 | 8795 | 41300 | 380 | 70 | 15250 | 140 | 414 | 31 | 23400 | 1 | 62 | 21 | 14 | 45 | 55 |
| 111 | Galveston | 29.22 | 95.08 | 8828 | 42500 | 400 | 75 | 16000 | 120 | 312 | 32 | 23800 | 0.1 | 65 | 22 | 13 | 46 | 53 |
| 112 | Galveston | 29.21 | 94.58 | 8933 | 44600 | 470 | 85 | 17000 | 160 | 643 | 34 | 25200 | 0.1 | 64 | 35 | 16 | 41 | 25 |
| 113 | Galveston | 29.20 | 95.06 | 11080 | 53100 | 700 | 90 | 19500 | 190 | 787 | 11 | 31000 | 7 | 80 | 130 | 64 | 30 | 32 |
| 114 | Galveston | 29.20 | 95.06 | 12992 | 50400 | 1230 | 170 | 18250 | 190 | 506 | 8 | 29300 | 41 | 99 | 150 | 110 | 59 | 49 |
| 115 | Brazoria | 29.20 | 95.20 | 9715 | 81026 | 903 | 196 | 30600 | 216 | 0 | 11 | 49100 | 0 | 90 | 154 | 0 | 0 | 1 |
| 116 | Brazoria | 29.20 | 95.20 | 12402 | 92612 | 4621 | 535 | 29090 | 306 | 560 | 0 | 57500 | 999 | 110 | 657 | 0 | 1 | 1 |
| 117 | Brazoria | 29.24 | 95.17 | 10497 | 98500 | 1010 | 180 | 37900 | 292 | 600 | 12 | 59500 | 0.1 | 60 | 157 | 0 | 65 | 94 |
| 118 | Brazoria | 29.16 | 95.18 | 12558 | 235000 | 22600 | 1535 | 69700 | 1218 | 30 | 16 | 152000 | 0.1 | 60 | 0 | 0 | 0 | 342 |
| 119 | Brazoria | 29.22 | 95.15 | 10858 | 56600 | 330 | 60 | 22700 | 171 | 1280 | 21 | 34000 | 8 | 95 | 50 | 0 | 56 | 80 |
| 120 | Brazoria | 29.19 | 95.12 | 8610 | 42800 | 380 | 70 | 16250 | 140 | 361 | 43 | 24000 | 1 | 68 | 25 | 11 | 45 | 59 |
| 121 | Brazoria | 29.19 | 95.12 | 8615 | 40200 | 280 | 60 | 15250 | 120 | 427 | 43 | 22500 | 0.1 | 75 | 22 | 8.5 | 44 | 59 |
| 122 | Brazoria | 29.19 | 95.12 | 8845 | 40000 | 180 | 40 | 15750 | 110 | 525 | 42 | 22400 | 0.1 | 74 | 19 | 11 | 45 | 50 |
| 123 | Brazoria | 29.19 | 95.12 | 8615 | 42100 | 290 | 60 | 16500 | 130 | 397 | 39 | 23200 | 0.1 | 70 | 22 | 9 | 42 | 60 |

Table 4 (continued)

| No. | County | Latitude | Longitude | Depth (ft) | TDS | Ca | Mg | Na | K | Alkalinity | SO4 | Cl | Fe | SiO2 | Sr | Ba | B | Br |
|-----|-----------|----------|-----------|------------|--------|------|-----|-------|-----|------------|-----|-------|-----|------|------|-----|----|-----|
| 124 | Brazoria | 29.19 | 95.12 | 9780 | 42000 | 130 | 30 | 16500 | 120 | 582 | 25 | 23800 | 0.1 | 84 | 22 | 12 | 40 | 38 |
| 125 | Brazoria | 29.19 | 95.12 | 11360 | 73300 | 2000 | 220 | 26500 | 400 | 333 | 3 | 42700 | 10 | 87 | 365 | 290 | 35 | 52 |
| 126 | Brazoria | 29.19 | 95.12 | 10690 | 63700 | 710 | 90 | 25000 | 280 | 269 | 11 | 36300 | 0.1 | 81 | 130 | 61 | 35 | 59 |
| 127 | Brazoria | 29.19 | 95.12 | 11164 | 63000 | 1700 | 200 | 22000 | 270 | 262 | 5 | 37500 | 15 | 63 | 360 | 240 | 27 | 43 |
| 128 | Brazoria | 29.19 | 95.12 | 9255 | 33400 | 130 | 25 | 13000 | 90 | 562 | 57 | 18100 | 0.1 | 84 | 12 | 7 | 48 | 46 |
| 129 | Brazoria | 29.19 | 95.12 | 9285 | 35800 | 160 | 35 | 14000 | 90 | 632 | 59 | 19600 | 8 | 95 | 13 | 6.8 | 47 | 37 |
| 130 | Brazoria | 29.19 | 95.12 | 11286 | 60700 | 610 | 95 | 23250 | 220 | 302 | 11 | 35200 | 8 | 87 | 150 | 6.6 | 33 | 49 |
| 131 | Brazoria | 29.19 | 95.12 | 11725 | 68600 | 2000 | 235 | 24000 | 300 | 317 | 1 | 40500 | 8 | 87 | 380 | 370 | 30 | 45 |
| 132 | Brazoria | 29.19 | 95.12 | 9278 | 36600 | 140 | 30 | 14000 | 100 | 596 | 17 | 20400 | 1 | 78 | 14 | 8 | 48 | 33 |
| 133 | Brazoria | 29.19 | 95.12 | 9281 | 34300 | 170 | 30 | 12500 | 100 | 484 | 59 | 19600 | 2 | 79 | 13 | 7.3 | 50 | 32 |
| 134 | Brazoria | 29.17 | 95.08 | 13650 | 58000 | 1800 | 170 | 20500 | 180 | 356 | 16 | 34500 | 22 | 110 | 170 | 59 | 91 | 32 |
| 135 | Brazoria | 29.17 | 95.08 | 12770 | 50200 | 1600 | 185 | 17750 | 240 | 400 | 6 | 29300 | 17 | 95 | 170 | 110 | 46 | 31 |
| 136 | Matagorda | 29.04 | 95.54 | 8940 | 100000 | 1620 | 286 | 37400 | 310 | 230 | 15 | 61000 | 0.1 | 47 | 213 | 0 | 48 | 80 |
| 137 | Matagorda | 29.04 | 95.54 | 8996 | 98800 | 1660 | 277 | 36000 | 359 | 242 | 6 | 59100 | 0.1 | 49 | 213 | 0 | 51 | 79 |
| 138 | Matagorda | 29.04 | 95.54 | 8708 | 93700 | 1070 | 225 | 35900 | 260 | 257 | 7 | 56900 | 0.1 | 52 | 182 | 0 | 50 | 66 |
| 139 | Matagorda | 28.59 | 95.55 | 8893 | 39048 | 118 | 26 | 15040 | 110 | 1251 | 11 | 22480 | 2.1 | 73 | 0 | 12 | 0 | 0 |
| 140 | Matagorda | 28.57 | 96.10 | 8322 | 83540 | 1230 | 356 | 30900 | 0 | 171 | 6 | 50800 | 21 | 0 | 0 | 71 | 0 | 0 |
| 141 | Matagorda | 28.57 | 96.10 | 8348 | 57341 | 671 | 153 | 21500 | 0 | 469 | 18 | 34500 | 10 | 0 | 0 | 30 | 0 | 0 |
| 142 | Matagorda | 29.04 | 95.54 | 9195 | 78600 | 2006 | 648 | 27061 | 0 | 854 | 1 | 46718 | 65 | 0 | 0 | 140 | 0 | 0 |
| 143 | Matagorda | 29.04 | 95.54 | 8897 | 98836 | 2890 | 401 | 35000 | 0 | 279 | 1 | 60200 | 14 | 0 | 0 | 61 | 0 | 0 |
| 144 | Matagorda | 29.04 | 95.54 | 8980 | 90938 | 2380 | 23 | 33000 | 0 | 263 | 360 | 54800 | 23 | 0 | 0 | 112 | 0 | 0 |
| 145 | Matagorda | 29.04 | 95.54 | 8920 | 109673 | 1710 | 349 | 40600 | 0 | 260 | 78 | 66600 | 35 | 0 | 0 | 79 | 0 | 0 |
| 146 | Matagorda | 29.00 | 95.50 | 8735 | 95418 | 1188 | 239 | 36200 | 270 | 515 | 6 | 57000 | 0 | 74 | 188 | 0 | 0 | 1 |
| 147 | Matagorda | 29.00 | 95.50 | 8961 | 104612 | 1770 | 296 | 38900 | 379 | 561 | 6 | 62700 | 0 | 82 | 217 | 0 | 0 | 1 |
| 148 | Matagorda | 29.00 | 95.50 | 10798 | 47256 | 4784 | 130 | 12590 | 144 | 286 | 22 | 29300 | 41 | 34 | 607 | 0 | 1 | 0 |
| 149 | Matagorda | 29.00 | 95.50 | 11690 | 14540 | 100 | 9 | 5840 | 61 | 0 | 60 | 8470 | 0 | 179 | 8 | 0 | 1 | 1 |
| 150 | Matagorda | 29.00 | 95.50 | 9397 | 30796 | 92 | 20 | 12097 | 80 | 0 | 7 | 18500 | 1 | 101 | 26 | 0 | 0 | 0 |
| 151 | Matagorda | 29.00 | 95.50 | 9378 | 10992 | 16 | 2 | 4822 | 30 | 0 | 22 | 6100 | 0 | 107 | 2 | 0 | 0 | 0 |
| 152 | Jackson | 29.08 | 96.40 | 9246 | 114000 | 8260 | 730 | 33500 | 767 | 59 | 4 | 68100 | 0.1 | 18 | 1080 | 0 | 56 | 107 |
| 153 | Calhoun | 28.12 | 96.32 | 7636 | 19200 | 34 | 16 | 7900 | 56 | 1710 | 44 | 10800 | 0.1 | 61 | 14 | 0 | 40 | 49 |
| 154 | Calhoun | 28.12 | 96.32 | 8840 | 57300 | 189 | 52 | 23000 | 139 | 1130 | 15 | 34100 | 0.1 | 61 | 55 | 0 | 49 | 110 |
| 155 | Calhoun | 28.12 | 96.32 | 9293 | 70100 | 450 | 111 | 27200 | 171 | 574 | 24 | 41500 | 0.1 | 58 | 162 | 0 | 51 | 131 |
| 156 | Calhoun | 28.17 | 96.40 | 8882 | 59800 | 2100 | 170 | 22600 | 130 | 120 | 5 | 42050 | 0.3 | 10 | 160 | 0 | 46 | 140 |
| 157 | Calhoun | 28.17 | 96.40 | 8780 | 49100 | 740 | 105 | 17100 | 110 | 710 | 23 | 27800 | 0.2 | 46 | 95 | 0 | 50 | 125 |
| 158 | Calhoun | 28.17 | 96.40 | 8796 | 31000 | 185 | 31 | 11200 | 85 | 1300 | 45 | 17050 | 0.1 | 66 | 19 | 0 | 46 | 105 |
| 159 | Calhoun | 28.34 | 96.50 | 6750 | 63847 | 1320 | 163 | 22379 | 0 | 138 | 105 | 39671 | 6 | 0 | 0 | 6 | 0 | 0 |
| 160 | Calhoun | 28.20 | 96.50 | 8384 | 44859 | 158 | 40 | 17300 | 90 | 1436 | 35 | 25800 | 0 | 89 | 37 | 0 | 1 | 1 |
| 161 | Calhoun | 28.20 | 96.50 | 9312 | 70527 | 450 | 111 | 27200 | 171 | 1090 | 5 | 41500 | 0 | 93 | 162 | 0 | 1 | 0 |
| 162 | Calhoun | 28.20 | 96.50 | 8918 | 61332 | 231 | 62 | 25000 | 132 | 0 | 7 | 35900 | 0 | 98 | 46 | 0 | 1 | 0 |
| 163 | Calhoun | 28.20 | 96.50 | 10532 | 18111 | 44 | 7 | 7400 | 63 | 0 | 47 | 10550 | 0 | 130 | 8 | 0 | 0 | 1 |
| 164 | Calhoun | 28.20 | 96.50 | 8836 | 29937 | 163 | 32 | 10710 | 90 | 1932 | 0 | 17010 | 999 | 114 | 18 | 0 | 1 | 1 |

Table 4 (continued)

| No. | County | Latitude | Longitude | Depth (ft) | TDS | Ca | Mg | Na | K | Alkalinity | SO4 | Cl | Fe | SiO2 | Sr | Ba | B | Br |
|-----|---------|----------|-----------|------------|-------|-------|----|-------|------|------------|------|-------|-----|------|-----|------|---|----|
| 165 | Kleberg | 27.30 | 97.30 | 7298 | 87880 | 8100 | 95 | 25600 | 150 | 60 | 25 | 53850 | 1 | 70 | 500 | 0 | 1 | 0 |
| 166 | Kleberg | 27.30 | 97.30 | 8856 | 54135 | 1780 | 77 | 18990 | 131 | 0 | 7 | 33150 | 23 | 112 | 288 | 0 | 1 | 0 |
| 167 | Kleberg | 27.30 | 97.30 | 8498 | 61513 | 3490 | 61 | 20860 | 95 | 0 | 7 | 37000 | 85 | 37 | 335 | 0 | 1 | 0 |
| 168 | Hidalgo | 26.10 | 98.30 | 7997 | 55762 | 8720 | 38 | 12600 | 164 | 400 | 130 | 33710 | 114 | 18 | 563 | 0.6 | 0 | 0 |
| 169 | Hidalgo | 26.10 | 98.30 | 7997 | 54996 | 6800 | 34 | 12700 | 257 | 0 | 15 | 35190 | 220 | 29 | 491 | 1.8 | 0 | 0 |
| 170 | Hidalgo | 26.10 | 98.30 | 9522 | 7017 | 150 | 3 | 2630 | 45 | 0 | 59 | 4130 | 0 | 160 | 10 | 0 | 0 | 0 |
| 171 | Hidalgo | 26.10 | 98.30 | 9361 | 9017 | 430 | 7 | 2920 | 260 | 0 | 150 | 5250 | 4 | 117 | 19 | 0 | 0 | 0 |
| 172 | Hidalgo | 26.10 | 98.30 | 9414 | 7616 | 430 | 2 | 2530 | 46 | 0 | 20 | 4588 | 1 | 136 | 19 | 0 | 0 | 1 |
| 173 | Hidalgo | 26.10 | 98.30 | 6908 | 6693 | 380 | 14 | 2050 | 19 | 0 | 230 | 4000 | 120 | 8 | 7 | 0 | 0 | 0 |
| 174 | Hidalgo | 26.10 | 98.30 | 7908 | 13559 | 130 | 6 | 4940 | 33 | 0 | 1880 | 6570 | 5 | 110 | 5 | 0 | 0 | 0 |
| 175 | Hidalgo | 26.10 | 98.30 | 8741 | 9127 | 110 | 3 | 3510 | 31 | 0 | 750 | 4723 | 17 | 90 | 8 | 0 | 0 | 1 |
| 176 | Hidalgo | 26.10 | 98.30 | 9728 | 13343 | 910 | 6 | 4100 | 97 | 0 | 40 | 8190 | 11 | 168 | 46 | 0 | 0 | 1 |
| 177 | Hidalgo | 26.10 | 98.30 | 6839 | 14244 | 1110 | 12 | 4400 | 92 | 0 | 60 | 8570 | 35 | 192 | 60 | 0 | 0 | 1 |
| 178 | Hidalgo | 26.10 | 98.30 | 7997 | 69962 | 10200 | 72 | 14800 | 2290 | 0 | 10 | 42590 | 54 | 16 | 819 | 11.4 | 0 | 0 |

Economic Geology in August-September 1987 were analyzed for major and minor ions, isotopes, organic acids, and organic composition of oils (tables 5 through 7). Methods for selection, collection, and analysis are listed below.

8.1 Sample Selection

Thirty-two samples were collected from the Texas Gulf Coast oil and gas fields (tables 5 and 6). Several criteria were used in selecting sites, including API gravity of the oils, geographic location, and sample depth. Wells in the same zone as secondary recovery operations were avoided.

Heavy Oils--Because one of the effects of biodegradation and water washing of oils is to decrease its API gravity, wells that produce the heavier, relatively low API gravity oils were chosen. Most of the samples were taken from fields with oils that have API gravities of 25.0 or lower. Samples were also collected from fields with lighter oils in order to investigate waters associated with nondegraded oils.

Geographic Distribution--Samples were taken in the Texas Gulf Coast from Jim Wells County in the south to Jefferson County in the north (fig. 63). Sample locations were fairly evenly distributed throughout the Gulf Coast.

Depth--Samples were taken from depths of 3,000 ft to 10,000 ft. Owing to the lack of appropriate deep wells in the South Gulf Coast, more samples from shallow wells (3,000 to 6,000 ft) were collected there. There is a good representation for all depths between 3,000 and 10,000 ft.

8.2 Sample Collection

Samples were collected from the wellhead, separator, or "heater treater." In several instances operators added a chemical at the wellhead as a scale inhibitor. For this the feedline for the chemical was turned off and the well line was flushed for several minutes to avoid contamination of the field sample with the inhibitor. Samples were collected in a 5-gallon bucket, which was cleaned with distilled water and acetone and rinsed with the sample. After the brine and oil separated, the brine was filtered through glass wool to remove any oil and solids remaining in the sample and poured into a pressure filtration chamber, which was also cleaned and rinsed with distilled water and sample water. Samples were then filtered through a 0.45- μ m filter using nitrogen gas to avoid atmospheric contamination. Samples taken for cation analysis were collected in 500-ml polyurethane bottles and acidified with 5 ml of 6N HCl. Samples taken for anion analysis were collected untreated in a 500-ml polyurethane bottle. Isotope samples were collected untreated in a 250-ml glass bottle. Organic acid samples were collected in a 500-ml glass bottle and treated with

Economic Geology in August-September 1987 were analyzed for major and minor ions, isotopes, organic acids, and organic composition of oils (tables 5 through 7). Methods for selection, collection, and analysis are listed below.

8.1 Sample Selection

Thirty-two samples were collected from the Texas Gulf Coast oil and gas fields (tables 5 and 6). Several criteria were used in selecting sites, including API gravity of the oils, geographic location, and sample depth. Wells in the same zone as secondary recovery operations were avoided.

Heavy Oils--Because one of the effects of biodegradation and water washing of oils is to decrease its API gravity, wells that produce the heavier, relatively low API gravity oils were chosen. Most of the samples were taken from fields with oils that have API gravities of 25.0 or lower. Samples were also collected from fields with lighter oils in order to investigate waters associated with nondegraded oils.

Geographic Distribution--Samples were taken in the Texas Gulf Coast from Jim Wells County in the south to Jefferson County in the north (fig. 63). Sample locations were fairly evenly distributed throughout the Gulf Coast.

Depth--Samples were taken from depths of 3,000 ft to 10,000 ft. Owing to the lack of appropriate deep wells in the South Gulf Coast, more samples from shallow wells (3,000 to 6,000 ft) were collected there. There is a good representation for all depths between 3,000 and 10,000 ft.

8.2 Sample Collection

Samples were collected from the wellhead, separator, or "heater treater." In several instances operators added a chemical at the wellhead as a scale inhibitor. For this the feedline for the chemical was turned off and the well line was flushed for several minutes to avoid contamination of the field sample with the inhibitor. Samples were collected in a 5-gallon bucket, which was cleaned with distilled water and acetone and rinsed with the sample. After the brine and oil separated, the brine was filtered through glass wool to remove any oil and solids remaining in the sample and poured into a pressure filtration chamber, which was also cleaned and rinsed with distilled water and sample water. Samples were then filtered through a 0.45- μ m filter using nitrogen gas to avoid atmospheric contamination. Samples taken for cation analysis were collected in 500-ml polyurethane bottles and acidified with 5 ml of 6N HCl. Samples taken for anion analysis were collected untreated in a 500-ml polyurethane bottle. Isotope samples were collected untreated in a 250-ml glass bottle. Organic acid samples were collected in a 500-ml glass bottle and treated with

Table 5. All chemical analyses of Frio waters collected for this study. Ionic concentrations in mg/L.

| Sample No. | Ca | Mg | Na | K | Alkalinity† | SO4 | Cl | TDS | Depth (ft) | Si | Sr | Ba | Br | I | pH †† | del O18 |
|------------|------|------|-------|-----|-------------|-----|-------|--------|------------|------|------|------|-----|----|-------|---------|
| 1 | 934 | 183 | 24000 | 170 | 258 | 7 | 36600 | 62563 | 6023 | 15.7 | 230 | 75.1 | 79 | 18 | 7.15 | 4.75 |
| 2 | 1730 | 284 | 25100 | 234 | 319 | <5 | 39300 | 67438 | 3499 | 8.7 | 196 | 81.4 | 168 | 17 | 7.52 | 4.01 |
| 3 | 184 | 360 | 12000 | 106 | 631 | <5 | 17400 | 30824 | 4226 | 14.7 | 19.1 | 12.7 | 81 | 15 | 7.72 | 3.32 |
| 4 | 1700 | 287 | 25100 | 155 | 186 | <5 | 40300 | 68257 | 5545 | 14.3 | 233 | 89.2 | 173 | 19 | 7.50 | 4.11 |
| 5 | 769 | 2980 | 24800 | 176 | 515 | <5 | 38200 | 67731 | 3606 | 16.5 | 104 | 87.2 | 70 | 13 | 7.12 | -0.25 |
| 6 | 5280 | 173 | 26400 | 162 | 423 | 7 | 47600 | 80861 | 6652 | 17.2 | 405 | 159 | 219 | 23 | 7.07 | 3.92 |
| 7 | 67 | 27 | 10900 | 114 | 845 | 7 | 15800 | 27848 | 3930 | 18.0 | 13.9 | 4.3 | 39 | 20 | 7.76 | 1.06 |
| 8 | 2130 | 173 | 23300 | 150 | 309 | 14 | 38500 | 64887 | 5000 | 15.5 | 106 | 36.6 | 143 | 24 | 6.65 | 1.33 |
| 9 | 863 | 118 | 18000 | 195 | 274 | <5 | 28000 | 47683 | 4768 | 15.9 | 52.5 | 23.7 | 125 | 16 | 6.70 | 4.09 |
| 10 | 2230 | 267 | 26600 | 187 | 237 | <5 | 43700 | 73830 | 4537 | 12.3 | 284 | 109 | 185 | 19 | 6.60 | 3.47 |
| 11 | 2430 | 327 | 28000 | 167 | 165 | <5 | 46600 | 78295 | 4388 | 10.7 | 268 | 104 | 203 | 20 | 6.79 | 3.36 |
| 12 | 281 | 51 | 8710 | 147 | 468 | <5 | 13100 | 22864 | 3040 | 29.8 | 9.8 | 2.9 | 47 | 17 | 6.77 | 0.42 |
| 13 | 131 | 24 | 8670 | 94 | 695 | <5 | 12500 | 22213 | 3942 | 15.4 | 8.7 | 6.5 | 50 | 18 | 7.32 | 3.11 |
| 14 | 818 | 168 | 18400 | 195 | 264 | <5 | 29000 | 49012 | 4640 | 15.2 | 70.4 | 27.4 | 36 | 18 | 6.48 | 4.22 |
| 15 | 243 | 17 | 10400 | 71 | 948 | <5 | 15100 | 26893 | 5000 | 19.1 | 16.6 | 12.4 | 44 | 22 | 7.01 | 2.97 |
| 16 | 8970 | 346 | 32600 | 144 | 124 | 15 | 64000 | 106914 | 6304 | 15.2 | 397 | 72.1 | 230 | 16 | 6.77 | 2.00 |
| 17 | 9460 | 463 | 34700 | 153 | 58 | 22 | 68900 | 114411 | 5700 | 13.3 | 369 | 30.2 | 247 | 17 | 6.68 | 1.01 |
| 18 | 1450 | 249 | 25600 | 157 | 412 | <5 | 40200 | 68373 | 4682 | 14.7 | 117 | 73.9 | 80 | 19 | 6.46 | 3.63 |
| 19 | 2160 | 480 | 27500 | 159 | 225 | <5 | 45000 | 75859 | 5096 | 11.5 | 137 | 84 | 80 | 22 | 6.44 | 2.44 |
| 20 | 2660 | 658 | 40600 | 262 | 93 | <5 | 67700 | 112401 | 6571 | 10.0 | 225 | 83.7 | 89 | 20 | 6.26 | 6.40 |
| 23 | 393 | 97 | 18900 | 149 | 1696 | 120 | 27500 | 49027 | 9646 | 27.7 | 54.7 | 4.6 | 66 | 19 | 7.19 | 5.47 |
| 24 | 2687 | 368 | 28133 | 207 | 1226 | 19 | 46800 | 79848 | 8760 | 17.7 | 274 | 36.4 | 78 | 21 | 6.69 | 4.72 |
| 25 | 2890 | 520 | 43300 | 229 | 193 | <5 | 71400 | 118802 | 7752 | 11.7 | 120 | 43.6 | 76 | 19 | 6.00 | 1.88 |
| 26 | 2290 | 448 | 38100 | 188 | 355 | 11 | 63000 | 104621 | 8310 | 15.9 | 103 | 36.5 | 66 | 19 | 5.93 | 1.01 |
| 27 | 2630 | 623 | 37100 | 230 | 212 | <5 | 61500 | 102643 | 6721 | 12.2 | 176 | 79 | 63 | 18 | 5.70 | 2.05 |
| 28 | 2170 | 538 | 38500 | 211 | 185 | 6 | 63200 | 105173 | 4574 | 11.2 | 179 | 87.5 | 72 | 19 | 6.31 | 2.46 |
| 29 | 12 | 2 | 3730 | 23 | 2448 | <5 | 4300 | 10598 | 7666 | 23.7 | 2.2 | 1.5 | 23 | 33 | 8.24 | 4.63 |
| 31 | 992 | 150 | 28900 | 356 | 1253 | 9 | 44000 | 76095 | 9950 | 30.2 | 219 | 112 | 58 | 25 | 6.72 | 3.58 |
| 32 | 1190 | 261 | 35700 | 250 | 460 | 15 | 56600 | 94834 | 9074 | 23.1 | 187 | 81.1 | 64 | 18 | 6.31 | 3.08 |
| 33 | 1660 | 490 | 38400 | 278 | 322 | <5 | 61300 | 102738 | 5902 | 13.4 | 143 | 56 | 57 | 19 | 6.12 | 2.72 |
| 34 | 1860 | 451 | 38400 | 288 | 245 | 11 | 61300 | 102975 | 6244 | 14.1 | 252 | 66 | 82 | 17 | 6.13 | 4.19 |
| 35 | 1760 | 369 | 34500 | 217 | 804 | 17 | 55400 | 93399 | 8382 | 18.3 | 163 | 39.1 | 115 | 14 | 6.21 | 3.99 |

Table 5 (continued)

| Sample No. | del D | API Gravity ††† | Total Alkalinity | Acetate | Propionate | Butyrate | HCO3- | Tot. Org. Acids | Titrated Org. Alk. | Temp (°C)†††† |
|------------|-------|-----------------|------------------|---------|------------|----------|-------|-----------------|--------------------|---------------|
| 1 | -14.9 | 26.0 | 258 | 0 | 0 | 0 | 258 | 0 | na | 69 |
| 2 | -14.4 | 23.0 | 319 | 0 | 0 | 0 | 319 | 0 | na | 49 |
| 3 | -14.0 | 24.0 | 631 | 0 | 0 | 0 | 631 | 0 | 131 | 54 |
| 4 | -13.3 | 28.0 | 186 | 0 | 0 | 0 | 186 | 0 | na | 66 |
| 5 | -5.6 | 29.1 | 515 | 0 | 0 | 0 | 515 | 0 | na | 50 |
| 6 | -10.6 | 23.8 | 423 | 300 | 32 | 3 | 88 | 335 | 399 | 75 |
| 7 | -14.7 | 26.0 | 845 | 6.5 | 0 | 0 | 839 | 6.5 | 44 | 52 |
| 8 | -15.0 | 25.0 | 198 | 104 | 38 | 3.5 | 53 | 145.5 | 199 | 62 |
| 9 | -13.2 | 25.0 | 274 | 4.7 | 0 | 0 | 269 | 4.7 | na | 59 |
| 10 | -12.4 | 24.0 | 237 | 0 | 0 | 0 | 237 | 0 | na | 58 |
| 11 | -10.7 | 23.0 | 165 | 0 | 0 | 0 | 165 | 0 | na | 56 |
| 12 | -15.5 | 22.8 | 468 | 0 | 0 | 0 | 468 | 0 | na | 44 |
| 13 | -14.9 | 24.0 | 695 | 0 | 0 | 0 | 695 | 0 | 60 | 52 |
| 14 | -14.0 | 20.5 | 264 | 0 | 0 | 0 | 264 | 0 | na | 59 |
| 15 | -11.8 | 22.0 | 948 | 440 | 135 | 15 | 358 | 590 | 678 | 62 |
| 16 | -10.6 | 23.0 | 124 | 47 | 9 | 0 | 68 | 56 | 283 | 72 |
| 17 | -15.5 | 23.0 | 58 | 0 | 0 | 0 | 58 | 0 | na | 67 |
| 18 | -15.1 | 25.0 | 412 | 0 | 0 | 0 | 412 | 0 | na | 59 |
| 19 | -15.2 | 23.0 | 225 | 0 | 0 | 0 | 225 | 0 | 68 | 62 |
| 20 | -13.0 | 29.5 | 93 | 0 | 0 | 0 | 93 | 0 | na | 74 |
| 23 | -12.2 | 30.0 | 1696 | 814 | 95 | 10 | 777 | 919 | 1000 | 104 |
| 24 | -10.7 | 33.5 | 1226 | 697 | 71 | 8 | 450 | 776 | 887 | 99 |
| 25 | -19.6 | 26.3 | 193 | 40 | 3.5 | 0 | 150 | 43.5 | 146 | 88 |
| 26 | -24.0 | 29.1 | 355 | 136 | 22 | 3 | 194 | 161 | 217 | 94 |
| 27 | -18.0 | 29.0 | 212 | 0 | 0 | 0 | 212 | 0 | na | 77 |
| 28 | -16.3 | 28.0 | 185 | 0 | 0 | 0 | 185 | 0 | na | 58 |
| 29 | -12.3 | 32.4 | 2448 | 1270 | 207 | 23.5 | 948 | 1500.5 | 1476 | 87 |
| 31 | -15.3 | 28.0 | 1253 | 728 | 113 | 18 | 394 | 859 | 857 | 107 |
| 32 | -15.5 | 28.0 | 460 | 190 | 40 | 5 | 225 | 235 | na | 101 |
| 33 | -16.4 | 28.0 | 322 | 0 | 0 | 0 | 322 | 0 | na | 68 |
| 34 | -17.4 | 31.3 | 245 | 0 | 0 | 0 | 245 | 0 | na | 71 |
| 35 | -12.6 | 30.4 | 804 | 326 | 2 | 4 | 472 | 332 | 538 | 95 |

Alkalinity† field alkalinity titration

pH †† field pH

API Gravity ††† API gravity from Railroad Commission of Texas, Oil and Gas Division proration schedules

Temp (°C)†††† temperatures estimated from geothermal gradient † ‡

Table 6. Water samples with location and operator information of Frio waters collected for this study. Ionic concentrations in mg/L.

| Sample No. | 1 | 2 | 3 | 4 | 5 |
|--------------------------|------------------------------|--------------------------|----------------------|-------------------------------|--------------|
| Field | Placedo | Lonnie Glasscock | Tynan, E | Placedo, E | Tesoro |
| County | Victoria | Victoria | Bee | Victoria | Duval |
| Operator | Global Natural Resources | Three Mile Joint Venture | TXO Production Corp. | Westland Oil Development Inc. | A. H. Garcia |
| Lease/Well No. | Henderson & Pickering No. 14 | M.S. Welder No. G-5 | Ramirez No. B-2 | Vendenberge & Hill No. 10 | Parr No. 2A |
| Depth (feet) | 6019'-6023' | 3499'-3503' | 4222'-4226' | 5545' | 3606' |
| TDS | 62570 | 67443 | 30829 | 68262 | 67736 |
| Ca | 934 | 1730 | 184 | 1700 | 769 |
| Mg | 183 | 284 | 360 | 287 | 2980 |
| Na | 24000 | 25100 | 12000 | 25100 | 24800 |
| K | 170 | 234 | 106 | 155 | 176 |
| Alkalinity | 258 | 319 | 631 | 186 | 515 |
| SO4 | 7 | <5 | <5 | <5 | <5 |
| Cl | 36600 | 39300 | 17400 | 40300 | 38200 |
| Si | 15.7 | 8.7 | 14.7 | 14.3 | 16.5 |
| Sr | 230 | 196 | 19.1 | 233 | 104 |
| Ba | 75.1 | 81.4 | 12.7 | 89.2 | 87.2 |
| Br | 79 | 168 | 81 | 173 | 70 |
| I | 18 | 17 | 15 | 19 | 13 |
| ∂ O18 | 4.75 | 4.01 | 3.32 | 4.11 | -0.25 |
| ∂ D | -14.9 | -14.4 | -14 | -13.3 | -5.6 |
| pH | 7.15 | 7.52 | 7.72 | 7.5 | 7.12 |
| Acetate | trace | trace | trace | trace | trace |
| Propionate | 0 | 0 | 0 | 0 | 0 |
| Butyrate | 0 | 0 | 0 | 0 | 0 |
| Tot. Org. Acids | 0 | 0 | 0 | 0 | 0 |
| Titrated Org. Alkalinity | na | na | 131 | na | na |

Table 6 (continued)

| Sample No. | 6 | 7 | 8 | 9 | 10 |
|--------------------------|--------------------------|---------------------|---------------------------------|---------------------|-----------------|
| Field | Triple -A- | Magnolia City, W | Minnie Bock | Pridham Lake, W | Lake Pasture |
| County | San Patricio | Jim Wells | Nueces | Victoria | Refugio |
| Operator | Robinson Interests, Inc. | Verado Energy, Inc. | Sanchez-O'Brien Oil & Gas Corp. | Mandarin Oil & Gas | T-C Oil Co. |
| Lease/Well No. | A. E. Nelson No. 4 | Perez No. 1 | Wright Trust No. 1 | Calhoun Farms No. 2 | O'Connor No. 79 |
| Depth (feet) | 6652' | 3930' | 5000' | 4768' | 4537' |
| TDS | 80868 | 27855 | 64901 | 47688 | 73835 |
| Ca | 5280 | 67 | 2130 | 863 | 2230 |
| Mg | 173 | 27 | 173 | 118 | 267 |
| Na | 26400 | 10900 | 23300 | 18000 | 26600 |
| K | 162 | 114 | 150 | 195 | 187 |
| Alkalinity | 423 | 845 | 309 | 274 | 237 |
| SO4 | 7 | 7 | 14 | <5 | <5 |
| Cl | 47600 | 15800 | 38500 | 28000 | 43700 |
| SI | 17.2 | 18 | 15.5 | 15.9 | 12.3 |
| Sr | 405 | 13.9 | 106 | 52.5 | 284 |
| Ba | 159 | 4.3 | 36.6 | 23.7 | 109 |
| Br | 219 | 39 | 143 | 125 | 185 |
| I | 23 | 20 | 24 | 16 | 19 |
| ∂ O18 | 3.92 | 1.06 | 1.33 | 4.09 | 3.47 |
| ∂ D | -10.6 | -14.7 | -15 | -13.2 | -12.4 |
| pH | 7.07 | 7.76 | 6.65 | 6.7 | 6.6 |
| Acetate | 300 | 6.5 | 104 | 4.7 | trace |
| Propionate | 32 | 0 | 38 | 0 | 0 |
| Butyrate | 3 | 0 | 3.5 | 0 | 0 |
| Tot. Org. Acids | 335 | 6.5 | 145.5 | 4.7 | 0 |
| Titrated Org. Alkalinity | 399 | 44 | 199 | na | na |

Table 6 (continued)

| Sample No. | 11 | 12 | 13 | 14 | 15 | 16 |
|--------------------------|----------------------|-----------------------|--------------------|--------------------|----------------------|---------------|
| Field | Tom O'Connor | Silva, SW | Silva, SW | Blanconia, N | Richard King | Luby |
| County | Refugio | Bee | Bee | Bee | Nueces | Nueces |
| Operator | Hewit & Dougherty | Good Day Energy | KTX Management | Legacy Exploration | Kamllok, Inc. | Kamllok, Inc. |
| Lease/Well No. | M. F. Lampert No. 95 | Riggle-Wendland No. 3 | Paul Treptow No. 2 | Roberts No. 1 | Richard King No. C-9 | McCann No. 38 |
| Depth (feet) | 4388' | 3040' | 3942' | 4640' | 5000' | 6304' |
| TDS | 78300 | 22869 | 22218 | 49017 | 26898 | 106929 |
| Ca | 2430 | 281 | 131 | 818 | 243 | 8970 |
| Mg | 327 | 51 | 24 | 168 | 17 | 346 |
| Na | 28000 | 8710 | 8670 | 18400 | 10400 | 32600 |
| K | 167 | 147 | 94 | 195 | 71 | 144 |
| Alkalinity | 165 | 468 | 695 | 264 | 948 | 124 |
| SO4 | <5 | <5 | <5 | <5 | <5 | 15 |
| Cl | 46600 | 13100 | 12500 | 29000 | 15100 | 64000 |
| Si | 10.7 | 29.8 | 15.4 | 15.2 | 19.1 | 15.2 |
| Sr | 268 | 9.8 | 8.7 | 70.4 | 16.6 | 397 |
| Ba | 104 | 2.9 | 6.5 | 27.4 | 12.4 | 72.1 |
| Br | 203 | 47 | 50 | 36 | 44 | 230 |
| I | 20 | 17 | 18 | 18 | 22 | 16 |
| ∂ O18 | 3.36 | 0.42 | 3.11 | 4.22 | 2.97 | 2 |
| ∂ D | -10.7 | -15.5 | -14.9 | -14 | -11.8 | -10.6 |
| pH | 6.79 | 6.77 | 7.32 | 6.48 | 7.01 | 6.77 |
| Acetate | trace | trace | trace | trace | 440 | 47 |
| Propionate | 0 | 0 | 0 | 0 | 135 | 9 |
| Butyrate | 0 | 0 | 0 | 0 | 15 | 0 |
| Tot. Org. Acids | 0 | 0 | 0 | 0 | 590 | 56 |
| Titrated Org. Alkalinity | na | na | 60 | na | 678 | 283 |

123

Table 6 (continued)

| Sample No. | 31 | 32 | 33 | 34 | 35 |
|--------------------------|------------------------|------------------------|---------------------------|--------------------------------|----------------|
| Field | Sugar Valley, S | Sugar Valley, N | Clear Lake | Webster | Fishers Reef |
| County | Brazoria | Brazoria | Harris | Harris | Chambers |
| Operator | Exxon | Exxon | Exxon | Exxon | Exxon |
| Lease/Well No. | Truitt & Grevaer No. 8 | John F. Grant No. 11-J | Exxon West Fee "C" No. 85 | West Production Co. A/C No. 29 | FR Tract No. 2 |
| Depth (feet) | 9950' | 9074' | 5902' | 6244' | 8382' |
| TDS | 76104 | 94849 | 102743 | 102986 | 93416 |
| Ca | 992 | 1190 | 1660 | 1860 | 1760 |
| Mg | 150 | 261 | 490 | 451 | 369 |
| Na | 28900 | 35700 | 38400 | 38400 | 34500 |
| K | 356 | 250 | 278 | 288 | 217 |
| Alkalinity | 1253 | 460 | 322 | 245 | 804 |
| SO4 | 9 | 15 | <5 | 11 | 17 |
| Cl | 44000 | 56600 | 61300 | 61300 | 55400 |
| Si | 30.2 | 23.1 | 13.4 | 14.1 | 18.3 |
| Sr | 219 | 187 | 143 | 252 | 163 |
| Ba | 112 | 81.1 | 56 | 66 | 39.1 |
| Br | 58 | 64 | 57 | 82 | 115 |
| I | 25 | 18 | 19 | 17 | 14 |
| ∂ O18 | 3.58 | 3.08 | 2.72 | 4.19 | 3.99 |
| ∂ D | -15.3 | -15.5 | -16.4 | -17.4 | -12.6 |
| pH | 6.72 | 6.31 | 6.12 | 6.13 | 6.21 |
| Acetate | 728 | 190 | trace | trace | 326 |
| Propionate | 113 | 40 | 0 | 0 | 2 |
| Butyrate | 18 | 5 | 0 | 0 | 4 |
| Tot. Org. Acids | 859 | 235 | 0 | 0 | 332 |
| Titrated Org. Alkalinity | 857 | na | na | na | 538 |

Table 7. Oxygen and hydrogen isotopic data for Frio and Wilcox Formations. "EPA data" are samples collected for this study. "Frio data" from L.S. Land. Wilcox data from Fisher (1982). Ionic concentrations in mg/L.

| EPA Data | | | | Frio Data | | | Wilcox Data | | |
|------------|--------------|------------|--------------|--------------|------------|--------------|--------------|------------|--------------|
| Sample No. | $\delta O18$ | δD | Depth (feet) | $\delta O18$ | δD | Depth (feet) | $\delta O18$ | δD | Depth (feet) |
| 1 | 4.75 | -14.9 | 6023 | 5.22 | -17.0 | 9312 | 1.20 | -21.0 | 8453 |
| 2 | 4.01 | -14.4 | 3499 | 4.91 | -9.5 | 8843 | -2.50 | 1.4 | 9345 |
| 3 | 3.32 | -14.0 | 4226 | 4.65 | -8.1 | 8613 | -5.40 | -20.8 | 10198 |
| 4 | 4.11 | -13.3 | 5545 | 4.65 | -8.1 | 9778 | -0.30 | -15.0 | 7984 |
| 5 | -0.25 | -5.6 | 3606 | 5.70 | -17.0 | 11359 | 2.10 | -11.0 | 6471 |
| 6 | 3.92 | -10.6 | 6652 | 4.93 | -18.8 | 10690 | 2.10 | -15.0 | 9505 |
| 7 | 1.06 | -14.7 | 3930 | 5.64 | -18.0 | 11723 | 2.20 | -10.0 | 6068 |
| 8 | 1.33 | -15.0 | 5000 | 4.00 | -10.4 | 8794 | 2.10 | -13.0 | 6849 |
| 9 | 4.09 | -13.2 | 4768 | 5.92 | -14.1 | 10683 | 5.40 | -2.4 | 10407 |
| 10 | 3.47 | -12.4 | 4537 | 7.57 | -14.3 | 10726 | 4.20 | -4.0 | 10463 |
| 11 | 3.36 | -10.7 | 4388 | 6.74 | -11.7 | 11526 | 4.60 | -11.9 | 10995 |
| 12 | 0.42 | -15.5 | 3040 | 7.56 | -15.0 | 10548 | 0.80 | 6.6 | 7000 |
| 13 | 3.11 | -14.9 | 3942 | 5.96 | -13.7 | 12116 | -4.70 | -42.0 | 8597 |
| 14 | 4.22 | -14.0 | 4640 | 4.45 | -16.1 | 11880 | 3.60 | -10.0 | 11897 |
| 15 | 2.97 | -11.8 | 5000 | | | | -3.20 | -35.0 | 10630 |
| 16 | 2.00 | -10.6 | 6304 | | | | -3.70 | -15.5 | 10000 |
| 17 | 1.01 | -15.5 | 5700 | | | | -3.10 | -15.7 | 6029 |
| 18 | 3.63 | -15.1 | 4682 | | | | -4.10 | -13.1 | 5258 |
| 19 | 2.44 | -15.2 | 5096 | | | | -4.40 | -7.1 | 4595 |
| 20 | 2.50 | -13.0 | 6571 | | | | -3.10 | -13.4 | 5858 |
| 23 | 5.47 | -12.2 | 9646 | | | | -4.40 | -17.2 | 4854 |
| 24 | 4.72 | -10.7 | 8760 | | | | -5.40 | -20.0 | 7167 |
| 25 | 1.88 | -19.6 | 7752 | | | | 1.90 | 3.3 | 7554 |
| 26 | 1.01 | -24.0 | 8310 | | | | 2.00 | -4.3 | 7564 |
| 27 | 2.05 | -18.0 | 6721 | | | | 2.70 | 2.6 | 7606 |
| 28 | 2.46 | -16.3 | 4574 | | | | 2.70 | -5.7 | 8174 |
| 29 | 4.63 | -12.3 | 7666 | | | | 1.20 | -11.0 | 9154 |
| 31 | 3.58 | -15.3 | 9950 | | | | 0.20 | -5.6 | 7797 |
| 32 | 3.08 | -15.5 | 9074 | | | | -4.20 | -17.4 | 7921 |
| 33 | 2.72 | -16.4 | 5902 | | | | -3.90 | -15.0 | 5081 |
| 34 | 4.19 | -17.4 | 6244 | | | | -2.10 | -16.0 | 4920 |
| 35 | 3.99 | -12.6 | 8382 | | | | -3.90 | -7.0 | 5960 |
| | | | | | | | 3.00 | 3.0 | 7560 |
| | | | | | | | -0.70 | 1.0 | 9056 |
| | | | | | | | -0.90 | 3.0 | 7150 |
| | | | | | | | 2.10 | 2.0 | 8239 |
| | | | | | | | ± ↓ 3.20 | -12.0 | 8177 |
| | | | | | | | 1.30 | -2.0 | 7311 |
| | | | | | | | 2.30 | -7.0 | 9197 |
| | | | | | | | 2.80 | -6.0 | 8125 |

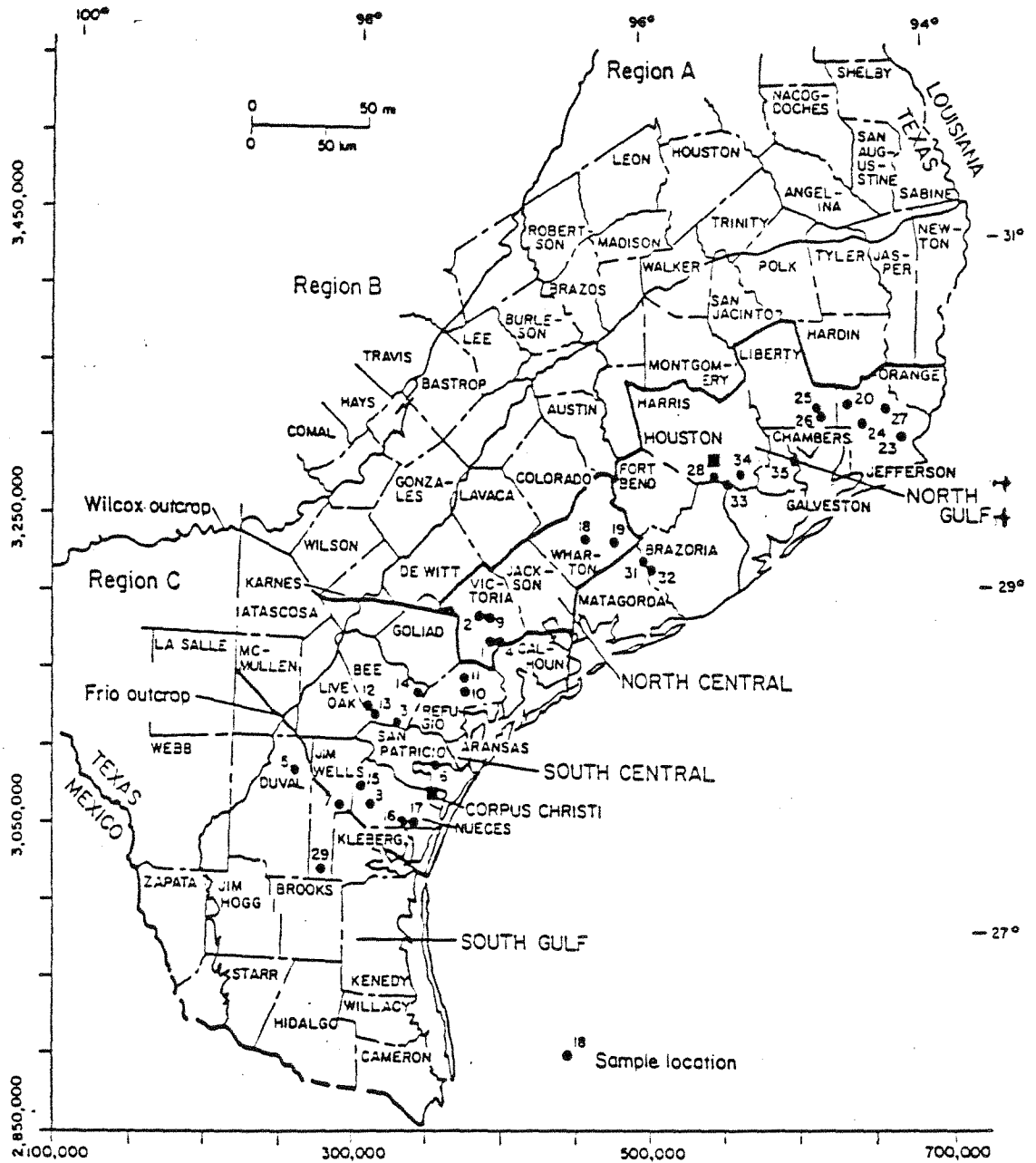


Figure 63. Location of wells sampled for this study.

a few drops of HgCl_2 . A sample diluted with deionized water in a proportion of 1:10 was collected in a 1-L polyurethane bottle. An untreated, unfiltered sample was also taken. For each brine collected, an oil sample was gathered in a 125-ml glass bottle. All sample bottles were tightly capped and sealed with Parafilm.

Alkalinity titrations were done in the field. Dilute HCl was titrated into 50 ml of unfiltered sample in 1- to 2 ml-additions to a pH of 2.5. Sample collection followed Bureau of Economic Geology Specific Work Instruction (BEG SWI) 3.1.a, Quality Assurance document.

8.3 Sample Analysis

All samples were analyzed and archived at the Bureau of Economic Geology's Mineral Studies Laboratory. Samples were analyzed for major cations and anions, oxygen and hydrogen isotopes, and organic acids. Eleven samples were analyzed by ARCO Service Laboratory for evidence of degradation.

Inorganic Chemistry

Chloride: A small aliquot of the untreated, filtered sample (0.1-1 ml) was diluted with deionized water to approximately 100 ml and adjusted to a pH of 7 to 9. One ml of K_2CrO_4 indicator solution was added, and the solution was titrated with a silver nitrate solution to a light orange endpoint, which was then used to calculate the chloride concentration. Sample analysis followed BEG SWI 1.1.

Bromide: A 1-ml aliquot of untreated, filtered sample was diluted to 25 ml with deionized water. The solution was then reacted with $\text{Ca}(\text{ClO})_2$ to oxidize the bromide to bromate (BrO_3^-) at a pH of 7.2. The excess hypochlorite (ClO^-) was then eliminated, and the bromate was reacted with iodide to produce iodine, which was then measured spectrophotometrically in solution. Sample analysis followed BEG SWI 1.2.

Sulfate: An appropriate aliquot of sample (<10 ml) was acidified with HCl and stabilized (for the BaSO_4 suspension) with gum arabic solution. BaCl_2 was then added and was mixed to dissolve all crystals. After at least 8 minutes the turbidity was measured at 420 nm using the secondary light path on the spectrophotometer. This result was compared to curves prepared with standard sulfate solutions. Sample analysis followed BEG SWI 1.3.

Ammonia: A small portion of each sample was extracted with cyclo-hexane, to eliminate any organic nitrogen present, and then steam distilled. The remaining distillate was then titrated with standardized hydrochloric acid to determine $\text{NH}_3\text{-N}$ concentrations (Mineral Studies Laboratory Procedure No. 001).

a few drops of HgCl_2 . A sample diluted with deionized water in a proportion of 1:10 was collected in a 1-L polyurethane bottle. An untreated, unfiltered sample was also taken. For each brine collected, an oil sample was gathered in a 125-ml glass bottle. All sample bottles were tightly capped and sealed with Parafilm.

Alkalinity titrations were done in the field. Dilute HCl was titrated into 50 ml of unfiltered sample in 1- to 2 ml-additions to a pH of 2.5. Sample collection followed Bureau of Economic Geology Specific Work Instruction (BEG SWI) 3.1.a, Quality Assurance document.

8.3 Sample Analysis

All samples were analyzed and archived at the Bureau of Economic Geology's Mineral Studies Laboratory. Samples were analyzed for major cations and anions, oxygen and hydrogen isotopes, and organic acids. Eleven samples were analyzed by ARCO Service Laboratory for evidence of degradation.

Inorganic Chemistry

Chloride: A small aliquot of the untreated, filtered sample (0.1-1 ml) was diluted with deionized water to approximately 100 ml and adjusted to a pH of 7 to 9. One ml of K_2CrO_4 indicator solution was added, and the solution was titrated with a silver nitrate solution to a light orange endpoint, which was then used to calculate the chloride concentration. Sample analysis followed BEG SWI 1.1.

Bromide: A 1-ml aliquot of untreated, filtered sample was diluted to 25 ml with deionized water. The solution was then reacted with $\text{Ca}(\text{ClO})_2$ to oxidize the bromide to bromate (BrO_3^-) at a pH of 7.2. The excess hypochlorite (ClO^-) was then eliminated, and the bromate was reacted with iodide to produce iodine, which was then measured spectrophotometrically in solution. Sample analysis followed BEG SWI 1.2.

Sulfate: An appropriate aliquot of sample (<10 ml) was acidified with HCl and stabilized (for the BaSO_4 suspension) with gum arabic solution. BaCl_2 was then added and was mixed to dissolve all crystals. After at least 8 minutes the turbidity was measured at 420 nm using the secondary light path on the spectrophotometer. This result was compared to curves prepared with standard sulfate solutions. Sample analysis followed BEG SWI 1.3.

Ammonia: A small portion of each sample was extracted with cyclo-hexane, to eliminate any organic nitrogen present, and then steam distilled. The remaining distillate was then titrated with standardized hydrochloric acid to determine $\text{NH}_3\text{-N}$ concentrations (Mineral Studies Laboratory Procedure No. 001).

Iodide: A ~2-ml aliquot of untreated, filtered sample was diluted to 10 ml. The sample was mixed with bromine water and then with sodium formate to destroy excess bromine. KI was then added to form iodine, which was then measured spectrophotometrically. Sample analysis followed BEG SWI 1.4.

Major and Minor Cations: Major and minor cations were analyzed using an inductively coupled plasma-optical emission spectrometer (ICP-OES). For K, Mg, Na, Sr, Ba, Si, and Ca the sample was diluted to approximately 1000 mg/L Na and acidified with 6N HCl and diluted further with double deionized water. This was then heated, cooled, and then analyzed on the ICP-OES, using seawater as a reference sample. For minor elements 10 ml of the sample was acidified with 5 ml of 6N HCl and heated and cooled as above. The solution was analyzed with the ICP-OES, with special attention given to elements with concentrations near the detection limits of the system. Sample analysis followed BEG SWI 1.5 and 1.6.

Isotopic Analyses

Oxygen: An aliquot of water (2 ml) was acidified with concentrated phosphoric acid and degassed three times under vacuum. Carbon dioxide was added to the water (18 ml and ~60 torr) and allowed to equilibrate with the water for 80 to 130 hours. The equilibrated carbon dioxide was transferred back to the vacuum line and purified. The purified gas was then analyzed with a VG SIRA 12 mass spectrometer to determine the relative abundances of the oxygen isotopes.

Hydrogen: An aliquot of water (5 μ l) was reduced in a sealed tube under vacuum pressure over hot zinc (430°C) for 24 hours. The evolved hydrogen gas was analyzed directly with a VG SIRA 12 mass spectrometer to determine the relative abundance of hydrogen isotopes.

Organic Acids

Organic acid concentrations were determined using a Hewlett-Packard Gas Chromatograph equipped with a Flame Ionization Detector (FID) and a 0.32 mm ID x 6 m long fused silica capillary column coated with 0.1 μ m Superox. The column was run isothermally at 110°C. The flow rate was 7 ml/min, and the carrier gas was helium. Before gas chromatograph analysis the samples were acidified to a pH of 1-2 with concentrated phosphoric acid in order to convert organic salts into organic acids. The sample was then injected in sample sizes of 2.5 μ m. A standard solution of acetic, propionic, and i- and n- butyric acids in ~100,000 ppm NaCl was used to calibrate the FID response. To check the accuracy of the gas chromatograph analyses, 14 samples were analyzed for total aliphatic acids by the titration (fig. 64)

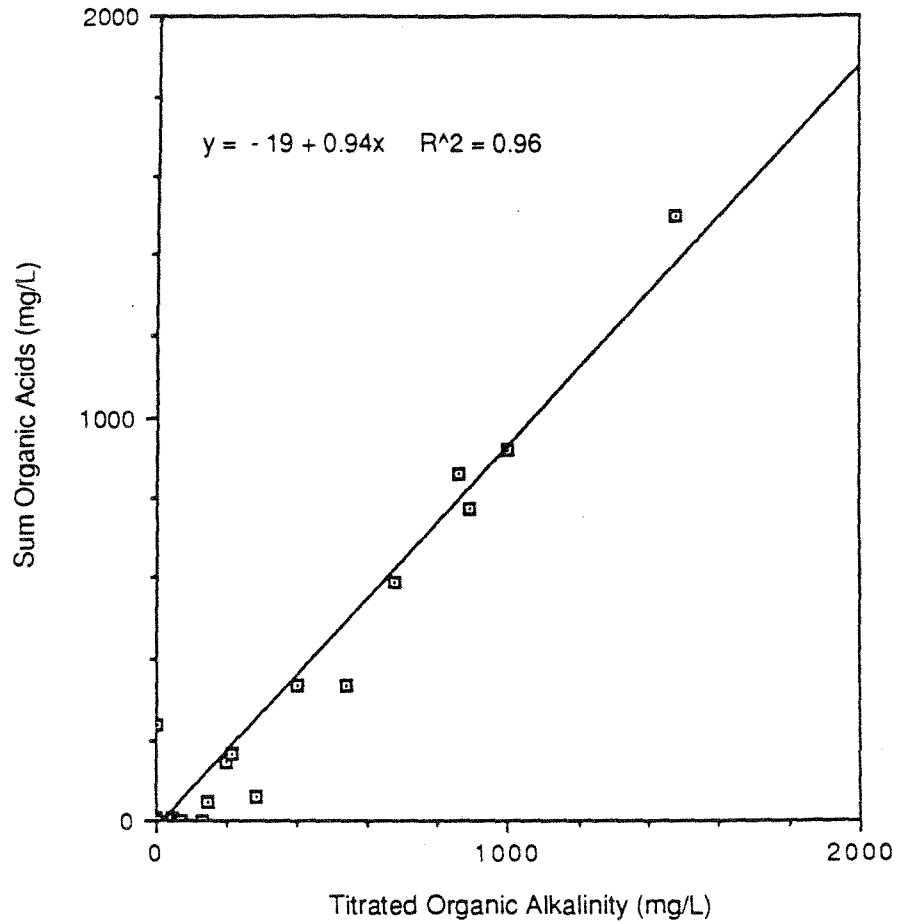


Figure 64. Titration of organic alkalinity versus sum of acetate, propionate, and butyrate. Note that titration concentrations are consistently higher than the summation of organic acids. This suggests the presence of other organic acids in the waters.

as defined in the manual of Standard Methods for the Examination of Water and Wastewater (1975). There is a linear trend of total aliphatic acids from titration versus the sum of the aliphatic acids from gas chromatograph analysis (fig. 65 and table 3), but concentrations from titration results generally are greater than the sum of the acids from the gas chromatograph analysis. This may indicate the presence of other short-chained aliphatic acids that were not analyzed.

Total Organic Alkalinity: Total organic alkalinity titrations were done on approximately half of the samples. The titration procedure followed was from Standard Methods for the Examination of Water and Wastewater (1975). The sample was acidified with six drops of concentrated HCl, and thymol blue was added. Then 5 ml of the sample was drawn through a column of silicic acid by vacuum, which was immediately followed by 65 ml of a chloroform-butanol mix. A phenolphthalein indicator was added, and the sample was then titrated to the phenolphthalein endpoint with .02N NaOH in absolute methanol.

Gas chromatographic analyses of oil: Eleven samples were analyzed by Research and Technical Services, ARCO Oil and Gas Co., to determine whether the oils exhibited biodegradation. Oils were analyzed with a Hewlett-Packard 558 gas chromatograph fitted with a 25-mm. cross-linked 5% phenolmethyl styrene column. Column temperature was initiated at -60°C , then $20^{\circ}/\text{min}$ up to 40°C , then 5.5°C per minute up to 240° then $6^{\circ}/\text{min}$ up to 300°C and held for 23 minutes (M. Robinson-Lewis, personal communication, 1988). Two blind samples were included in the set sent for analysis to test the reproducibility of their analysis. The duplicates are identical to original samples sent (fig. 65).

8.4 Quality Assurance

For all analyses except the organic acids analysis, strict quality assurance methods were adhered to. For inorganic analyses, 10 percent of the samples were analyzed several times to ensure the reproducibility of results. For oxygen and hydrogen isotopes, multiple analyses were also performed on several samples to ensure accuracy of the results. Because the organic acid analysis was new, no standard quality assurance methods exist. Multiple analyses were performed on one sample, and reasonable reproducibility was found.

9. WATER CHEMISTRY - RESULTS

The inorganic and organic chemical and isotopic composition, depth, and location of the 32 water samples collected for this study are shown in tables 5 and 6 and

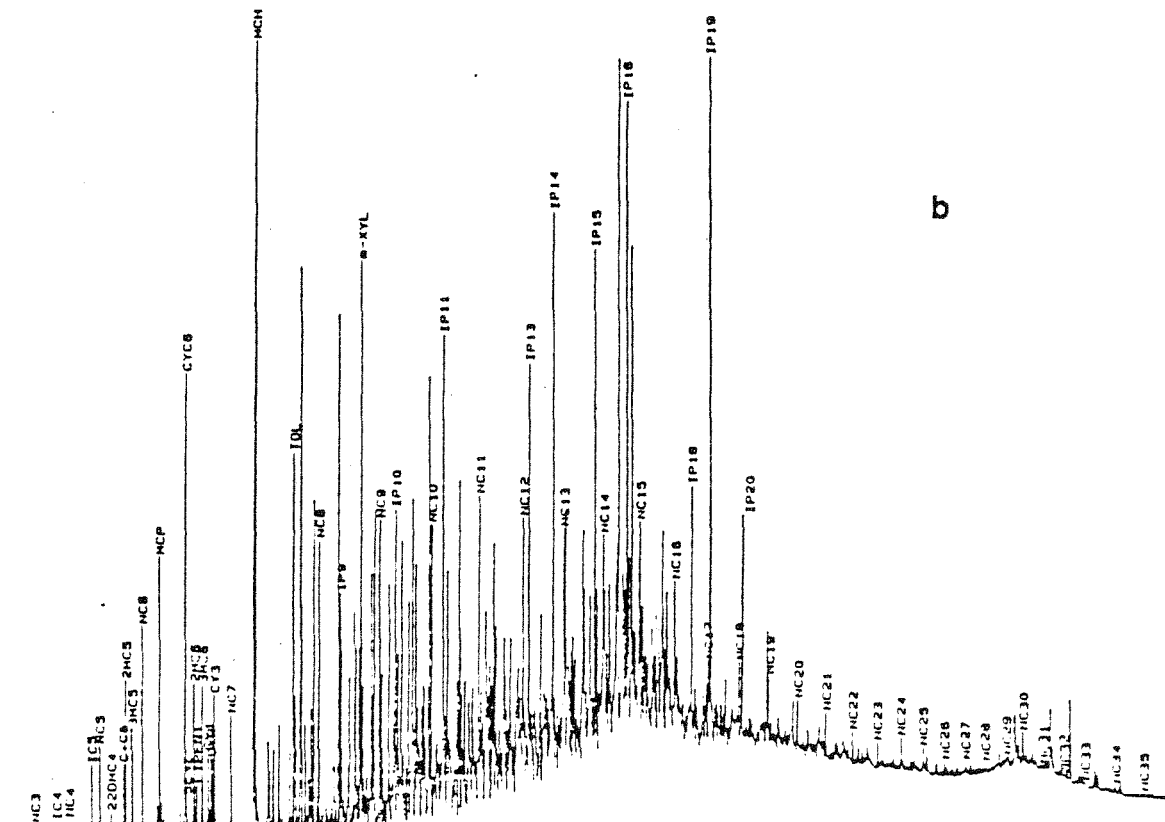
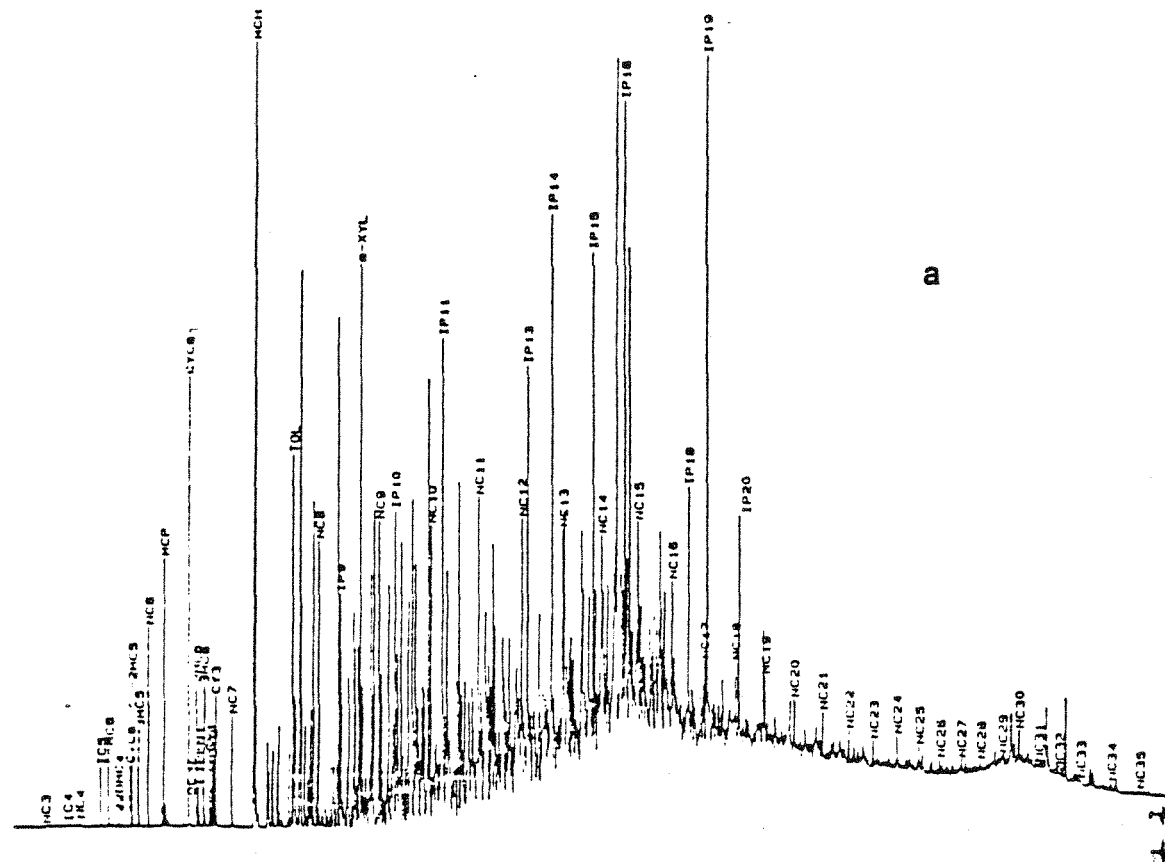


Figure 65. a, b, c, and d. Comparison of gas chromatograph traces for samples ARCO-1989 (TBEG-1) to ARCO-2000, and ARCO-1997 (TBEG-29) to ARCO-2001. ARCO-2000 and ARCO-2001 were unidentified duplicate samples sent to ARCO Service labs to provide a check on their quality. Good replication was found.

figure 63. For trilinear diagrams and maps, these data are based on the Frio chemistry data base previously collected by Kreitler and Richter (1986) (table 3a through d). Scatter diagrams include information from samples collected specifically for this study, or from both this study and the Frio data from Kreitler and Richter (1986). The data set used in the following figures is specified in the captions. In the presentation of the stable isotope data (table 7), the data collected from this study is integrated with Fisher (1982), and unpublished data from Lynton S. Land (Department of Geological Sciences, The University of Texas at Austin). Data from Kreitler and Richter (1986) are presented geographically as the total data set, by county or general region of the Texas Gulf Coast (table 3a through d). It was found that reasonable subregions for our study were Northgulf, Northcentral, Southcentral, and Southgulf. Northgulf region includes Brazoria, Chambers, Fort Bend, Galveston, Harris, Jefferson, Matagorda, and Newton Counties. Northcentral region includes Jackson, Victoria, and Wharton Counties. Southcentral region includes Aransas, Bee, Calhoun, Goliad, parts of Jim Wells, parts of Kleberg, Nueces, Refugio, and San Patricio Counties. Southgulf region includes Brooks, Duval, Hidalgo, parts of Jim Wells, Kenedy, parts of Kleberg, and Starr Counties.

9.1 Trilinear Diagrams

Trilinear diagrams for the Frio show a gradual shift from Na-Cl water in the north and north-central region to Na-Ca-Cl water in the south-central region and Na-Ca-Cl-SO₄ in the south (fig. 66a through d). These trends are similar to those observed by Morton and Land (1987) deeper in the Frio section. Their data show higher Ca concentrations in the south but lower SO₄ values in this southern area.

9.2 Major Anion Distributions (Cl, SO₄)

Chloride

Chloride concentrations in the Frio range from less than 5000 mg/L to approximately 100,000 mg/L. Chloride concentrations typically represent more than 90% of the anions (fig. 66a through d) and therefore are generally correlative with salinity (TDS). The highest Cl concentrations for all depths are generally found in the northern Gulf region, the region that encompasses the Houston Embayment and its salt domes (fig. 67a through d). Kreitler and Richter (1986) and Morton and Land (1987) suggest that these high Cl values are related to salt dome dissolution. A smaller salt basin is present in South Texas, but chloride concentrations in this region are variable with depth, as indicated on the Cl versus depth plot for each county (appendix). Previous authors have suggested that salinity decreases with depth and

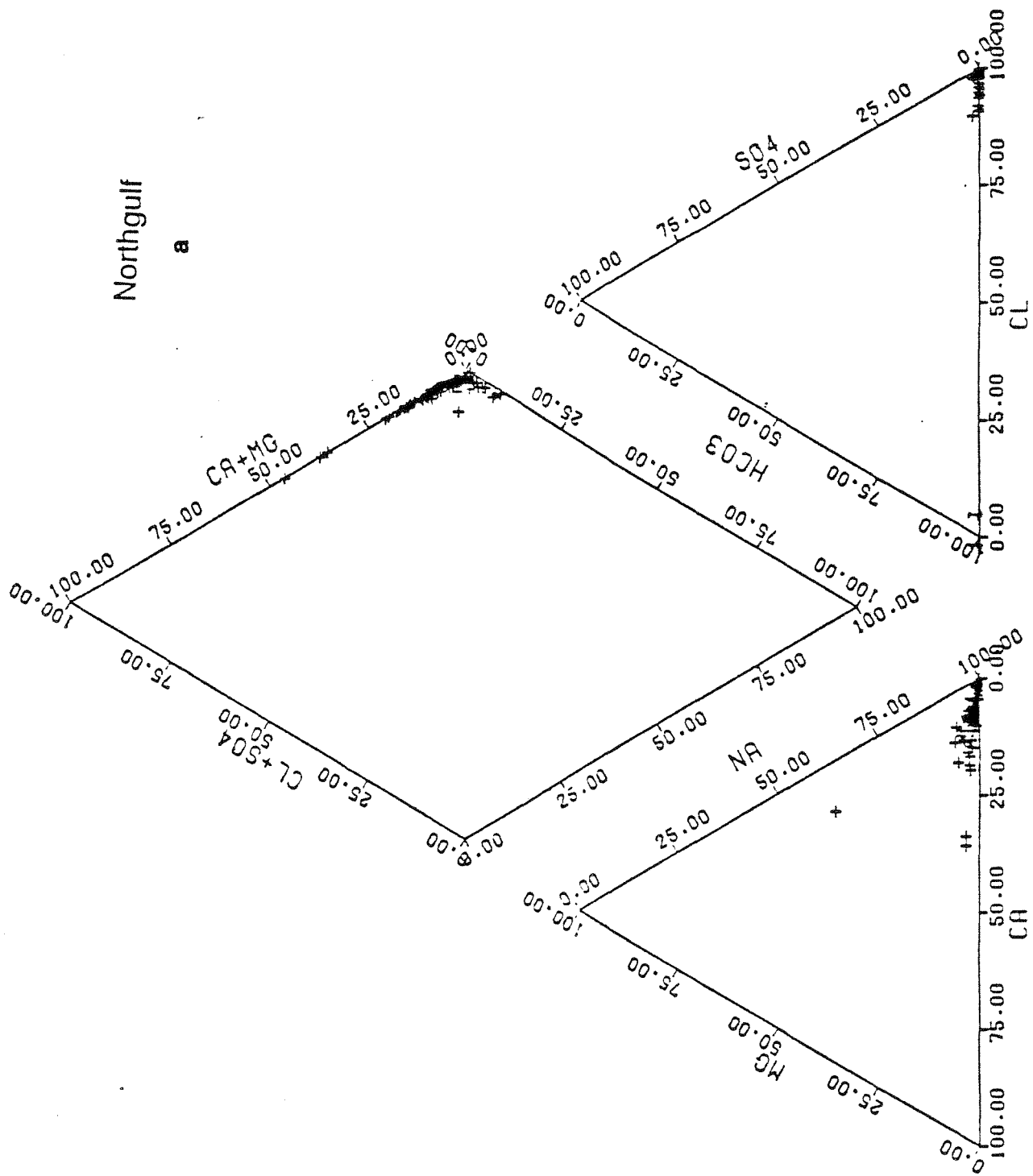


Figure 66. a, b, c, d. Trilinear diagrams for Northgulf, Northcentral, Southcentral, and Southgulf regions of the Frio Formation. Chemical compositions based on Table 1a, b, c, and d.

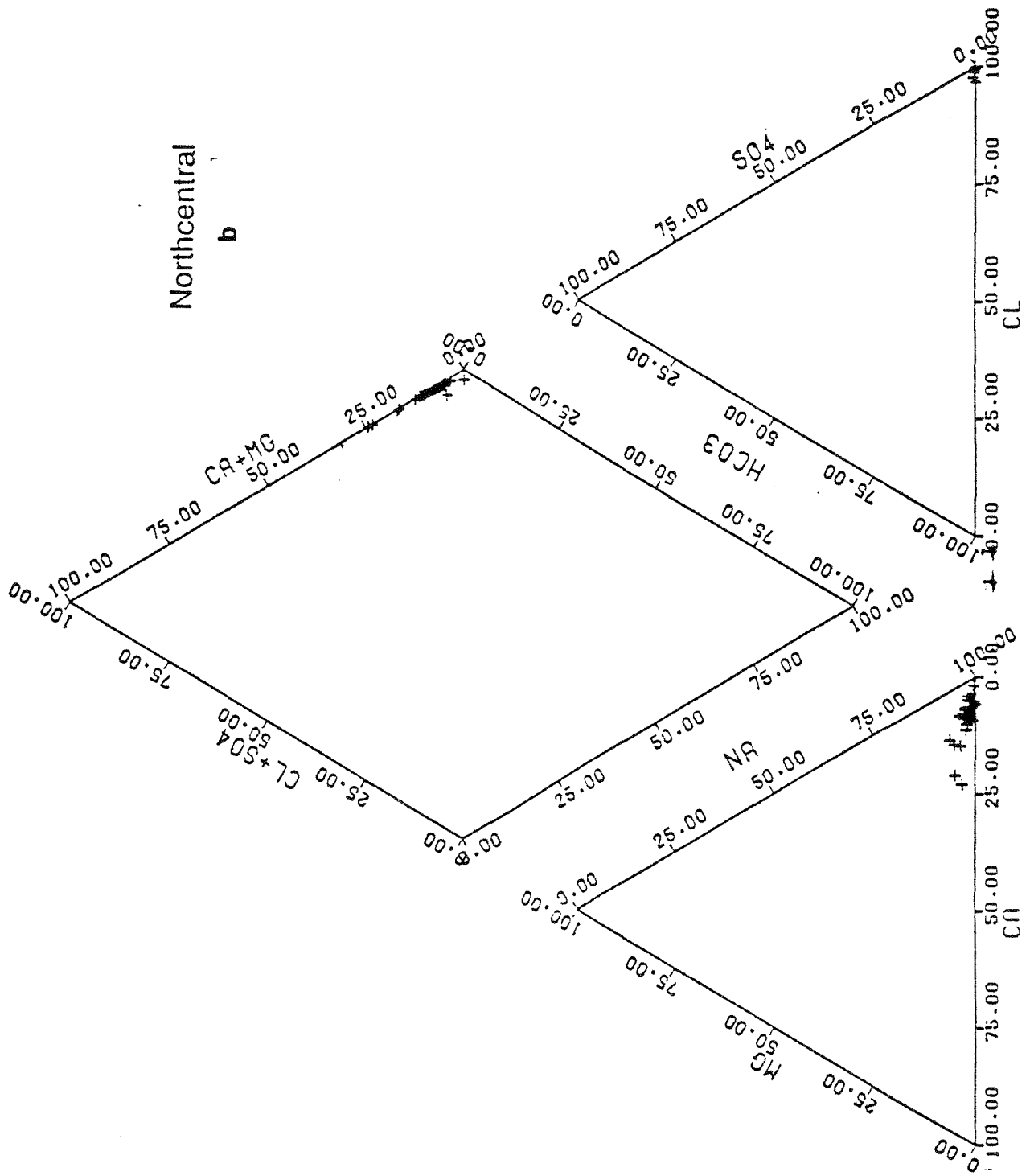


Figure 66 (continued)

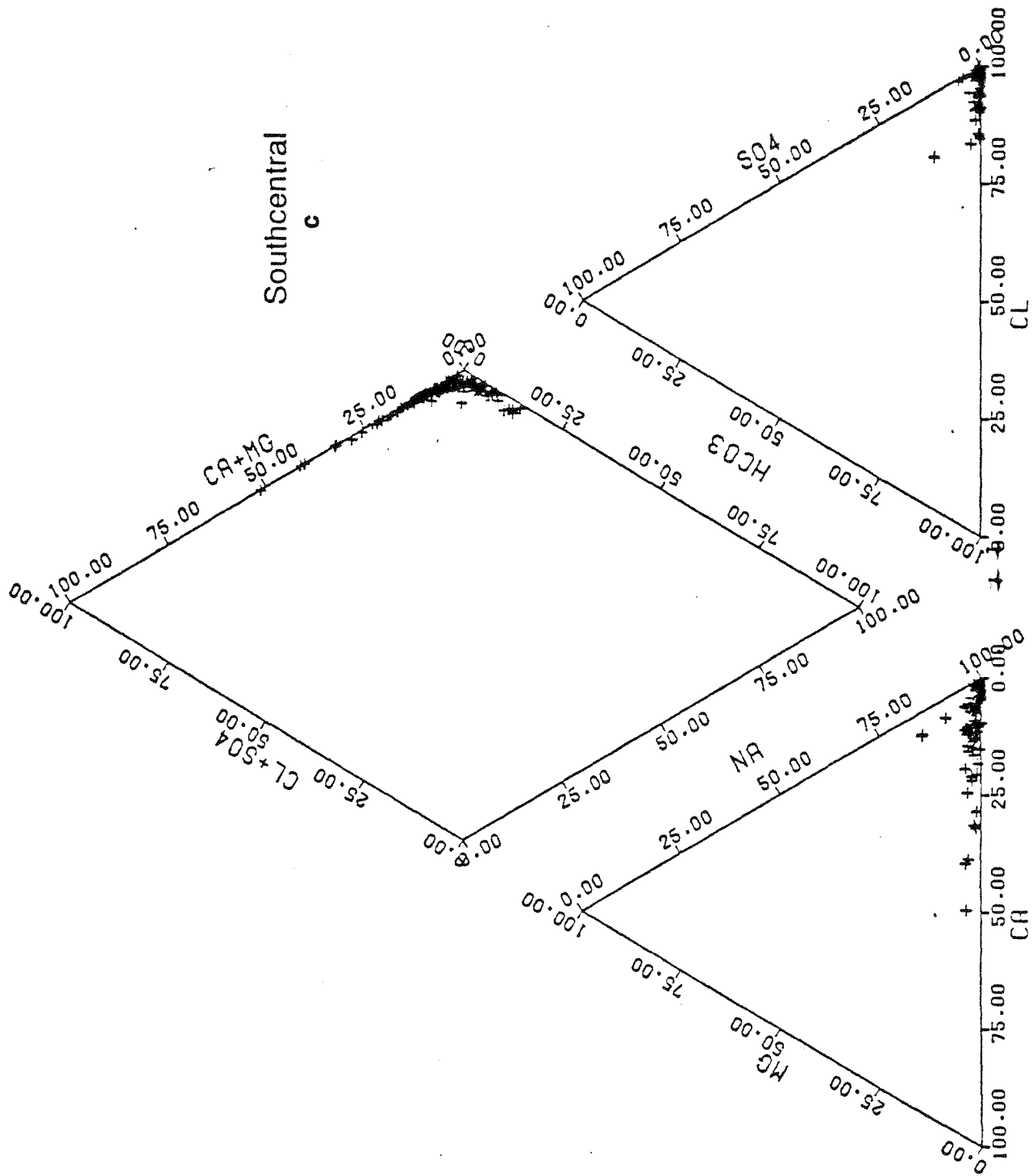


Figure 66 (continued)

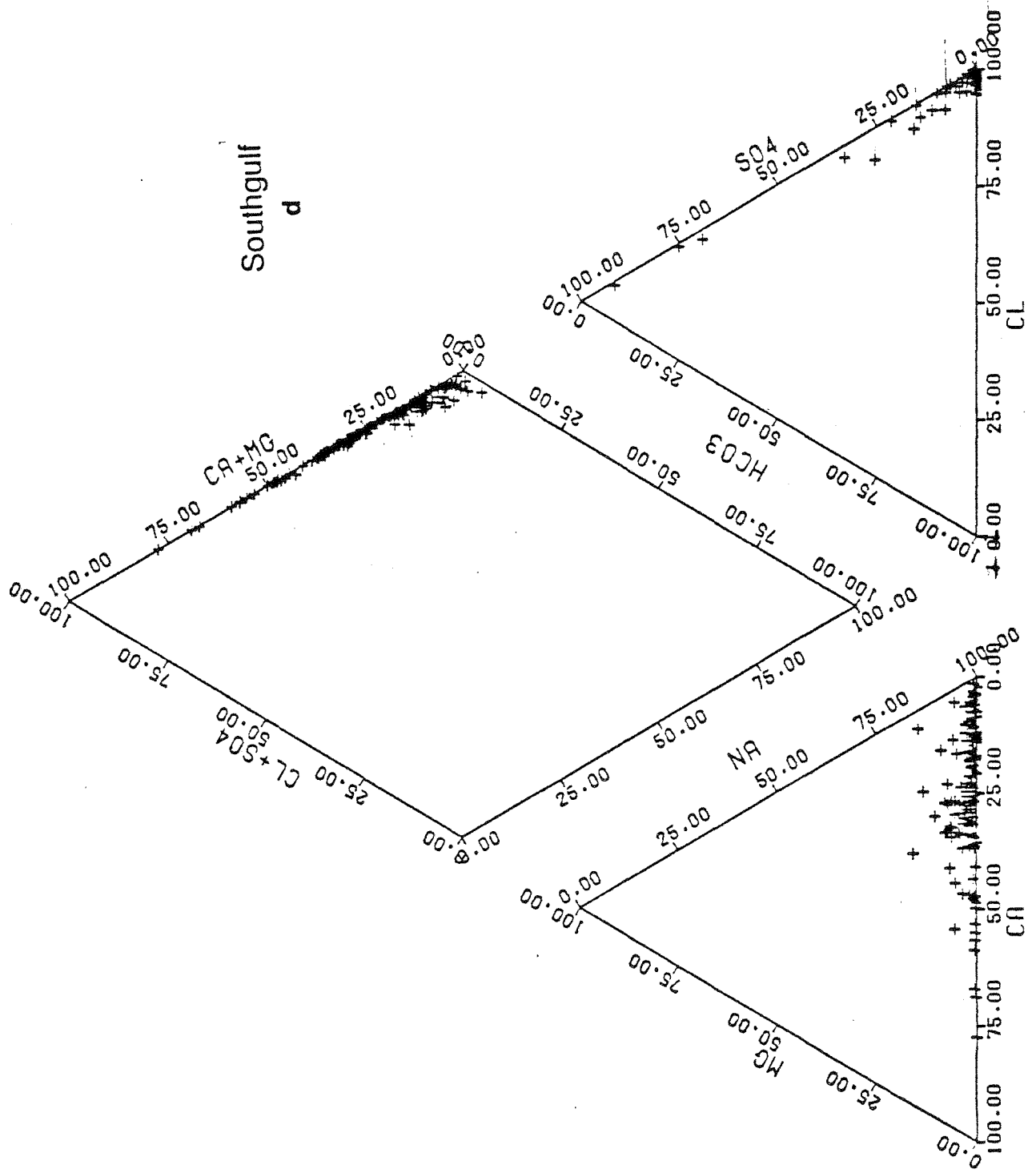


Figure 66 (continued)

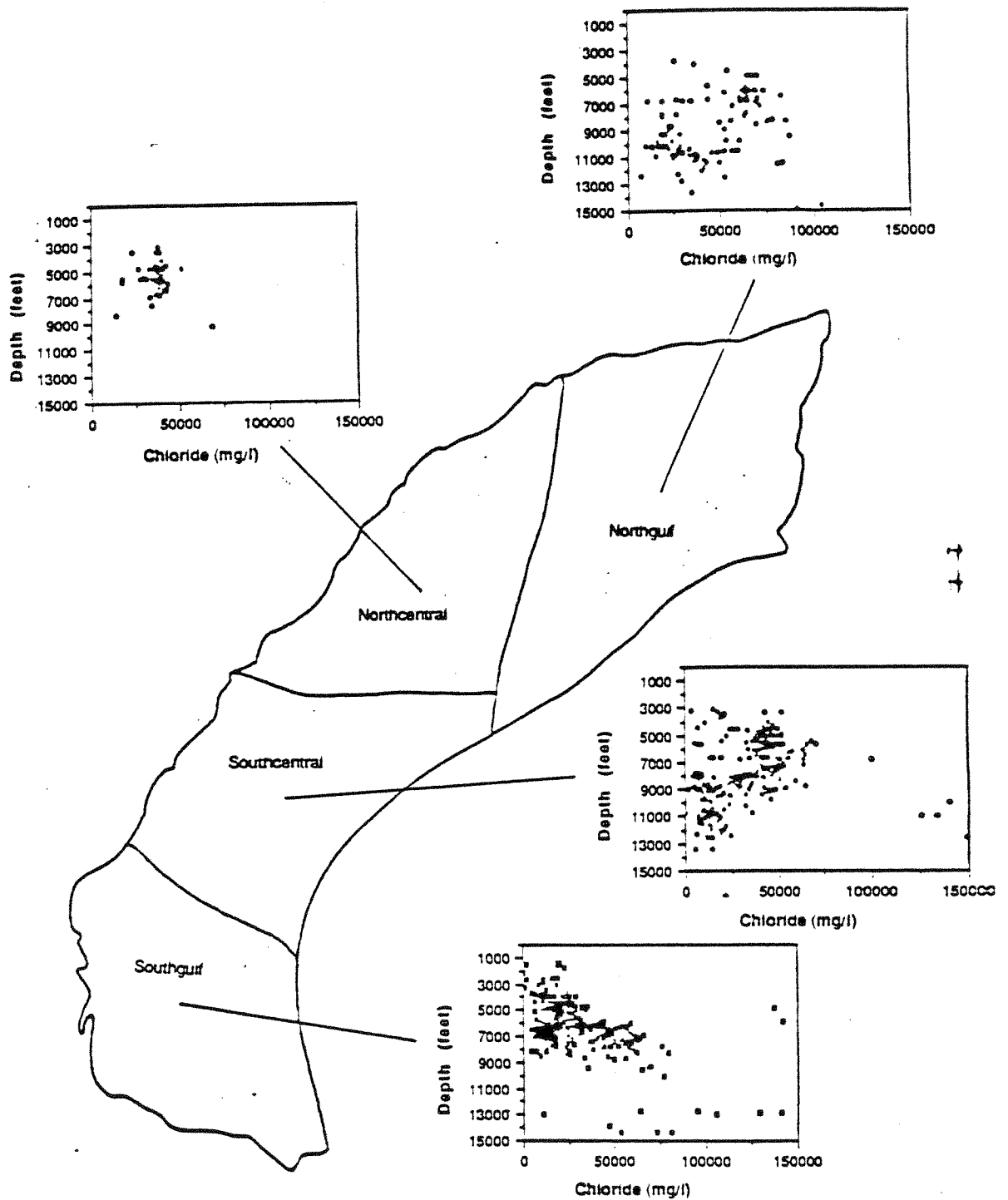


Figure 67. Chloride distribution for the Frio Formation for various depths from Northgulf, Northcentral, Southcentral and Southgulf regions. Chemical compositions based on Table 1a ,b ,c, and d. Units in mg/l.

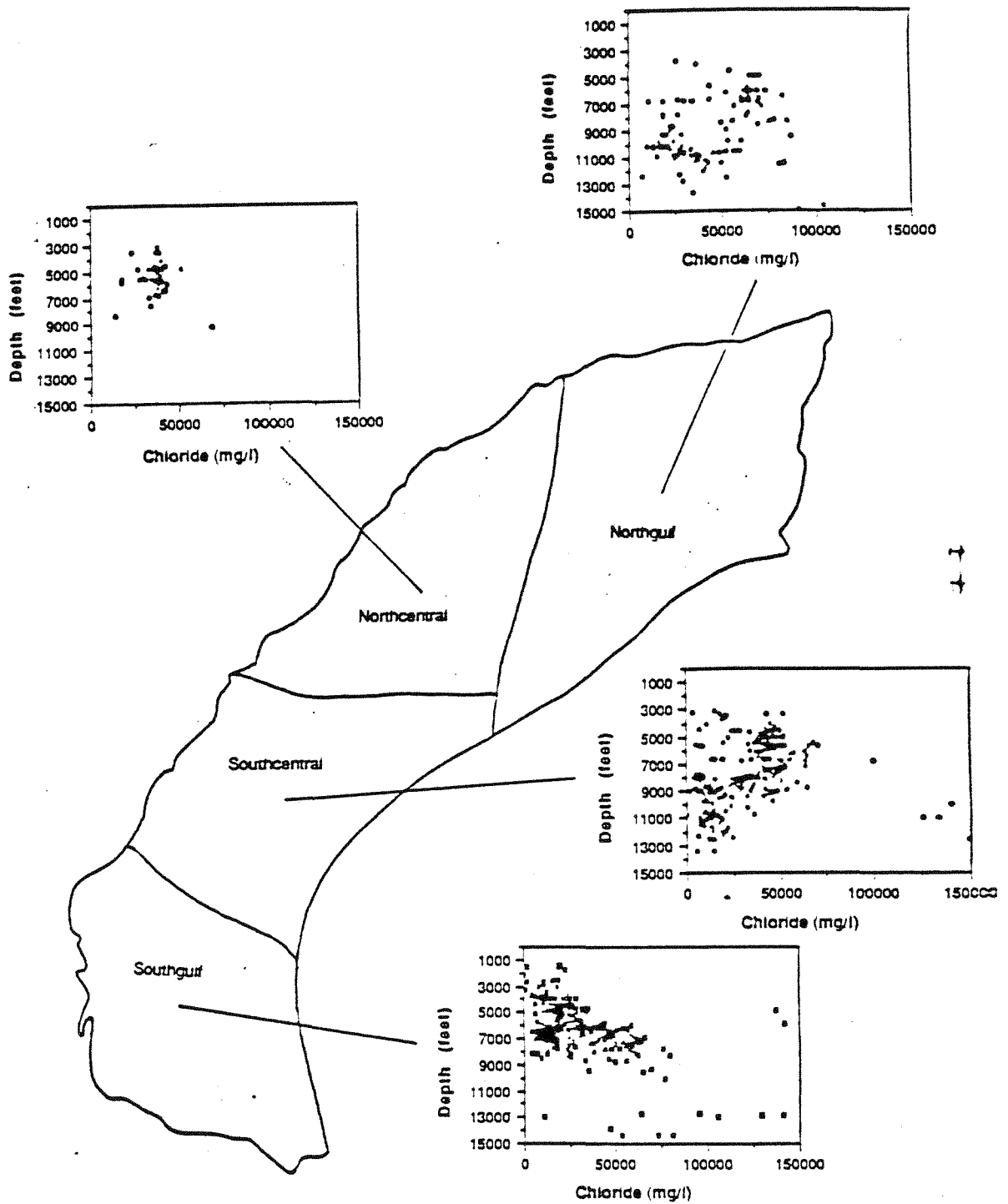


Figure 67. Chloride distribution for the Frio Formation for various depths from Northgulf, Northcentral, Southcentral and Southgulf regions. Chemical compositions based on Table 1a ,b ,c, and d. Units in mg/l.

may be related to the transition from hydrostatic to geopressed conditions. This trend of decreasing salinities is observed in San Patricio and Nueces Counties (fig. 68a, b).

Our pressure/depth plot from the previous description on hydrostatic section of the Frio Formation (fig. 11) also indicates variable salinities. Two hydrostatic lines are evident: one line with a slope of 0.433, which indicates low total dissolved solids, and a second line or zone with a slope of 0.465, which indicates brines of 80,000 mg/L or greater salinities. These two different distributions of data suggest waters with different salinities. We were unable to integrate our pressure data base with chemical composition to the pressure data base to confirm the different salinities for the different hydrostatic lines. It is interesting to note that the hydrostatic line for the middle Wilcox Formation (fig. 57), which generally contains lower TDS values than the Frio, has only the 0.433 hydrostatic line; the 0.465 line is absent.

Sulfate

Sulfate concentrations generally are low in Frio Formation waters (fig. 69a through e). Only in Southgulf are higher values evident. Low sulfate concentrations probably result from a reducing environment in the organic-rich Frio Formation.

9.3 Major Cation Distributions (Na, Ca)

Sodium concentrations increase linearly with chloride for most of the samples except for the Southgulf region (fig. 70a through e). Calcium concentrations versus chloride form a dogleg for Southgulf, Southcentral, and Northgulf (fig. 71a through e). Land and Prezbindowski (1983), Fisher and Kreitler (1987), and Kreitler and Seni (1984) have suggested that the increase in calcium results from cation exchange reactions where Na from a NaCl brine is replaced by Ca from either clays or calcic feldspars. This reaction may be the cause of high calcium in the Southgulf region. Morton and Land (1987) observed similar calcium-rich brines in the geopressed section of this South Texas region and suggest that these calcium-rich brines are deeper brines that have migrated to shallower depths.

9.4 Minor Elements (Br), and Cl/Br and Na/Cl Ratios

A plot of bromide versus chloride (fig. 72) shows two different populations of data, a population where bromide increases linearly with chloride (this will be referred to as Na-Cl, high-Br water type, and a population where bromide concentration remains constant with increasing chloride (this will be referred to as Na-Cl, low-Br water type; all discussion of these two water types is based on this differentiation in

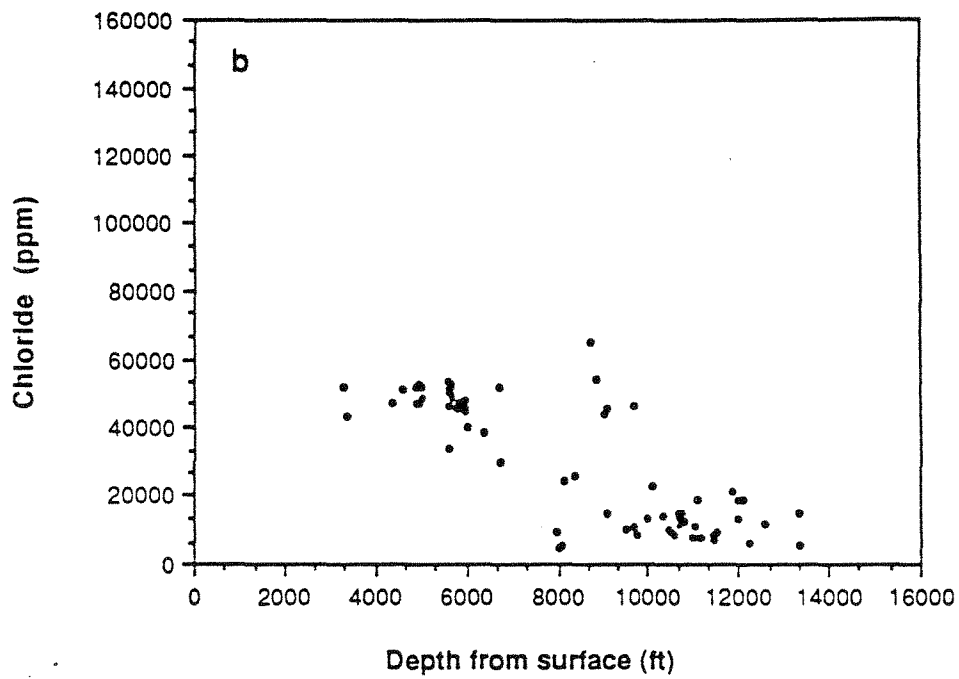
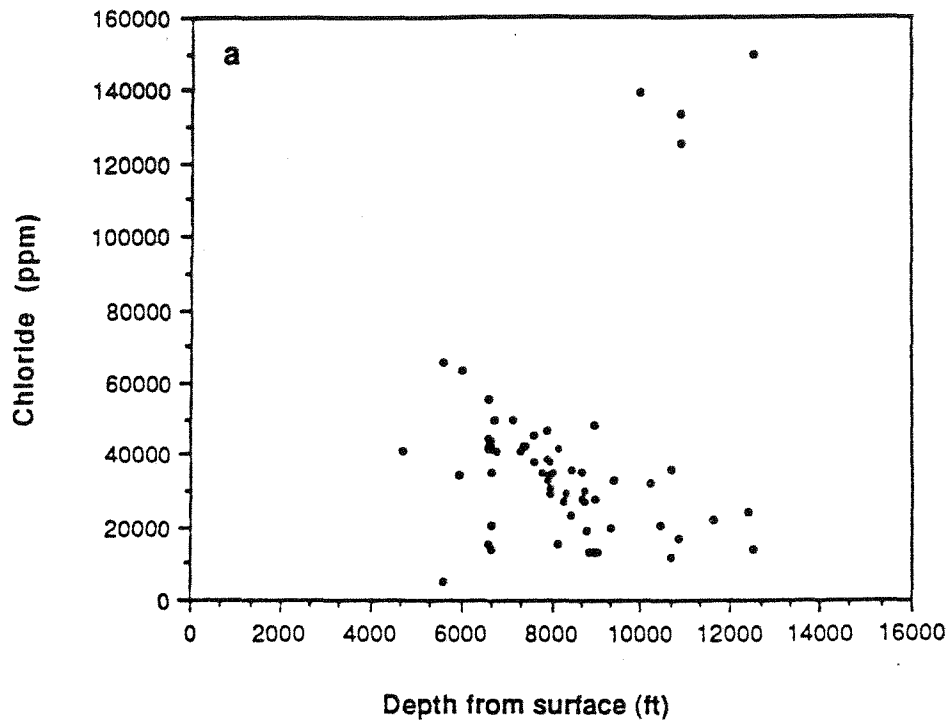


Figure 68. (a) Cl versus depth for Nueces County, (b) Cl versus depth for San Patricio County. Data from Kreitler and Richter (1986).

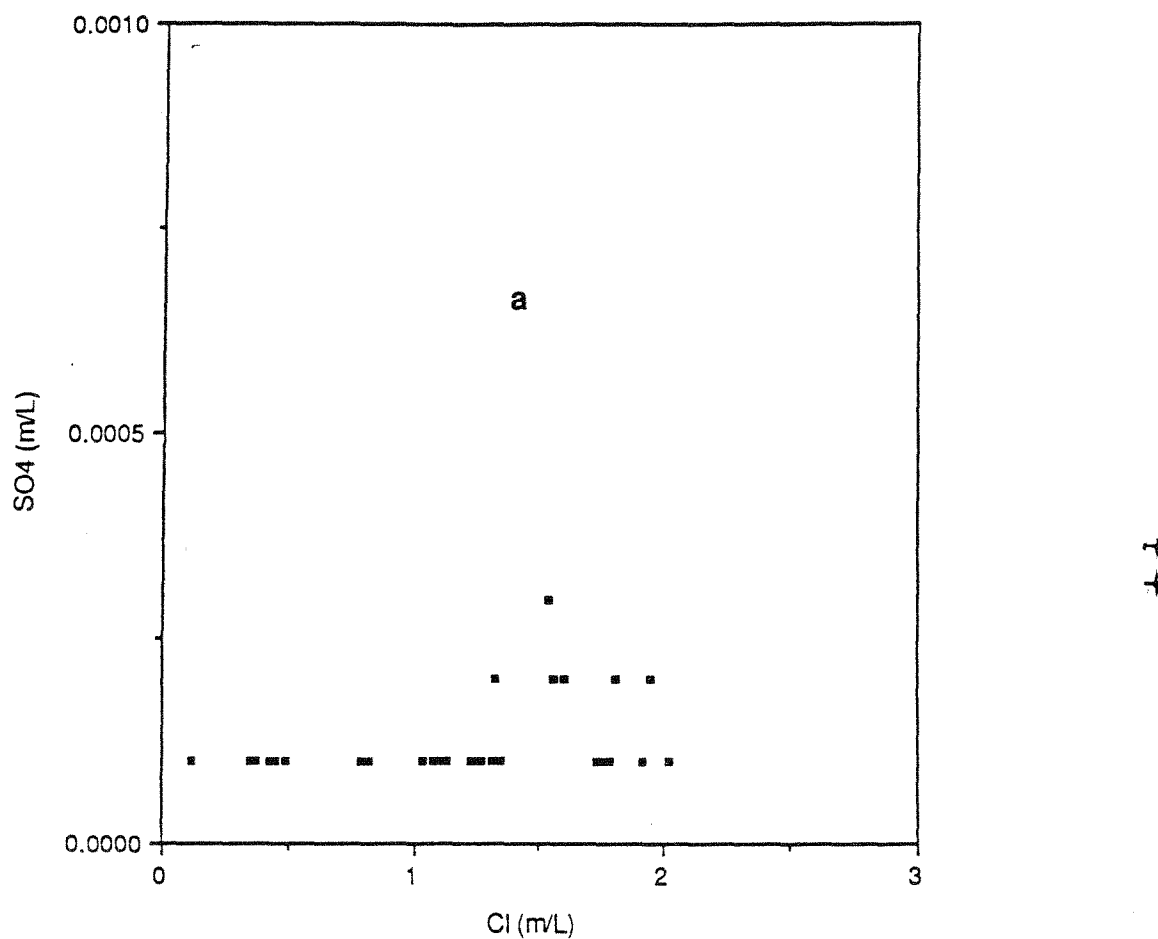
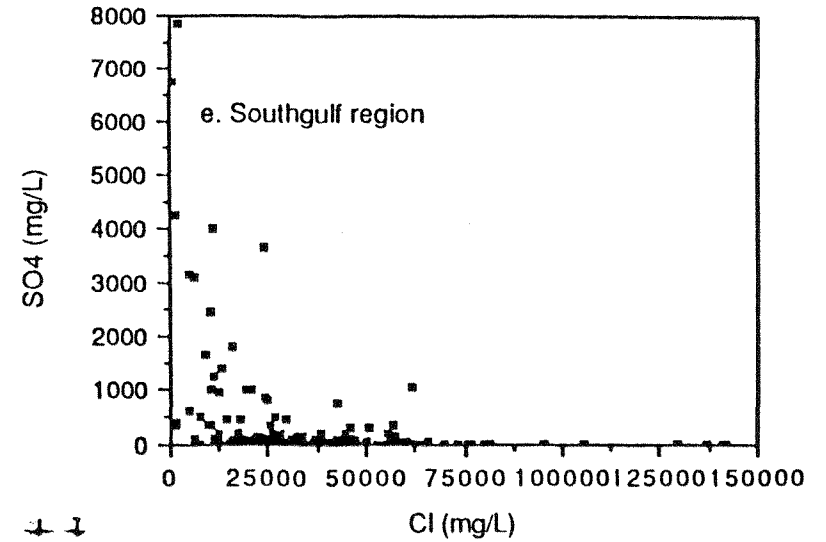
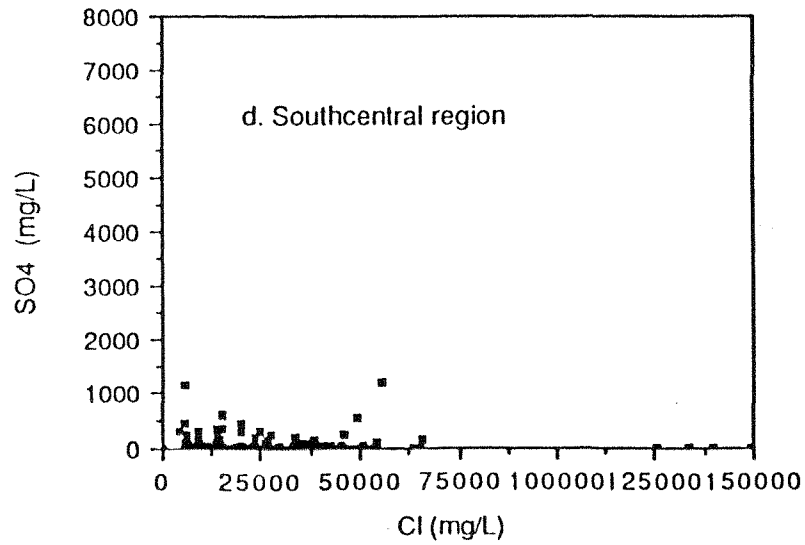
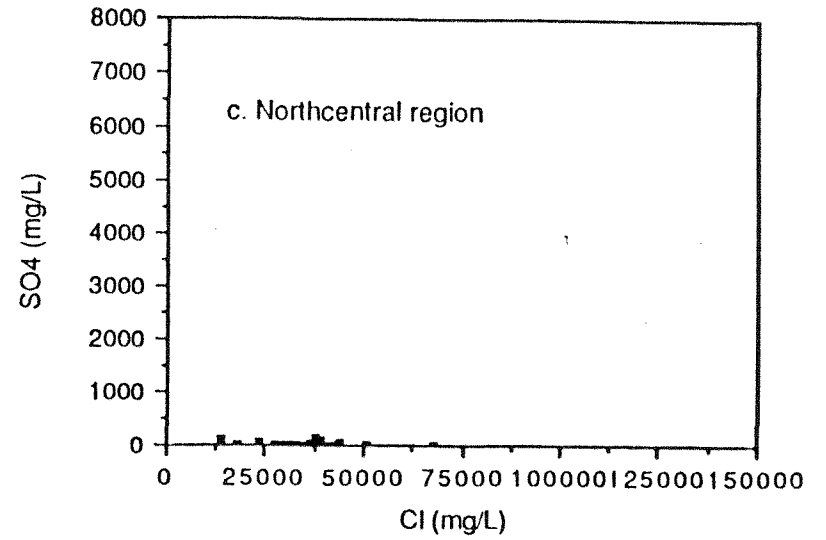
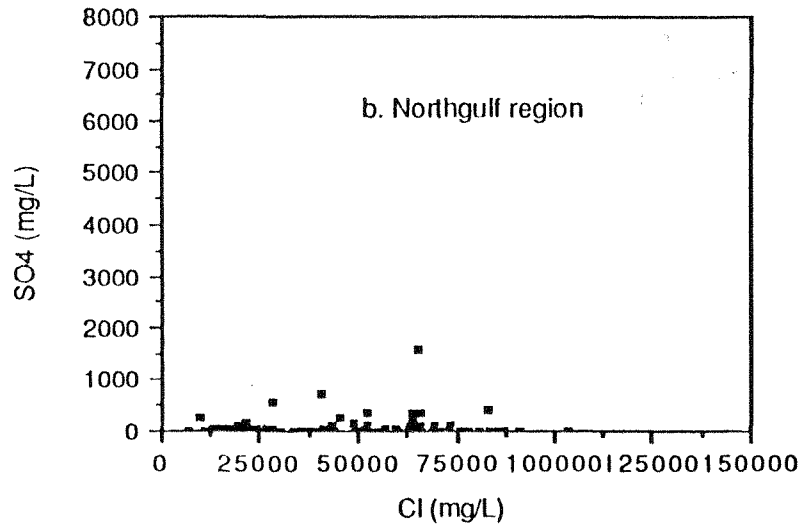


Figure 69. (a) Sulfate concentrations versus chloride in the Frio Formation collected for this study (Table 3). Sulfate concentrations versus chloride for the Frio Formation for Northgulf (b), Northcentral (c), Southcentral (d), and Southgulf (e). Chemical compositions based on Table 2.

Figure 69 (continued)



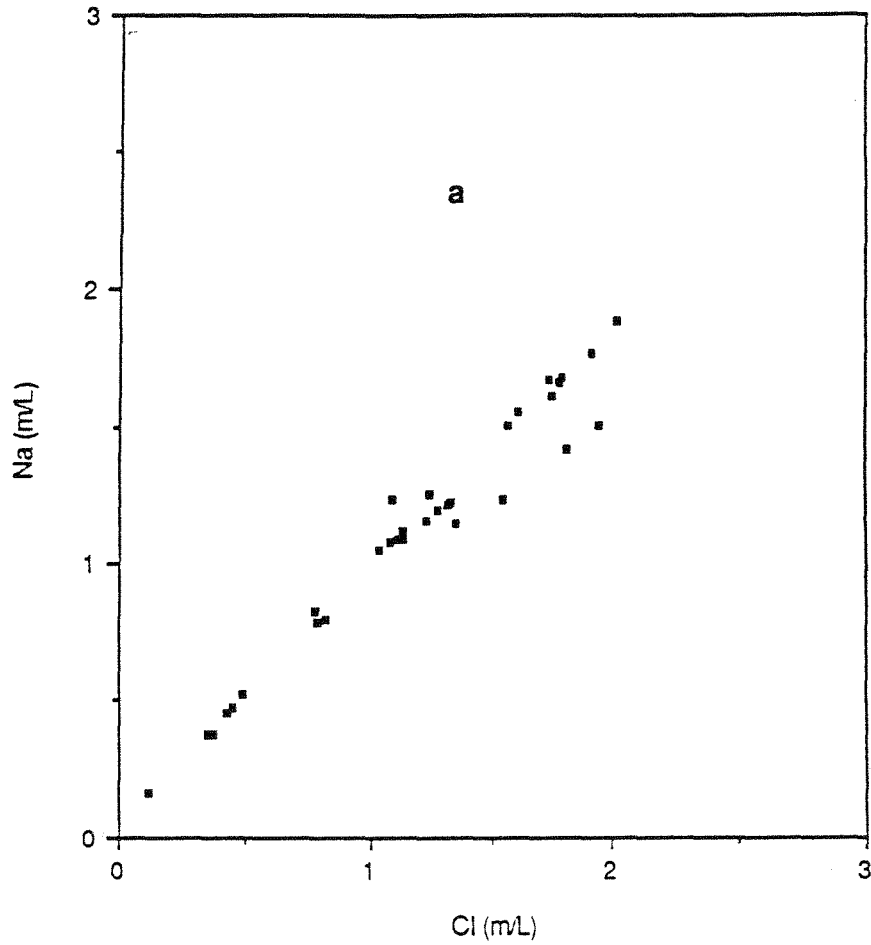
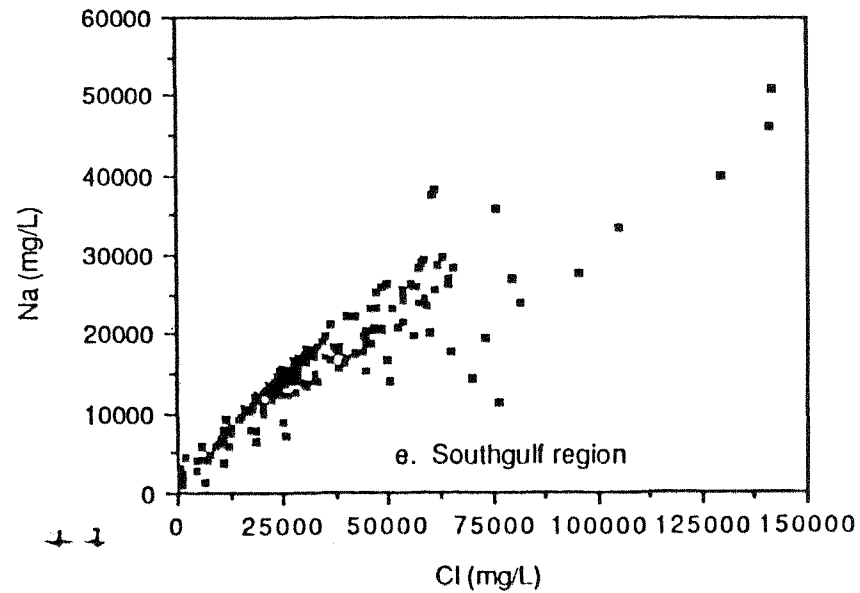
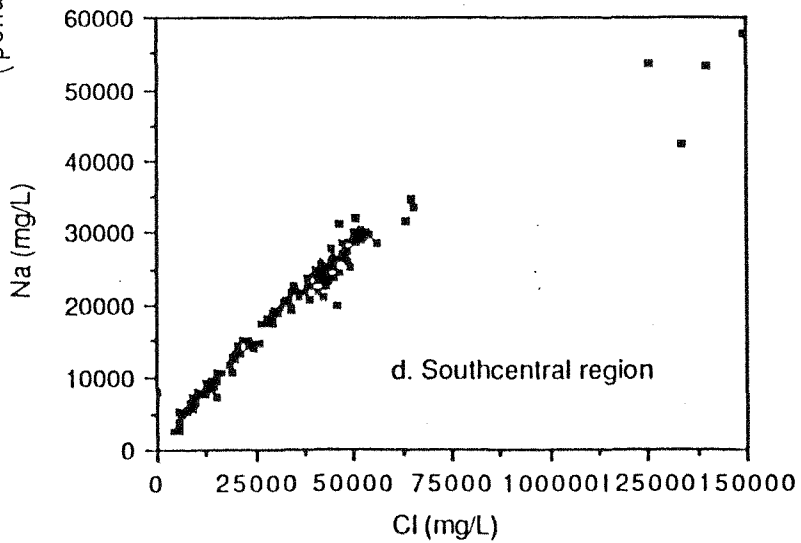
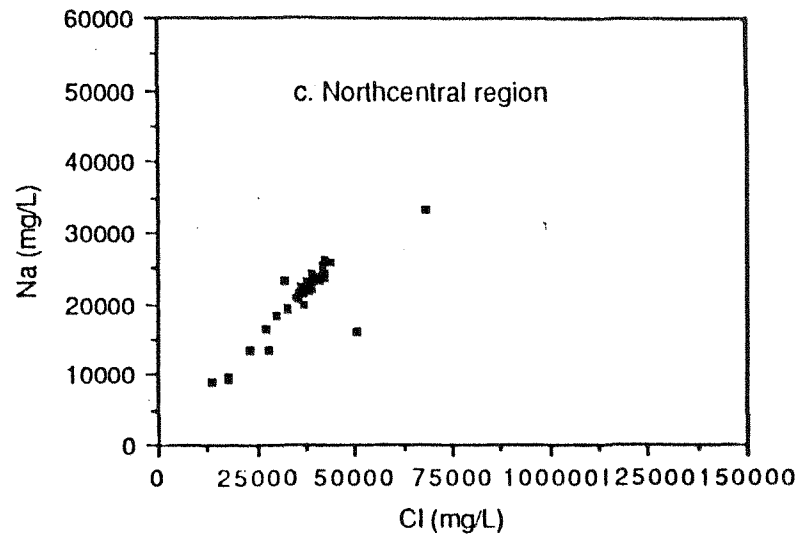
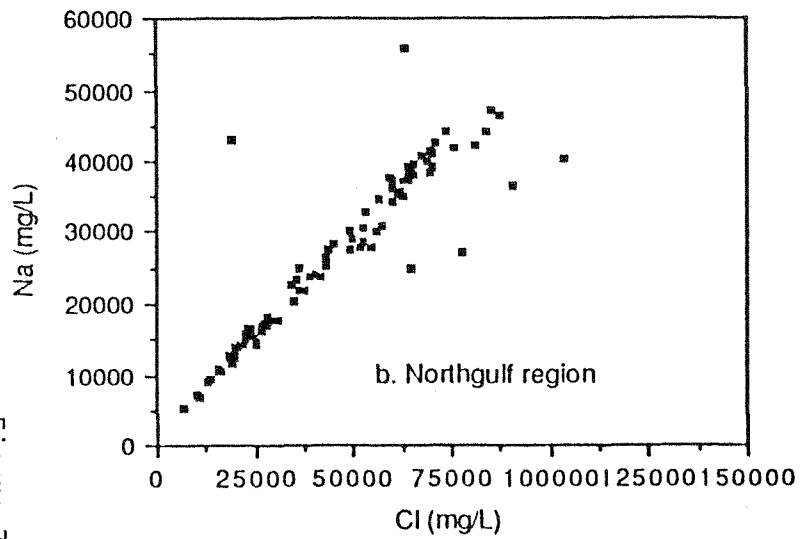


Figure 70. (a) Sodium concentration in the Frio Formation from data collected for this study (Table 3). Sodium concentrations versus chloride for the Frio Formation for Northgulf (b), Northcentral (c), Southcentral (d), and Southgulf (e). Chemical compositions based on Table 1a, b, c, and d.

Figure 70 (continued)



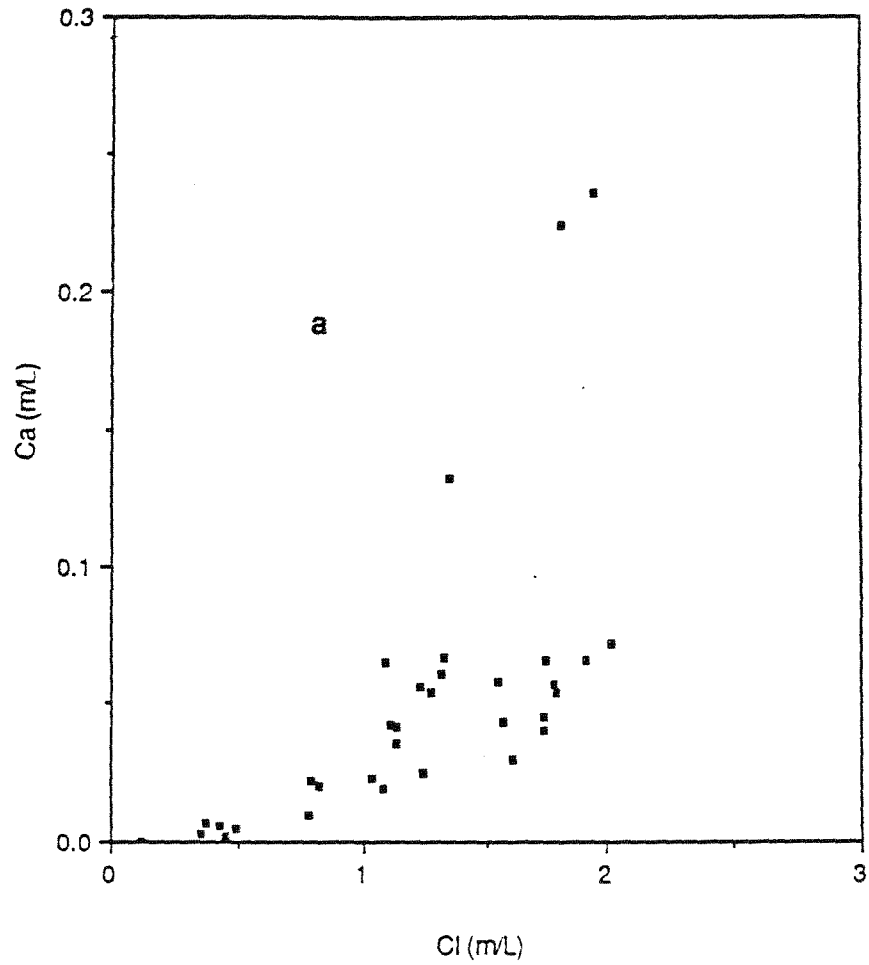
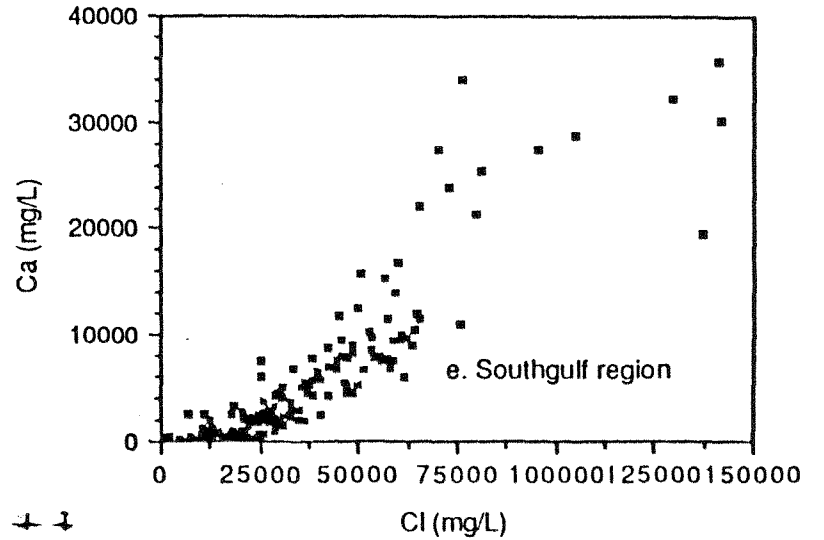
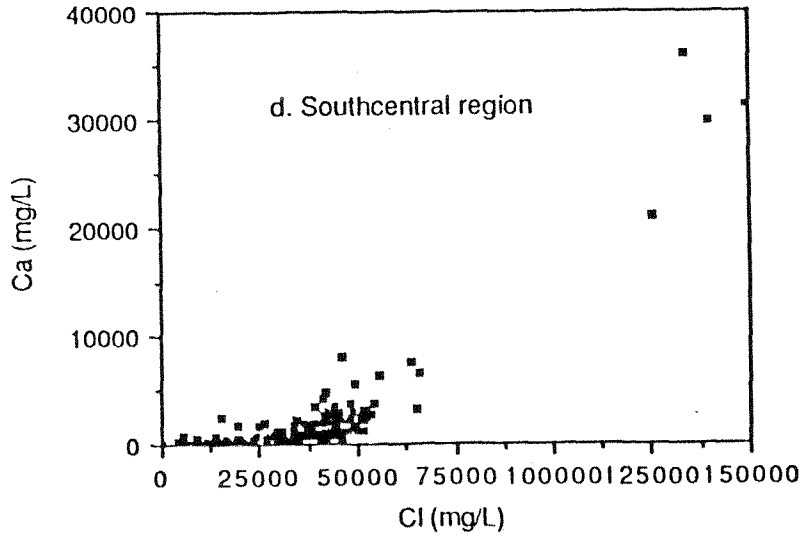
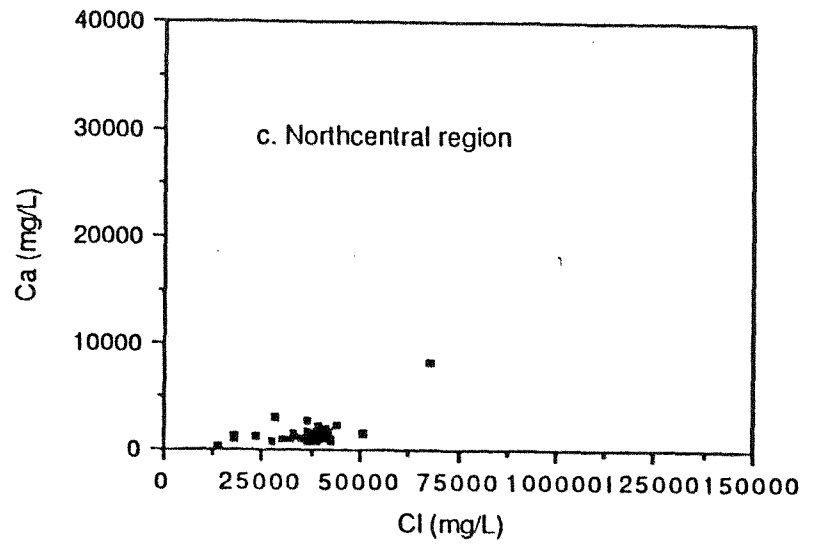
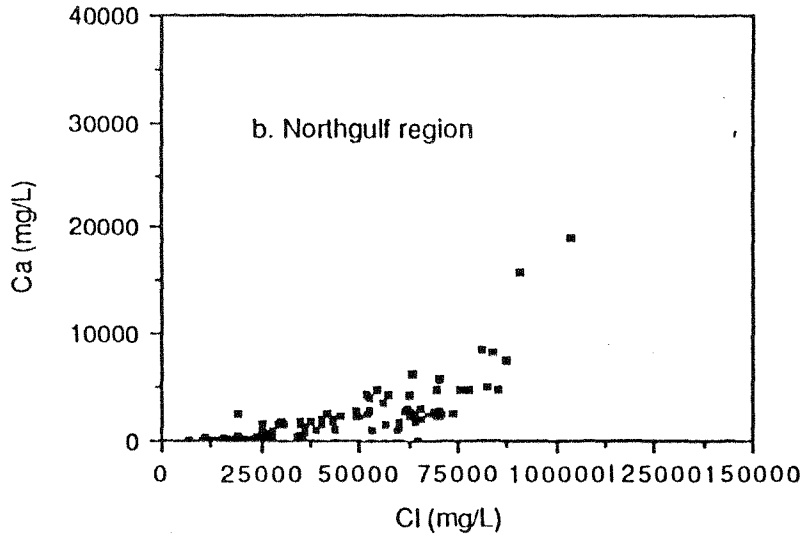


Figure 71. (a) Calcium concentrations versus chloride in the Frio Formation from data collected for this study (Table 3). Calcium concentrations versus chloride for the Frio Formation for Northgulf (b), Northcentral (c), Southcentral (d), and Southgulf (e). Chemical composition based on Table 1a, b, c, and d.

Figure 71 (continued)



↑ ↓

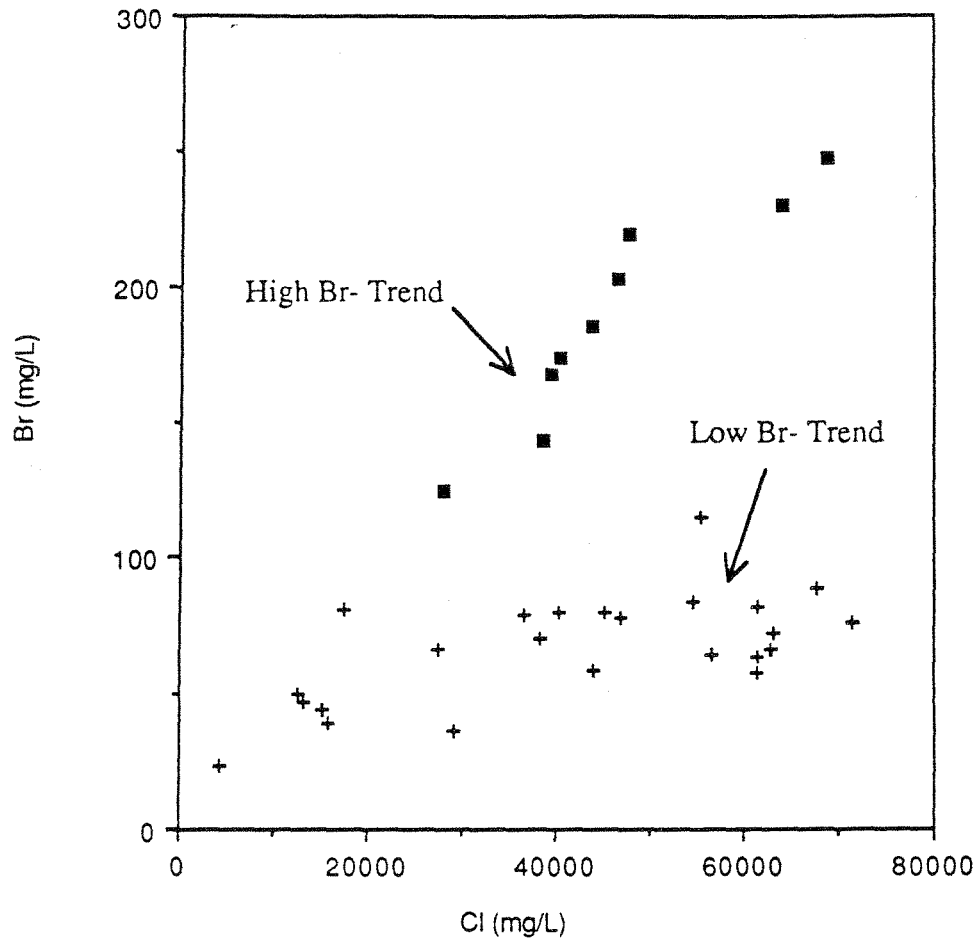


Figure 72. Plot of bromide versus chloride from data collected for this study (Table 3). Note two different populations of data.

fig. 72). With the addition of Southgulf region data, the linear relationship of the high-Br trend is extended to much higher Br concentrations (fig. 73). Figure 74, a plot of Cl/Br versus Cl, shows a similar separation of the two populations. Bromide and Cl/Br ratios have been used as an effective tool for determining the source of chloride in a brine. High Cl/Br ratios indicate that halite dissolution is the source of chloride (Whittemore and others, 1981; Richter and Kreitler, 1986). Low Cl/Br ratios are typical of the average basinal brine (Richter and Kreitler, 1986), seawater, and residual brines from bittern salt precipitation (Carpenter, 1978). The ratio of Na/Cl is another effective tool for determining the source of Cl in a brine. Seawater has a molar Na/Cl ratio of 0.77, whereas brines resulting from halite dissolution approximate 1.0. Low-salinity meteoric waters typically have an Na/Cl ratio > 1.0 , because of possible generation of sodium bicarbonate waters that is independent of chloride. Figure 75, a plot of Na/Cl versus Cl again shows two different populations. The low-Br waters trend from approximately 1.1 to 0.95, whereas the high-Br waters trend from 1.0 to 0.75. The Cl/Br and the Na/Cl ratios for the low-Br data both suggest halite dissolution as the source of NaCl in these waters. The geographic location of these samples in the salt basin further confirms halite dissolution (fig. 76 a and b). These two populations are geographically distributed such that the low-Br values are predominantly in the Houston Embayment salt dome region. The high-Br waters occur predominantly in the middle to south coastal region. The source of the high Br cannot be as easily determined. A high-Br water is mixing with a low-Br, low-salinity water. A plot of Br versus Ca (fig. 77) shows that the high Br also correlates with the high Ca previously discussed and may result from mixing. High Br also correlates with high Sr concentrations and follows a slope of 9:10 (a molar ratio of approximately 1:1) (fig. 78). Deeper formation waters in the Gulf of Mexico basin are high in Ca, Sr, and Br (Morton and Land, 1987). These waters may be leaking into shallower sections, resulting in the observed chemistry changes. Figure 79 shows the increase in Br with depth for the samples from the high-Br population. Plotting Na/Cl versus Cl/Br (fig. 80) again separates the two trends. Both populations (low Br and high Br) appear to originate from the same source, a water with a Na/Cl ratio of 1.0 or higher and a Cl/Br ratio of about 200. These ratios suggest a continental ground water, or possibly brackish water in a deltaic setting like the original water, and not a marine water as has been previously suggested. If this initial water is an original depositional (connate) water, then the hypothesis of a more continental-deltaic water like the original water may be reasonable for the Frio, which is composed predominantly of fluvial and deltaic, not marine, facies.

fig. 72). With the addition of Southgulf region data, the linear relationship of the high-Br trend is extended to much higher Br concentrations (fig. 73). Figure 74, a plot of Cl/Br versus Cl, shows a similar separation of the two populations. Bromide and Cl/Br ratios have been used as an effective tool for determining the source of chloride in a brine. High Cl/Br ratios indicate that halite dissolution is the source of chloride (Whittemore and others, 1981; Richter and Kreitler, 1986). Low Cl/Br ratios are typical of the average basinal brine (Richter and Kreitler, 1986), seawater, and residual brines from bittern salt precipitation (Carpenter, 1978). The ratio of Na/Cl is another effective tool for determining the source of Cl in a brine. Seawater has a molar Na/Cl ratio of 0.77, whereas brines resulting from halite dissolution approximate 1.0. Low-salinity meteoric waters typically have an Na/Cl ratio > 1.0 , because of possible generation of sodium bicarbonate waters that is independent of chloride. Figure 75, a plot of Na/Cl versus Cl again shows two different populations. The low-Br waters trend from approximately 1.1 to 0.95, whereas the high-Br waters trend from 1.0 to 0.75. The Cl/Br and the Na/Cl ratios for the low-Br data both suggest halite dissolution as the source of NaCl in these waters. The geographic location of these samples in the salt basin further confirms halite dissolution (fig. 76 a and b). These two populations are geographically distributed such that the low-Br values are predominantly in the Houston Embayment salt dome region. The high-Br waters occur predominantly in the middle to south coastal region. The source of the high Br cannot be as easily determined. A high-Br water is mixing with a low-Br, low-salinity water. A plot of Br versus Ca (fig. 77) shows that the high Br also correlates with the high Ca previously discussed and may result from mixing. High Br also correlates with high Sr concentrations and follows a slope of 9:10 (a molar ratio of approximately 1:1) (fig. 78). Deeper formation waters in the Gulf of Mexico basin are high in Ca, Sr, and Br (Morton and Land, 1987). These waters may be leaking into shallower sections, resulting in the observed chemistry changes. Figure 79 shows the increase in Br with depth for the samples from the high-Br population. Plotting Na/Cl versus Cl/Br (fig. 80) again separates the two trends. Both populations (low Br and high Br) appear to originate from the same source, a water with a Na/Cl ratio of 1.0 or higher and a Cl/Br ratio of about 200. These ratios suggest a continental ground water, or possibly brackish water in a deltaic setting like the original water, and not a marine water as has been previously suggested. If this initial water is an original depositional (connate) water, then the hypothesis of a more continental-deltaic water like the original water may be reasonable for the Frio, which is composed predominantly of fluvial and deltaic, not marine, facies.

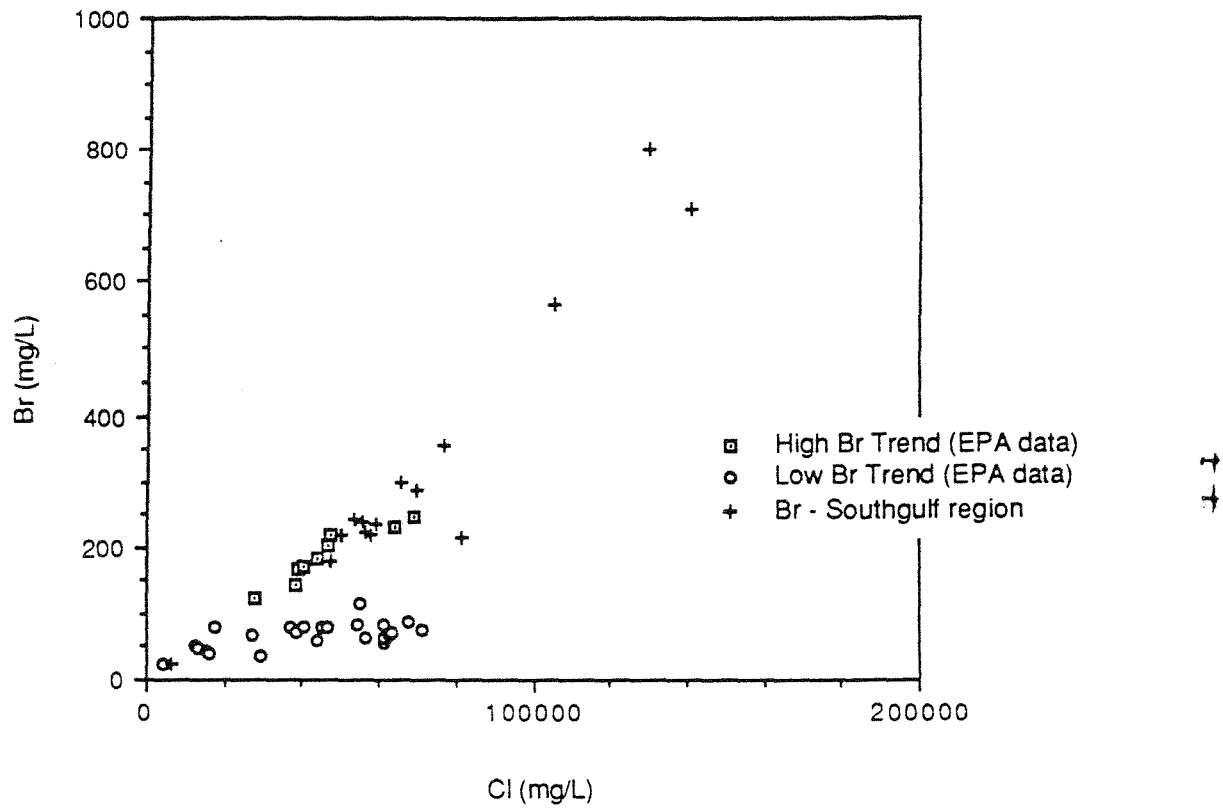


Figure 73. Br versus Cl for high Br trend and low Br trend based on EPA data (Table 3) and Southgulf region data (Table 2). Note linear increase of Br with Cl to very high Br concentrations.

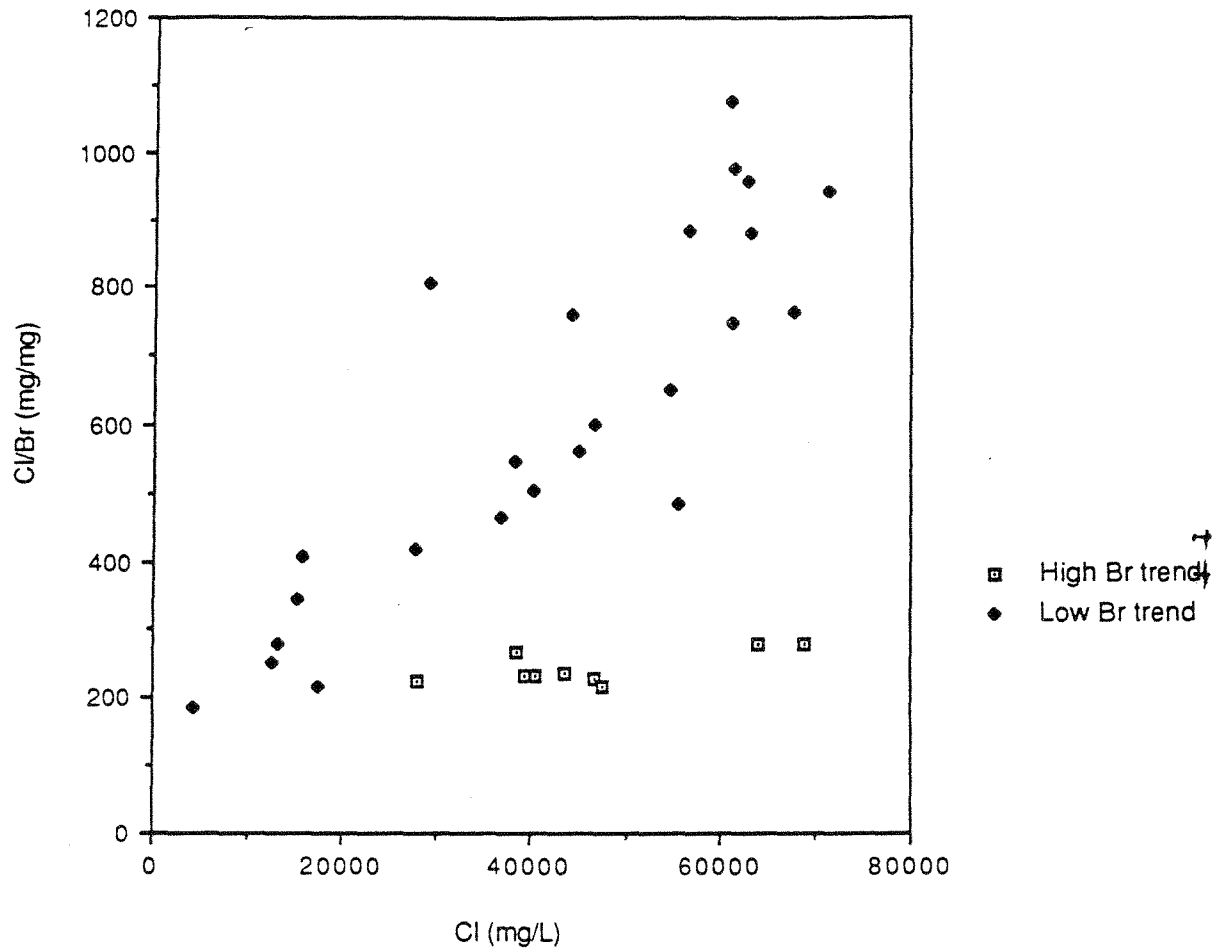


Figure 74. Plot of Cl/Br versus chloride, Frio Formation, from data collected for this study (Table 3).

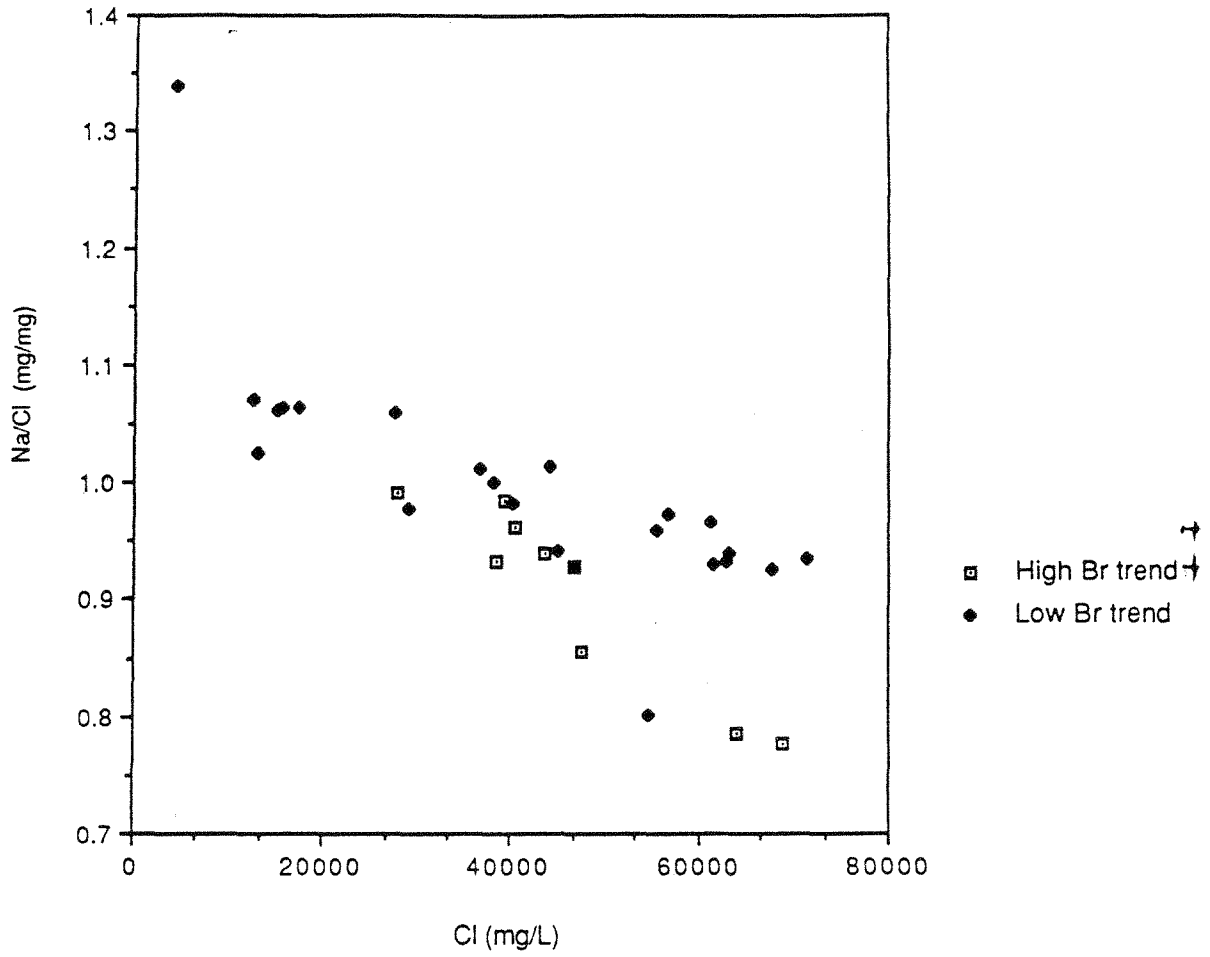


Figure 75. Na/Cl versus chloride, Frio Formation, from data collected for this study (Table 3).

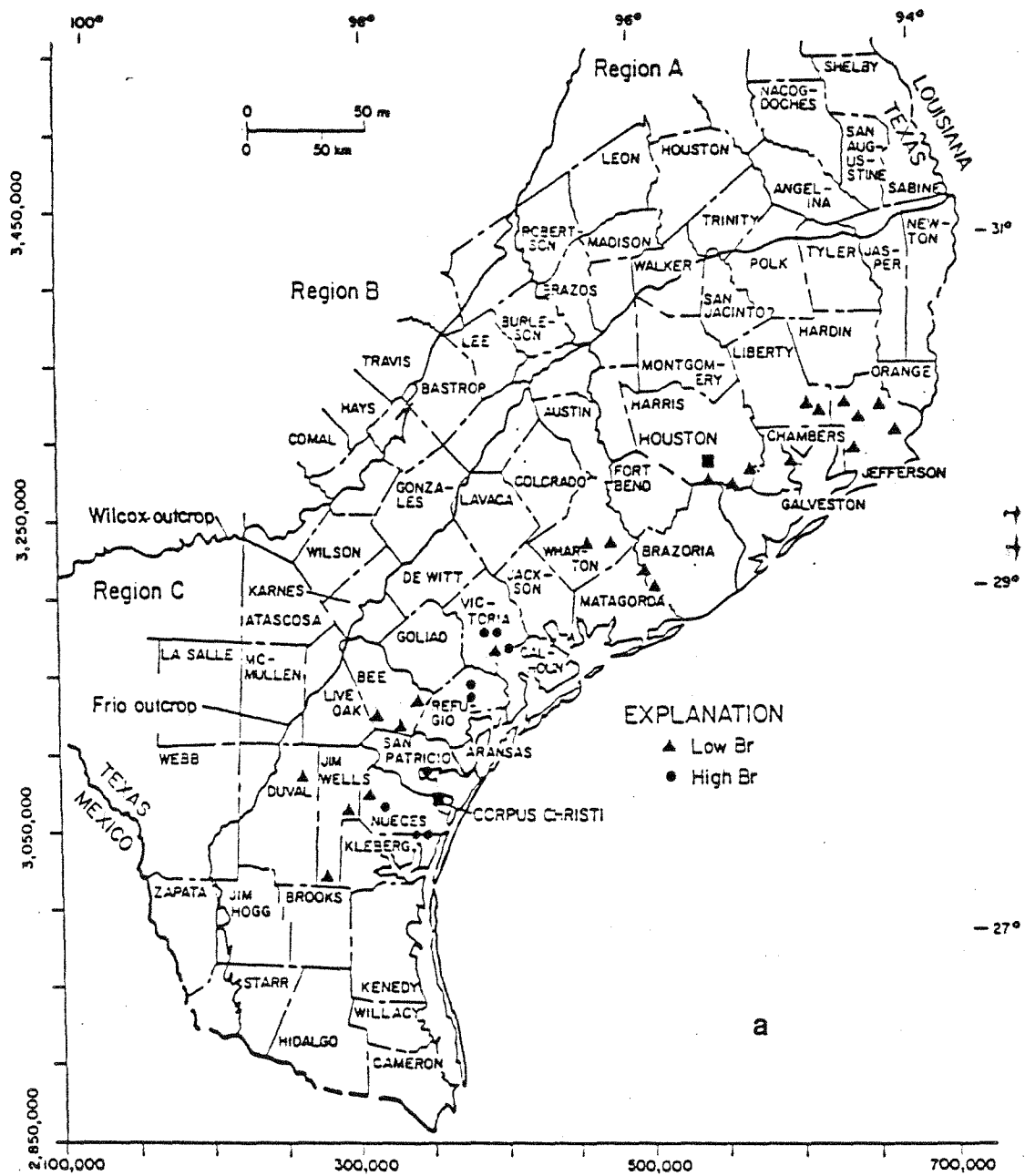


Figure 76. (a) Geographic distribution of the two different populations of data, Na-Cl, low-Br waters and Na-Cl, high Br waters, and (b) salt dome locations. Note the low-Br waters are predominantly in the Houston Embayment salt dome region. The low-Br waters in Duval, Jim Wells and Nueces Counties are near two salt domes in Duval County. Data from this study (Table 3).

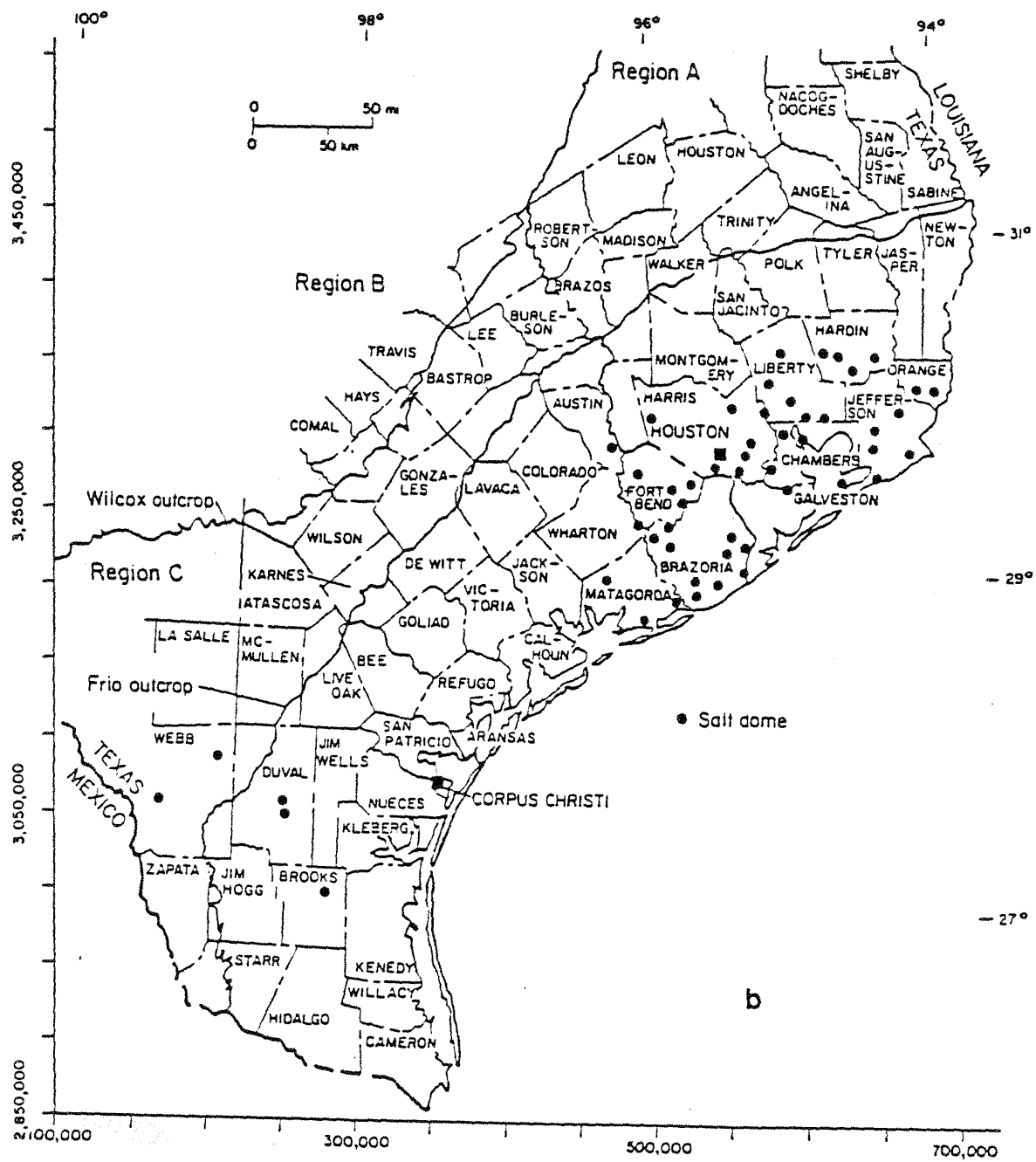


Figure 76 (continued)

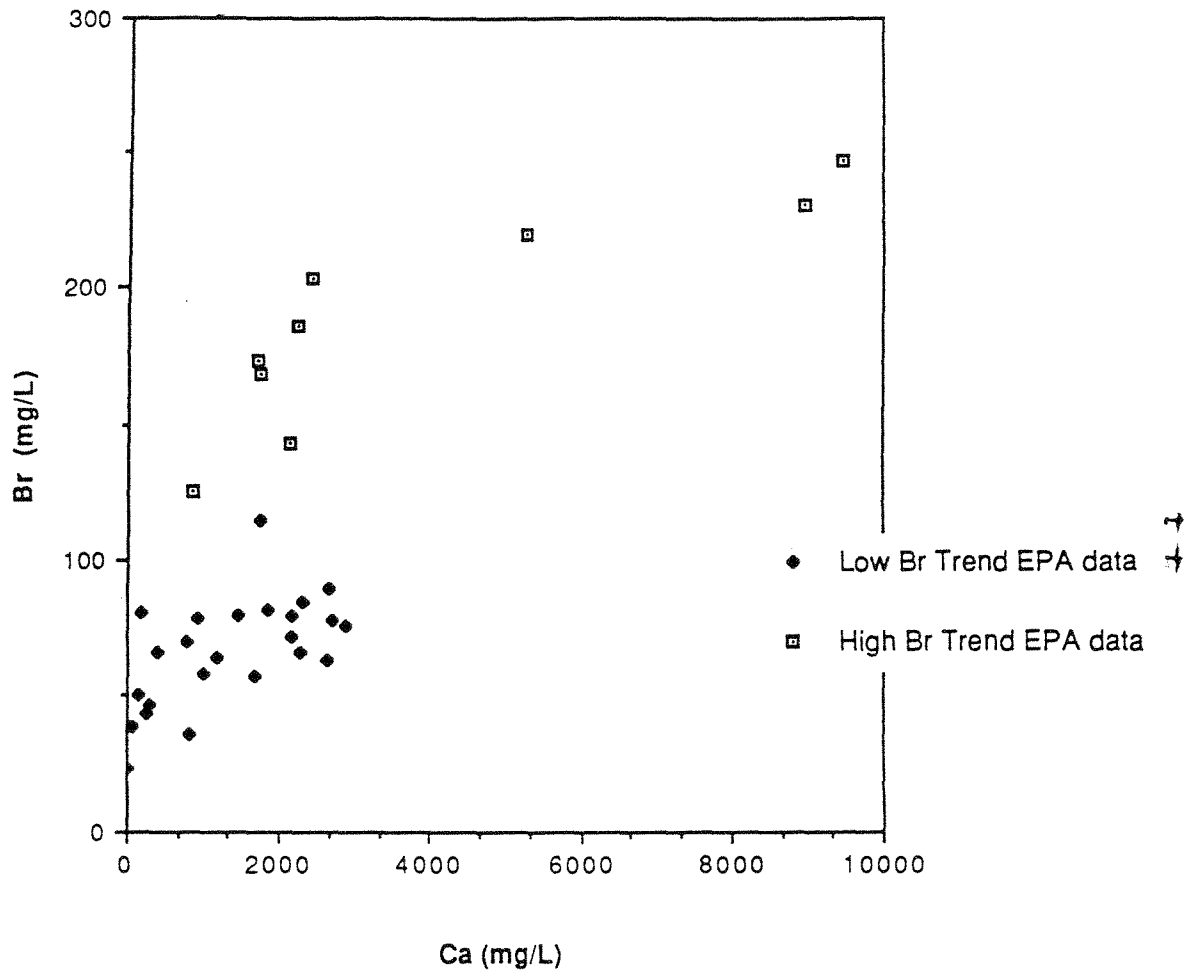


Figure 77. Plot of Br versus Ca or Frio Formation. Data from this study (Table3).

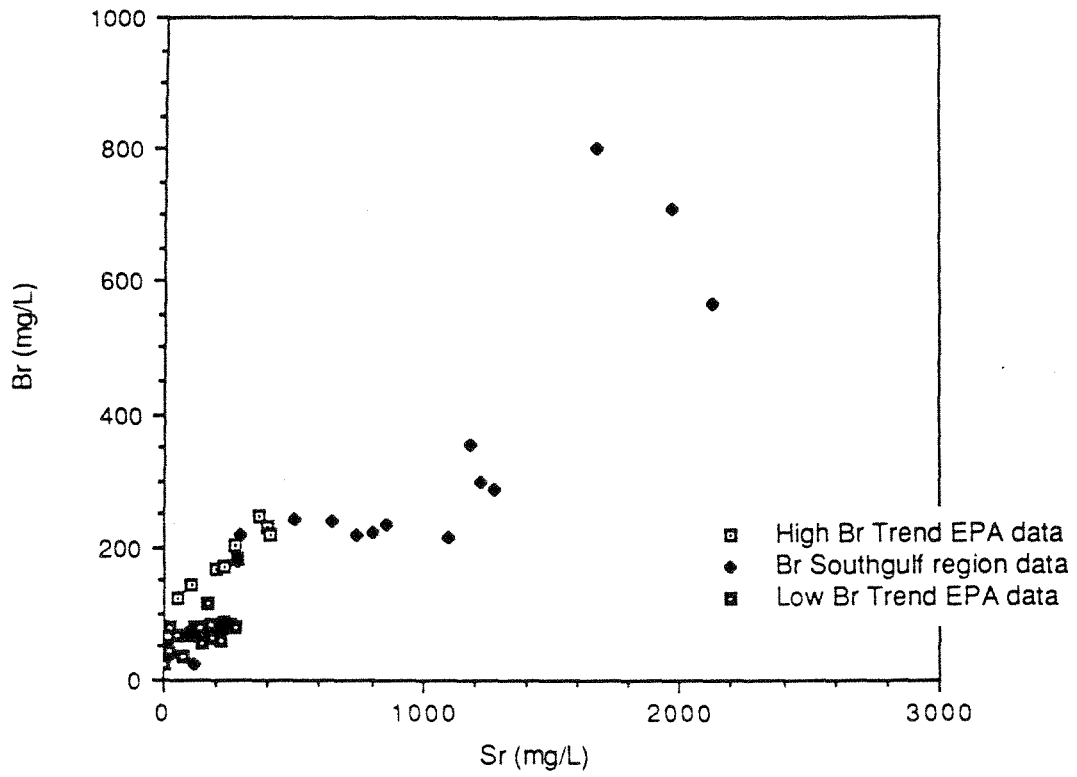


Figure 78. Plot of Br versus Sr. Data from this study (Table 3) and Southgulf region (Table 2).

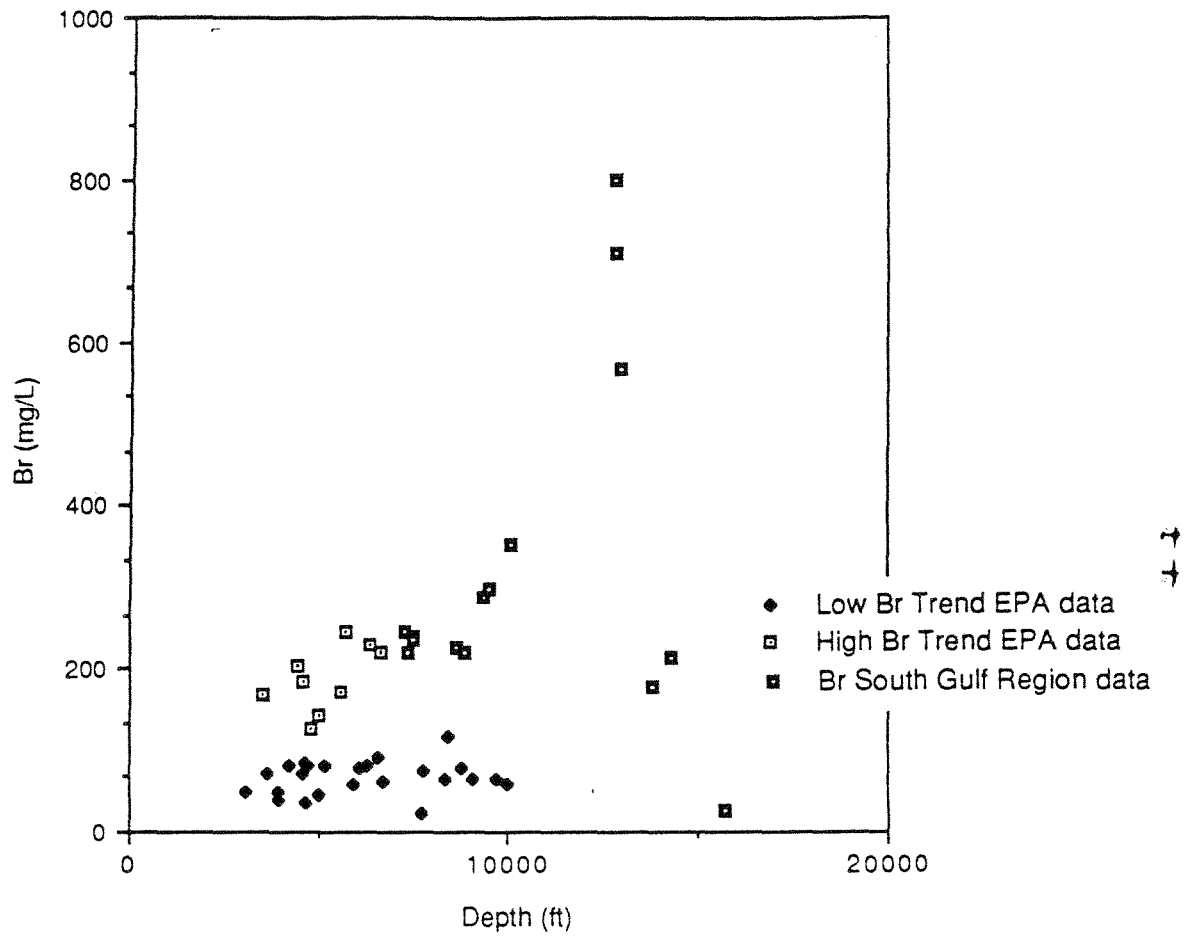


Figure 79. Plot of Br versus depth. Data from this study (Table 3) and Southgulf region (Table 2).

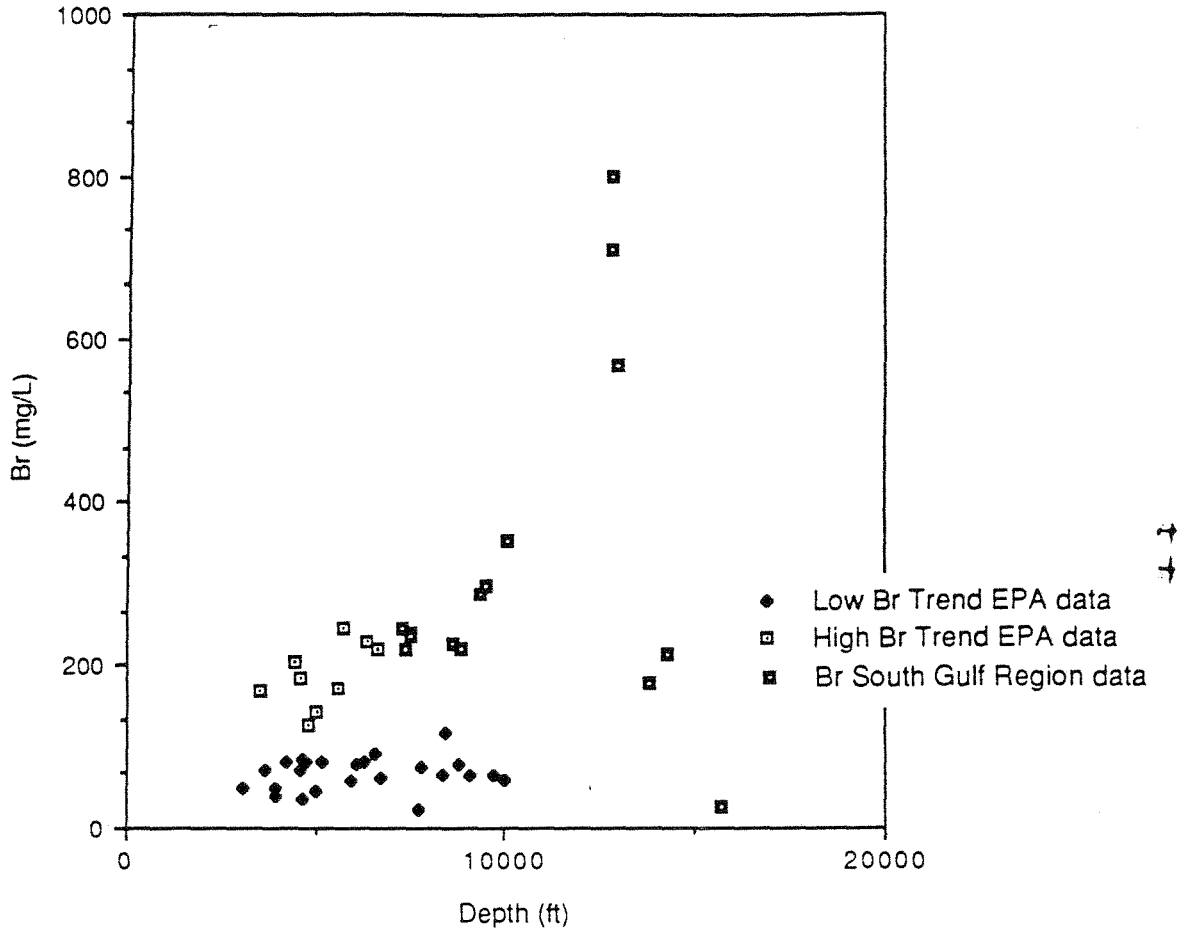


Figure 79. Plot of Br versus depth. Data from this study (Table 3) and Southgulf region (Table 2).

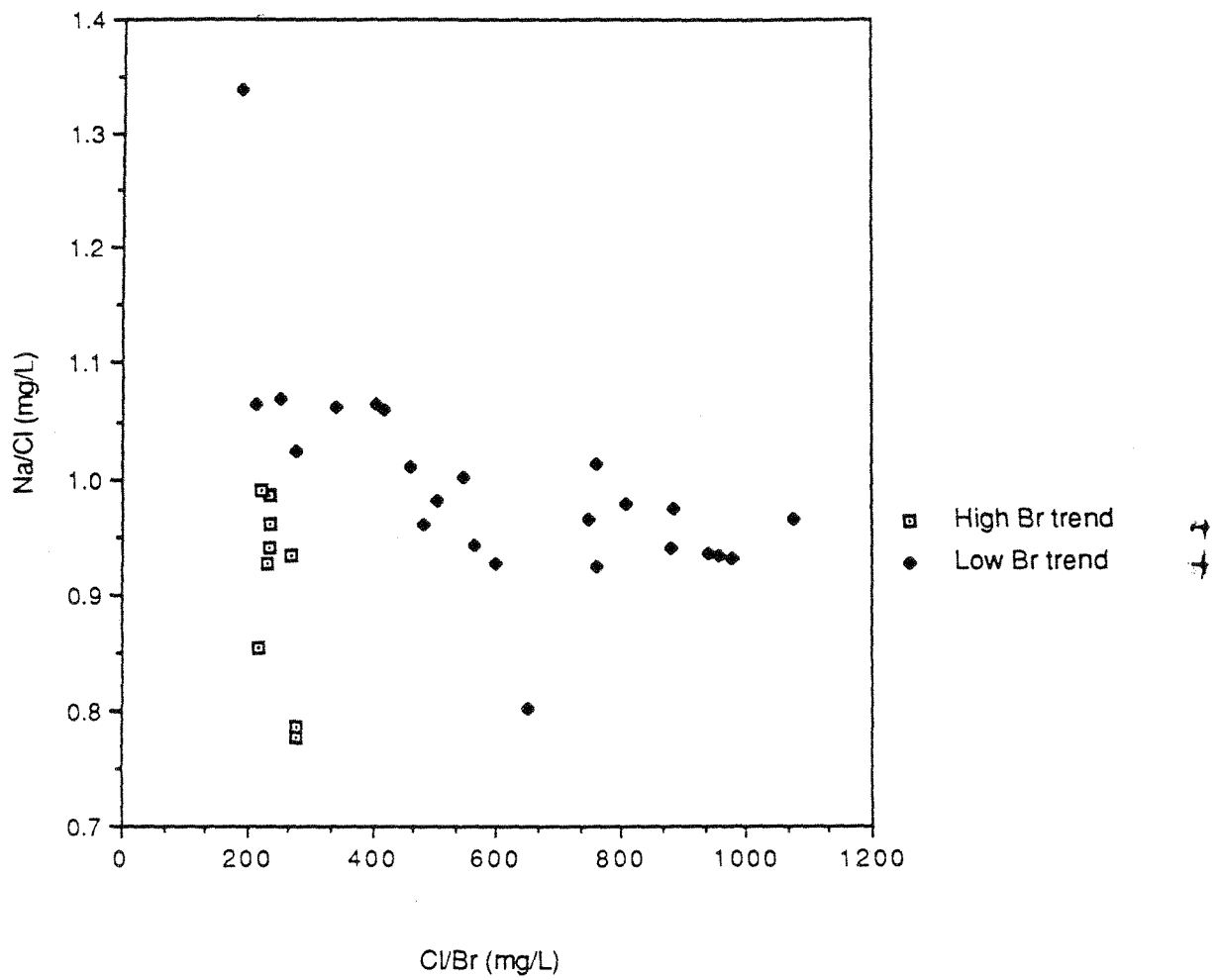


Figure 80. Plot of Na/Cl versus Cl/Br, Frio Formation. Data from this study (Table 3).

9.5 Alkalinity

Total field-titrated alkalinity is a qualitative estimate of the organic acids in deep formation waters (Carothers and Kharaka, 1980; Fisher, 1987; Morton and Land, 1987). A plot of total alkalinity versus organic alkalinity (fig. 81) shows two trends for the Frio: (1) organic acid concentration that increases linearly with total alkalinity, and (2) total alkalinity for samples with some total alkalinity but little or no organic acids. Trend 1 shows a linear relationship with approximately 50% of the total alkalinity attributable to organic acids. The data from Lundegard (1985) also follow this 1:1 molar slope (fig. 82). Most of the organic alkalinity is acetate with minor amounts of propionate and butyrate (fig. 83). The 1:1 molar ratio between organic alkalinity and inorganic alkalinity suggests that the inorganic alkalinity is integrally related to the organic acids. Carothers and Kharaka (1980) suggested that decarboxylation of acetate produces bicarbonate and methane. Light $\delta^{13}\text{C}$ of the bicarbonate of oil-field brines further substantiated the decarboxylation reaction. This 1:1 ratio of organic acids to bicarbonate suggests that this reaction is in equilibrium. →

Trend 2 data indicate trace to zero concentrations of organic acids for total alkalinity concentrations less than 800 mg/L. Carothers and Kharaka (1980) suggested that organic acid concentrations should be very low if not absent because of biodegradation of the acids in formations where temperatures were below 80°C. Data from this study suggest that the upper temperature for degradation is approximately 70°C (fig. 84), slightly lower than Carothers and Kharaka's estimate. As the organic acids degraded to CO_2 , they increased the total inorganic alkalinity by a similar amount. The high inorganic alkalinity of 900 ppm suggests that the organic acids up to 450 ppm may have been originally present but have been degraded. The degradation of 450 ppm organic acids suggests a healthy appetite for the bacteria as well as a significant CO_2 source (up to ~8 mmoles) for other diagenetic reactions. The complete loss of organic acids also indicates that more degradation could have occurred if there had been greater concentrations of the available organic acids. This biodegradation reaction of organic acids has important implications to deep-well injection of chemical wastes. It suggests that organic waste could be degraded biologically by naturally occurring bacteria within the formations with temperatures below 70°C. †

Redox Environment

Low sulfate concentrations and occurrence of organic acids and oil indicate a general reducing environment. Eh measurements were not made.

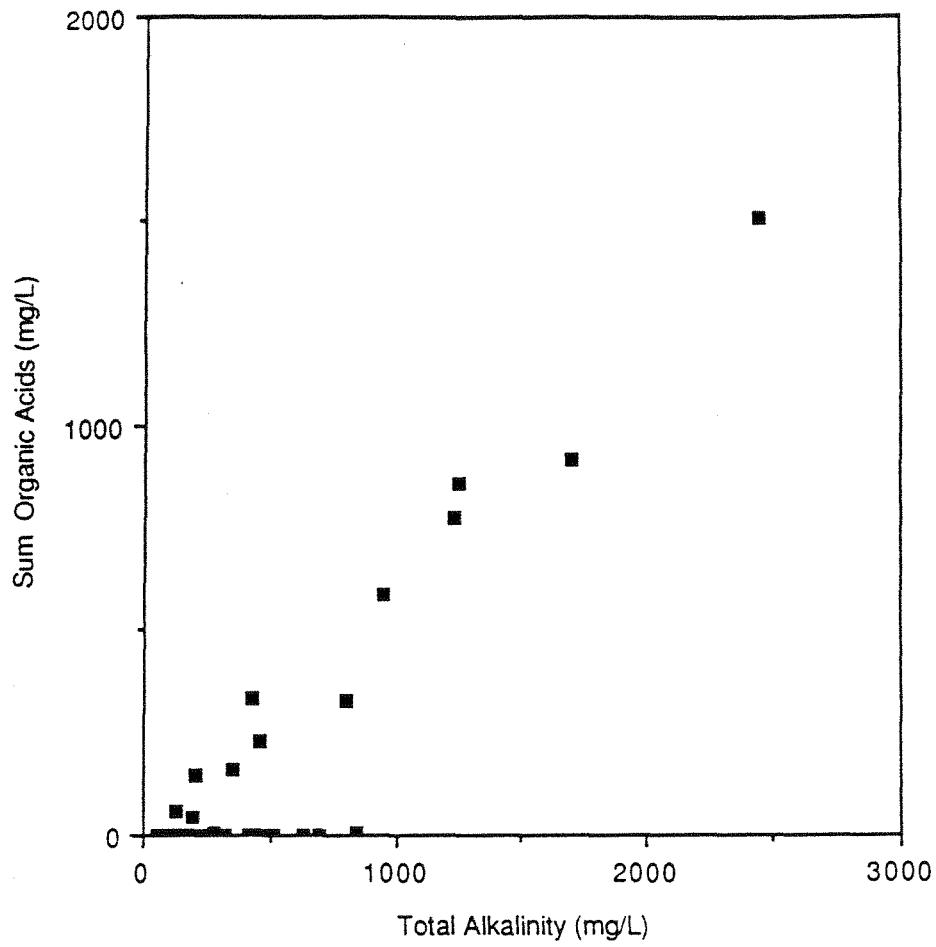


Figure 81. Plot of total field alkalinity versus sum of organic acids. Note the two different populations of data. Data from this study (Table 3).

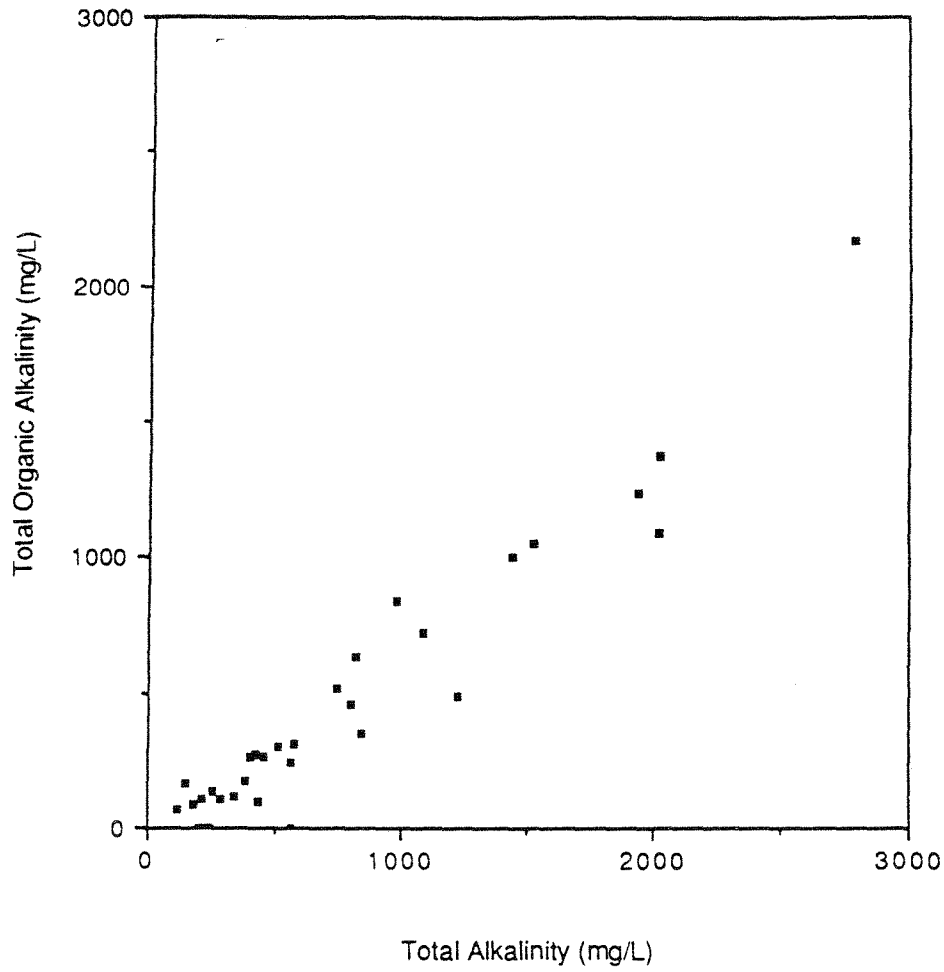


Figure 82. Plot of total field alkalinity versus sum of organic alkalinity from Lundegard (1985). Note how Lundegard's data follow the same trend as observed in Figure 17.

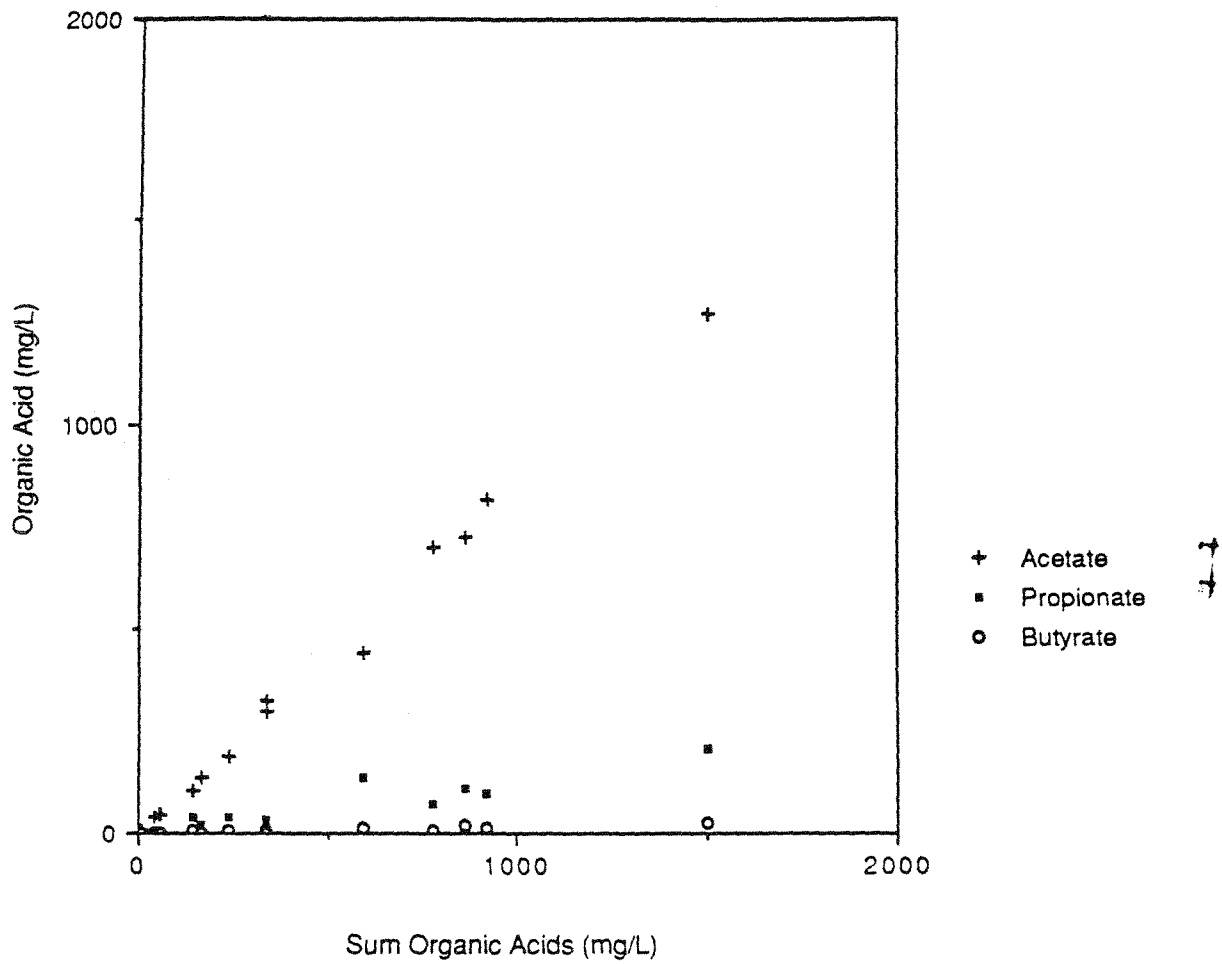


Figure 83. Plot of total alkalinity versus the individual organic acids, acetate, propionate and butyrate. The organic acids are composed predominantly of acetate.

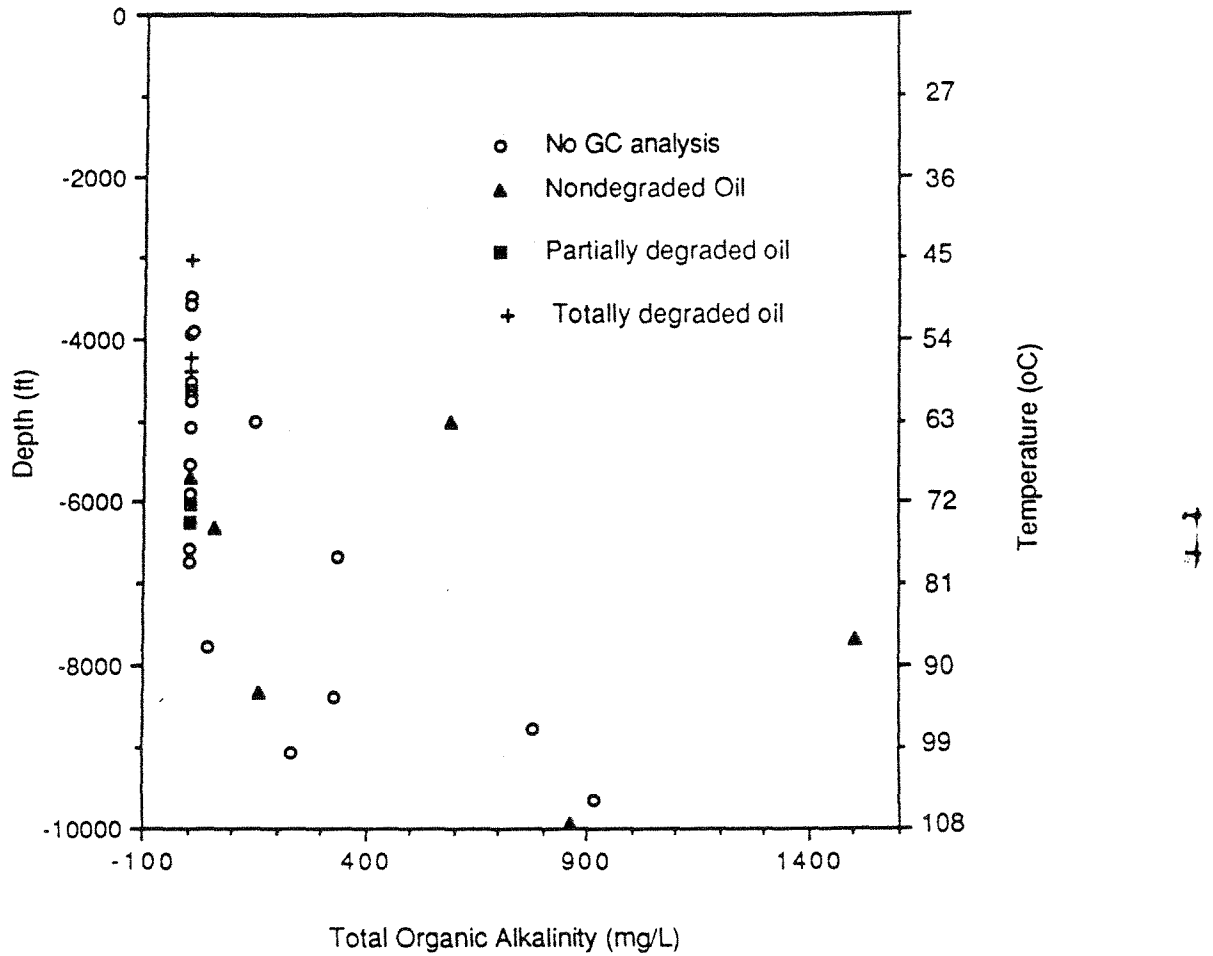


Figure 84. Total organic acids versus depth. All samples with degraded and partially degraded oils contain no organic acids.

9.6 Gas Chromatographic Analysis of Oil

The high concentrations of inorganic alkalinity and zero to trace organic acids could also represent deep penetration of meteoric waters and not the product of biodegradation. Kreitler and Wuerch (1981) observed HCO_3 concentrations as high as 1,000 mg/L in the fresh-water section of the Wilcox Formation in East Texas. A second approach to further test this hypothesis of biodegradation reaction is gas chromatograph analysis of whole oils associated with these waters. Eleven whole oils were analyzed by gas chromatograph to determine whether there was evidence of biodegradation. Nearly all organic compounds in crude oil are susceptible to biodegradation. The normal paraffins degrade before the isoprenoids or naphthalenes. The paraffins between C5-C10 are the most susceptible (Bailey and others, 1973b). Milner and others (1977) suggest that C12 and C13 are the most susceptible. Another test for degradation is the ratio of NC17 to IP19. Degraded oils will show the loss of the NC17 peak in comparison to the IP19 peak (Zvi Sofer, personal communication, 1988). Samples 15, 16, 17, 26, 29, and 31 (figs. 85 through 90) do not appear to be degraded. They contain high concentrations of the normal paraffins (NC) and the isoprenoids (IP), which appear to dominate the composition of these oils. Samples 3, 11, and 12 exhibit significant biodegradation (figs. 91 through 93) with the loss of nearly all organic compounds. Samples 1 and 34 (figs. 94 and 95) appear to exhibit less degradation, not because of the loss of the heavy paraffins (greater than NC15) but because of the loss of the light paraffins (C5-C13). These interpretations of biodegradation are qualitative, because of the variables that control the basic distributions of the organics in crude oil. The composition of the unaltered oils is affected by source, maturation processes, and migration, all of which may alter the concentrations of the different organic compounds. Water washing may also alter the oil (LaFargue and Barker, 1988). Ground water flowing through an oil field may dissolve some of the more soluble compounds and chemically change the unaltered oil. Water washing may also occur concomitantly with biodegradation, because the flowing ground water may be carrying the bacteria for biodegradation. Precise identification of biodegradation is difficult because of these factors. Even though these interpretations should be considered preliminary, there has been a significant change in gas chromatograph pattern of samples 1, 3, 11, 12, and 34 (figs. 91 through 95) in comparison to the gas chromatograph traces for the unaltered oils, and therefore are considered to be biodegraded.

There is also a correlation between the biodegraded oil and the concentration of short-chained organic acids (fig. 84). None of the water samples with strongly or

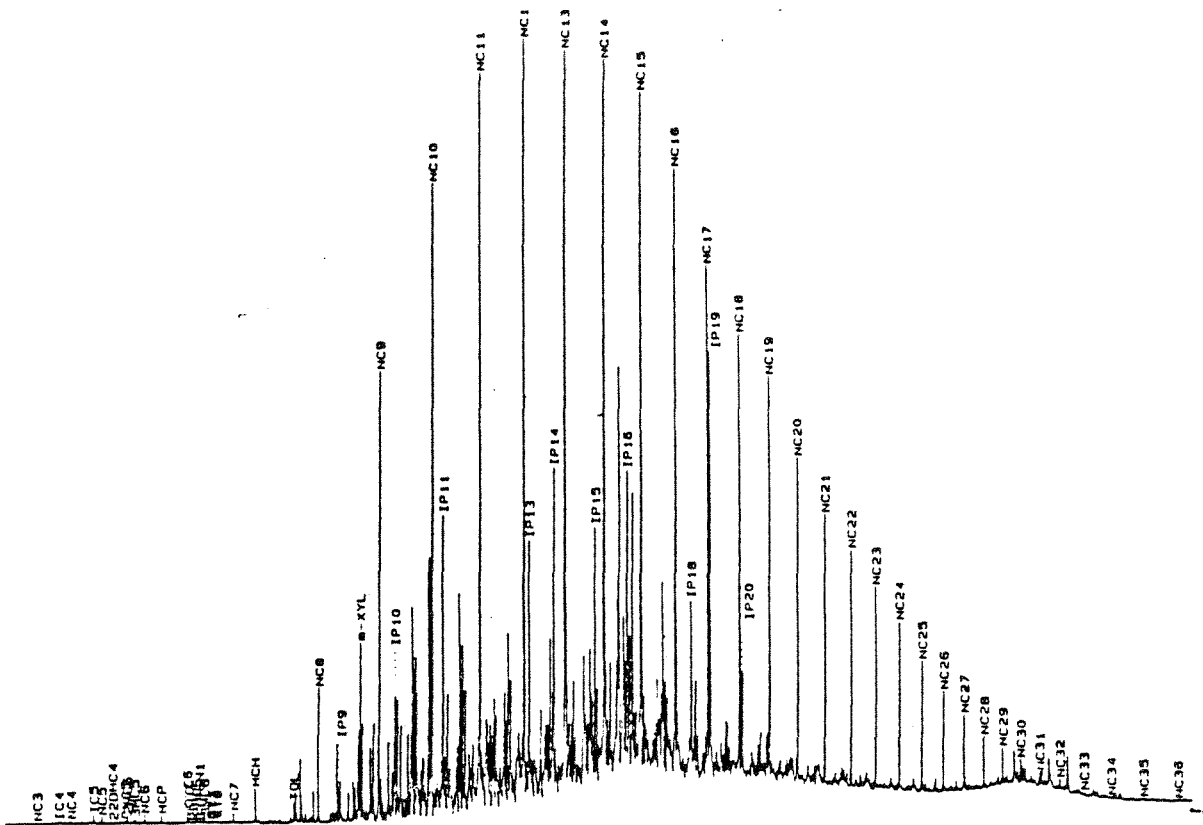


Figure 85. Gas chromatograph trace of whole oil sample TBEG-15. Sample does not appear to be degraded. Sample depth is 5,000 ft.

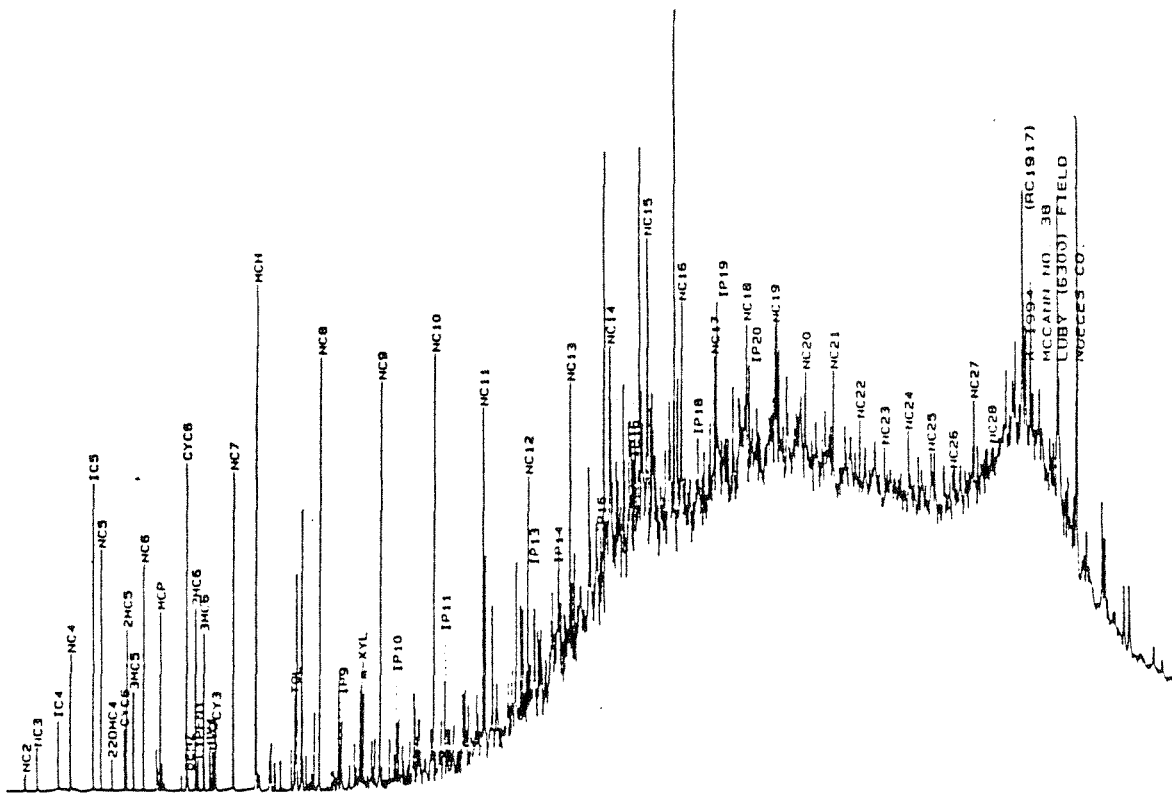


Figure 86. Gas chromatograph trace of whole oil sample TBEG-16. Sample does not appear to be degraded. Sample depth is 6,304 ft.

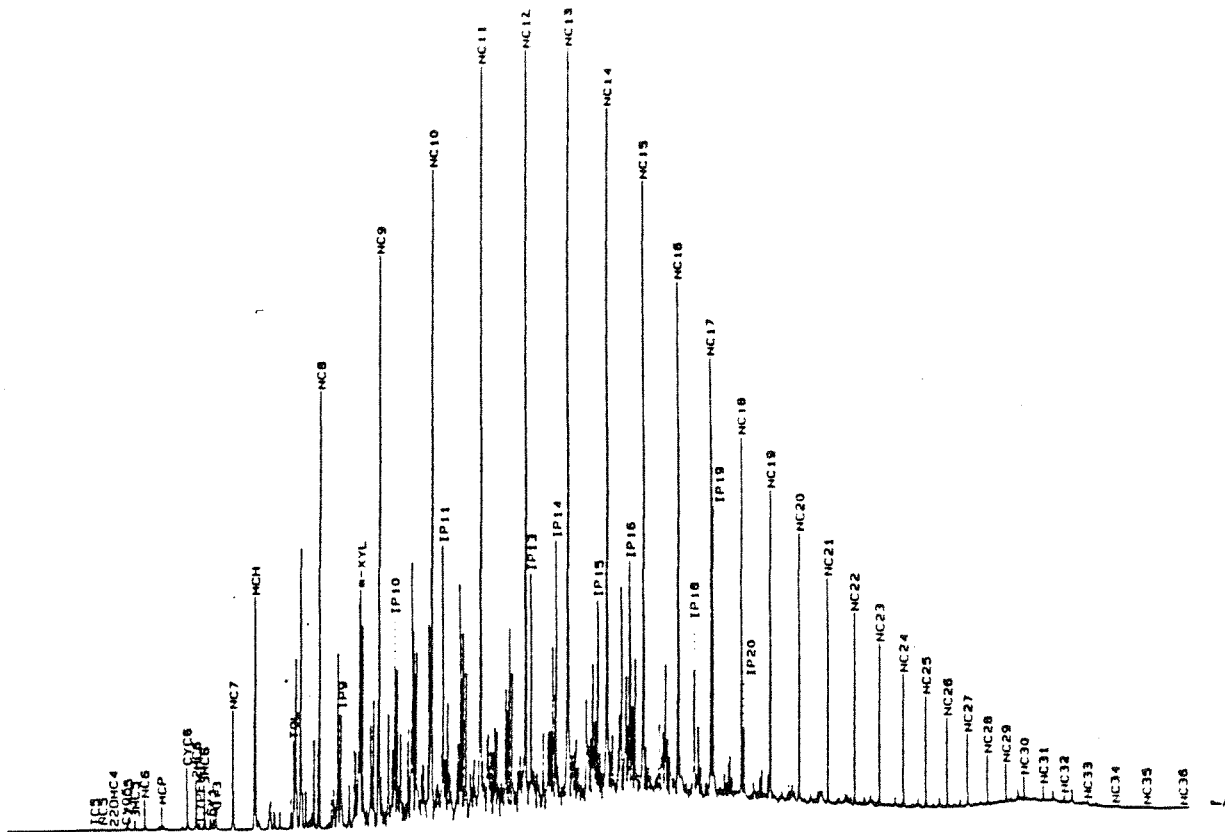


Figure 87. Gas chromatograph trace of whole oil sample TBEG-17. Sample does not appear to be degraded. Sample depth is 5,700 ft.

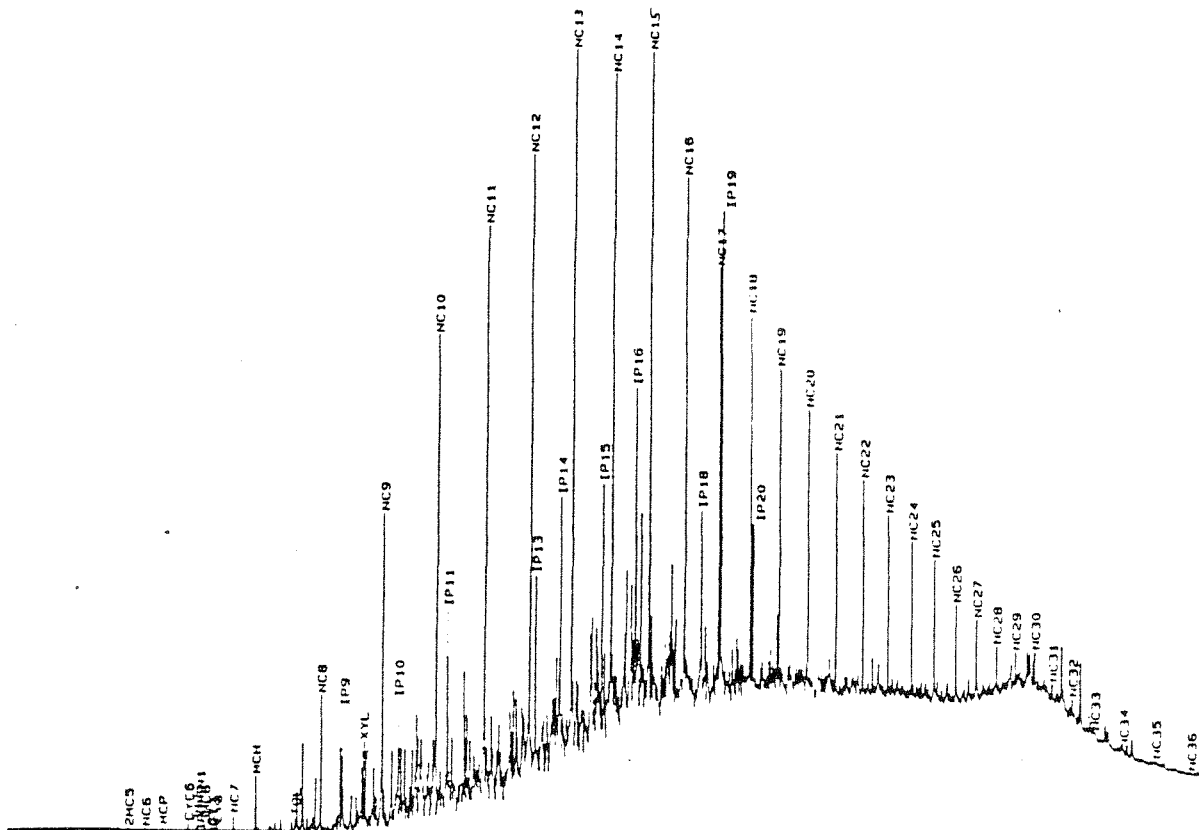


Figure 88. Gas chromatograph trace of whole oil sample TBEG-26. Sample does not appear to be degraded. Sample depth is 8,310 ft.

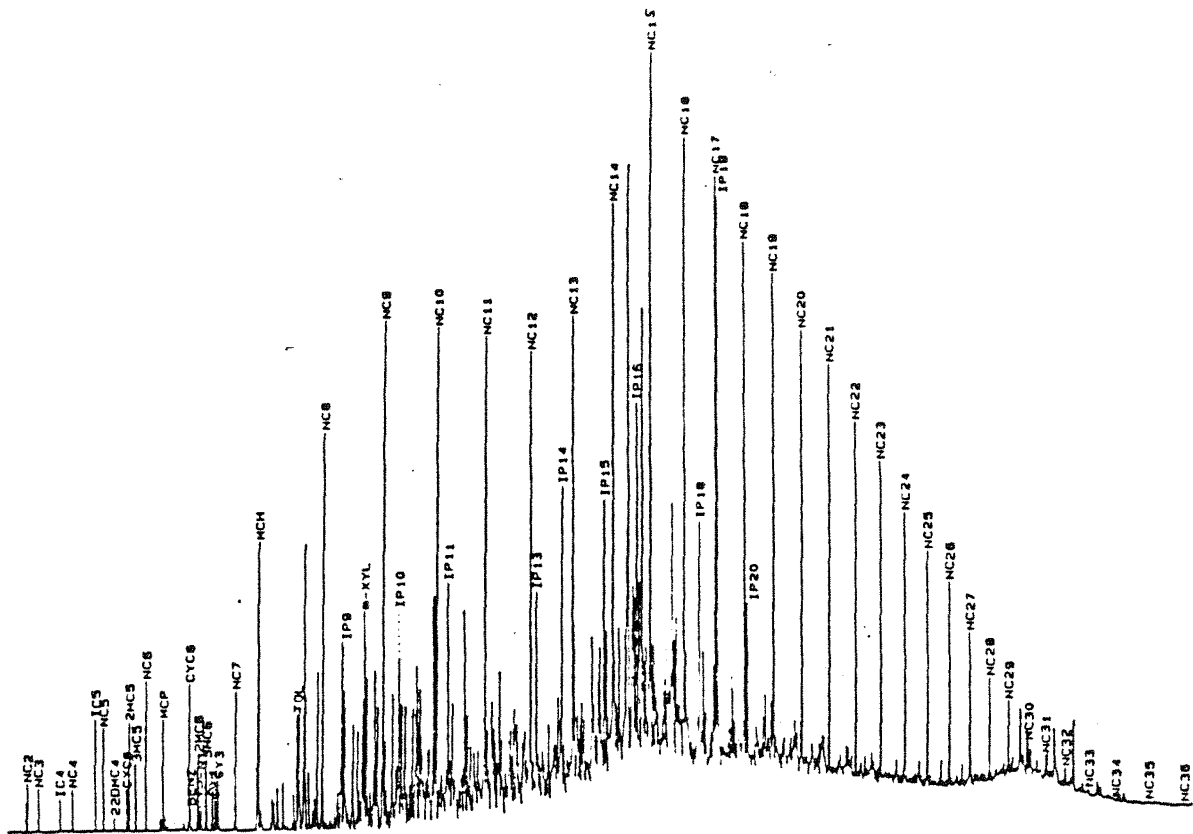


Figure 89. Gas chromatograph trace of whole oil sample TBEG-29. Sample does not appear to be degraded. Sample depth is 7,666 ft.

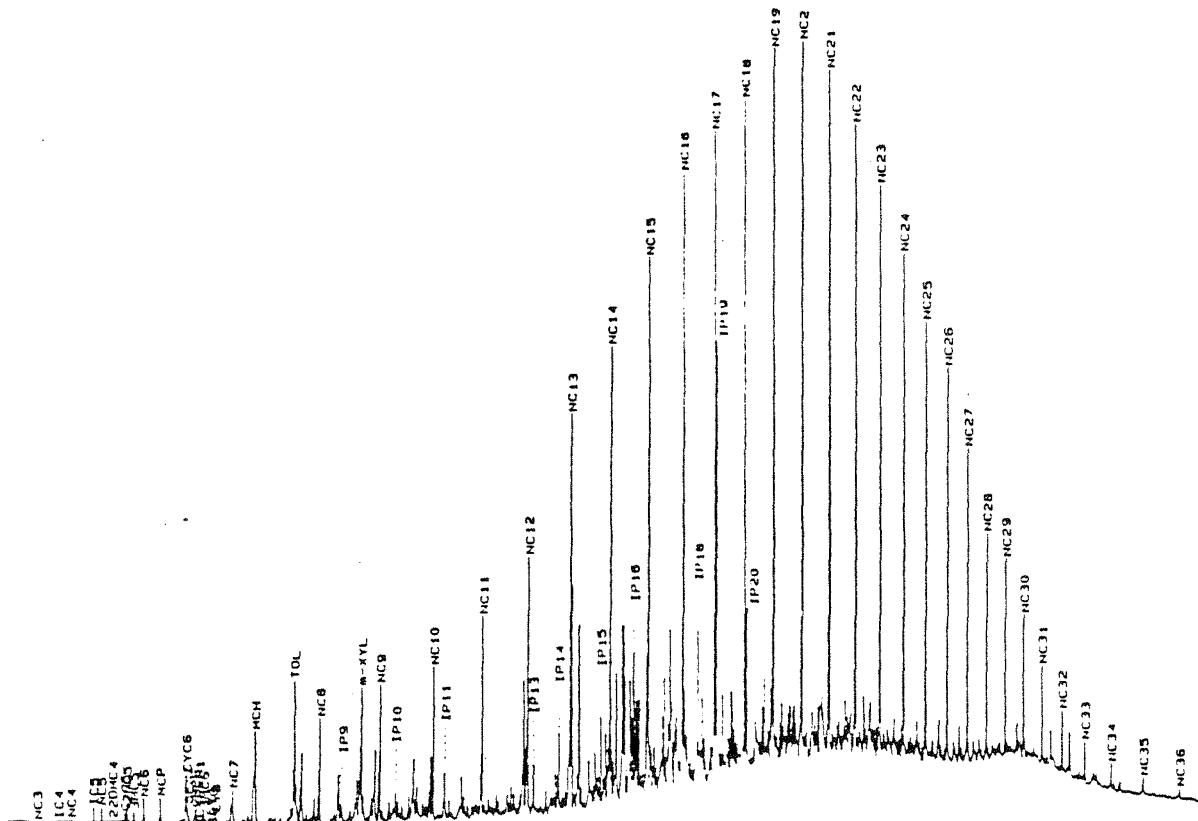


Figure 90. Gas chromatograph trace of whole oil sample TBEG-31. Sample does not appear to be degraded. Sample depth is 9,950 ft.

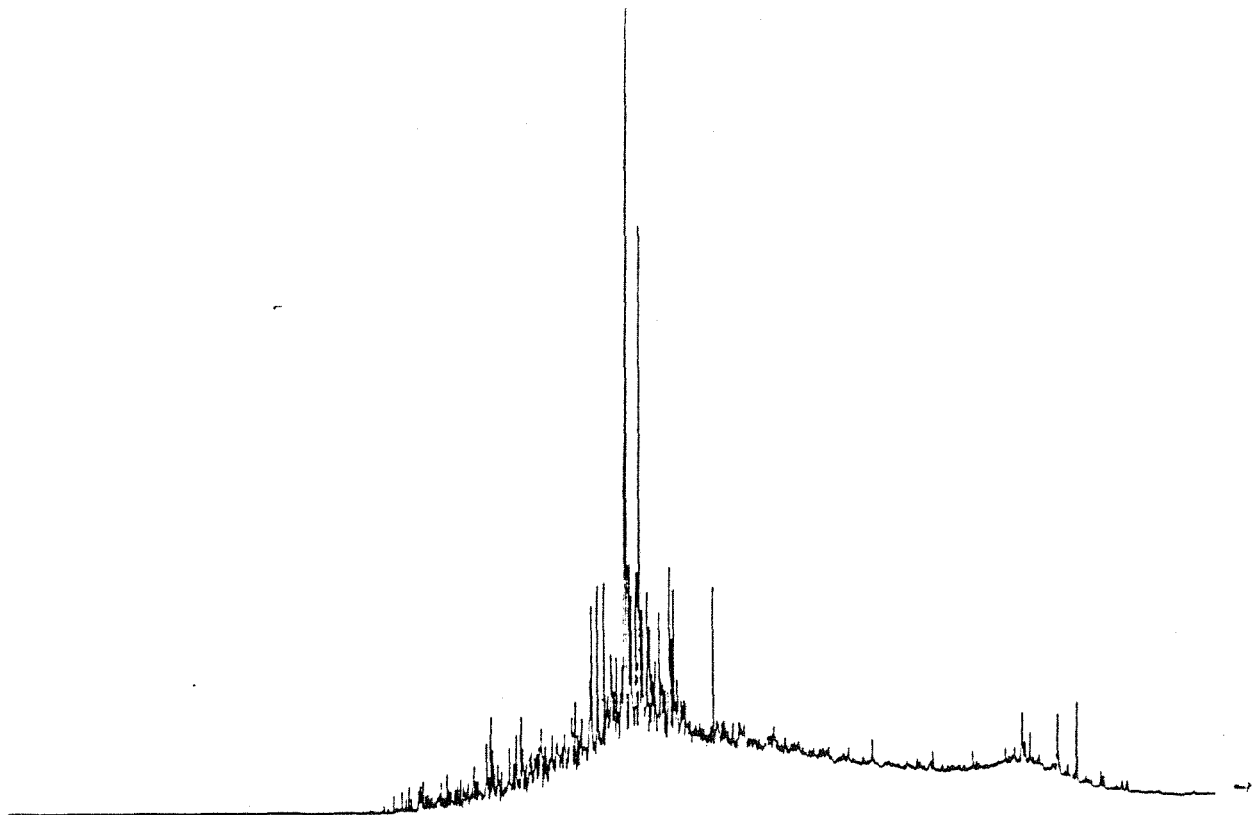


Figure 91. Gas chromatograph trace of whole oil sample TBEG-3. Sample appears to be significantly degraded. Sample depth is 4,222-4,226 ft.

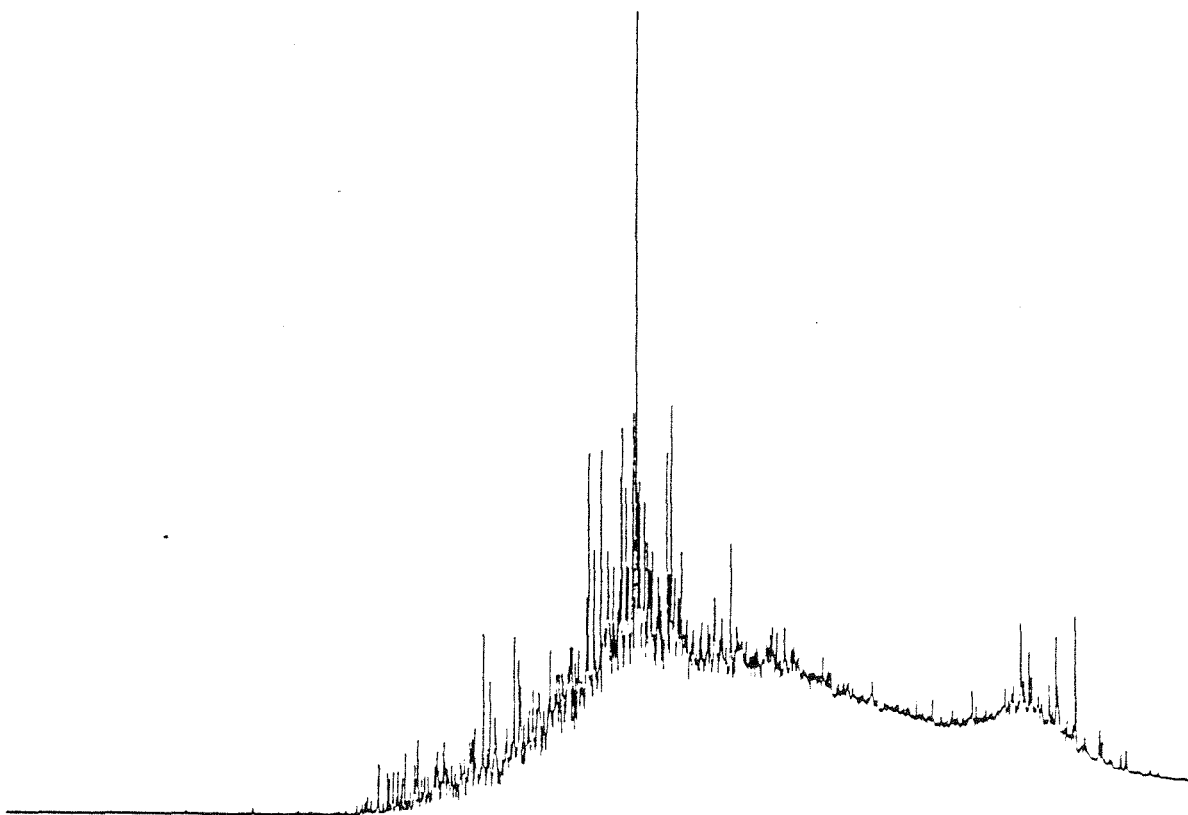


Figure 92. Gas chromatograph trace of whole oil sample TBEG-11. Sample appears to be significantly degraded. Sample depth is 4,388 ft.

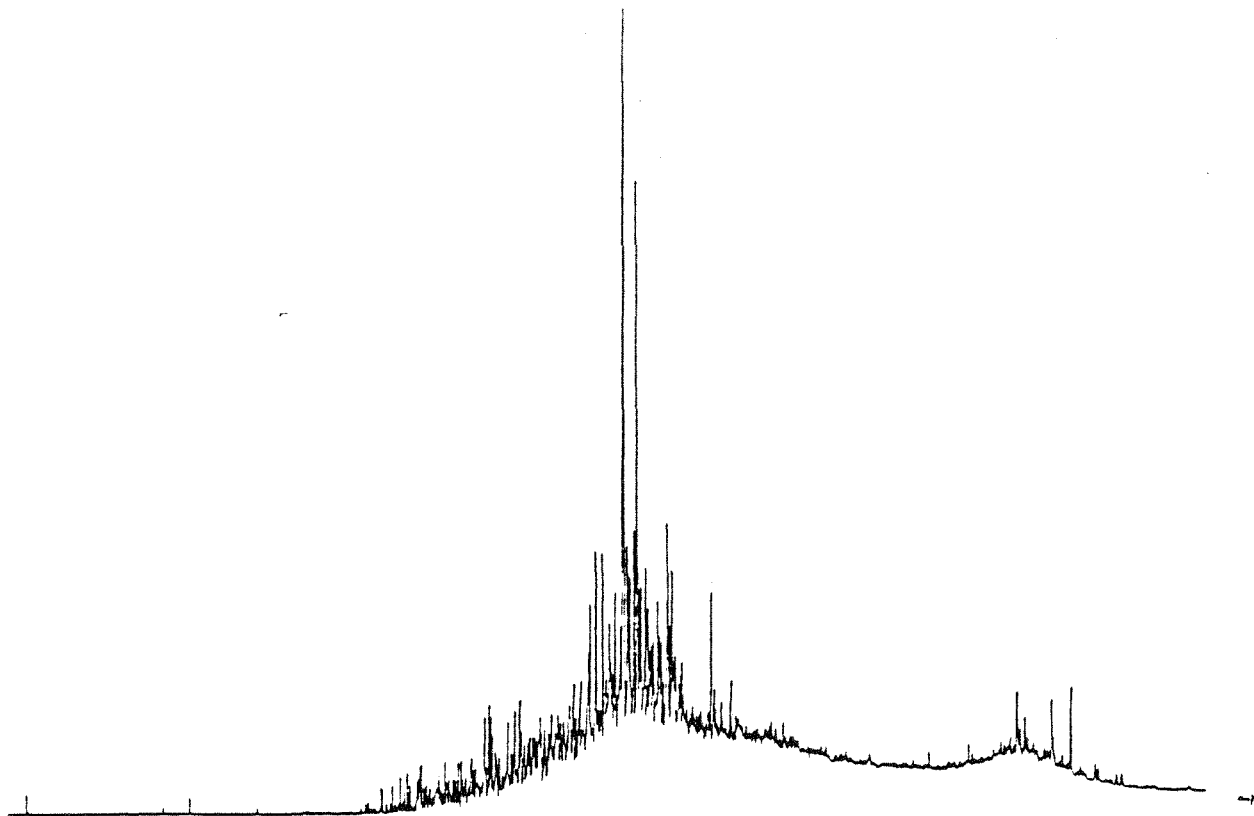


Figure 93. Gas chromatograph trace of whole oil sample TBEG-12. Sample appears to be significantly degraded. Sample depth is 3,040 ft.

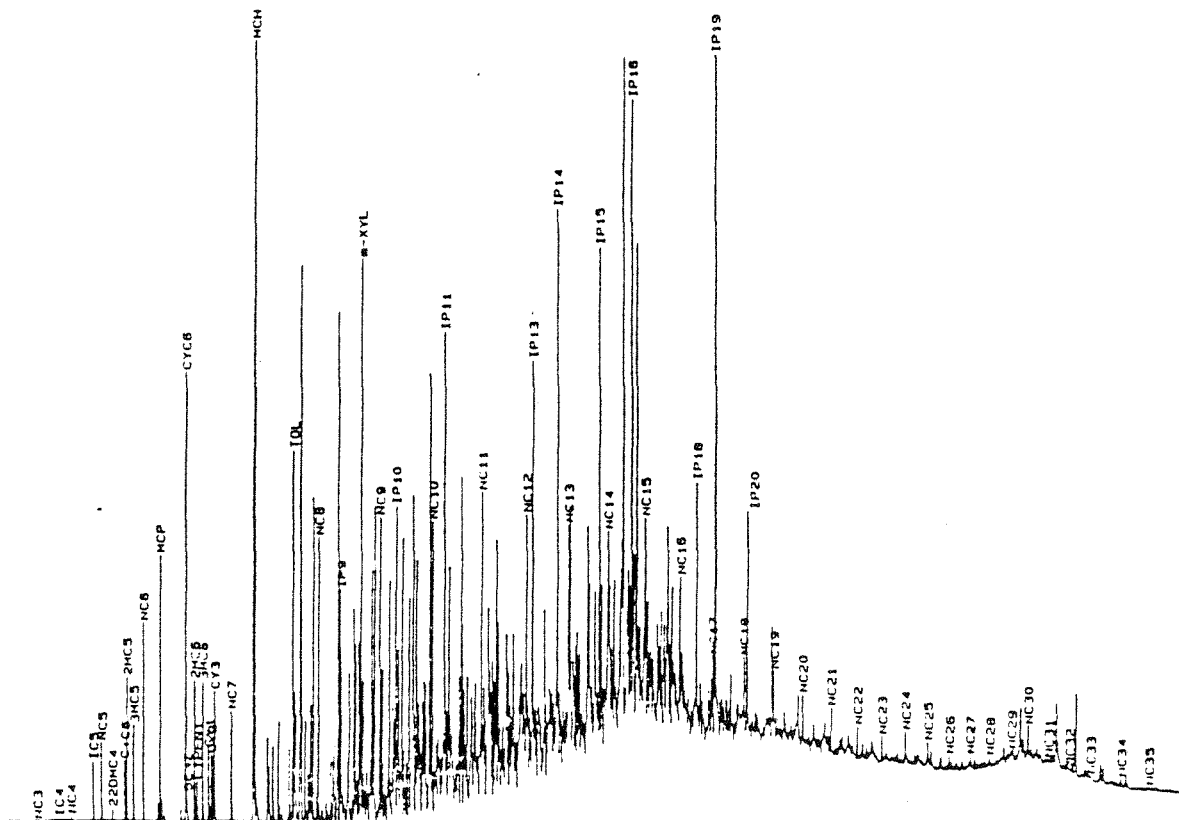


Figure 94. Gas chromatograph trace of whole oil sample TBEG-1. Sample appears to be degraded but less than samples TBEG-3, 11, or 12. Sample depth is 6,019-6,023 ft.

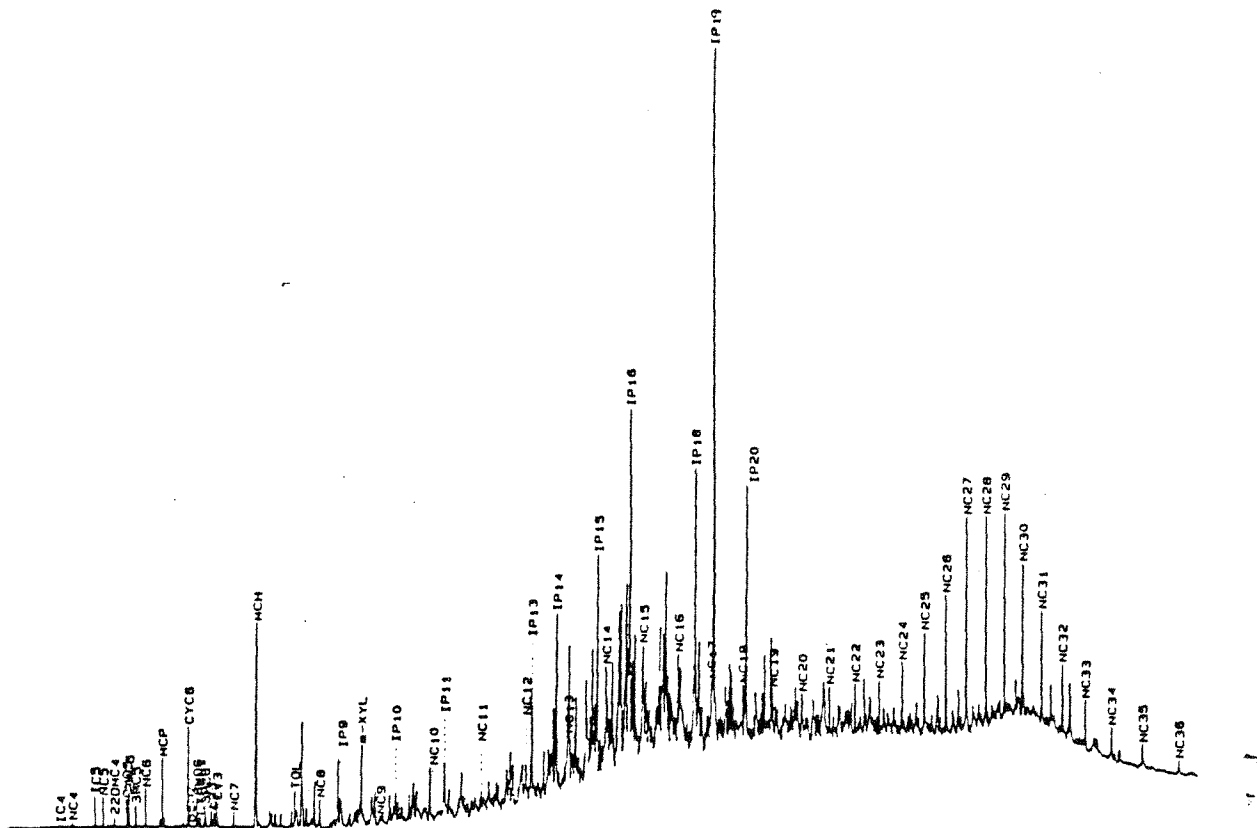


Figure 95. Gas chromatograph trace of whole oil sample TBEG-34. Sample appears to be degraded but less degraded than samples TBEG-3, 11, or 12. Sample depth is 6,244 ft.

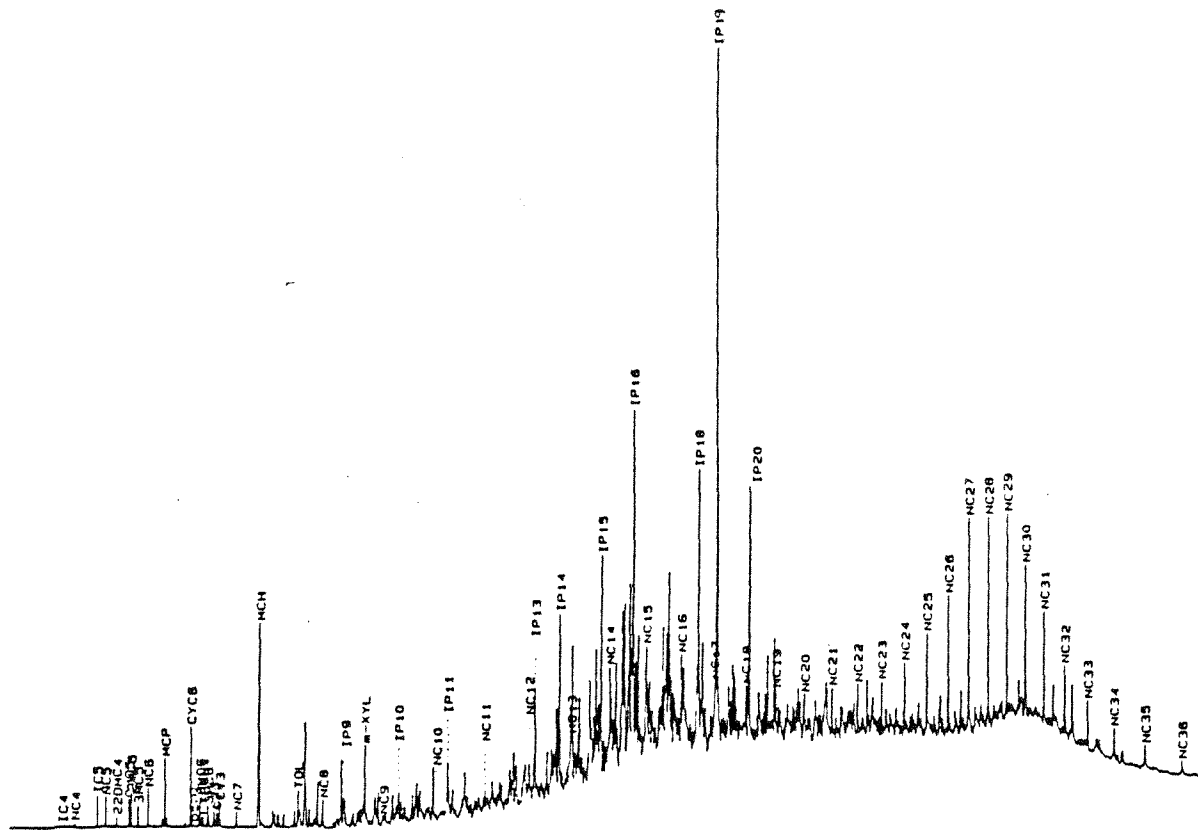


Figure 95. Gas chromatograph trace of whole oil sample TBEG-34. Sample appears to be degraded but less degraded than samples TBEG-3, 11, or 12. Sample depth is 6,244 ft.

partially degraded oils (1, 3, 11, 12, and 34) (figs. 91, 92, 93 and 94, respectively) had measurable organic acids. Conversely, five of the six nondegraded oils had appreciable organic acid concentrations. (Sample 17, a nondegraded oil, contained no organic acids.)

The API gravities of the totally degraded oils were 24 or less. Nondegraded oils ranged from 23 to 31, and the partially degraded oil ranged from 26 to 31. The API number of an oil does not appear to be a reliable indicator of biodegradation.

Presence of degraded oil and absence of short-chained organic acids appear to be good geochemical indicators of biologic activity at depths shallower than 7,000 ft and temperatures lower than 70-80°C. The good correlation between zero to trace concentrations of organic acids and degraded oil indicates that the organic acids had probably been there originally and had been subsequently degraded. An alternate hypothesis, that the organic acids were never present and that the field alkalinity represents high bicarbonate in meteoric water, is considered to be incorrect. Another important question is whether biodegradation is still occurring or whether it represents a geologically dead process. The occurrence of both degraded oil and zero organic acid concentrations suggests that the degradation process occurred after oil migration. This assumes that the occurrence of oil and organic acids followed two separate geochemical pathways. The coincidence of two degradation products indicates that the reactions occurred in situ. The potential for biodegradation may still be present. Oil degradation also indicates that these subsurface organisms are capable of consuming organic compounds far more complex than simple organic acids such as acetate. If the degradation of organic compounds is occurring biotically (rather than abiotically) then the degradation reactions may be occurring almost instantaneously in the context of geologic time. Bailey and others (1973) showed experimentally that biotically-driven degradation of hydrocarbons occurred within weeks. These hypotheses have significant implications to the possibility of biologic degradation of chemical wastes disposed of by deep-well injection.

9.7 Estimated In-Situ pH

The pH of deep basinal brines has always been considered unreliable because of CO₂ degassing as the sample depressurizes when it comes up the well bore or comes in contact with the atmosphere. The loss of CO₂ shifts the pH to more basic values. Neutral to basic pH values were measured for all samples indicating degassing (fig. 96). This degassing, however, does not cause a significant loss of inorganic alkalinity in the samples. The previous discussion on organic acids

demonstrated that 50% of the field titrated total alkalinity represents the in situ concentration of inorganic alkalinity. The consistency of the slope of total alkalinity versus sum of the organic acids (figs. 81 and 82) indicates that the samples are not losing significant quantities of inorganic alkalinity by CO_2 degassing either as the water flows from the well or where water is stored in separator tanks. An in situ pH in the range of 5-6 can also be estimated from the alkalinity titration data. A plot of pH versus inorganic alkalinity (fig. 96) shows a general trend of increasing pH with increasing concentrations of inorganic alkalinity. This degassing permits an estimate of in situ pH. This linear trend of higher pH for higher alkalinities results because the higher alkalinities have higher initial CO_2 pressures and therefore undergo greater degassing when these waters come in contact with the lower partial pressure of CO_2 in the atmosphere. The greater the degassing, the greater the shift toward more basic pH. Assuming that subsurface Frio conditions are acidic, then the inorganic CO_2 species will be in the carbonic acid form, and HCO_3^- concentrations (total inorganic alkalinity) should be very low. The pH of zero bicarbonate value should approximate the in situ value (fig. 96). An in situ pH of 5-6 is estimated. (This approximation does not account for pH shifts and changes in carbonate equalization associated with the higher temperatures of in situ conditions at depth.)

9.8 Oxygen and Hydrogen Isotopes

Oxygen and hydrogen isotopes for 32 samples collected for this study plus 14 analyses provided by L. S. Land (personal communication, 1987) are shown in figures 97 through 99 and table 5. Most surface water, ground water, and precipitation worldwide have hydrogen and oxygen isotope compositions that plot approximately on a single line, referred to as the global meteoric water line (fig. 97) (Craig, 1961). Sedimentary basin waters typically trend away from that line toward heavier oxygen and hydrogen isotope values because of isotopic reactions between the water and sediments (Clayton and others, 1966). If deep-basinal brines have isotopic compositions similar to the isotopic composition of shallow, low-TDS ground waters, then there is a hydrologic connection between the shallow and the deep system, and the lack of isotopic enrichment suggests that this recharge process is relatively recent (in the context of geologic time). A plot of $\delta^{18}\text{O}$ versus $\delta^2\text{H}$ for Frio waters (fig. 97) shows a general trend of isotopic enrichment for $\delta^{18}\text{O}$ away from the meteoric water line. The trend appears to be controlled by isotopic fractionation of the water with the sediments. The amount of fractionation of the oxygen increases with increasing temperature. A plot of $\delta^{18}\text{O}$ versus depth (fig. 98) shows an enrichment of $\delta^{18}\text{O}$ with depth (and therefore temperature). An increase in $\delta^{18}\text{O}$ is expected for

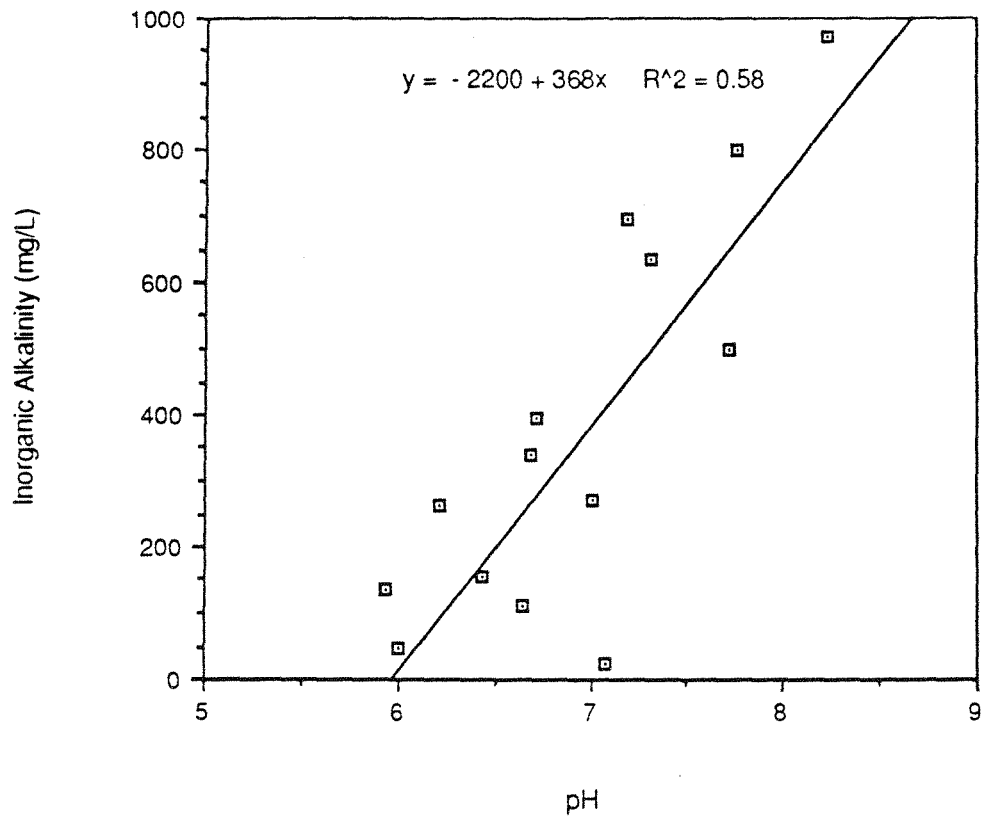


Figure 96. Inorganic alkalinity (total field alkalinity minus total titrated organic acids) versus pH. Note the rise in pH with higher alkalinities.

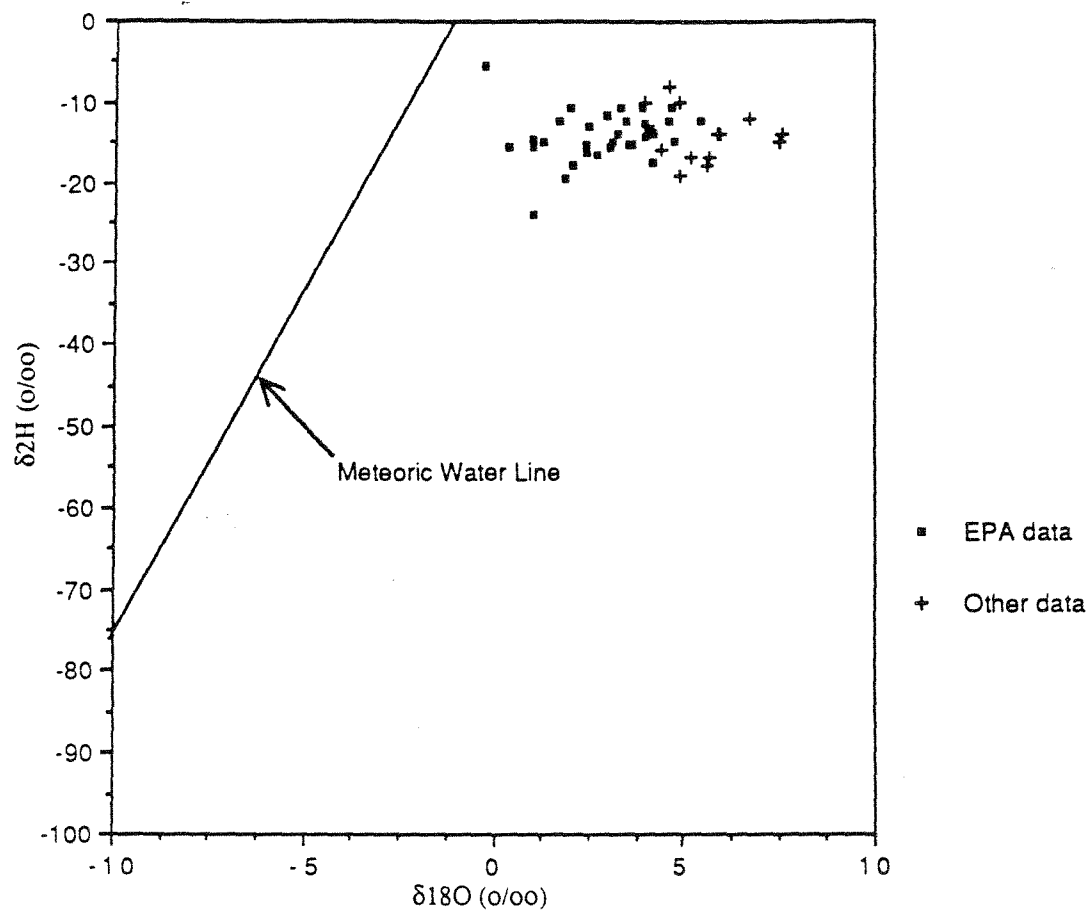


Figure 97. Hydrogen versus oxygen isotopic composition of waters from the Frio Formation. Data from this study (Table 5). Global meteoric water line from Craig (1961).

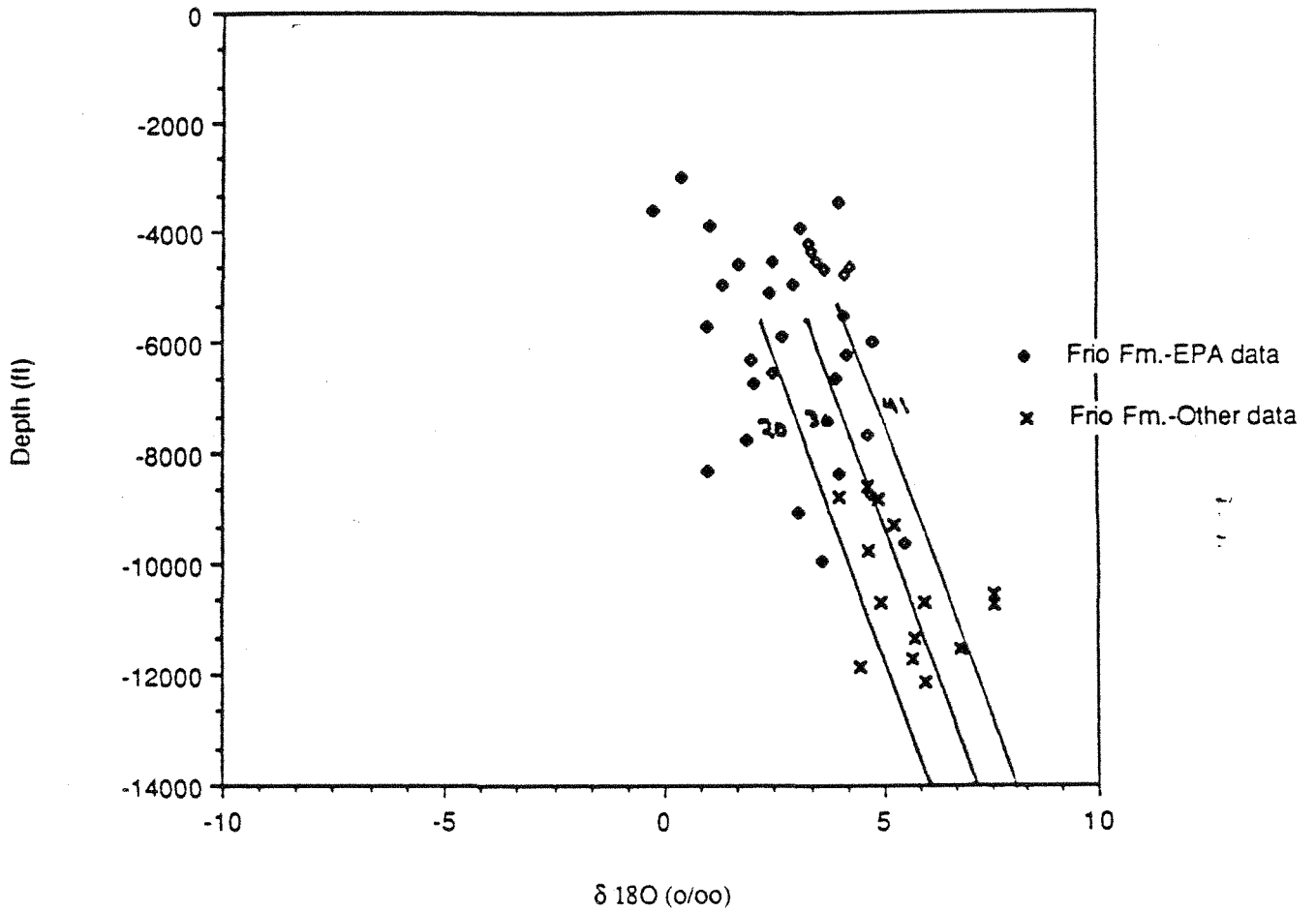


Figure 98. $\delta^{18}\text{O}$ versus depth. Data show a general enrichment of $\delta^{18}\text{O}$ with increasing depth (temperature). Data follows the isotope equilibration lines between water and illite (Epstein and Savin, 1973) for different geothermal gradients. Data from this study (Table 5).

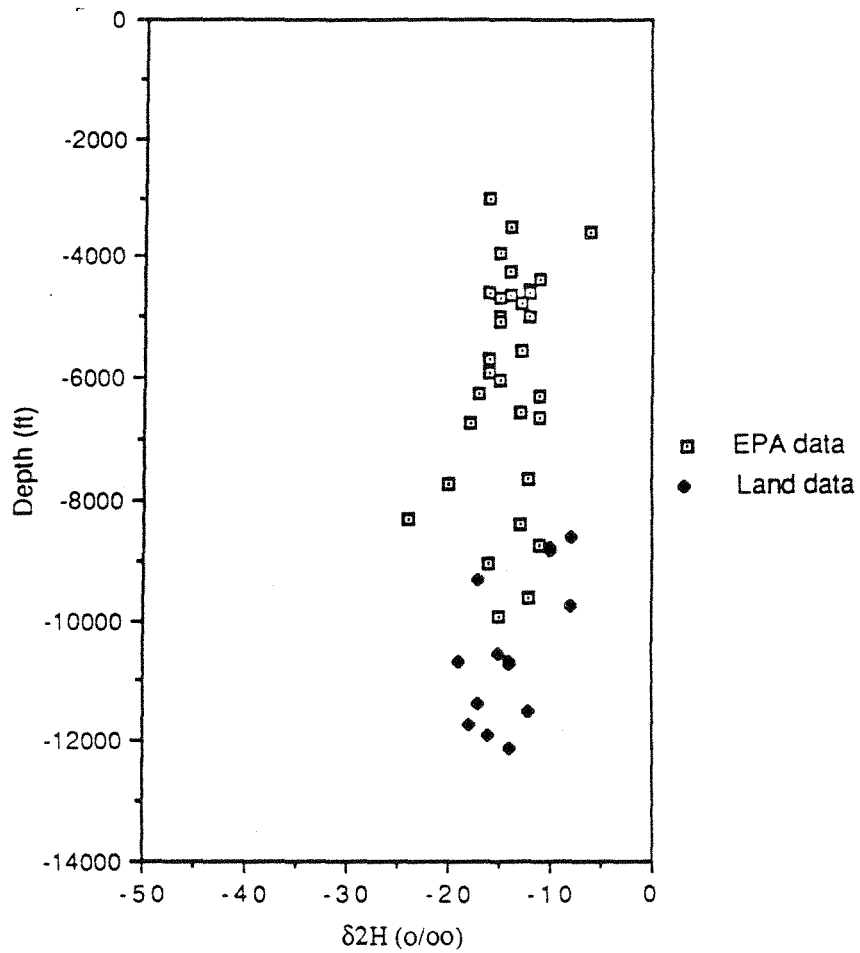


Figure 99. $\delta^2\text{H}$ versus depth for waters in the Frio Formation. Note consistency of isotopic composition with depth. Data from this study (Table 5).

Gulf Coast formation waters with increased temperature if the waters have equilibrated with the clays in the formation (Fisher, 1982). Whether these waters are in isotopic equilibrium can be estimated by plotting the isotope equilibration line between illite and water (Epstein and Savin, 1973) for different geothermal gradients (fig. 98). The equation used is:

$$10^3 \ln \alpha = 2.43 \times 10^{-6} T^{-2} - 4.82$$

If the water data plot close to these equilibrium curves, the waters are considered to have equilibrated with the clay in the formation. Most of the Frio data appear to be approaching these equilibrium lines.

The hydrogen isotope composition appears relatively constant versus depth, with $\delta^2\text{H}$ values ranging from -10 to -20‰. This consistency of isotopic values with depth strongly suggests isotopic equilibrium of the hydrogen in the water with hydrogen in clays. The clay with which the waters are equilibrating probably is montmorillonite, the dominant clay in the Gulf of Mexico basin. O'Neil and Kharaka (1976) in laboratory experiments identified rapid hydrogen isotope exchange between water and clays in temperatures as low as 100°C. They also argued that the process should occur in nature at lower temperatures. This exchange appears to be occurring in our Frio samples. Fisher (1982) constructed an equilibrium curve from Yeh (1980) for expected hydrogen isotopic compositions of waters equilibrated with illite. This curve predicts that the isotopic composition of the waters should progressively decrease with depth (fig. 99). This relationship is not observed for the Frio water data.

9.9 Age Determination

Determining the age of these Frio waters is important for understanding the hydrogeology of the saline Frio Formation as well as its implications for residence time of wastes injected into the Frio. There are, however, no appropriate radioisotopes for determining the absolute age of old saline waters such as in the Frio Formation. Absolute ages of ground waters can be estimated from radioactive isotopes such as ^3H (tritium), ^{14}C , ^{36}Cl , and ^{129}I , which have half-lives of 12.3 years, 5,730 years, 300,000 years, and 16 million years, respectively (Fritz and Fontes, 1980; Fabryka-Martin and others, 1985; Bentley and others, 1986). Of these, ^{14}C , ^{36}Cl , or ^{129}I are the most appropriate for dating old ground waters. All dating techniques relying on radioactive decay, however, have limitations, whether they be restricted by the short half-life of the radioisotope (for example, ^3H) or the complexities created by multiple sources or competing chemical reactions. For example, ^{36}Cl cannot be used for dating deep-basin brines. The radioactive isotope, ^{36}Cl , which results from cosmogenic fallout (Bentley and others, 1986), is overwhelmed by other chloride

Gulf Coast formation waters with increased temperature if the waters have equilibrated with the clays in the formation (Fisher, 1982). Whether these waters are in isotopic equilibrium can be estimated by plotting the isotope equilibration line between illite and water (Epstein and Savin, 1973) for different geothermal gradients (fig. 98). The equation used is:

$$10^3 \ln \alpha = 2.43 \times 10^{-6} T^{-2} - 4.82$$

If the water data plot close to these equilibrium curves, the waters are considered to have equilibrated with the clay in the formation. Most of the Frio data appear to be approaching these equilibrium lines.

The hydrogen isotope composition appears relatively constant versus depth, with $\delta^2\text{H}$ values ranging from -10 to -20‰. This consistency of isotopic values with depth strongly suggests isotopic equilibrium of the hydrogen in the water with hydrogen in clays. The clay with which the waters are equilibrating probably is montmorillonite, the dominant clay in the Gulf of Mexico basin. O'Neil and Kharaka (1976) in laboratory experiments identified rapid hydrogen isotope exchange between water and clays in temperatures as low as 100°C. They also argued that the process should occur in nature at lower temperatures. This exchange appears to be occurring in our Frio samples. Fisher (1982) constructed an equilibrium curve from Yeh (1980) for expected hydrogen isotopic compositions of waters equilibrated with illite. This curve predicts that the isotopic composition of the waters should progressively decrease with depth (fig. 99). This relationship is not observed for the Frio water data.

9.9 Age Determination

Determining the age of these Frio waters is important for understanding the hydrogeology of the saline Frio Formation as well as its implications for residence time of wastes injected into the Frio. There are, however, no appropriate radioisotopes for determining the absolute age of old saline waters such as in the Frio Formation. Absolute ages of ground waters can be estimated from radioactive isotopes such as ^3H (tritium), ^{14}C , ^{36}Cl , and ^{129}I , which have half-lives of 12.3 years, 5,730 years, 300,000 years, and 16 million years, respectively (Fritz and Fontes, 1980; Fabryka-Martin and others, 1985; Bentley and others, 1986). Of these, ^{14}C , ^{36}Cl , or ^{129}I are the most appropriate for dating old ground waters. All dating techniques relying on radioactive decay, however, have limitations, whether they be restricted by the short half-life of the radioisotope (for example, ^3H) or the complexities created by multiple sources or competing chemical reactions. For example, ^{36}Cl cannot be used for dating deep-basin brines. The radioactive isotope, ^{36}Cl , which results from cosmogenic fallout (Bentley and others, 1986), is overwhelmed by other chloride

sources (for example, salt dome dissolution, connate brines, etc.), which, because of their old age, no longer contain original cosmogenic ^{36}Cl . In addition, there is subsurface generation of ^{36}Cl by neutron flux from the decay of radioactive minerals (Feige and others, 1968; Kuhn, 1984). Next, ^{129}I , another long-lived radioisotope with a half-life of 16 million years may be appropriate for dating old waters but has problems similar to those of ^{36}Cl ; iodide is leached from the basinal formations and ^{129}I is produced in the subsurface by neutron flux (Fabryka-Martin and others, 1985). Even though these radiometric dating techniques have serious problems, they may provide general ages or, more importantly, approximate minimum ages. The presence of high ^{36}Cl or ^{14}C activities indicates a relatively young water, whereas the absence of these species may indicate an older water.

Carbon-14 (^{14}C), the best method for dating waters less than 20,000 to 40,000 years old, was considered for the Frio, but was not analyzed for two reasons. Based on the following reasoning, Frio waters are considered to be older than can be dated with ^{14}C . Previous work by Pearson and White (1967) showed that the deep, downdip, fresh waters in the Gulf Coast Carrizo-Wilcox aquifer had reached the lower limit of ^{14}C activity. Fisher (1982) sampled waters farther downdip in the Wilcox than those sampled by Pearson and White (1967) (fig. 100) and found depleted $\delta^{18}\text{O}$ values that are significantly lighter than the isotope equilibration curves for clay-mineral reactions. These light values indicate a meteoric component of geologically recent recharge. In contrast, the Frio waters are significantly heavier and appear to be equilibrated. Because the Frio waters have equilibrated and the Wilcox waters have not, they are assumed to be older than the Wilcox waters which, in turn, were collected downdip from the Carrizo-Wilcox water sampled by Pearson and White (1967). On the basis of this line of reasoning, the Frio waters are considered to be older than 20,000 to 40,000 years, that is, older than can be easily dated by ^{14}C . In general, ^{14}C analyses are routinely done by liquid scintillation or proportional counting techniques, which limits the maximum age of the water sample to approximately 40,000 years.

Accelerator mass spectrometry has extended the possible maximum age such that older waters can be analyzed. Application of more sensitive methods of analysis is precluded, however, by the second problem, the source of the dissolved carbon in deep saline formations. Dating of ground waters depends upon our adding a naturally occurring radioisotope in the recharge zone, knowing the decay rate, and measuring the radioisotope activity at the point of sampling. With this information, we can estimate how long the radioisotope has been within the aquifer. In saline aquifers, ^{14}C has problems similar to those of ^{36}Cl and ^{129}I in that there are subsurface sources for

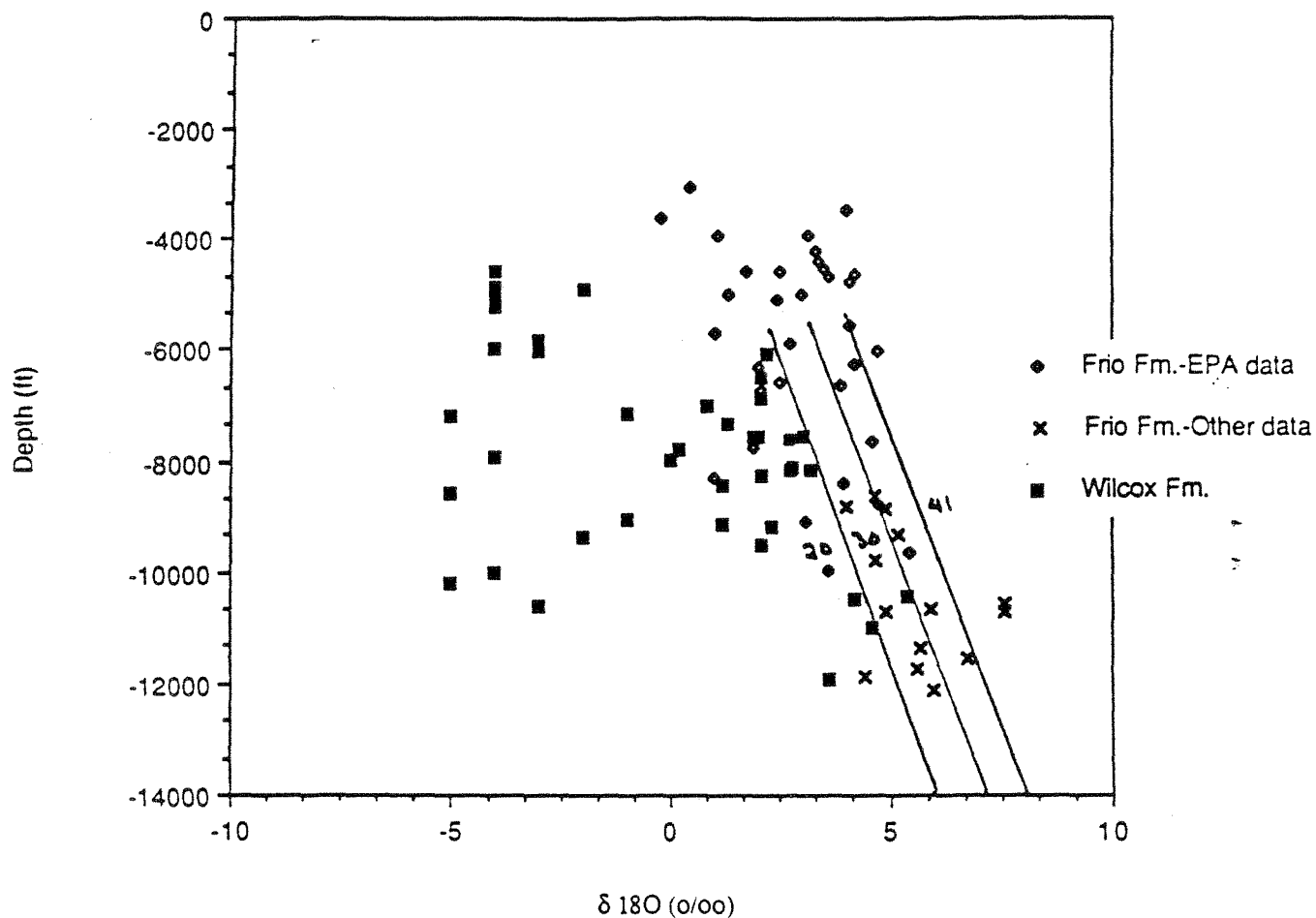


Figure 100. Comparison of $\delta^{18}\text{O}$ composition of Wilcox waters (Fisher, 1982) to Frio waters collected for this study (Table 5). Wilcox waters are much lighter and do not appear to be in isotopic equilibrium with sediments.

carbon as there are for chlorine and iodine. As discussed previously, the source of dissolved carbon (as either an organic acid or bicarbonate/ CO_2) in saline Gulf Coast formation waters probably is from the maturation of organic material. The dissolved carbon therefore is derived from Oligocene-aged Frio sediments and not from the recharge at the outcrop. Saline formation waters are not expected to be datable with ^{14}C because of their pre- ^{14}C age and in situ source of carbon.

10. WATER CHEMISTRY - DISCUSSION

10.1 Hydrochemical Environment

The hydrochemistry of Frio formation water within a depth range of 4,000-7,000 ft. the range used for deep-well injection, typically is slightly acidic (pH 5-6), very saline to briny (Cl generally ranges from 20,000 to greater than 60,000 ppm), reducing (presence of NH_4), warm (less than 80°C), and potentially biologically active (zero to trace organic acid concentrations and degraded oil). Each of the above geochemical conditions may have an impact on the long-term fate of injected chemical wastes.

The varying salinity of natural brines may affect the flow of wastes away from an injection well. Salinity determines whether injected wastes would float on top because of lower density, sink to the bottom because of higher density, or flow from the well as a plug flow because of similar densities (Miller and others, 1985). The potential for wastes floating on top because of a density contrast probably is much greater in other sedimentary basins used for injection where brines have typical chlorinities of greater than 100,000 ppm (such as the Illinois basin). Figure 68a and b and the appendix provide salinity information on a county scale, which enabled us to estimate density of formation waters.

The estimated pH range of 5-6 is controlled by rock-water chemical reactions. The pH of the chemical wastes, regardless of whether they are acidic or basic, should ultimately reach this slightly acidic range. Scrivner and others (1985) suggested that hydrolysis reactions are important for waste degradation (for example, decomposition of cyanide). The speed of reaction (the kinetics) for hydrolysis, however, strongly favors either high or low pH, and not the neutral values of the natural conditions. Hydrolysis reactions of wastes need to be completed before acid or basic liquids are neutralized by the sedimentary formation.

Increased temperatures may increase reaction rates, but to significantly benefit, higher temperatures (probably above 100°C) are needed (O'Neil and Kharaka, 1976;

Lundegard, 1985; Boles and others, 1988). The lower temperatures in the shallow hydrostatic section may be optimal because of the possibility of biologically mediated waste degradation reactions. In the Texas Gulf Coast the predominant injected waste types are organics. If these wastes will degrade biotically, reaction rates may be significantly faster than for abiotic reactions such as hydrolysis. Under natural conditions, acetate and complex organic admixtures, such as crude oil, appear to be biologically consumed as deep as 7,000 ft and at temperatures as high as 70°C.

The presence of bacteria or other microorganisms was not investigated during this study. Bacteria have been identified as deep as 1,300 ft at Savannah River, Georgia (Wobber, 1986). If bacteria are present, they could be anaerobic (reducing environment) and may utilize methane. Methane occurs pervasively through the subsurface of the Gulf Coast (Lundegard, 1985). Previous investigators of hydrocarbon biodegradation have assumed that shallower oxidizing conditions were necessary and that aerobic bacteria were the dominant bacterial type (Bailey and others, 1973a). Neither the type of bacterial population in the subsurface (up to 70°C) nor whether they now exist is known. The presence of degraded oil may only indicate previous reactions. If bacteria are present, they may or may not be capable of degrading organic wastes. Even if they are not, this geochemical environment may be suitable for anaerobic bacteria, which can degrade organic wastes. This possibility needs to be investigated.

10.2 Hydrochemical Interpretation of Hydrogeologic Environment

The chemical and isotopic compositions of the sampled brines indicate two types of water in the shallower hydrostatic section (in comparison to the deeper geopressured horizons sampled by Morton and Land [1987]): an Na-Cl, low-Br water type (A), and an Na-Cl, high-Br water type (B). The chemical composition of Type A is controlled by halite dissolution. These waters occur in the Houston Embayment region and have high Na-Cl concentration as deep as 10,000 ft. The Na-Cl, high-Br waters typically are in the San Marcos Arch (central region) and South Texas region. These waters exhibit an increase of Br with depth, suggesting leakage of high-Br, high-Sr, and high-Ca waters from deeper in the section. Chemically both water types A and B appear to have originated from the same water type because both appear to be in isotopic equilibrium with oxygen and hydrogen. Both water types contain degraded oils and zero to trace concentrations of organic acids.

Based on these hydrochemical characteristics, what can we say about the hydrogeology of the Frio saline aquifer? Three scenarios were suggested in the introduction to hydrochemistry:

1. A meteoric origin for Frio waters
2. Original depositional (connate) waters
3. Waters leaking up from the deeper geopressed sections.

1. Meteoric origin: Active recharge of continental waters is not occurring in the Frio. All waters sampled appear in isotopic equilibrium with the rock matrix (figs. 98 and 99). This is in contrast with the underlying Wilcox, which contains isotopically nonequilibrated waters (fig. 99). Total dissolved solutes are also much higher than in the Wilcox (Kreitler and Richter, 1986). The inverse correlation of salinity and total alkalinity observed by Kreitler and Richter (1986) does not appear to correlate with shallow depths but to the deep section at the top of geopressure in South Texas (Land and Morton, 1987). The original water (before salt dome dissolution or deeper brine leakage) in the Frio had a Na/Cl ratio slightly greater than 1.0, which could suggest a post-depositional circulating water or a connate water that had a continental rather than a marine origin. The occurrence of biodegraded oils and lack of organic acids to depths of 7,000 ft imply biodegradation. Previous authors investigating biodegradation, however, believe that circulating meteoric waters are needed for transport of bacteria to the oils. Bacteria here, however, are found as deep as 1,300 ft in fresh-water aquifers. The other chemical data argue against an active circulation system.

2. and 3. Original depositional water and leakage: The Frio waters may predominantly represent original depositional waters that have subsequently dissolved salt domes or been mixed with a high-Br Na-Cl brine: the presence of Br-rich brines in the shallow hydrostatic sections offers geochemical evidence of fluid leakage from the undercompacted, geopressed section. It is surprising that high-Br concentrations occur only in Central and South Texas and not in the Houston Embayment region. In this region salt dome dissolution is the dominant reaction, but the increase in NaCl still should not mask this leakage. If there is leakage, Br concentrations should still rise. The Br concentrations in the salt dome region, however, remain constant regardless of NaCl concentrations. Vertical migration appears to occur in Central and South Texas but not in the Houston Embayment. This appears contradictory because of the extensive growth faults and salt domes in the Houston Embayment, which should provide excellent pathways for fluid migration. Lead-zinc mineralization along salt dome flanks in this region has been used for evidence of upward fluid migration. This paradox needs further explanation.

The evidence of salt dome dissolution and leakage in the hydrostatic section of the Frio indicates that hydrologic conditions are not stagnant. For salt dome dissolution to occur, advection or diffusion must be occurring. Fluid leakage from depth also implies fluid movement. This fluid movement may be geologic in time-scale and not critical for short timespans such as the time period needed for isolation of chemical wastes.

11. SUMMARY AND CONCLUSIONS

1. A very large pressure data base is available from which potentiometric maps and pressure depth plots can be constructed. More than 17,000 pressure measurements are available for the Frio Formation in Texas. Potentiometric maps can be made on a regional to site-specific scale. The regional scale is too large for evaluating individual injection facilities. Site-specific potentiometric surfaces are probably too small to identify the impact of oil production on an injection operation. County-scale maps appear appropriate. These data can be used to provide boundary conditions as well as confirm numerical models of injection.
2. Although some previous researchers have discredited the value of DST data, the pressure data from DSTs and other bottom-hole pressure measurements appear to be reliable. Good tests have been obtained from Gulf Coast Tertiary formations because of good porosity and permeability, which permit rapid pressure equilibrium within the tool. The pressure data have been invaluable for constructing potentiometric maps and, to some extent, for calculating permeability values. Other researchers attempting to describe regional or site-specific hydrology in the Texas Gulf Coast are strongly encouraged to use the pressure files, not only for research in hazardous waste disposal but also for studies related to oil and gas recovery.
3. Construction of potentiometric maps required development of arbitrary zones of investigations. Formations such as the Frio are thick and contain more than one hydrologic regime. A single integrated potentiometric surface is therefore not representative of the potential distribution at any specific depth within the Frio. For analysis of specific injection zones, a balance is needed between analyzing a thin injection zone and trying to develop a reasonable size data base. A similar problem occurs with the temporal distribution of pressure analysis; data have been collected for 50 years. It is important to use limited time intervals for construction of

potentiometric maps. Maintaining a balance between site-specific and time-specific data versus the use of large data bases to better understand a hydrologic system requires a subjective interpretation of the data and therefore a subjective interpretation of the maps. In that context, it must be remembered that these maps represent interpretations.

4. Because of the large amount of pressure data available, development of a computerized data base as well as computerized mapping proved to be the most efficient use of time and staff.

5. The Frio Formation was chosen because of the large volumes of wastes injected into the formation and because of the extensive geochemical, geologic, and pressure data bases available for interpretations. It was an excellent formation to use as a test case. Similar approaches can be developed for the other formations used for injection.

6. The geohydrologic environment of the Texas Gulf Coast saline formations is a complex interaction of the region's geology and hydrology. Pressure-depth plots indicate the presence of different pressure regimes that influence the fluid flow directions in and between the various hydrologic units. Formation fluid pressures are a good indicator of the hydrologic regime within a given formation. Thus, pressure gradients may be used as hydrologic markers for delineating different flow regimes. These pressure regimes can be classified as: shallow fresh- to moderately saline water hydropressured (<4,000 ft), intermediate depth (4,000 to 8,000 ft) brine hydrostatic, and deep overpressured. The pressure-depth profiles show that the transition to overpressured sediments is encountered at a depth shallower (around 6,500 ft) than what has been proposed by earlier researchers during drilling and geophysical logging measurements. Using the pressure gradient of 0.465 psi/ft as a marker, a new base of hydrostatic and top of geopressured section were delineated (figs. 52 and 53). As outlined in figure 53, there are areas where overpressured sediments are interspersed within the hydrostatic section.

7. Pressure/depth and potentiometric surface analyses indicate extensive depressurization in the 4,000- to 8,000-ft-depth range. This presumably results from the production of 20 billion barrels of oil and gas equivalent as well as large volumes of brine produced with the oil. If this depressurization results from oil and brine production, then the oil fields potentially become the ultimate sinks and pathways to

the biosphere for chemical wastes. Based on the available permeability data and flow gradients calculated from potentiometric surfaces, average horizontal linear flow velocity in the Frio Formation ranges from 0.01 to 105 ft/year. This reflects the flow potential toward a moderately depressurized oil field. For a better estimate of flow potential between an injection zone and an oil field, additional pressure distribution data in the injection sites are required. This process may be enhanced by the typical high permeability (greater than 1 darcy) of Gulf Coast sands. Conversely, flow may be impeded by geologic barriers such as growth faults. The use of pressure data in conjunction with structure and geology is the most appropriate technique for a complete hydrogeologic characterization. Detailed geologic investigations were not conducted for this study. They are needed, however, for a complete characterization of an injection site. Oil field depressurization may be a transient process. When the fields are depleted and production stops, reservoir pressures should return to higher values. The time or percentage of recovery, however, is unknown. It is important to bear in mind that the current study is based mainly on formation pressures from the oil- and gas-producing areas and is thus biased toward describing the complexity of those systems.

Because of this depressurization, a potentiometric surface cannot be constructed to determine natural gradients or natural points of discharge. Present hydrologic conditions do not mimic natural conditions. Conversely, hydrochemical tracers (such as high-Br waters) and mineralogical indicators (such as lead-zinc mineralization along salt dome flanks) do not represent current hydrologic conditions but represent preproduction, natural flow patterns.

9. Upward migration of water in hydrostatic section is currently limited by depressurization, density differences between shallow fresh water aquifers and the deeper saline aquifers and the interlayered low-permeability shales. The densities of the injected wastes and formation waters should be used in comparing the potential for vertical migration. Environmental heads maps rather than fresh-water head equivalent maps provide a more accurate picture of vertical flow potential. Using environmental head maps further decreases the potential for upward migration of brine into shallower fresh waters. Potentiometric surfaces that are above land surface using fresh water head equivalent may correct to a below-land-surface elevation when density is taken into consideration. However, density measurements rarely are included with pressure data for a well. Regional interpretation of salinity, and therefore density, can be estimated with the county salinity depth profiles shown in the appendix.

10. Hydrochemical data from the Frio suggest that a slow-moving, sluggish hydrologic environment existed under natural conditions. The Frio is not being actively recharged in geologic time by continental meteoric waters, as the Wilcox appears to be. Frio waters are considered to be older than can be dated by ^{14}C methods. Brines from the deeper geopressed section may be leaking into the hydrostatic section of the central and southern Frio. Vertical leakage does not appear to be occurring in the northern region. In this northern region the chemical composition of the brines is strongly influenced by salt dome dissolution. This leakage presumably extends only to the shallow saline hydrostatic section and not into the fresh ground water. The Gulf of Mexico sedimentary basin typically has been referred to as a compacting basin (Galloway and Hobday, 1983). This term "compacting" has been misapplied because it implies that waters from both the hydrostatic and geopressed section are migrating up faults or up structural dip to the outcrop. The only part in the Gulf of Mexico sedimentary basin out of compaction equilibrium (and therefore capable of fluid flow because of compaction) is the geopressed section. As the geopressed section compacts, fluids migrate to the brine hydrostatic section either by porous media flow or along faults. The only pathways through which compactional waters can reach land surface or the fresh-water section and bypass the brine hydrostatic section is up structural discontinuities such as faults and flanks of salt domes. Waters from the brine hydrostatic section are not expected to be currently flowing into the fresh-water sections because these brines appear from geochemical data to be relatively stagnant and from hydrologic data to be either depressurized or at hydrostatic pressures (i.e., no potential for upward migration) as well as being denser than the shallower fresh waters.

11. The presence of degraded hydrocarbons and the absence of organic acids suggest that bacteria may be degrading organic compounds as deep as 7,000 ft. Most injection zones should be in this potentially biologically active zone. If biodegradation of oils has occurred, it probably took place at rates significantly faster than abiotic reactions such as hydrolysis. Though these bacteria may not be capable of degrading other organic compounds, such as injected wastes, their presence does suggest that these shallow saline zones are in suitable biologic environments that might support the bacteria capable of degrading wastes. Hydrocarbon degradation may have occurred only in the past and may not be ongoing. The presence of bacteria in these zones needs to be documented.

12. FUTURE RESEARCH DIRECTIONS

This study has raised some important issues that need to be addressed to ensure safe disposal of hazardous chemical wastes. These issues are also relevant to the oil and gas industry.

12.1 Better Understanding of Depressurization

A more detailed study of the extent and effects of underpressuring is needed to determine the ultimate fate of the injected chemical wastes. The severe pressure depletion has altered the hydrologic equilibrium in the subsurface. Depressurization has enhanced the potential for migration of injected fluids toward oil fields. In a depleted field, high-permeability sediments may accentuate flow velocities. Other issues linked to depressurization are: land subsidence in oil fields, possible activation of faults, and efficiency of primary and secondary hydrocarbon recovery operations. For example, is it possible to reenter an old depleted oil field and conduct enhanced recovery operations, or does the extreme depressurization alter the fluid dynamics to such an extent that such operations become infeasible?

During mapping of potentiometric surfaces it was observed that not all the cones of depression circled by negative contours centered on oil and gas fields. Thus, in addition to hydrocarbon production, there may be other factors contributing to depressurization. Severe depressurization may also lead to stress alteration in the rocks. These factors require further investigation.

The Wilcox and Miocene formations do not seem to be as severely affected by depressurization as the Frio. This may be due to less hydrocarbon production from these formations. Determinations of the areal extent of depressurization and of the rates of pressure equilibration and pressure recovery due to fluid injection require integration of transient pressure data with static pressure information. The limitation of working with static pressures alone is that localized and temporal effects may become significant. Efforts need to be directed toward acquisition of transient pressure data from oil and gas fields for assessment of the effects of depressurization. The effects of extensive reinjection of brine also need to be investigated in the context of pressure equilibration.

12.2 Research in Overpressure Formation Mechanisms

The top of geopressed sediments, as observed from the pressure-depth profiles and potentiometric surfaces, is shallower than was previously recognized. Similarities between the character of the pressure-depth profiles in the Frio, Wilcox, and Miocene

indicate similar processes controlling the formation of overpressuring in all these sediments.

At this point the following questions still need to be answered:

1. Why does overpressuring start at approximately 6,000 ft in depth?
2. Why does the maximum gradient lie close to 0.9 psi/ft line (fig. 101)? Is this related to a formation fracture gradient? How does it correlate to the lithostatic gradient of 1.0 psi/ft?
3. What light can overpressuring shed on the processes of sediment compaction?
4. What path do the sediments traverse during burial? Do they follow the 0.465 trend line and then move into the overpressured zone, or first into the overpressured zone and then along a curved overpressured trend?
5. What role does the extensive faulting of Gulf Coast sediments play in the formation of overpressures? Do the faults impede compaction and diagenesis, or do they act as conduits for migration of overpressured brines to the shallower regions?
6. How does the process of equilibration of overpressures take place? Is the shallow occurrence of overpressuring a result of continued compaction, or is it due to the release of deep pressured brines that have not yet equilibrated to the lithostatic load?

The understanding of overpressuring phenomenon is also linked to the exploitation of energy resources and involves the synthesis of hydrologic data with geologic and geochemical information.

12.3 Potential for Biodegradation

The possibility of biodegradation as an important mechanism for waste degradation needs to be investigated. Organic wastes represent the largest type of waste injected in the Gulf Coast saline formations. If biodegradation is occurring or could occur, then reaction rates may be significantly faster than if degradation is dependent on abiotic reactions.

Investigating the potential for biodegradation may be a multistage program. Initially subsurface brines in this potentially biologically active zone should be tested for the presence of bacteria and other indicators of biologic activity. Secondly, an injection well needs to be tested to determine whether there are bacterial populations associated with the injection process. Bacterial populations for both studies need to be sampled so that types and population densities can be determined. Thirdly, laboratory experiments need to be designed to evaluate this potential for deep subsurface biodegradation, its potential for degrading organic wastes, and possible enhancement of the process.

indicate similar processes controlling the formation of overpressuring in all these sediments.

At this point the following questions still need to be answered:

1. Why does overpressuring start at approximately 6,000 ft in depth?
2. Why does the maximum gradient lie close to 0.9 psi/ft line (fig. 101)? Is this related to a formation fracture gradient? How does it correlate to the lithostatic gradient of 1.0 psi/ft?
3. What light can overpressuring shed on the processes of sediment compaction?
4. What path do the sediments traverse during burial? Do they follow the 0.465 trend line and then move into the overpressured zone, or first into the overpressured zone and then along a curved overpressured trend?
5. What role does the extensive faulting of Gulf Coast sediments play in the formation of overpressures? Do the faults impede compaction and diagenesis, or do they act as conduits for migration of overpressured brines to the shallower regions?
6. How does the process of equilibration of overpressures take place? Is the shallow occurrence of overpressuring a result of continued compaction, or is it due to the release of deep pressured brines that have not yet equilibrated to the lithostatic load?

The understanding of overpressuring phenomenon is also linked to the exploitation of energy resources and involves the synthesis of hydrologic data with geologic and geochemical information.

12.3 Potential for Biodegradation

The possibility of biodegradation as an important mechanism for waste degradation needs to be investigated. Organic wastes represent the largest type of waste injected in the Gulf Coast saline formations. If biodegradation is occurring or could occur, then reaction rates may be significantly faster than if degradation is dependent on abiotic reactions.

Investigating the potential for biodegradation may be a multistage program. Initially subsurface brines in this potentially biologically active zone should be tested for the presence of bacteria and other indicators of biologic activity. Secondly, an injection well needs to be tested to determine whether there are bacterial populations associated with the injection process. Bacterial populations for both studies need to be sampled so that types and population densities can be determined. Thirdly, laboratory experiments need to be designed to evaluate this potential for deep subsurface biodegradation, its potential for degrading organic wastes, and possible enhancement of the process.

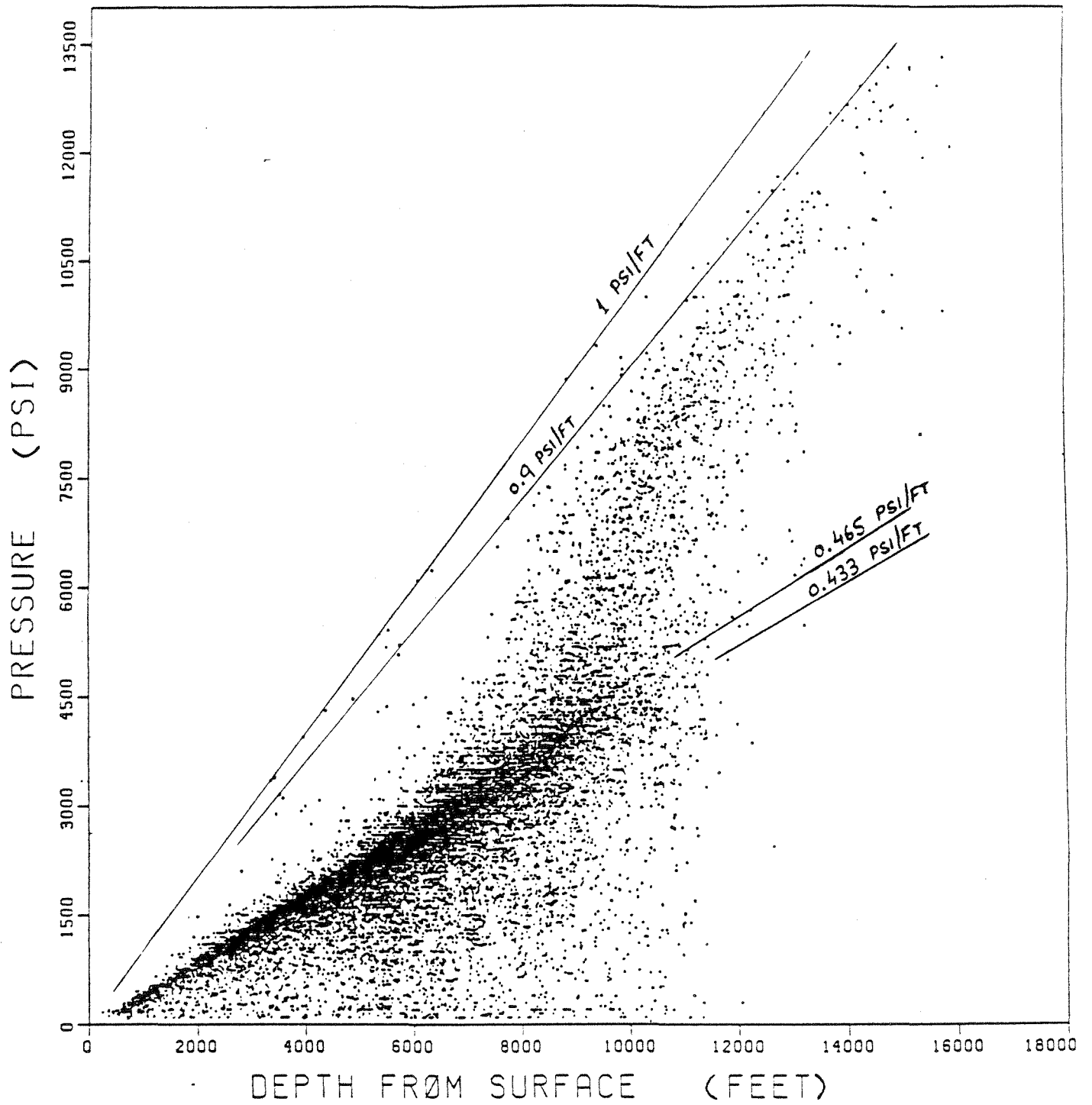


Figure 101. Pressure-depth diagram for Frio regions A-B-C data with overburden pressure line 1 psi/ft, and possible fracture gradient 0.9 psi/ft.

The presence of biodegradation within the Wilcox Formation should also be investigated. Low-TDS ground water appears to extend significantly deeper in the Wilcox than in the Frio. The effects of biodegradation, therefore, may also extend significantly deeper.

12.4 Thermal Regimes

A complete characterization of the Gulf Coast Tertiary formations is viable only when the thermal component of fluid properties is also integrated with the hydrologic description. A significant amount of temperature data was retrieved from the PI data base and was plotted as the temperature-depth profile of the Frio in region C (fig. 102). An in-depth screening and evaluation of these data is needed because it may provide new insight into the thermal gradients and their influence on the mechanism of overpressure formation. The thermal environment may play a critical role in the chemical degradation of injected wastes.

12.5 Geohydrologic Computer Modeling

The synthesis of geologic, hydrologic, geochemical, and geothermal information facilitates compilation of models that can provide practical answers to questions of chemical waste injection, confinement, migration, and degradation within the Gulf Coast injection zones. These answers need to be corroborated by the development of analytical processes and mathematical computer models. Efforts are underway at the Bureau of Economic Geology, Austin, to develop analytical capabilities and to test certain geochemical simulators that can be incorporated in the modeling process. A program is in place to compile a comprehensive data base of formation fluid and injected fluid chemistry. Subsequently, research will continue in parameter estimation to describe the chemical degradation reactions. These need to be integrated with laboratory and field studies.

12.6 Other Gulf Coast Formations Used for Injection

The hydrology of other Texas Gulf Coast formations used for deep-well injection of chemical wastes should be investigated with the approaches developed in this report. Data are available, as is evident in the pressure-depth profiles of the Wilcox and undifferentiated Miocene strata (figs. 57 and 58).

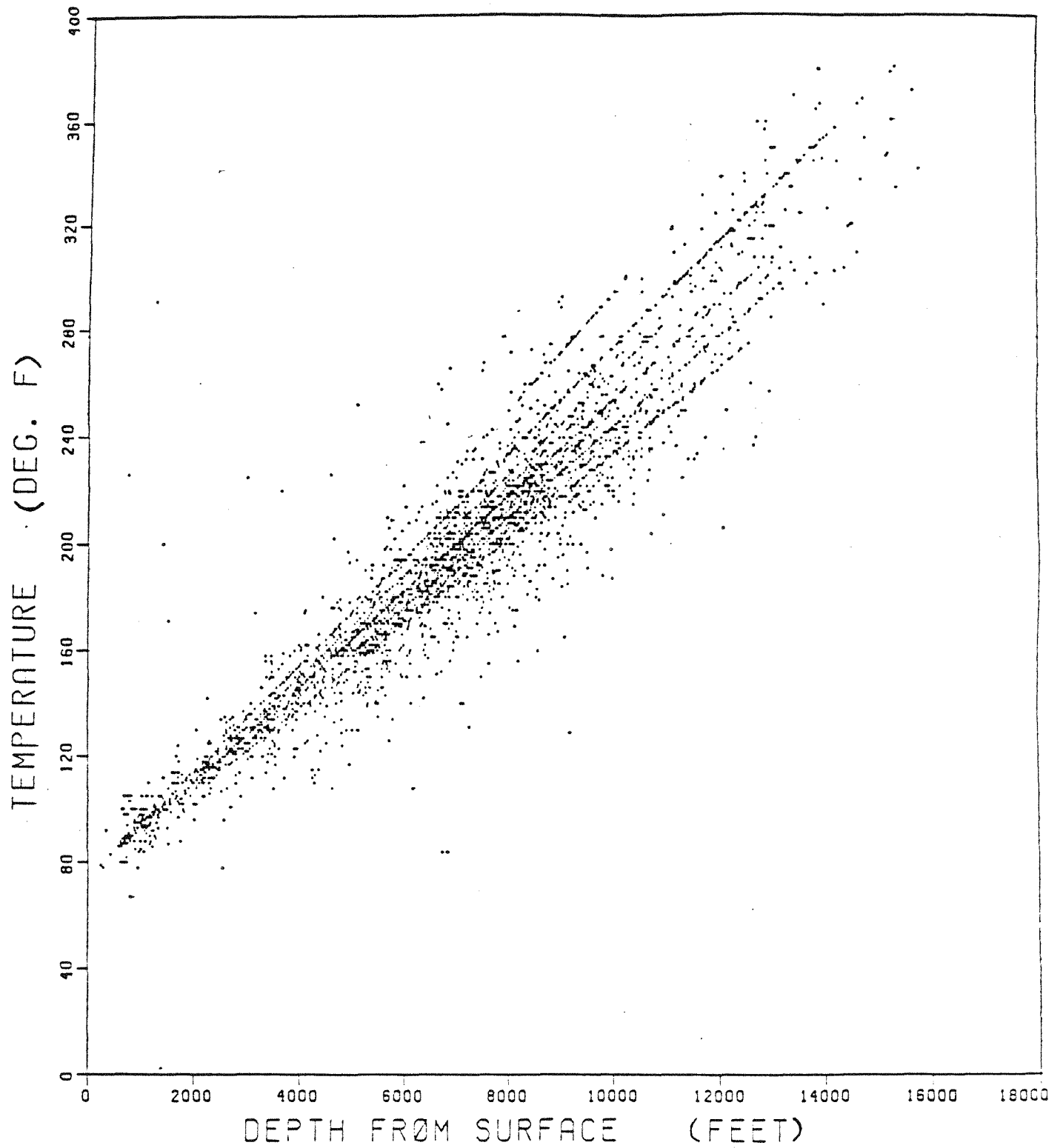


Figure 102. Temperature-depth profile for Frio Formation, region C. Data reliability has not been confirmed.

13 ACKNOWLEDGMENTS

Funding for this research was provided by the U.S. Environmental Protection Agency under Cooperative Agreement ID No. CR812786-01-0. The support provided by Jerry Thornhill, Project Officer, U.S. Environmental Protection Agency (Robert S. Kerr Environmental Research Laboratory, Ada, Oklahoma), was greatly appreciated. Numerous oil field operators willingly provided access to oil wells for water chemistry sampling. Zvi Sofer of the Mineral Studies Laboratory, Bureau of Economic Geology, performed the isotopic and organic carbon analyses. Steve Tweedy of the Bureau's Mineral Studies Laboratory provided the chemical analyses. Merrill Robinson-Lewis of ARCO Services Laboratory conducted the gas chromatographic analyses. Regina Capuano provide valuable comments during the final writing of this report. Maria Saenz drafted the illustrations, under the direction of Richard L. Dillon.

14. REFERENCES

- Bachman, A. L., 1979, Subsurface Disposal of Geopressed Fluids: Potential Geologic and Operational Problems with Recommendations for Disposal System Testing, in Dorfman, M. H., and Fisher, W. L., Proceedings, 4th U.S. Gulf Coast Geopressed-Geothermal Energy Conference; Research and Development: The University of Texas at Austin, Center for Energy Studies, v. 2, p. 972-999.
- Bailey, N. J. L., Krouse, H. R., Evans, C. R., and Rogers, M. A., 1973a, Alteration of Crude Oil by Waters and Bacteria - Evidence from Geochemical and Isotope Studies: American Association of Petroleum Geologists Bulletin, v. 57(7), p. 1276-1290.
- Bailey, N. J. L., Jobson, A. M., and Rogers, M. A., 1973b, Bacterial Degradation of Crude Oil: Comparison of Field and Experimental Data: Chemical Geology, v. 11, p. 203-221.
- Baker, E. T., Jr., 1979, Stratigraphic and Hydrogeologic Framework of Part of the Coastal Plain of Texas: Texas Department of Water Resources, Austin, Texas, Report no. 236.
- Bebout, D. G., Loucks, R. G., and Gregory, A. R., 1978, Frio Sandstone Reservoirs in the Deep Subsurface along the Texas Gulf Coast: The University of Texas at Austin, Bureau of Economic Geology Report of Investigations No. 91, 92 p.
- Bentley, H. W., Phillips, F. M., and Davis, S. N., 1986, ^{36}Cl in the Terrestrial Environment, in Handbook of Environmental Isotope Chemistry (Fritz, P., and Fontes, J. C., eds.), v. 2, p. 427-480.
- Boles, J. S., Crerar, D. A., Grissom, G., and Key, T. C., 1988, Aqueous Thermal Degradation of Gallic Acid: Geochimica et Cosmochimica Acta, v. 52, p. 341-344.
- Bond, D. C., 1972, Hydrodynamics in Deep Aquifers of the Illinois Basin: Illinois State Geological Survey, Circular 470, p. 51.
- Bradley, J. S., 1975, Abnormal Formation Pressure: American Association of Petroleum Geologists Bulletin, v. 59, no. 6, p. 957-973.
- Carothers, W. W., and Kharaka, Y. K., 1978, Aliphatic Acid Anions in Oil-field Waters--Implications for Origin of Natural Gas: American Association of Petroleum Geologists Bulletin, v. 62, no. 12, p. 2441-2453.
- _____ 1980, Stable Carbon Isotopes of HCO_3 in Oil-Field Waters - Implications for the Origin of CO_2 : Geochimica et Cosmochimica Acta, v. 44, p. 323-332.

- Carpenter, A. B., 1978, Origins and Chemical Evolution of Brines in Sedimentary Basins: Oklahoma Geological Survey Circular 79, p. 60-77.
- Carpenter, R., 1987, The Road to Recovery: Texas Engineering Experimental Station Windows, v. 6, no. 3, p. 3-5.
- Clayton, R. N., Friedman, I., Graf, D. L., Mayeda, T. K., Meents, M. F., and Shrimp, N. F., 1966, The Origin of Saline Formation Waters - 1. Isotopic Composition: Journal of Geophysical Research, v. 77(16), p. 3869-3882.
- Craig, H., 1961, Isotopic Variations in Meteoric Waters: Science, v. 133, p. 1702-1703.
- Dickey, P. A., Shriram, C. R., and Paine, W. R., 1968, Abnormal Pressures in Deep Wells of Southwestern Louisiana: Science, v. 160, no. 3828, p. 609-615.
- Dodge, M. M., and Posey, J. S., 1981, Structural Cross Sections, Tertiary Formations, Texas Gulf Coast: The University of Texas at Austin, Bureau of Economic Geology Cross Sections, 6-p. text, 23 cross sections.
- Drez, P. E., 1988, Rock-Water Interaction between Injected Waste and Host Formations and Mineralogy during Deep Well Injection (abs.): EOS, v. 69, no. 16, p. 350.
- DuBar, J. R., 1982, unpublished, Structure Map, Top of Undifferentiated Miocene Formation: The University of Texas at Austin, Bureau of Economic Geology Open-File Report.
- Earlougher, R. C., 1977, Advances in Well Test Analysis: Society of Petroleum Engineers of American Institute of Mining and Metallurgical Engineers, Monograph Volume 5, p. 93-94.
- Epstein, E. V., and Savin, S. M., 1973, Oxygen Isotope Geothermometry of the Burial Metamorphic Rocks of the Precambrian Belt Supergroup, Glacier National Park, Montana: Geological Society of America Bulletin, v. 84, p. 2549-2560.
- Fabryka-Martin, J., Bentley, H., Elmore, D., and Airey, P. L., 1985, Natural Iodine-129 as an Environmental Tracer: Geochimica et Cosmochimica Acta, v. 49, p. 337-347.
- Federal Register, August 27, 1987: Environmental Protection Agency, Proposed Rule, Part III, v. 52, no. 166.
- Feige, Y., Oltman, B. G., and Kastner, J. M., 1968, Production of Neutrons in Soils due to Natural Radioactivity: Journal of Geophysical Research, v. 37, p. 3135-3142.

- Fisher, J. B., 1987, Distribution and Occurrence of Aliphatic Acid Anions in Deep Subsurface Waters: *Geochimica et Cosmochimica Acta*, v. 51, p. 2459-2468.
- Fisher, R. S., 1982, Diagenetic History of Eocene Wilcox Sandstones and Associated Formation Waters, South-Central Texas: The University of Texas at Austin, Ph.D. dissertation, 185-p.
- Fisher, R. S., and Kreitler, C. W., 1987, Origin and Evolution of Deep-Basin Brines, Palo Duro Basin, Texas: The University of Texas at Austin, Bureau of Economic Geology Report of Investigations No. 166, 33 p.
- Frank, J. C., 1986, Injection Zone Pressure Profile at E. I. Du Pont de Nemours and Company, Victoria Site, Texas, in Proceedings of the International Symposium on Subsurface Injection of Liquid Wastes, New Orleans, p. 509-519.
- Fritz, P., and Fontes, J. C., 1980, Handbook of Environmental Isotope Geochemistry: Elsevier, Amsterdam, 545 p.
- Galloway, W. E., 1982, Epigenetic Zonation and Fluid Flow History of Uranium-bearing Fluvial Aquifer Systems, South Texas Uranium Province: The University of Texas at Austin, Bureau of Economic Geology Report of Investigations No. 119, 31 p.
- Galloway, W. E., Hobday, D. K., and Magara, K., 1982, Frio Formation of the Texas Gulf Coast Basin--depositional systems, structural framework, and hydrocarbon origin, migration, distribution, and exploration potential: The University of Texas at Austin, Bureau of Economic Geology Report of Investigations No. 122, 78 p.
- Galloway, W. E., and Hobday, D. K., 1983, Terrigenous Clastic Depositional Systems: Applications to Petroleum, Coal, and Uranium Exploration: Springer-Verlag, New York, 423 p.
- Hanor, J. S., and Bailey, J. E., 1983, Use of Hydraulic Head and Hydraulic Gradient to Characterize Geopressured Sediments and the Direction of Fluid Migration in the Louisiana Gulf Coast: Gulf Coast Association of Geological Societies Transactions, v. 33, p. 115-122.
- Hantush, M. S., and Jacob, C. E., 1954, Plain Potential Flow of Groundwater with Linear Leakage: EOS Transactions of the American Geophysical Union, v. 35, p. 917-936.
- Hubbert, M. K., 1957, Darcy's Law and the Field Equations of the Flow of Underground Fluids: Bulletin of the International Association of Scientific Hydrology, no. 5, p. 24-59.

- Jessen, F. W., and Rolshausen, F. W., 1944, Waters from the Frio Formation, Texas Gulf Coast: American Institute of Mining and Metallurgical Engineers Transactions, v. 7, no. 3, p. 1-16.
- Jones, P. H., 1968, Hydrology of Neogene Deposits in the Northern Gulf of Mexico: U.S. Geological Survey Open-File Report, 132 p.
- Jones, P. H., 1975, Geothermal and Hydrocarbon Regimes, Northern Gulf of Mexico Basin, in Dorfman, M. H., and Deller, R. W., eds., Proceedings, First Geopressured Geothermal Energy Conference, Center for Energy Studies, The University of Texas at Austin, p. 42-44.
- Knape, B. K., 1984, Underground Injection Operations in Texas - a classification and assessment of underground injection activities: Texas Department of Water Resources Report 291, 207 p.
- Kreitler, C. W., 1979, Ground-Water Hydrology of Depositional Systems, in Galloway, W. E., and others, Depositional and Ground-Water Flow Systems in the Exploration for Uranium: A Research Colloquium: The University of Texas at Austin, Bureau of Economic Geology, p. 118-176.
- Kreitler, C. W., 1986, Hydrogeology of Sedimentary Basins as it Relates to Deep-Well Injection of Chemical Wastes: preprint of paper presented at the International Symposium on Subsurface Injection of Liquid Wastes, New Orleans, March 3-5, 27 p.
- Kreitler, C. W., and Richter, B. C., 1986, Hydrochemical Characterization of Saline Aquifers of the Texas Gulf Coast Used for the Disposal of Industrial Waste: The University of Texas at Austin, Bureau of Economic Geology, contract report to the U.S. Environmental Protection Agency, Contract No. R-812785-01-0, 164 p.
- Kreitler, C. W., and Seni, S. J., 1983, Origin and Evolution of Na-Cl to Na-Ca-Cl Brines, East Texas Basin (abs.): Geological Society of America, v. 15(6), p. 618-619.
- Kreitler, C. W., and Wuerch, H. V., 1981, Water Chemistry, Oakwood Salt Dome: in Kreitler, C. W., and others, Geology and Geohydrology of the East Texas Basin, A Report on the Progress of Nuclear Waste Isolation Feasibility Studies: The University of Texas at Austin, Bureau of Economic Geology Geological Circular 81-7, p. 156-161.
- Kuhn, M. W., 1984, Subsurface Neutron Production and Its Impact on ³⁶Cl Ground Water Dating: The University of Arizona, Master's thesis, 45 p.
- LaFargue, E., and Barker, C., 1988, Effect of Water Washing on Crude Oil Compositions: American Association of Petroleum Geologists Bulletin, v. 72, no. 3, p. 263-276.

- Land, L. S., and Prezbindowski, D. R., 1981, The Origin and Evolution of Saline Formation Water, Lower Cretaceous Carbonates, South-Central Texas, U.S.A.: *Journal of Hydrology*, v. 54, p. 51-74.
- _____ 1985, Chemical Constraints and Origins of Four Groups of Gulf Coast Reservoir Fluids: *American Association of Petroleum Geologists Bulletin*, v. 69, no. 1, p. 119-129.
- Lewis, C. T., and Rose, S. C., 1970, A Theory Relating High Temperatures to Overpressures: *Journal of Petroleum Technology*, v. 22, p. 11-16.
- Lundegard, P. D., 1985, Carbon Dioxide and Organic Acids: Origin and Role in Burial Diagenesis (Texas Gulf Coast Tertiary Formations): The University of Texas at Austin, Ph.D. dissertation, 145 p.
- Luszczynski, N. J., 1961, Head and Flow of Ground Water of Variable Density: *Journal of Geophysical Research*, v. 66, no. 12, p. 4247-4256.
- Magara, Kinji, 1976, Water Expulsion from Clastic Sediments during Compaction - Directions and Volumes: *American Association of Petroleum Geologists Bulletin*, v. 60, no. 4, p. 543-553.
- Miller, C., Fisher, T. A., II, Clark, J. E., Hales, C. H., Porter, W. M., and Tilton, J. N., 1986, Flow and Containment of Injected Waste, *in* Proceedings, International Symposium: Subsurface Injection of Liquid Wastes, New Orleans, March 3-5, p. 520-559.
- Milner, C. W. D., Rogers, M. A., and Evans, C. R., 1977, Petroleum Transformations in Reservoirs: *Journal of Geochemical Exploration*, v. 7, p. 101-153.
- Morton, R. O., and Land, L. S., 1987, Regional Variations in Formation Water Chemistry, Frio Formation (Oligocene), Texas Gulf Coast: *American Association of Petroleum Geologists Bulletin*, v. 71(2), p. 191-206.
- O'Neil, J. R., and Kharaka, Y. K., 1976, Hydrogen and Oxygen Isotope Exchange between Clay Minerals and Water: *Geochimica et Cosmochimica Acta*, v. 40, p. 241-246.
- Pearson, F. J., and White, D. E., 1967, Carbon 14 Ages and Flow Rates of Water in Carrizo Sand, Atascosa County, Texas: *Water Resources Research*, v. 3, 251 p.
- Pearson, F. J., Jr., Fisher, D. W., and Plummer, L. N., 1978, Correction of Ground-Water Chemistry and Carbon Isotopic Composition for Effects of CO₂ Outgassing: *Geochimica et Cosmochimica Acta*, v. 42, p. 1799-1807.
- Powers, M. C., 1967, Fluid Release Mechanisms in Compacting Marine Mudrocks and their Importance in Oil Exploration: *American Association of Petroleum Geologists Bulletin*, v. 51, no. 7, p. 1240-1254.

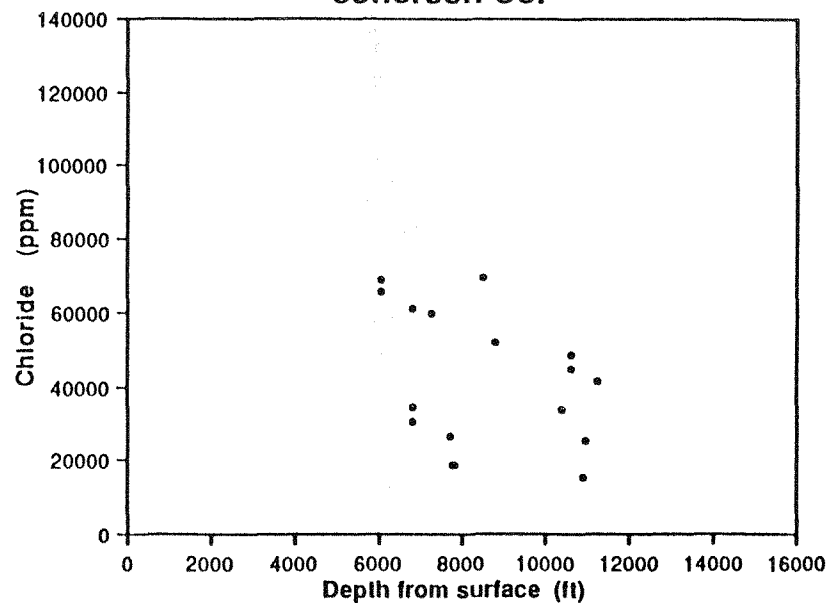
- Railroad Commission of Texas, 1978, A Survey of Secondary and Enhanced Recovery Operations in Texas to 1976: Railroad Commission of Texas, Oil and Gas Division Bulletin 76, 487 p.
- Richter, B. C., and Kreitler, C. W., 1986, Geochemistry of Salt-Spring and Shallow Subsurface Brines in the Rolling Plains of Texas and Southwestern Oklahoma: The University of Texas at Austin, Bureau of Economic Geology Report of Investigations No. 155, 47 p.
- Scrivner, N. C., Bennett, K. E., Pease, R. A., Kopatsis, A., Sanders, S. J., Clark, D. M., and Rafal, M., 1986, Chemical Fate of Injected Waste, in Proceedings, International Symposium on Subsurface Injection of Liquid Wastes: New Orleans, p. 560-609.
- Standard Methods for the Examination of Water and Wastewater, 1975, 14th ed., American Public Health Association - American Waterworks Association - Water Pollution Control Federation, p. 527-529.
- Texas Water Commission, Austin, Texas, 1987, Annual Injection Data Book.
- Toth, J., 1978, Gravity-Induced Cross-Formational Flow of Formation Fluids, Red Earth Region, Alberta, Canada - Analysis, Patterns, and Evolution: Water Resources Research, v. 14, no. 5, p. 805-843.
- Tyler, N., Light, M. P. R., and Ewing, T. E., 1985, Saline Fluid Flow and Hydrocarbon Migration and Maturation as Related to Geopressure, Frio Formation, Brazoria County, Texas, in Dorfman, M. H., and Morton, R. A., eds., Proceedings, Sixth Geopressured Geothermal Energy Conference, Center for Energy Studies, The University of Texas at Austin, p. 83-92.
- Ulrich, M. R., Kyle, J. R., and Price, P. E., 1984, Metallic Sulfide Deposits of the Winnfield Salt Dome, Louisiana: Evidence for Episodic Introduction of Metalliferous Brines During Cap Rock Formation: Gulf Coast Association of Geological Societies Transactions, v. 34, p. 435-442.
- Whittemore, D. O., Basel, C. L., Galle, O. K., and Waugh, T. C., 1981, Geochemical Identification of Saltwater Sources in the Smoky Hill River Valley, McPherson, Saline, and Dickinson Counties, Kansas: Kansas Geological Survey Open-File Report 81-6, 78 p.
- Wobber, F. L., 1986, Proceedings, Microbiology of Subsurface Environments: Second Investigators' Meeting - Savannah River Exploratory Probe, September 23, 1986, 24 p.
- Wood, L. A., Gabrysch, R. K., and Marvin, R., 1963, Reconnaissance Investigation of the Ground-Water Resources of the Gulf Coast Region, Texas: Texas Water Commission Bulletin 6305, 114 p.

- Yeh, H. W., 1980. D/H Ratios and Late-Stage Dehydration of Shales during Burial: *Geochimica et Cosmochimica Acta*, v. 42, p. 140-143.
- Young, A., Monaghan, P. H., and Schweisberger, R. T., 1977. Calculation of Ages of Hydrocarbons in Oils: *Physical Chemistry Applied or Petroleum Geochemistry*, Part I: American Association of Petroleum Geologists Bulletin, v. 61, p. 573-600.

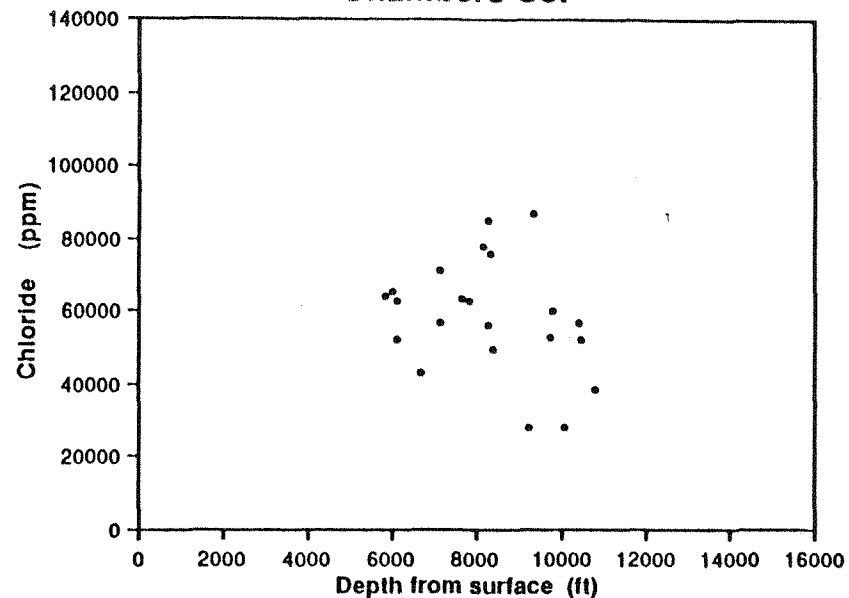
Appendix. Chloride versus depth for Gulf Coast counties.

201

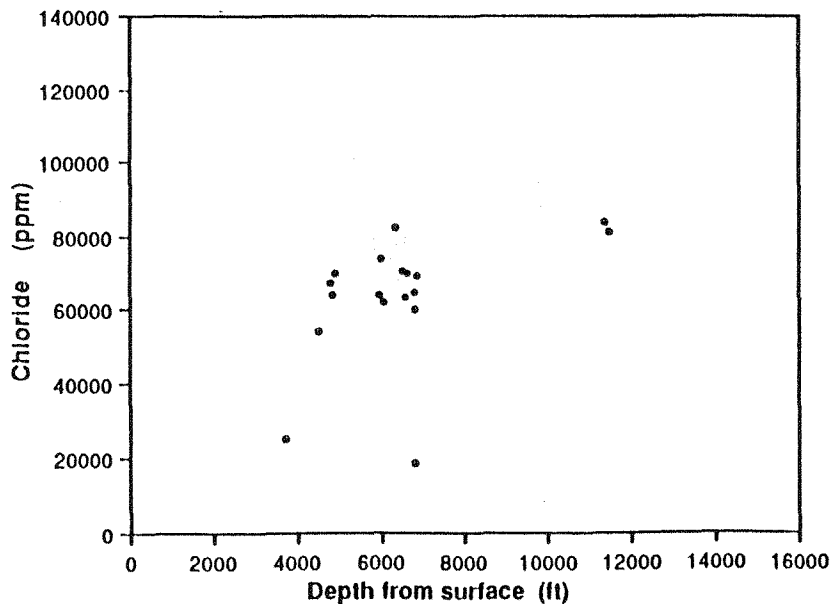
Jefferson Co.



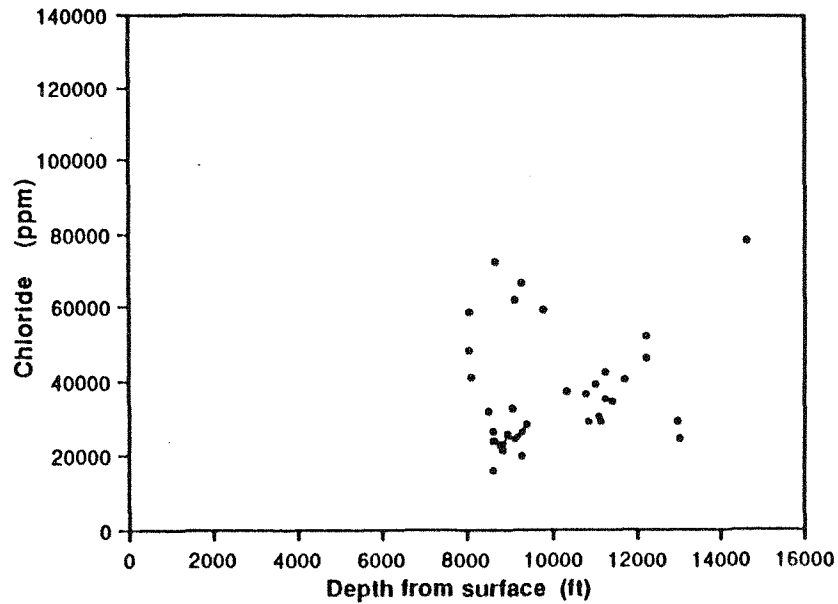
Chambers Co.



Harris Co.

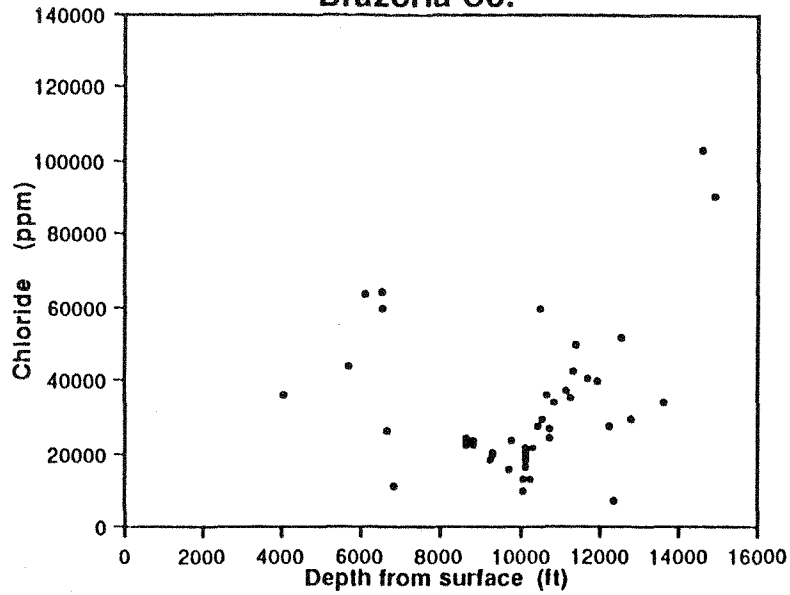


Galveston Co.

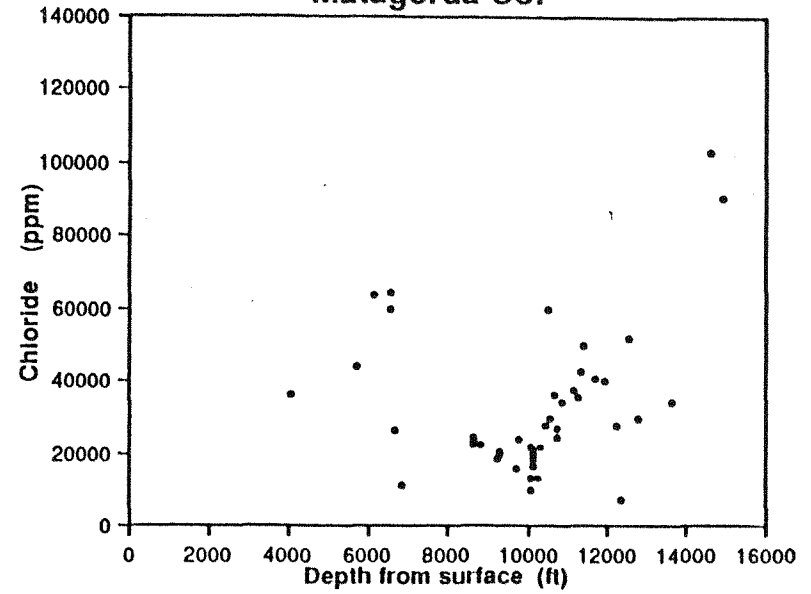


Appendix (continued)

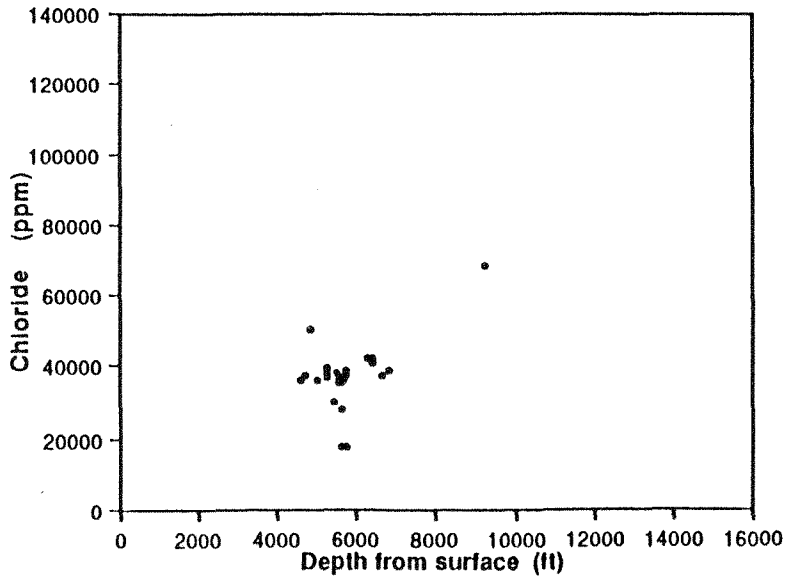
Brazoria Co.



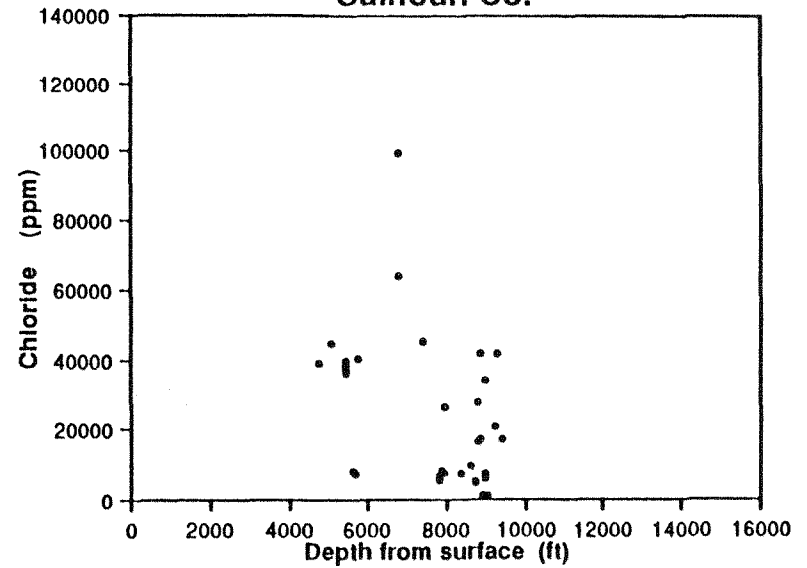
Matagorda Co.



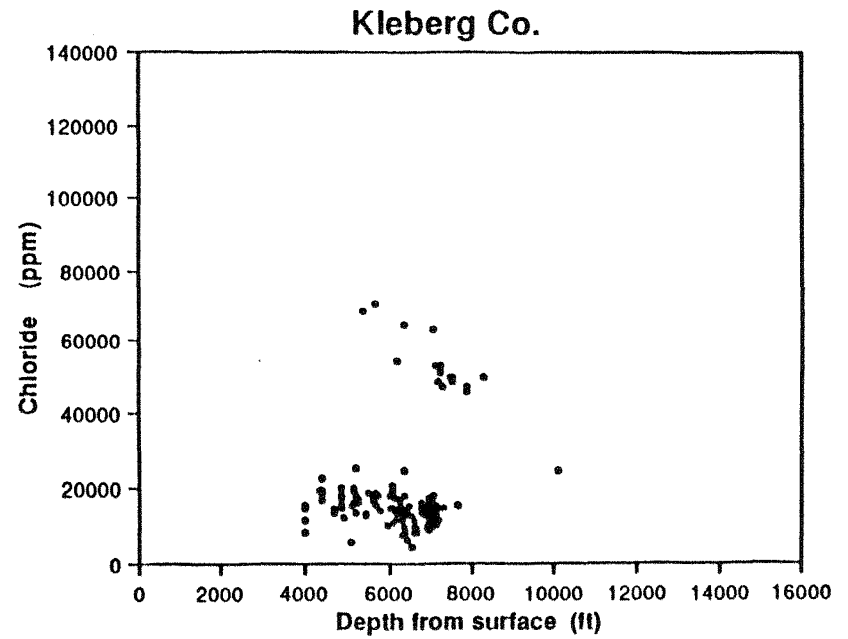
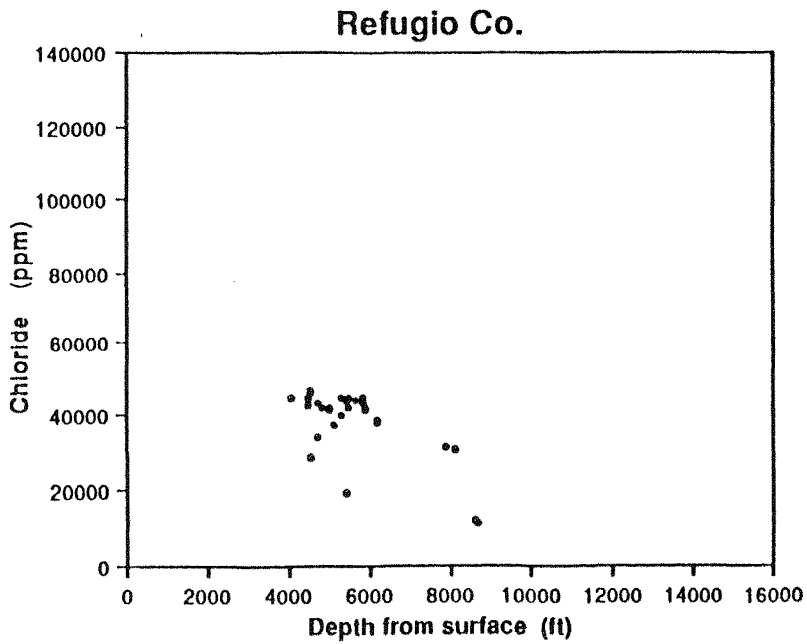
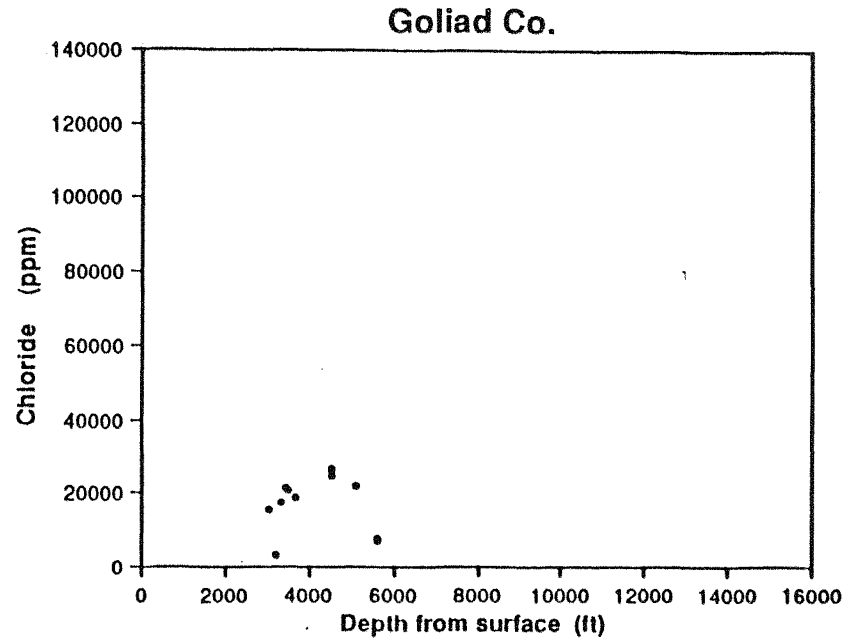
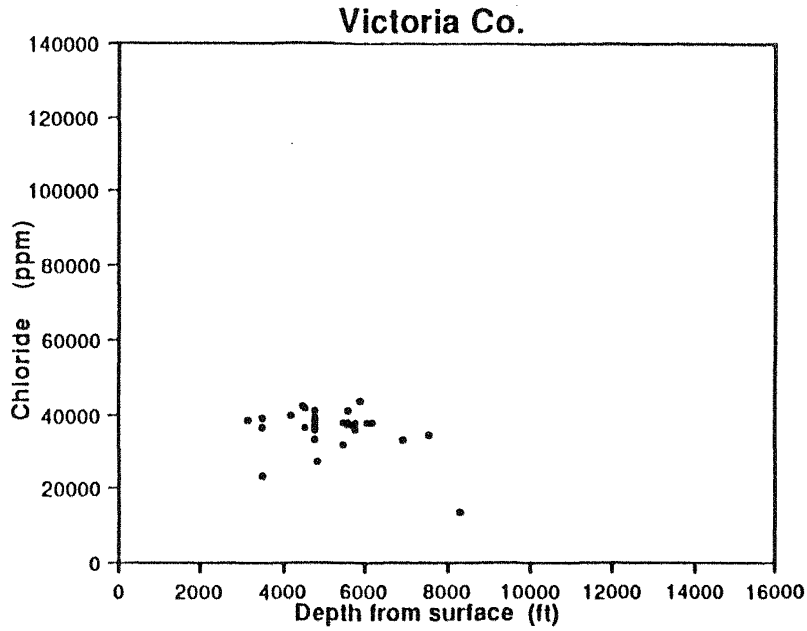
Jackson Co.



Calhoun Co.

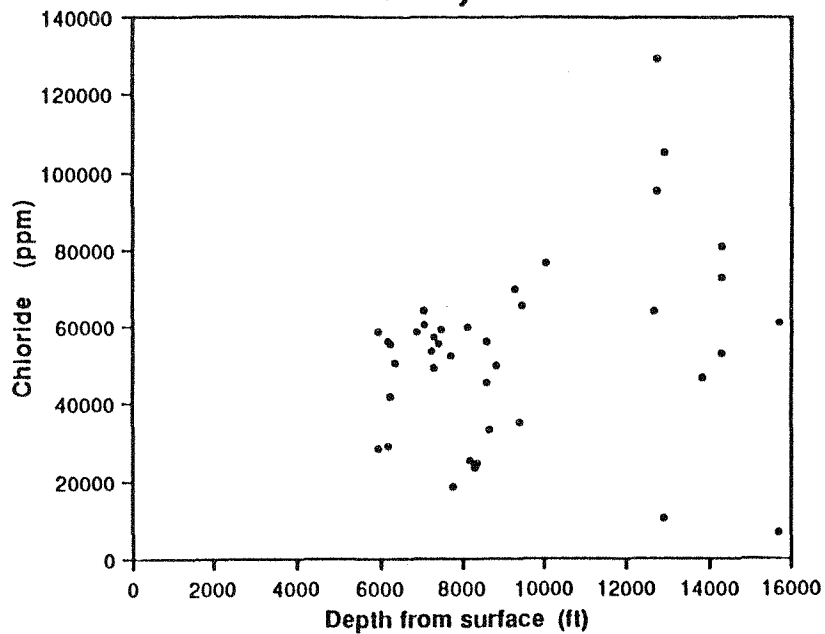


Appendix (continued)

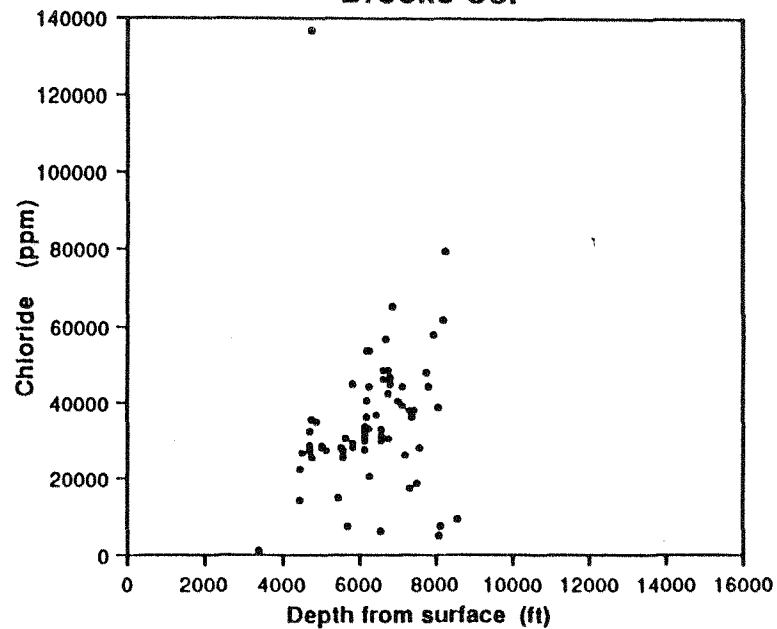


Appendix (continued)

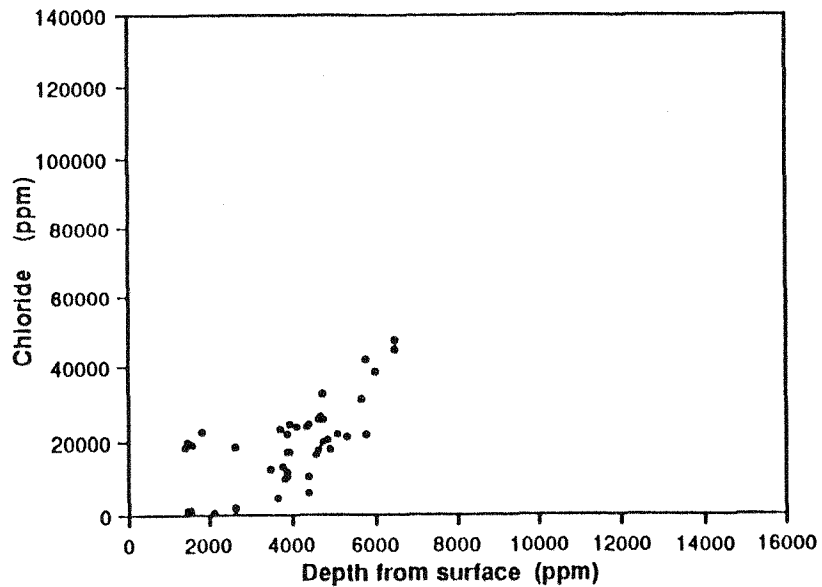
Kenedy Co.



Brooks Co.



Starr Co.



Hidalgo Co.

